UNIVERSIDAD DE MURCIA

FACULTAD DE INFORMÁTICA

Design of PID Controllers for Uncertain Plants

Diseño de Controladores PID para Plantas Inciertas

D. Pedro Mercader Gómez

2017

UNIVERSIDAD DE MURCIA
FACULTAD DE INFORMÁTICA

Design of PID Controllers for Uncertain Plants

Ph.D. Thesis

Author:
Pedro Mercader Gómez

Supervisor:
Dr. Alfonso Baños Torrico

2017

UNIVERSIDAD DE MURCIA
FACULTAD DE INFORMÁTICA

Diseño de Controladores PID para Plantas Inciertas

Tesis Doctoral

Presentada por:
Pedro Mercader Gómez

Supervisada por:
Dr. Alfonso Baños Torrico

2017

Agradecimientos

En primer lugar quiero mostrar mi mayor agradecimiento a mi director Alfonso Baños, por su excelente labor realizada durante el desarrollo de esta tesis y por sus valiosas enseñanzas. A Aurelio Arenas le agradezco haberme introducido en el mundo del control y su constante disponibilidad. También agradecer a los miembros (o antiguos miembros) del grupo de investigación de Informática Industrial con los que he tenido el placer de trabajar durante estos años: Ángeles, Paco, Quino, José Carlos, Joaquín, Juan Ignacio, Julio, Félix, Ovidio, Cristian David y José Francisco. Una mención especial se merece Miguel Ángel con el que he compartido innumerables cafés e interesantes discusiones. También quiero mostrar mi gratitud a Antonio Barreiro y a los miembros de su grupo de investigación con los que he tenido la oportunidad de compartir reuniones y congresos.

I would like to thank Tore Hägglund and Karl Johan Åström for receiving me at the Department of Automatic Control of Lund University and sharing with me their immense knowledge. I also thank Kristian Soltesz for the work we have done on some part of this thesis. I am not less grateful to Per-Olof Gutman who hosted me at the Technion – Israel Institute of Technology and gave me interesting projects to work on. I feel very fortunate to have met such great mentors and awesome people.

Por último, deseo expresar mi más sincero agradecimiento a mi familia y a mi novia por el incondicional apoyo recibido durante todo este proceso.

Financiación

Dar las gracias al Ministerio de Educación, Cultura y Deporte de España por la financiación de esta tesis doctoral bajo la beca de Formación de Profesorado Universitario FPU12/01026.

Abstract

This thesis is devoted to the problem of designing Proportional-Integral-Derivative (PID) controllers for uncertain, linear time-invariant (LTI), single-input-single-output (SISO) plants. The uncertainty of the plant is explicitly taken into account in the design stage of the controller. It is assumed that any mathematical model used to describe a real plant is an approximation, and hence, its ignorance should be quantified and taken into account when designing a control system. In addition, the most valuable feature of feedback control is its ability to reduce the effect of uncertainty, both model mismatch and unknown external disturbances. It should be noted that in absence of uncertainty or when it is acceptably small, feedback control is not necessary at all. In such cases, more advantageous solutions could be adopted by means of open-loop control.

The choice of a PID control structure is because of the fact that it is by far the most used form of feedback. It is present in more than 95 % of the industrial control loops. Even with the advent of more advanced control techniques, this situation has not changed. As a matter of fact, the only of such techniques that have achieved a significant presence in the industry is the predictive control, and it is generally deployed at a supervisory level, e.g., generating set-points for the bottom level PID controllers. Therefore, the overall performance of a control system based on predictive control is usually subordinated to the existence of properly tuned PID controllers. Nevertheless, the consideration of this control structure should not be a limitation, since most of the presented methods could be applied to more complex control structures.

The task of modeling uncertainty comprises a trade-off between obtaining a mathematically amenable model (unstructured uncertainty) and an accurate description of the uncertainty (structured uncertainty). This thesis adopts the latter approach. Interval parametric models are considered throughout this thesis, but some results are also applicable to the case of nonparametric multi-models in the frequency domain. The control design problems are posed as constrained optimization problems. Different kinds of problems are considered, depending on which control specification is most

important to the designer. In addition, a probabilistic description of the uncertainty is also tackled. The major strength of this approach is that it allows to state (soft) specification in terms of probability of constraint violation; then a considerable increase of performance may be obtained with respect to a design based on (hard) worst-case specifications, even when considering small values of probability constraint violation.

The practical problem of (easily) obtaining plant models is acknowledged. A breakthrough in the problem of identifying for PID control design was the relay autotuner method. A novel autotuning method is presented through its application in an industrial in-line pH problem. Its most outstanding features are the short duration of the experiment and its ability to estimate and employ for synthesis an uncertainty model of the obtained parameters.

Resumen Extendido

Esta tesis presenta varios procedimientos para el diseño de sistemas de control realimentado, también conocidos como sistemas de control en lazo cerrado. Se considera el caso en el que la planta a controlar es modelada por un sistema lineal e invariante en el tiempo con una entrada y una salida. En particular, se estudian métodos de diseño en los que el controlador es de tipo proporcional integrador derivativo (PID) y en los que se considera de forma explícita un modelado de la incertidumbre sobre la dinámica de la planta que se quiere controlar. Este último punto es de crucial importancia, ya que en ausencia de incertidumbre no hay necesidad de utilizar realimentación, entendiendo como incertidumbre los siguientes puntos: inexactitudes en el modelado de la planta y perturbaciones no medibles que actúan sobre ella. En tales casos, un controlador en lazo abierto ofrecería una solución al problema de control, sin la necesidad de embeber a la planta en un sistema de control realimentado. También puede darse el caso en el que el efecto de la incertidumbre sea aceptable en relación con las especificaciones de control, en tales casos la realimentación tampoco sería estrictamente necesaria. La realimentación es peligrosa en el sentido de que esta puede provocar inestabilidades, por lo tanto su uso está solamente justificado por la necesidad de reducir el efecto de la incertidumbre por debajo de unos límites marcados por las especificaciones de control. Además, es importante tener en cuenta que el diseño de un sistema de control realimentado se puede interpretar como un juego de suma cero (en el mejor de los casos) para cualquier planta real. Esto se deduce de la integral de Bode (también llamada de Horowitz) sobre la sensibilidad.

Dicho lo cual, cualquier método general de diseño (o síntesis) de controladores realimentados, que aspire a ser útil en la práctica y no solo un elegante ejercicio matemático, deberá incluir algún tipo de modelado de la incertidumbre de la planta así como unas especificaciones de diseño. En líneas generales, se podría decir que la incertidumbre se puede modelar con un modelo con mayor o menor nivel de detalle (incertidumbre estructurada), o bien de una forma más laxa, imponiendo unos ciertos márgenes de estabilidad sobre un modelo nominal (incertidumbre no estructurada). Con

respecto a las especificaciones, a grandes rasgos un tipo de especificación razonable es que el sistema diseñado exhiba una cierta insensibilidad con respecto a variaciones en la dinámica de la planta, esta propiedad es denominada como robustez en la terminología de la teoría del control. En otras palabras, se desea que el comportamiento del sistema diseñado mantenga unas ciertas características, a pesar de posibles cambios en la planta física. Estos cambios pueden ser debidos al envejecimiento de componentes, a la existencia de distintos puntos de operación, a cambios en el entorno, etc.

El problema de diseño de un sistema de control es un problema rico que debe tener en cuenta varios aspectos, como por ejemplo, la atenuación de perturbaciones de carga, el seguimiento de referencias, el ruido de la medida y las variaciones en la dinámica de la planta. Dentro del abanico de técnicas desarrolladas para tratar estos problemas, un enfoque en el dominio de la frecuencia aporta las herramientas necesarias para abordar este problema de una forma relativamente sencilla y efectiva. Una desventaja de este enfoque es la imposibilidad de tratar el caso de parámetros variables en el tiempo, imponiendo necesariamente la asunción de parámetros inciertos pero constantes. En particular, esta tesis considera la Teoría de Control Cuantitativa (QFT por sus siglas en inglés) desarrollada principalmente por Isaac Horowitz, que extiende y generaliza conceptos previamente estudiados por Hendrik W. Bode. Esta técnica ha demostrado su solvencia mediante un gran número de casos de éxito en aplicaciones prácticas, así como su extensión tanto a sistemas multivariables, no lineales, o de parámetros distribuidos. Por otro lado, también se hace uso de la metodología del espacio de parámetros del controlador, cuyos orígenes se remontan al menos a finales siglo XIX, época en la que ya era usada por Ivan A. Vishnegradsky. A la hora de formular los problemas de diseño del controlador, estos se modelan en esta tesis como problemas de optimización con restricciones. La especificación más importante tomará el papel de función de coste a optimizar, mientras que las otras especificaciones se incluirán como restricciones. Una formulación extensivamente empleada aquí es la optimización del rechazo de perturbaciones sujeta a restricciones sobre la robustez y la amplificación del ruido. Actualmente existen métodos de optimización que permiten resolver estos problemas de forma relativamente fiable. Además, algunos problemas de optimización tienen una cierta estructura (por ejemplo, linealidad o convexidad) que les dota de unas ciertas bondades, que permiten su resolución de forma altamente eficiente. Hoy en día, la optimización lineal es considerada una tecnología, mientras que la optimización convexa está cerca de serlo.

A la hora de modelar la incertidumbre en el dominio de la frecuencia, el método predominante en la literatura sobre control robusto es mediante incertidumbre no

estructurada. El uso de este tipo de modelado de la incertidumbre supone un sacrificio en cuanto a exactitud a cambio de obtener un modelo más ameno matemáticamente. Este tipo de modelos permite obtener propiedades de estabilidad robusta mediante la aplicación de resultados basados en el Teorema de la Ganancia Pequeña. En contra, el uso de un modelado estructurado de la incertidumbre permite reducir el conservadurismo inherente al modelado no estructurado, con el coste de plantear un problema de diseño sustancialmente más complejo. Por ejemplo, el enfoque de los valores singulares estructurados (o análisis mu) requiere la resolución de problemas de complejidad computacional NP-complejo. La Teoría de Control Cuantitativa, calificada a veces como un método práctico o semiformal, ofrece un buen compromiso entre exactitud y complejidad del proceso de diseño.

Por otro lado, el hecho de considerar controladores tipo PID es debido a que este tipo de controladores es con una amplia diferencia el más usado en la práctica. En la mayoría de casos prácticos este controlador es capaz de ofrecer una solución satisfactoria al problema de control cuando las especificaciones no son demasiado exigentes. Diferentes estudios cifran en más del 95 % su presencia en sistemas de control industriales. También se indica que muchos de estos controladores no utilizan la acción derivativa, resultando en controladores tipo proporcional integrador (PI). Además, el predominio de este tipo de controlador no se ha visto amenazado por la irrupción en entornos industriales de otras técnicas de control denominadas como avanzadas. La única clase de tales técnicas que ha tenido una penetración significante en la industria es la representada por el control predictivo, también conocido con otros nombres como control predictivo basado en modelo o realimentación óptima en lazo abierto, por nombrar algunos. En la mayoría de casos, los controladores predictivos conviven en el mismo sistema de control que los controladores tipo PID, de modo que los controladores PID se encargan de los lazos de control a bajo nivel, mientras que un controlador predictivo se encarga de las interacciones entre distintos lazos a un nivel superior. Gran parte del éxito del control predictivo se debe a su habilidad para poder tratar de forma sistemática con interacciones y, en especial, con restricciones sobre la señal de control y la salida de la planta. Estas restricciones pueden estar motivadas por limitaciones físicas, de seguridad o medioambientales. Cabe destacar que en un gran número de casos, el desempeño global de un sistema de control que incluye un controlador predictivo estará supeditado a la existencia de unos controladores tipo PID debidamente ajustados. Además, se reconoce que una parte del éxito atribuido al control predictivo es debido realmente a los avances en las técnicas de diseño de controladores tipo PID.

A pesar de lo dicho sobre los controladores PID, el hecho de considerar una estructura relativamente sencilla como la de estos puede parecer una limitación importante. Cabe destacar que varios de los métodos de diseño presentados en esta tesis son también aplicados a estructuras de control más generales.

Una primera parte de los resultados presentados en esta tesis corresponde a métodos de diseño para ciertos tipos de modelos, que describen el comportamiento de gran parte de las dinámicas encontradas en procesos industriales. Los dos modelos que se consideran son: integrador con retardo temporal y primer orden con retardo temporal. En estos casos, el modelado de la incertidumbre se realiza usando un conjunto de plantas definido mediante incertidumbre paramétrica intervalar en cada uno de los parámetros que aparecen en estos modelos. El enfoque adoptado en estos dos casos es la identificación de un número reducido de plantas que permita llevar a cabo el diseño para el conjunto inicial, de la forma menos conservadora posible. En el primer caso se obtiene un método de diseño en forma de una regla de ajuste; y en el segundo, el problema inicial, que considera un conjunto infinito de plantas, se resuelve considerando una única planta instrumental de orden fraccionario. Esta planta representa en un cierto modo al conjunto de plantas inicialmente considerado.

Posteriormente se estudia el caso en el que el modelo de la planta a controlar está compuesto por una conjunto finito de respuestas en frecuencia. Cabe destacar que el rango de aplicación de este último modelo es bastante amplio. Por una parte, es posible obtener la respuesta en frecuencia de cualquier modelo lineal invariante en el tiempo. Por otra parte, experimentos de identificación entrada salida mediante el análisis de la respuesta en frecuencia son ampliamente usados en diversas ramas de ingeniería. Estas características hacen que este procedimiento de diseño sea adecuado para una gran variedad de problemas de control prácticos. Otra ventaja del método es el uso de algoritmos basados en optimización convexa. Esto hace que una vez que el problema de control ha sido debidamente formulado, su resolución sea prácticamente trivial y no requiera de supervisión alguna por parte del usuario. Este método permite el diseño de controladores PID con especificaciones tipo QFT de una forma más sencilla y considerablemente más rápida que las ofrecidas por métodos previos.

Otro enfoque tratado en esta tesis es el estudio de un modelado probabilístico de la incertidumbre. De este modo, un parámetro incierto pero perteneciente a un intervalo acotado, puede ser descrito como una variable aleatoria continua sujeta a una distribución de probabilidad uniforme. La mayor parte de las técnicas de diseño de controladores consideran un modelado determinista de la incertidumbre, ya sea estructurado o no estructurado. Un modelado determinista resulta inevitablemente en

especificaciones tipo peor caso, donde una cierta propiedad se garantiza para todo el conjunto de parámetros inciertos. Una crítica a este enfoque es que la probabilidad de que ocurra el escenario asociado al peor caso podría ser muy baja. Por contra, un modelado probabilístico permite plantear especificaciones más ricas, como por ejemplo, en términos de probabilidad de cumplimiento de una cierta propiedad. Este enfoque permite obtener controladores que alcancen un desempeño superior a los diseñados con técnicas deterministas, con el coste de incumplir las especificaciones de diseño con una probabilidad predefinida por el usuario y típicamente pequeña. En uno de los ejemplos presentados, el cual está basado en un modelo de un sistema de transmisión mecánica tomado de la literatura, se muestra como es posible triplicar el rendimiento con respecto al caso determinista a costa de permitir una violación de la especificación con una probabilidad de tan solo el 2 %.

Por último se presenta un nuevo método de sintonía automático de controladores PID mediante su aplicación a un problema de control de pH en línea en una planta industrial. Normalmente, la obtención de un modelo para su uso en el diseño de un controlador tipo PID puede ser una tarea costosa en términos económicos. Es por ello que los métodos de sintonía automática basados en un experimento tipo relé son muy populares en la industria de control de procesos, donde una industria típica podría contener cientos o incluso miles de lazos de control. El método presentado tiene como ventajas con respecto a métodos previos: una duración del experimento sustancialmente más corta, y la habilidad de identificar y emplear para el diseño del controlador un modelo probabilístico de la incertidumbre de los parámetros estimados.

Contents

List of Figures

List of Tables

Chapter 1

Introduction

1.1 Preliminaries

Feedback control is one of the great concepts developed (mostly) in the last century, it has had an utmost impact on the technological development of modern society. Among its wide range of applications are aerospace, automotive, industrial processes, robotic, renewable energy, etc. In particular, control engineering aims to design systems that interact with the plant to be controlled, making the plant to behave in a desired way[1]. The purpose of a control system is generally that the plant output follows a reference signal as well as possible, in spite of disturbances acting on the plant or uncertainty about the plant model. The control system or controller has then the role of computing a signal that is fed into the plant with the aim of achieving this goal. An everyday example of a control system is the cruise control system, typically encountered in most of the modern cars. It attempts to maintain the velocity of the car close to a given desired velocity, in spite of uncertain factors such as changes in the road slope, different wind conditions, and several road surface properties.

Control systems may operate in one of two different modes: open loop or closed loop, see Figure 1.1 where both modes are sketched. There are three signals: the reference input r, the controller output u, and the plant output y. In an open-loop control system, the output of the controller is obtained from the reference input, and possibly a measurable disturbance, using a mathematical model of the plant. This operation mode is very sensitive to inaccuracies in the plant model. It only works well when the effects of inaccuracies in the model of the plant and unknown external

[1]The word plant is generally used in control engineering to denote the combination of a process and actuator.

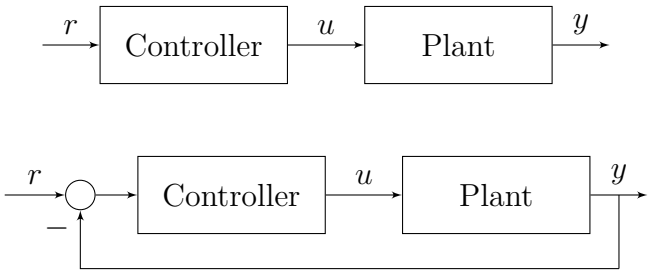

Figure 1.1 Open-loop (top) and closed-loop (bottom) control systems

disturbances acting on the plant are acceptable in relation to the desired specifications. Closed-loop control, also known as feedback control, attempts to overcome this caveat (sensitivity to uncertainty both in the model and in the disturbances) by measuring the output of the plant and using the error between the reference input and the measured output to generate the output of the controller.

The idea of feedback is at the core of control theory, it has interesting properties, such as making it possible to reduce the effect of unmeasured disturbances and uncertainty about the plant model. It is worth to point out that the only reason for using closed-loop control is because of uncertainty, both in the plant model and in the external disturbances acting on the plant [124]. In absence of these factors, more economical solutions can be adopted by means of open-loop control. On the other hand, its major drawback is that it may cause instability. An improper use of feedback may result in an unstable closed-loop system (a bounded input may generate an unbounded output), even when the plant to be controlled is stable (bounded inputs generate bounded outputs). In addition to the risk of instability, another limitations inherent to any feedback control system is due to the presence of the errors in the measuring signals (sensors have a certain accuracy), that inevitably imposes a lower bound on the error of the control system. Another issue is that high-frequency measurement noise causes actuator stress. These issues are generally disregarded in the control literature. There are some exceptions that to put emphasis on these issues, for example, [85, 125].

Let us consider the two-degrees-of-freedom (2-DOF) feedback control system of Figure 1.2. This system has three blocks corresponding to the plant P, the feedback controller C, and the feedforward controller F. There are three external signals: the reference input r, the load disturbance d, and the measurement noise n. Under the assumption that plant, controller, and prefilter are single-input-single-output (SISO) linear time-invariant (LTI) systems. The following equation, where the Laplace transform representation of these systems is used, relates the plant output with the

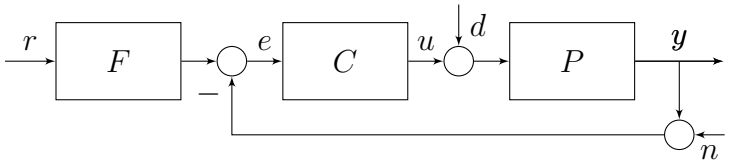

Figure 1.2 2-DOF feedback control system

external signals and serves to illustrate the properties of feedback[2]:

$$Y(s) = \frac{P(s)C(s)}{1+P(s)C(s)}F(s)R(s) + \frac{P(s)}{1+P(s)C(s)}D(s) - \frac{P(s)C(s)}{1+P(s)C(s)}N(s). \quad (1.1)$$

Assuming an ideal situation in which $N(s) = 0$, the desired output is practically achieved $Y(s) \approx F(s)R(s)$ if a controller with enough high gain is used, despite unknown disturbances and uncertainty about the plant model. The equation that relates the controller output with the external signals is

$$U(s) = \frac{C(s)}{1+P(s)C(s)}F(s)R(s) - \frac{C(s)P(s)}{1+P(s)C(s)}D(s) - \frac{C(s)}{1+P(s)C(s)}N(s). \quad (1.2)$$

It should be mentioned that the transfer functions[3] that appear in equations (1.1) and (1.2) have specific names [21]:

- Sensitivity function: $S(s) = \dfrac{1}{1+P(s)C(s)}$.
- Complementary sensitivity function: $T(s) = 1 - S(s) = \dfrac{P(s)C(s)}{1+P(s)C(s)}$.
- Load disturbance sensitivity function: $P(s)S(s) = \dfrac{P(s)}{1+P(s)C(s)}$.
- Noise sensitivity function: $C(s)S(s) = \dfrac{C(s)}{1+P(s)C(s)}$.

This group of equations is often called the *Gang of Four* [21]. Coming back to the situation where $N(s) \neq 0$, a controller with high gain may amplify and fed the measurement noise into the control signal, leading to undesirable effects [124]. Therefore, there is a trade-off between designing a controller that achieves sufficiently high gain for

[2]Lower- and upper-case versions of the same letter are used, the former denotes a time-domain signal and the latter denotes its Laplace transform.

[3]The transfer function of an LTI system is the Laplace transform of the output due to a unit impulse input; s is the complex variable.

obtaining a good performance and designing one with a sufficiently low gain in order to minimize the undesirable effects of the measurement noise and the risk of losing stability. As load disturbances typically have low frequencies and measurement noise has high frequencies, the loop transfer function $L(s) = P(s)C(s)$ should be designed with high gain at low frequencies and low gain at high frequencies[4]. Note that there are limitations imposed on LTI control systems by Bode's gain-phase relationship that states that gain and phase of an LTI system cannot be designed independently [42]. This constraint makes designing a control system a challenging problem. In addition to the previous requirements over the gain of the loop transfer function, the transfer function $L(s)$ should be shaped to have adequate stability margins, as gain and phase margins or peak of sensitivity functions. There are many aspects that have to be accounted for when designing a feedback control system, they can be summarized in the following points [19, 21]:

- the effect of load disturbance has to be reduced or minimized;
- the designed system has to be robust (at least maintain closed-loop stability) against plant model uncertainty;
- the amount of measurement noise fed into the plant should be limited or minimized;
- the output of the plant should follow the reference input.

From equations (1.1) and (1.2), it is clear that the role of the feedback controller C is to deal with the three first points. On the other hand, the prefilter F is in charge of the last one. Therefore, each one, the feedback controller and the prefilter, may be designed separately. A reasonable approach is to first design the feedback controller C for performance and robustness, and later the prefilter F to handle changes in the reference input.

Another important specifications are the constraints on the control signal and/or plant output, but this kind of specifications will not be treated in the present thesis. These constraints are present in any real control systems. Nevertheless, to the best of the author's knowledge, there is not a feedback control design method able to handle these constraints for continuous-time systems in a systematic manner[5].

[4]Performance of a control system will be poor in cases where frequency content of load disturbances and measurement noise are overlapped.

[5]The situation changes for discrete-time systems, in which several techniques can handle them, for example, Vertex control [113], Model Predictive Control [54, 170], and interpolation based techniques [196].

The number of degrees of freedom of a control system is defined as the number of closed-loop transfer functions that can be designed independently [125]. We have presented a 2-DOF control system, where it is assumed that the output of the plant and the reference are available to the control system. Therefore, closed-loop transfer functions from disturbance to output and reference to output can be designed independently. In 1-DOF control systems, $F(s)$ is restricted to be 1 since the control system only have available the error signal. The advantages of exploiting extra DOFs, when the corresponding signals are available to the control system, were presented by Horowitz [125]. Previously, a lot of development of feedback control was done on servomechanism [140], primarily for the radar problem, where only the error is available to the controller. After that, the feedback control academic community continues considering this constraint, even in cases where the output of the plant and the reference signals were available.

1.1.1 Introduction to PID Control

Taking into account the points discussed in the previous section, a good candidate for a feedback controller seems to be one that achieves high gain at low frequencies and low gain at high frequencies. A simple controller that meets these specifications is an integrator[6]. It has the following time and Laplace domain representations:

$$\begin{aligned} &\text{Time domain} \quad && u(t) = \int_0^t e(\tau)d\tau, \\ &\text{Laplace domain} \quad && U(s) = \frac{1}{s}E(s). \end{aligned} \tag{1.3}$$

Let us come back to the ideal situation in which $N(s) = 0$, an integrator as feedback controller achieves perfect reference tracking and disturbance rejection for constant references and disturbances in spite of plant model uncertainty, these facts follow from equation (1.1). In the time domain a similar analysis can be performed, if the output of an integrator is constant over an interval of time, then the input must be zero over the same interval. Now, assume that a system with constant references and disturbances inputs reaches steady state; then all signals, including integrator output reach constant steady-state values. This implies that the error (input of the integrator) is zero. Note that this property holds independently of

- the values of the constant references or disturbances,

[6]There is also some evidence that integral feedback appears in biological systems, where disturbance attenuation by integral feedback is usually known as perfect adaptation [242, 272].

- the initial conditions of the plant and controller,
- ignorance about the plant dynamics, and
- whether the plant and controller are linear or nonlinear.

The main drawback of using an integrator as feedback controller is that, in general, it makes the system less stable. Note that the integrator itself is not a stable system, for example, for a step input, a bounded signal, its output is a ramp, an unbounded signal. From a frequency domain perspective, the integrator has a constant phase lag of $\pi/2$ rad (or 90 degrees); then some elements that achieve phase lead are desirable[7]. A real zero is a simple element that is able to provide phase lead, its representation in the Laplace domain is given by the following transfer function:

$$\frac{s+a}{a}, \tag{1.4}$$

where a is a parameter. This transfer function corresponds to a zero at $s = -a$ and a gain equal to $1/a$ in order to have a steady-state gain equal to 1. The series combination of an integrator and a real zero (in addition to a gain factor) leads to a proportional-integral (PI) controller that is given by:

$$C_{\mathrm{PI}}(s) = k_p + \frac{k_i}{s}, \tag{1.5}$$

where k_p and k_i are the parameters of the controller, that are called proportional and integral gain, respectively. Although the phase lag of the controller (1.5) is $\pi/2$ rad at low frequencies, it is 0 rad at high frequencies. The frequency where the phase lag changes can be adjusted by tuning the parameters of the controller. In cases where more phase lead is necessary, another zero could be added in series leading to a proportional-integral-derivative (PID) controller

$$C_{\mathrm{PID}}(s) = k_p + \frac{k_i}{s} + k_d s, \tag{1.6}$$

where the new parameter k_d is the derivative gain. Note that transfer function (1.6) is not necessarily composed of an integrator and two real zeros, it could also be composed by an integrator (pole at the origin) and a pair of complex zeros. This

[7]Several nonlinear elements with the same gain characteristic of an integrator, but with less phase lag, in terms of the describing function approach, have been studied. See, for example, the Clegg Integrator (CI) [64], the split-path nonlinear (SPAN) filter [88], and an integrator with zero phase lag [150].

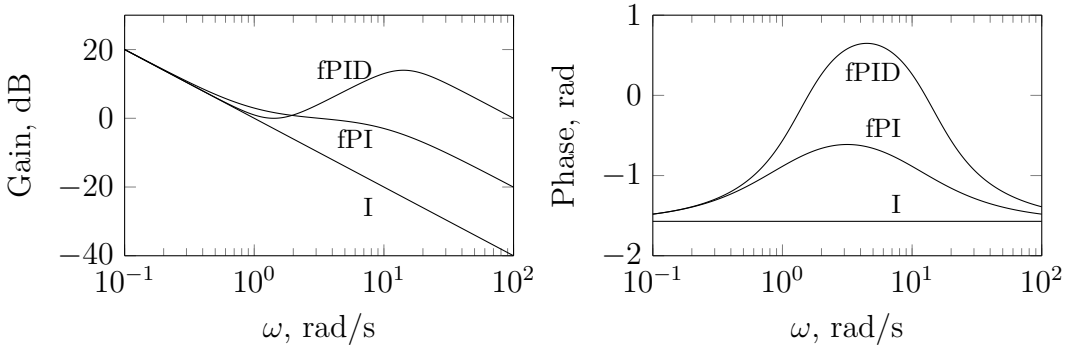

Figure 1.3 Bode plots for PID controllers

Bode plot for an integrator (I), a filtered PI (fPI), and a filtered PID (fPID).

ideal representation of the PID controller is not physically realizable (transfer function (1.6) is not proper when $k_d \neq 0$), but this issue is solved when a low-pass filter for noise measurement is added. Then, in order to guarantee amplitude roll-off at high frequencies, the feedback controller is usually combined in series with a measurement filter, that may be a first-order filter for a PI controller as

$$G_{\text{PI}}(s) = \frac{1}{T_f s + 1}, \tag{1.7}$$

or a second-order filter for a PID controller

$$G_{\text{PID}}(s) = \frac{1}{T_f^2 s^2/2 + T_f s + 1}. \tag{1.8}$$

This second-order filter has two complex poles with the smallest damping ratio for which there is no amplitude amplification. Other filter structures are possible [115], but this choice keeps the number of parameters as low as possible. Figure 1.3 shows an example of Bode plot of an integrator (I), a filtered PI (fPI), and a filtered PID (fPID).

Regarding the prefilter F, although the benefits of using a 2-DOF control structure was early emphasized by Horowitz [124, 125] at the end of the 1950s, this approach did not appear in the academic control community until the mid-1980s[8] [11, 84]. In PID control a common form of obtaining a simple control structure with 2 DOF is by means of set-point weighting, that consists in obtaining the error that enters into the

[8]Before this time, some industrial implementations of PID controllers applied derivative action only to the output of the plant. This is a simple implementation of a 2-DOF control structure.

proportional part as

$$e_p(t) = br(t) - y(t), \tag{1.9}$$

and the error that enters into the derivative part as

$$e_d(t) = cr(t) - y(t). \tag{1.10}$$

The use of set-point weighting corresponds to the following structure of the prefilter $F(s)$ (see [22]):

$$F_{\mathrm{SPW}}(s) = \frac{ck_d s^2 + bk_p s + k_i}{k_d s^2 + k_p s + k_i}, \tag{1.11}$$

where the parameters b and c are called set-point weights.

The PID controller, also known as the three-term controller, provides feedback using a relatively simple control structure, but despite its simplicity, it offers a very efficient solution to many real-world control problems. As it was presented before, the integral action provides very desirable properties while proportional action, and possibly derivative action, may improve the performance and robustness levels. Even with the advent of more advanced control techniques, the PID controller is by far the most used form of feedback in industry [17]. In fact, it has been the first and only controller to be mass produced for the market existing in the process industry [144]. One of the few advanced control techniques that has gained popularity in the industry is model predictive control (MPC), and it is common to use this technique in combination with PID control, in a way that the PID controllers are used in the lowest levels while a multivariable MPC controller provides the references [17]. According to a survey of over eleven thousand controllers in continuous process industries (among others refining, chemicals, and pulp and paper industries), the PID controller was used 97 % of the time [72]. Most of them are in fact PI controllers because derivative term is regarded as difficult to tune. Similar figures hold in the motion control and aerospace industries [231]. In addition, this type of controllers is also found in many devices used in everyday life, such as cruise control for cars, CD and DVD players, and mobiles phones. Therefore, due to its widespread use, any improvement in its design has the potential to have a significant engineering and economic impact. Aside from engineering, PID control also appears in areas like biology [21], or even, economy [102, 121].

The development of PID control traces back to at least 250 years [34–36]. Some of the milestones in its development are enlisted as follows:

- End of the eighteenth century. Windmills were operated at a constant speed by using centrifugal governors. In 1788, James Watt adapted it to the steam engine. Originally they provided proportional action, but the Périer brothers introduced the integral action around 1790. Later, the Siemens brothers, who also proposed an alternative implementation of integral action, proposed derivative action based on an inertial wheel [20].

- 1911. Elmer A. Sperry developed an automatic ship-steering mechanism that incorporated PID control and automatic gain adjustment to adapt to different sea conditions [215]. This device was designed to behave like an experienced helmsman. The U.S. Navy adopted it, remaining in use through World War II.

- 1939. Taylor Instrument Companies and Foxboro Instrument Company added a control action proportional to the derivative of the error signal (it was referred as "pre-act" by the first and "hyper-reset" by the latter) to previous commercial pneumatic controllers, that already had proportional and integral actions [34].

- 1942. John G. Ziegler and Nathaniel B. Nichols, employees of the Taylor Instrument Companies, published a method for obtaining the gains of a PID controller [280], this method was the result of empirical investigations.

- 1984. Karl J. Åström and Tore Hägglund proposed the relay autotuning method [14], that makes possible to tune a PID controller with no prior information of the process by performing a relatively short experiment. Computer implementations of PID controllers allow to incorporate this kind of functionalities.

1.1.2 Bibliometrics Analysis

The topic of PID control has attracted a great interest among the academic control community over the last decades. A considerable amount of books mainly focused on PID control have been published, particularly in the last decade, see the following books [7, 15, 16, 19, 43, 63, 67, 144, 201, 205, 232, 244, 245, 254, 255, 259, 275]. This topic has a tremendous impact on the scientific community, Table 1.1 shows some bibliometric figures retrieved from Scopus[9] when searching for *"PID control" OR "PID controller" OR "PID compensator"* in the article *title, abstract or keywords*. It is important to highlight that all the documents that appear in Table 1.1 are not mainly focused on PID control, but the presence of these words in the title, abstract

[9]Data retrieved 22 February 2017.

Table 1.1 Bibliometric figures about the presence of PID control on Scopus

Number of publications	26291
h-index	107
Publications per subject area	1) Engineering 20084
	2) Computer Science 9226
	3) Mathematics 3433
	4) Physics and Astronomy 1809
	5) Energy 1676
Publications per country/territory	1) China 10196
	2) United States 2183
	3) India 1956
	4) Japan 1293
	5) Taiwan 851
Publications per cites	1) Relay autotuning [14]
	2) Simple Internal Model Control [233]
	3) Particle Swarm Optimization [94]
	4) Internal Model Control [214]
	5) Analysis, Design, and Technology [9]

or keywords indicates some influence of the topic on them. The h-index of this group of documents is 110.

1.2 Motivation and Objectives

1.2.1 History of Feedback Control

Since the invention of the Watt's governor in 1788, the desire of obtaining control systems designed to work well under different operation points and external environment conditions, among other factors, has been implicit. These properties lead to the concept of robustness, that can be understood, as a "quantitative tolerance of large modeling uncertainties" [221]. Originally, it was clear that the main purpose of a feedback

control system was to cope with plant uncertainty. A central problem in the dawn of the telephone industry around the 1920s was to design amplifiers whose properties remain constant in spite of variations in supply voltage and component variations, this problem was solved by Harold S. Black by inventing the negative feedback amplifier [40]. Around these years, the well-known Nyquist criterion to determine the stability of feedback system in terms of its loop transfer function was developed in [200]. Hendrik W. Bode had designed feedback control systems for amplifiers that were robust to variations in the gain [42] and he had also used complex variable theory to prove that there are fundamental limitations in the design of feedback systems [223]. This may be considered the first systematic research in feedback theory. Isaac M. Horowitz extended the Bode's robust design to more general process variations resulting in a technique called Quantitative Feedback Theory (QFT) [125, 129]. This technique is regarded as the first mathematical formulation of a robust feedback control problem [221], although Horowitz did not use the word robust.

The significance of the Horowitz's works was unnoticed by the academic control community during the following decades. Most of the theory developed in these years considered a nominal model of the plant (that was assumed to be sufficiently accurate) ignoring the key problem of the uncertainty. During the period of time between 1960 and 1975, state-space and optimal control theories were developed. The Linear Quadratic Regulator (LQR) was developed in [8], it has very good robustness properties in terms of classic stability margins (infinite gain margin and 60 degrees of phase margin) over a nominal plant [148, 222]. In addition to the robustness property, this technique has the advantages of being well suited to numerical computations and extending well to the multivariable case. However, it leads to difficult implementations in which a constant gain controller is needed for each state. There was an extension of the LQR to the case of output feedback called Linear Quadratic Gaussian (LQG) controller, relying on the use of a Kalman-Bucy filter as a state observer. The separation principle states that the problem can be split into the design of an optimal observer and the design of an optimal controller. The robustness properties of the LQG controller were object of study, that culminated with the publication of a simple counterexample by John C. Doyle in a paper entitled "Guaranteed Margins for LQG Regulators" with possibly one of the shortest abstract "There are none" [76]. Some criticisms of these techniques had been reported earlier in [217], this work shows that these optimal control techniques have properties that cannot be achieved in most of real systems and also some highly undesirable properties. By this time, there was also criticism of the state-space theory in favor of frequency domain methods [132].

At the end of the 1970's, the analysis of robust stability became an emerging topic due to the publication of the Kharitonov Theorem [155]. This theorem states that the stability of an interval family of polynomials is equivalent to the stability of four elements of this family. This fact is independent of the degree of the polynomials. An extension of this result for the case where coefficients of the polynomials are affine functions of the uncertain parameters is presented in [33], it is known as the Edge Theorem. Extension of the latter to time-delay systems was published in [93].

Some progress was also made in the study of multivariable systems in the frequency domain during these years. The parameterization of stabilizing controller for a given plant was presented in [157, 273, 274]. The Nyquist stability criterion was generalized to multivariable systems in [168].

The drawbacks of optimal control methods and the advances on multivariable systems in the frequency domain motivate the development of a new wave of robust control methods. In the early 1980s, George Zames published a work [277] that laid the foundation for $\mathcal{H}_\infty$ control. This seminal work on $\mathcal{H}_\infty$ control was strongly motivated by Horowitz [86], Zames wrote on it: "Many of the ideas in this paper are foreshadowed by ... Horowitz ... who derived various limits on sensitivity imposed by the plant, and stressed the need to consider plant uncertainty in design". Further developments in $\mathcal{H}_\infty$ were done in [80, 278]. A brief historical review of $\mathcal{H}_\infty$ control can be found in [279]. The development of $\mathcal{H}_\infty$ control brought robustness to the forefront with techniques that also can be generalized to multivariable systems. As in LQR/LQG techniques, the control problem is expressed as a mathematical optimization problem, and the method yields the controller that solves the problem. Some caveats of this technique are that the approach to model uncertainty is generally by using conservative unstructured uncertainty and that $\mathcal{H}_\infty$ synthesis usually leads to high-order controllers. The problem becomes harder to solve when structural constraints on the controller are considered, in this case, the problem is not longer convex [139]. These methods can be used for structured uncertainty leading to the structured singular value framework [77]. Synthesis procedure for this method (D-K iterations) was proposed in [78, 220] and combines μ analysis and $\mathcal{H}_\infty$ synthesis in an iterative procedure. There are some drawbacks that limit the applicability of this method: calculation of structured singular value (also known as μ) is approximated by its upper bound and there is not guarantee for the convergence of the D-K iterations.

During the 1990s, there were several pessimistic results concerning the computational complexity of several algorithms used for analysis and synthesis of robust controllers [41, 194, 211]. These facts fueled a growing interest in using randomized algorithms

(RAs) for analysis and synthesis of control systems, see [246] for an overview of these techniques. In addition, from a more practical point of view, the usual approach for modeling uncertainty as unknown-but-bounded parameters, that leads to worst-case (hard) specifications, may result in conservative designs. The assignation of a probability density function to the uncertain parameters allows to consider probabilistic (soft) specifications, with designs that are expected to be less conservative than their deterministic counterpart.

1.2.2 Motivation

The brief exposition of the evolution of feedback control design methods, done in the previous section, serves as motivation for the desirable features that any practical control design method should exhibit. Some common characteristics of the several methods presented in this thesis are enlisted below:

- a structured model of the uncertainty is taken into account in the design stage;
- the approach to control SISO plants is restricted to output feedback;
- control design problems are cast as optimization problems;
- fixed controller structures are considered.

The design methods presented in this thesis range from a tuning rule for a simple parametric model with uncertainty to a convex-based optimization method for a family of plants given by frequency response data. Low-order controllers, such as PID, are considered, but many of the presented methods are extendable to more complex controller structures. In some cases, the extension to other controller structures is sketched in the application examples.

1.2.3 Objectives

Our target in this thesis is to obtain advances in the field of robust PID control. The general objectives of the thesis are exposed as follows.

Design Methods for Target Plant Models in the Process Industry

Most of the dynamics encountered in the process industry are relatively well modeled by either an integrating time-delay (ITD) or a first-order time-delay (FOTD) plant model. A wide variety of PID tuning rules and simple design methods has been

proposed for these plant models (see [201]). Nevertheless, almost all of them are developed for some nominal parameters of the plant model. There is no need to say that a desirable property that makes a method attractive for its use in industry is its simplicity. Therefore, it is necessary to find a compromise between simplicity and accuracy. An important issue in designing feedback control systems is to consider the ignorance about the plant model. In this context, one of the objectives of this thesis is to develop tuning rules or simple design methods able to account for the uncertainty of these models.

Design Methods for Nonparametric Plant Models

A very general method to model an uncertain plant is by means of a collection of frequency response data. For example, any LTI model can be transformed into a frequency response, and input/output identification experiments deliver a model in form of a frequency response. There are some methods able to deal with this kind of models, but almost all of them include some steps that require of user intervention. This issue may limit the applicability of such methods. A main objective of this thesis is to devise a PID design method that overcomes this caveat, or at least, one that requires a minimal user intervention.

Design Methods for Plant Models with Probabilistic Uncertainties

Robust control design methods generally consider a deterministic model of the uncertainty, guaranteeing some specifications for all the possible cases [209]. It is natural to claim that such approach may be quite conservative, since the occurrence of the worst-case scenario may be very unlikely. One of the aims of this thesis is to develop PID design method able to deal with models with a probabilistic parameterization.

Autotuning of PID Controllers

An important milestone in the history of PID control is the development of the relay autotuning method. A multitude of variants have been presented since its conception. Unfortunately, the issue of uncertainty, both in identification and synthesis, has not received much attention. In this context, another objective is to obtain a robust version of the relay autotuner method. It is considered its application to an industrial in-line pH control system.

1.3 List of Publications

Most of the results exposed in this thesis have been published (or submitted) to several peer-review conferences and journals [177–181, 185, 186, 238, 239]. In this section, we provide the list of publications:

- Mercader, P., Baños, A., Vilanova, R.: "Robust PID design for processes with interval parametric uncertainty". *IET Control Theory & Applications*, doi: 10.1049/iet-cta.2016.1239, 2017.

- Mercader, P., Baños, A.: "A PI tuning rule for integrating plus dead time processes with parametric uncertainty". *ISA Transactions*, doi: 10.1016/j.isatra.2017.01.025, 2017.

- Soltesz, K., Mercader, P., Baños, A.: "An automatic tuner with short experiment and probabilistic plant parametrization". *International Journal of Robust and Nonlinear Control*, doi: 10.1002/rnc.3640, 2016.

- Mercader, P., Åström, K. J., Baños, A., Hägglund, T.: "Robust PID design based on QFT and convex-concave optimization". *IEEE Transactions on Control Systems Technology*, doi: 10.1109/TCST.2016.2562581, 2017.

- Mercader, P., Soltesz, K., Baños, A.: "Autotuning of an in-line pH control system", *21st IEEE International Conference on Emerging Technologies and Factory Automation*, Berlin, Germany, 2016.

- Mercader, P., Soltesz, K., Baños, A.: "PID synthesis under probabilistic parametric uncertainty", *American Control Conference*, Boston, USA, 2016.

- Soltesz, K., Mercader, P.: "Identification for control of biomedical systems using a very short experiment", *International Conference on Systems in Medicine and Biology*, Kharagpur, India, 2016.

- Mercader, P., Baños, A.: "Robust PI compensator design for FOPDT systems with large uncertainty", *14th International Conference on Control, Automation and Systems*, Seoul, Korea, 2014.

- Mercader, P., Baños, A.: "Tuning of PI compensators for integrating systems with large parametric uncertainty", *19th IEEE International Conference on Emerging Technologies and Factory Automation*, Barcelona, Spain, 2014.

Below a list of additional publications, that have been submitted and are currently under review, is provided:

- Mercader, P., Soltesz, K., Baños, A.: "Robust PID design by chance-constrained optimization" (Submitted to journal).
- Rubin, D., Mercader, P., Nguyen, H.-N., Gutman, P.-O., Baños, A.: "Improvements on interpolation techniques based on linear programming for constrained control" (Submitted to conference).
- Mercader, P., Carrasco, J., Baños, A.: "IQC stability analysis of time-delay reset control systems" (Submitted to journal).

Finally, a list of publications obtained during the PhD studies of the author [182–184], whose results are not presented in the thesis, is given:

- Mercader, P., Davó, M. A., Baños, A.: "Performance analysis of PI and PI+CI compensation for an IPDT process", *23rd Mediterranean Conference on Control and Automation*, Torremolinos, Spain, 2015.
- Mercader, P., Carrasco, J., Baños, A.: "IQC Analysis for time-delay reset control systems with first order reset elements", *52nd IEEE Conference on Decision and Control*, Florence, Italy, 2013.
- Mercader, P., Davó, M. A., Baños, A.: "$\mathcal{H}_\infty/\mathcal{H}_2$ analysis for time-delay reset control systems", *3rd International Conference on Systems and Control*, Algiers, Algeria, 2013.

1.4 Overview of Contents

This thesis is organized as follows:

- Chapter 2 is devoted to provide a background in feedback control. After a general introduction, QFT and PID control are treated with more detail.
- Chapter 3 tackles the problem of designing a PI controller for an ITD plant model, in presence of interval parametric uncertainty. The design is based on optimization of load disturbance rejection with constraints on the magnitude of the sensitivity and complementary sensitivity functions, but instead of solving this problem with a brute force approach (grid the uncertainty set), we prove

that this problem can be solved by considering only two plants. That lets us to obtain a tuning rule after using some approximations. The proposed tuning rule is applied to some examples.

- Chapter 4 studies the design of PID controllers, with a second-order measurement filter, for FOTD plant models containing interval parametric uncertainty. The control design problem is posed as an optimization problem where performance is maximized subject to some stability margins over a family of transfer functions. We derive conditions that allow to obtain a solution to the resulting robust optimization problem by solving a nominal optimization problem. This simplification is made by introducing an instrumental fractional-order plant that characterizes the uncertain (interval) process and stating certain conditions over the fractional-order loop transfer function. The design approach is also applied to a Smith-Predictor (SP) based Dead-Time Compensator (DTC).

- Chapter 5 presents an automatic loop shaping (ALS) method for designing PID controllers. Criteria for load disturbance attenuation, measurement noise injection, set-point response, and robustness to plant uncertainty are given. One criterion is chosen to be optimized with the remaining ones as constraints. Two cases are considered: M-constrained integral gain optimization (MIGO) and minimization of the cost of feedback according to QFT. Optimization is performed using the convex-concave procedure (CCP). The method, that relies on solving a sequence of convex optimization problems, converges to a local minimum or a saddle point. The proposed method is illustrated by examples.

- Chapter 6 presents a method for synthesizing PID controllers for process models with probabilistic parametric uncertainty. The proposed method constitutes a stochastic extension to the well-studied MIGO approach. The underlying optimization problem is solved using a gradient-based algorithm once the stochastic objective and constraints have been approximated by deterministic ones. The approximated solution is then probabilistically verified using RAs. The proposed method is demonstrated through several realistic synthesis examples.

- Chapter 7 presents a novel autotuning procedure and its application to an industrial in-line pH control system. The procedure has three advantages over classical relay autotuners: experiment duration is very short (no need for limit-cycle convergence); all data is used for identification (instead of only peaks and

switch instances); a parameter uncertainty model is identified and utilized for robust controller synthesis.

- Chapter 8 summarizes the contributions of the thesis and presents some potential future works.

Chapter 2

Background

This chapter provides a general introduction to some concepts that will be used throught this thesis. Firstly, an overview of feedback control is given. After that, QFT and PID control are presented. These two topics are extensively used throughout this thesis.

2.1 Overview of Feedback Control

This section presents fundamental concepts of feedback control, such as closed-loop stability, relative stability, performance, trade-offs, and limitations of feedback control systems. These issues will be developed in the following sections. A deeper treatment of them can be found in [21, 101, 228].

2.1.1 Closed-Loop Stability

As it has been already mentioned in the first chapter, closed-loop stability is a crucial issue in a feedback control system. The reason is that feedback may cause instability when applied to any practical plant. We say that a system is stable if any bounded input produces a bounded output for all bounded initial conditions. That implies that the poles a transfer function representing an LTI model have to be in the open left half plane (OLHP) of the complex plane [101]. The next theorem states a stability condition of a closed-loop transfer function in terms of the loop transfer function.

Theorem 2.1 (Nyquist Criterion)**.** *Consider a closed-loop system with the loop transfer function $L(s)$ having P poles in the region enclosed by the Nyquist contour, this contour consists of the imaginary axis and a semicircle of arbitrary large radius in the right half-plane (RHP). Let N be the net number of clockwise encirclements of -1 by $L(s)$*

when s encircles the Nyquist contour Γ in the clockwise direction. The closed-loop system then has $Z = N + P$ poles in the RHP.

The image of $L(s)$ under the Nyquist contour, that is known as Nyquist plot, is usually reduced to the image of $L(s)$ under the positive imaginary axis, since the contour at infinity maps to 0 in the case of strictly proper transfer function[1] and the plot corresponding to the negative imaginary axis is the mirror of its positive counterpart.

This stability criterion has some great advantages. Some methods to analyze the stability of a closed-loop system, as by means of Lyapunov functions, only provides whether the system is stable or not. This criterion also provides information on how the controller has to be modified in order to obtain a stable closed-loop system, or a system with a desired stability margin, that is a measure of how close is the Nyquist plot to the critical point. More precisely, it makes possible to perform a loop shaping of the loop transfer function to obtain a closed-loop system with some desired characteristics.

The presence of a delay element in the feedback loop is very common in control practice, in these cases neither the latter criterion nor the Hurwitz stability criterion are applicable, both criteria assume that the plant is described by rational transfer functions. A popular method in these cases is to approximate the delay element by a rational approximation, but it is well-known that this approximation may lead to wrong conclusions [230]. Fortunately, the Nyquist criterion is also extendable to transfer function with time delay by means of the generalized Nyquist criterion developed by Yakov Tsypkin in 1946[2], that extends the Nyquist criterion to systems with time delay.

The Nyquist criterion can be reformulated in the Nichols plane instead of the complex plane. The Nichols plane displays gain in decibel (dB), i.e. $20 \log_{10} |\cdot|$, versus phase in radian (rad)[3]. The reformulation of the Nyquist criterion in the Nichols plane is based on the fact that counting the number of encirclements in the complex plane can be done by counting crossings instead of encirclements [253]. By defining a ray $R_0^p = (-\infty, -1)$, a crossing occurs when the Nyquist plot intersects the ray R_0^p. The crossing is positive if the direction of the plot is upward, and negative otherwise, see Figure 2.1. This reformulation in the Nichols plane is done by counting the net number of crossings of the Nichols plot [65], that is the Nyquist plot represented in the Nichols

[1] A transfer function where the degree of the numerator is less than the degree of the denominator.

[2] The original article was published in Russian, but a translation to English is included in the compilation of articles [248].

[3] The use of the degree as unit of the phase (angle) is more common in the control literature, but the author prefers to use the radian. It is the standard unit of angular measure.

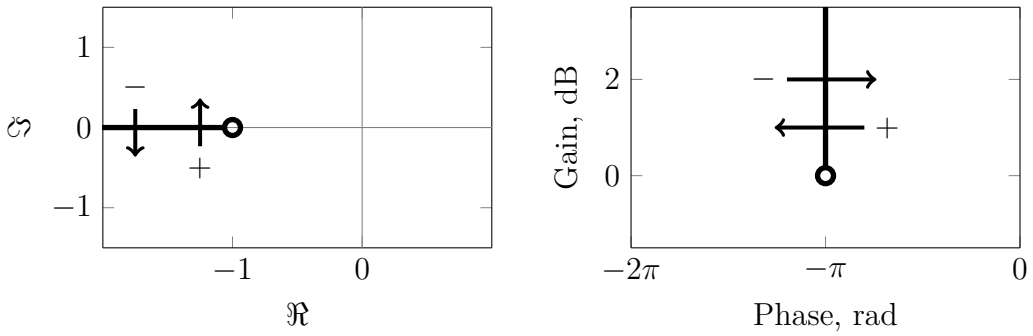

Figure 2.1 Crossing in the complex plane (left) and Nichols plane (right)

plane, with the family of rays

$$R_0^k = \left\{ [\phi \ r]^\top : \phi = (2k+1)\pi \text{ rad}, r > 0 \text{ dB}, k \in \mathbb{Z} \right\}, \tag{2.1}$$

with the left direction being positive and right direction being negative, see Figure 2.1. As we have already commented, it is common to use only half of the Nyquist plot due to symmetry properties (only nonnegative frequencies are considered). In such cases, each crossing of the half plot has to be counted twice. Special attention is required for crossings corresponding to $\omega = 0$ and infinite gain of the loop transfer function [95].

Example 2.1. This example aims to illustrate the convenience of using the Nyquist criterion in the Nichols plane instead of using it in the complex plane. Let us consider the following loop transfer function:

$$L(s) = 150 \frac{(1 + 0.94s + (0.67s)^2)(1 - 0.14s + (0.1s)^2)}{s(1+4s)^2(1 + 0.01s + (0.02s)^2)} e^{-0.01s}. \tag{2.2}$$

This loop transfer function has no RHP poles, therefore the closed-loop system will be stable if net number of encirclements of -1 by the Nyquist plot is zero, or equivalently, if the net number of crossings of the Nichols plot with the family of rays R_0^k is zero. Figure 2.2 shows the Nyquist plot (top) and the Nichols plot (bottom). The dashed line in the Nyquist plot corresponds to negative frequencies. On the other hand, the solid line in Nyquist and Nichols plots corresponds to nonnegative frequencies. Note that to perform a stability analysis using the Nyquist plot it is necessary to explore in different scales and the counting of encirclements may be messy. The counting of crossing is more clear, but it is also necessary to explore in different scales. Whereas, the situation is more clear when the Nichols plot is used. In this case, the closed-loop system is

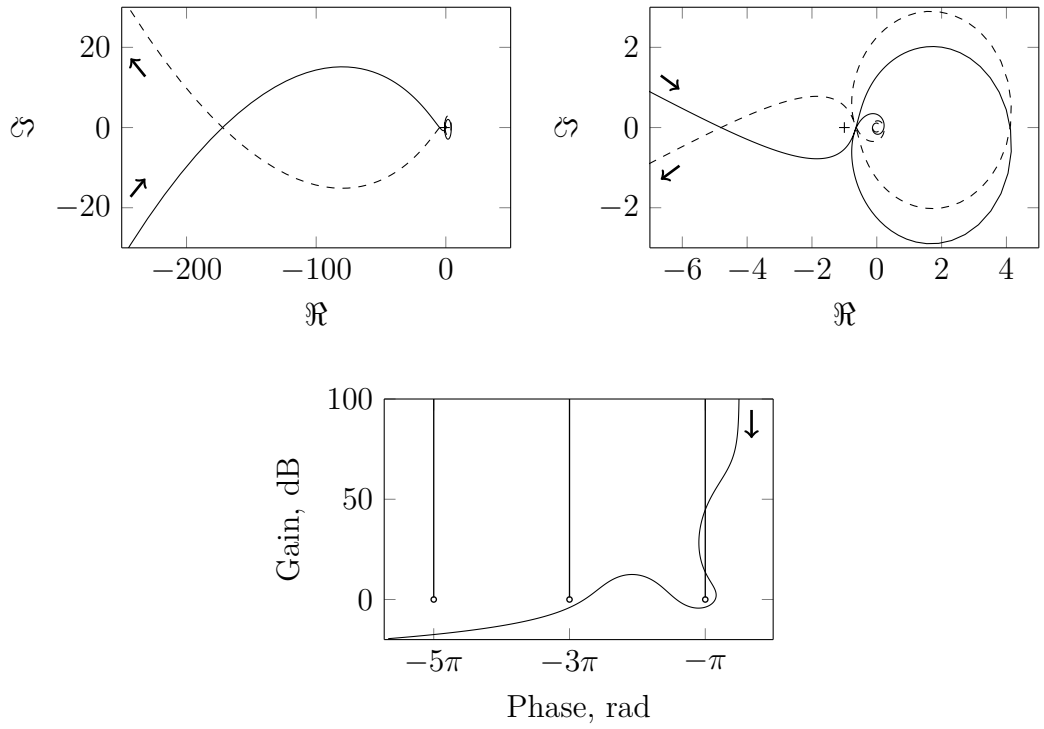

Figure 2.2 Nyquist plot (top) and Nichols plot (bottom) (Example 2.1)

stable, but we can easily deduce from the Nichols plot that small modifications of the gain of the loop transfer function may induce instability.

Besides the absence of RHP zeros in the transfer function $1 + L(s)$, there are more points that deserve attention when considering closed-loop stability. The presence of pole-zero cancellations in the closed RHP between $P(s)$ and $C(s)$ leads to unstable behaviors. This fact motivates the notion of internal stability, a feedback system is said to be internally stable if each of the transfer functions $T(s)$, $S(s)$, $P(s)S(s)$, and $C(s)S(s)$ are stable. Here, we are assuming that $F(s)$ is stable, otherwise the feedback system would be unstable. The following theorem can be found, e.g., in [79, 101].

Theorem 2.2. *A feedback control system is internally stable if and only if*

- *The transfer function* $1 + L(s)$ *has no RHP zeros.*
- *There are no pole-zero cancellations in the closed RHP between* $P(s)$ *and* $C(s)$*.*

Finally, a major limitation of the Nyquist criterion is that it is only applicable to LTI systems. An approximated extension exists in the case of feedback systems formed by a linear system and a static nonlinearity, that is known as describing function

analysis [99, 252]. It is based on considering the first harmonic of the output of the nonlinearity, neglecting the higher harmonics when the input of the nonlinearity is a sinusoidal signal; this analysis assumes a low-pass behavior of the linear system. The errors introduced by the approximation can be bounded for the case of slope-bounded single-valued nonlinearities [175].

2.1.2 Relative Stability

First of all, when designing a feedback controller, it is of utmost importance to guarantee closed-loop stability. While feedback controllers with sufficiently high gain immunize the closed-loop system against plant model uncertainties and unknown disturbances, these controllers have a destabilizing effect on any practical plant. However, plain stability is not sufficient, e.g. a stable closed-loop system may have a quasi-infinite settling time or a small variation in a parameter may lead to instability. Therefore, it is essential to consider any stability margin. They indicate how close the Nyquist plot is to the critical point -1. Classical stability margins are the gain and phase margins, which indicate how much gain can be added and how much phase can be subtracted, respectively, to the loop transfer function without the closed-loop system becoming unstable. They are introduced as follows.

Gain and phase margins. Let us denote by *phase crossover frequency* ω_{pc} the frequency where the phase lag of the loop transfer function $L(s)$ is equal to π rad, then the *gain margin* g_m is given by

$$g_m = \frac{1}{|L(j\omega_{pc})|}. \tag{2.3}$$

On the other hand, let us denote by *gain crossover frequency* ω_{gc} the frequency where the loop transfer function $L(s)$ has unit magnitude, then the *phase margin* φ_m is expressed as

$$\varphi_m = \pi + \arg L(j\omega_{gc}). \tag{2.4}$$

Sensible values for the gain and phase margins are in the intervals $6 - 14$ dB (or $2 - 5$) and $0.5 - 1$ rad (or $30 - 60$ degrees), respectively [19]. Figure 2.3 shows the gain and phase margins for a certain system in the complex plane and Nichols plane, note that they are easily calculable in the Nichols plane. These margins have been defined for the case when the Nyquist plot only intersects the unit circle and the negative real axis once, for multiple intersections (i.e. loop transfer functions with several phase

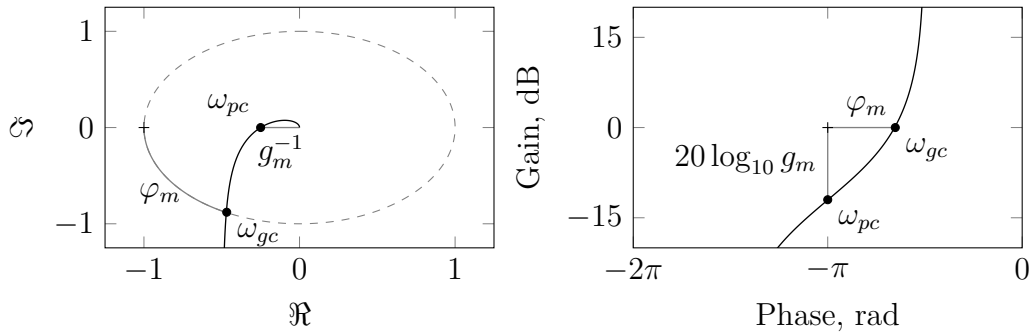

Figure 2.3 Classical stability margins

Gain margin g_m and phase margin φ_m in the complex plane (left) and Nichols plane (right).

crossover and/or gain crossover frequencies) it is necessary to consider the closest to the critical point.

These classical measures of robustness do not capture what happens if the gain and phase vary simultaneously. Stronger stability margins, that capture this behavior, are the maximum of the sensitivity and complementary sensitivity, they are defined below.

Sensitivity. The value of $|S(j\omega)|^{-1} = |1 + L(j\omega)|$ is equal to the distance from the point on the Nyquist curve (corresponding to frequency ω) to the critical point -1. Then, the maximum of the sensitivity (i.e. $\|S\|_\infty$) is equal to the inverse of the smallest distance to the critical point. Desirable values for $\|S\|_\infty$ are in the range $1.2 - 2$ (as indicated in the reference [19]). Constraints on the magnitude of the sensitivity transfer function have a graphical interpretation in the complex plane, they are represented by circles centered in -1 and radius equal to δ^{-1}, where δ is the value of the constraint, i.e. $\|S\|_\infty \leq \delta$. These circles are mapped into the Nichols plane as closed regions, that contain the critical point for values greater than 1 (or 0 dB). These circles in the complex plane (or closed regions in the Nichols plane) impose forbidden regions to the Nyquist plot (or Nichols plot). They are called *inverse M-circles*, where M is a positive real number indicating the value of the specification. In the Nichols plane, they are distorted into noncircular shapes.

Figure 2.4 shows these regions in the complex plane (left) and Nichols plane (right) for the values 1, 1.26, and 2; or equivalently 0, 2, and 6 dB. Furthermore, a constraint over the peak of the sensitivity function magnitude also guarantees closed-loop stability in presence of a static nonlinearity f in the loop satisfying [19] the following condition

$$\frac{\|S\|_\infty}{\|S\|_\infty + 1} < \frac{f(\alpha)}{\alpha} < \frac{\|S\|_\infty}{\|S\|_\infty - 1}. \tag{2.5}$$

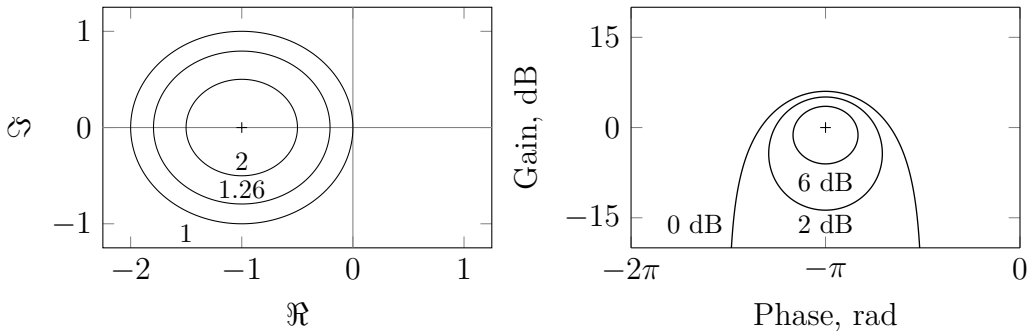

Figure 2.4 Inverse M-circles in the complex plane and Nichols plane

Constraints over the magnitude of the sensitivity in the complex plane (left) and Nichols plane (right).

A reasonable assumption is that actuator nonlinearities may be modeled by a static nonlinearity confined to a conic sector[4].

Complementary sensitivity. The complementary sensitivity as robustness measure indicates how large additive uncertainty can be added to the plant before losing stability. If the plant model changes from $P(s)$ to $P(s)+\Delta P(s)$ being $\Delta P(s)$ stable, a condition for stability is

$$\left|\frac{\Delta P(j\omega)}{P(j\omega)}\right| < \left|\frac{1}{T(j\omega)}\right|, \quad \forall\omega \geq 0. \tag{2.6}$$

Then, $\|T\|_\infty$ is clearly another robustness measure, whose desirable values are in the same range as $\|S\|_\infty$.

Constraints on the maximum peak of magnitude of the complementary sensitivity transfer function also have a graphical interpretation in the complex plane, they are represented by circles of center

$$-\frac{\delta^2}{\delta^2-1}, \tag{2.7}$$

and radius equal to

$$\frac{\delta}{\delta^2-1}, \tag{2.8}$$

being $\delta > 1$ the value of the constraint, i.e. $\|T\|_\infty \leq \delta$. In the Nichols plane, these circles are mapped to closed regions, that contain the critical point. For a value $\delta = 1$, the forbidden region in the complex plane is a semiplane containing the critical point, that is defined by the vertical line across -0.5 (see Figure 2.5 (left)). These constraints are displayed in Figure 2.5, both in the complex plane (left) and Nichols plane (right)

[4]More general nonlinear plants can be treated in the framework of QFT by means of the Schauder fixed point theorem [31].

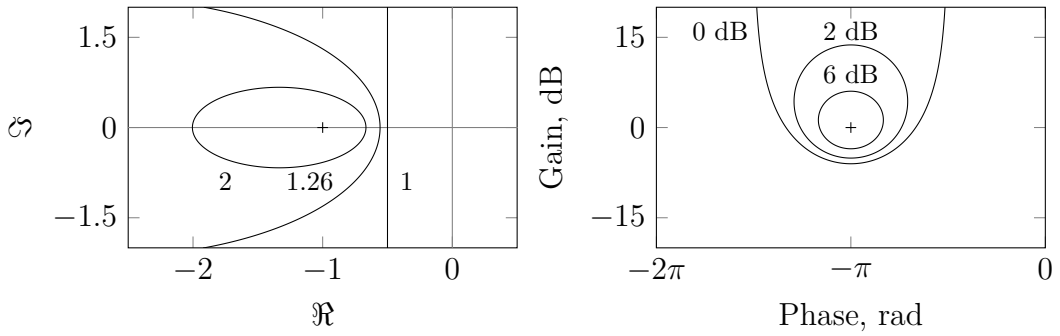

Figure 2.5 M-circles in the complex plane and Nichols plane

Constraints over the magnitude of the complementary sensitivity in the complex plane (left) and Nichols plane (right).

for the values 1, 1.26, and 2; or equivalently 0, 2, and 6 dB. Observe that the loci of constant $|T|$ in the Nichols plane are symmetric with respect to the horizontal line defined by 0 dB to the corresponding to the loci of constant $|S|$, that were displayed in Figure 2.4. Similarly to the previous regions, they are known as *M-circles*.

2.1.3 Performance of Feedback Control Systems

After guaranteeing closed-loop stability with pre-specified stability margins, the following step is to consider the performance of the control system. In terms of performance, the feedback controller is in charge for reducing the effect of load disturbances and plant model uncertainty, while feeding a limited or a minimum amount of measurement noise into the plant.

Reducing the Effect of Load Disturbances

The effect of load disturbances acting on the input or output of the plant can be determined by the sensitivity function $S(s)$. Let us consider a disturbance $d(t) = d_0 e^{j\omega t}$. Then, the steady-state response of the plant output y is given by

$$y_{ss}(t) = P(j\omega)S(j\omega)d_0 e^{j\omega t} \tag{2.9}$$

for the case of a disturbance entering at the plant input. On the other hand, for a disturbance entering at the plant output[5], the steady-state response of the plant output

[5]This case was not considered before in equations (1.1)–(1.2), but it can be easily taken into account using the same arguments as in the other case.

y is given by

$$y_{ss}(t) = S(j\omega)d_0 e^{j\omega t}. \tag{2.10}$$

Therefore, the effect of disturbances may be reduced by requiring $|P(j\omega)S(j\omega)| \ll 1$ and/or $|S(j\omega)| \ll 1$ over a range of frequencies representative of the disturbances.

Reducing the Effect Due to Plant Model Uncertainty

The sensitivity function quantifies the effect that small changes with respect to the plant model cause in the closed-loop transfer function from the reference signal to the plant output, i.e. $T(s)$. This is illustrated as follows:

$$\frac{dT(s)}{dP(s)} = \frac{C(s)}{(1 + P(s)C(s))^2} = \frac{T(s)S(s)}{P(s)}, \tag{2.11}$$

this equation can be rearranged as

$$\frac{dT(s)}{T(s)} = S(s)\frac{dP(s)}{P(s)}. \tag{2.12}$$

The latter equation applies only for small changes of $P(s)$. Horowitz extended it to finite changes in [125]. Let us consider the nominal transfer functions $T_0(s)$ and $P_0(s)$, and their perturbed counterparts defined as follows:

$$\begin{aligned} T_p(s) &= T_0(s) + \Delta T(s), \\ P_p(s) &= P_0(s) + \Delta P(s). \end{aligned} \tag{2.13}$$

Then, the Horowitz sensitivity function [167] is defined as:

$$S_H(s) = \frac{\Delta T(s)/T_f(s)}{\Delta P(s)/P_f(s)} = \frac{1}{1 + P_0(s)C(s)}. \tag{2.14}$$

Therefore, the response of the control system is hardly influenced by variations with respect to the plant model in the range of frequencies where the magnitude of the sensitivity function is very small.

Reducing the Effect Due to Measurement Noise

The effect of measurement noise on the plant output is determined by the complementary sensitivity function $T(s)$. Consider a noise signal $n(t) = n_0 e^{j\omega t}$. Then, the steady-state

response of the plant output y due to this signal is given by

$$y_{ss}(t) = -T(j\omega)n_0 e^{j\omega t}. \tag{2.15}$$

On the other hand, the steady-state response of the controller output u due to the same signal is given by

$$u_{ss}(t) = -C(j\omega)S(j\omega)n_0 e^{j\omega t}. \tag{2.16}$$

Therefore, the effect of measurement noise on the plant output may be reduced by requiring $|T(j\omega)| \ll 1$, or in the case of the effect on the controller input by imposing $|C(j\omega)S(j\omega)| \ll 1$. Note that this requirement implies a trade-off between achieving good performance and reducing the effect of measurement noise. Since the first two specifications require a controller with sufficiently high gain, while the latter specification demands one with low gain. This results in an unavoidable trade-off.

Performance Specifications in the Nichols Plane

Performance specifications can be thus stated in terms of upper bounds on the magnitude of the sensitivity and the complementary sensitivity transfer functions for a given range of frequencies. This kind of specifications has been presented as stability margins, but the same idea is used to specify a desired level of performance. There are some differences with respect to their use as stability margins. Performance specifications may be stated as upper bounds with values less than 1 (or 0 dB). When they act like stability margins, the value of the specifications is restricted to be greater than or equal to 1 (or 0 dB) (these values lead to regions that protect in some way the critical point). In addition, the value of the upper bound is usually given as function of the frequency (or even, it may be given for a finite range of frequencies), instead of being a constant value for all nonnegative frequencies.

Now, we are going to consider specifications in terms of an upper bound of the magnitude of the sensitivity and the complementary sensitivity for a given frequency and an arbitrary nonnegative value. That generalizes the presentation done for this class of specifications when introducing stability margins in Section 2.1.2. Let us firstly consider the specification $|S(j\omega)| \leq \delta$, this specification is translated to the complex plane as circles centered at -1 (critical point) and with radius δ^{-1}. That is easily proved by considering $L(j\omega) = x + jy$, then we can obtain contours of constant values

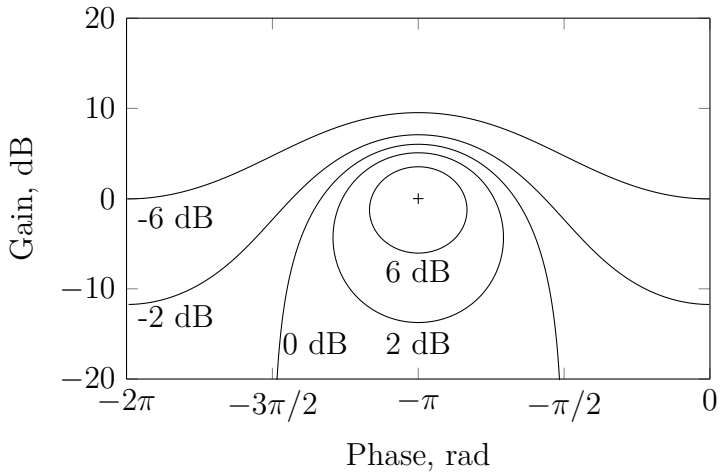

Figure 2.6 Curves of constant values of $|S|$ in the Nichols plane

of $|S(j\omega)| = |(1 + L(j\omega))^{-1}| = \delta$ as

$$((x+1)^2 + y^2) = \delta^{-2}. \tag{2.17}$$

These circles impose forbidden regions to the loop transfer function at the considered frequency. When they are translated to the Nichols plane, the three following cases are possible:

- The curves for $\delta > 1$ are closed curves that enclose the critical point, i.e. $-\pi$ rad and 0 dB, and are contained in a range of phases that expands from $-3\pi/2$ to $-\pi/2$ rad.

- The curve for $\delta = 1$ is an asymptotic curve to $-3\pi/2$ and $-\pi/2$ rad.

- The curves for $\delta < 1$ are open curves that impose a minimum amount of gain of the loop transfer function for each possible value of the phase.

Figure 2.6 shows some curves of constant values of $|S|$. These curves, that are symmetric about the vertical line at $-\pi$ rad, are repeated every 2π rad. This kind of diagram is known as *inverse Nichols chart*.

On the other hand, the specification $|T(j\omega)| \leq \delta$ is also translated to the complex plane as circles of center

$$-\frac{\delta^2}{\delta^2 - 1}, \tag{2.18}$$

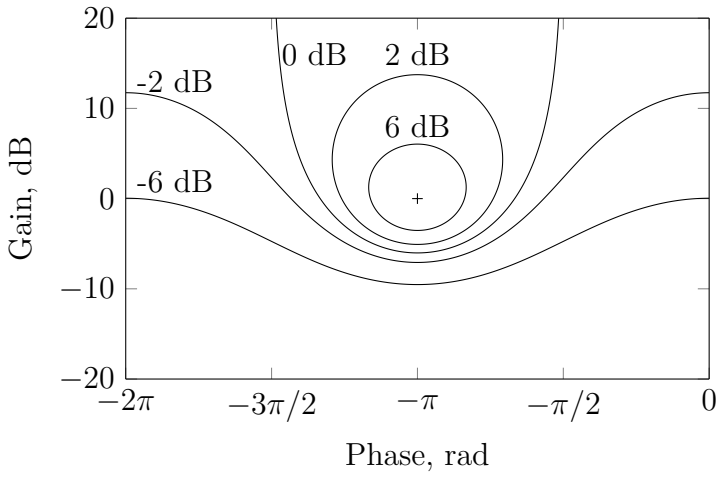

Figure 2.7 Curves of constant values of $|T|$ in the Nichols plane

and radius equal to

$$\frac{\delta}{|\delta^2 - 1|}, \tag{2.19}$$

when $\delta \neq 1$, and a semiplane containing the critical point, whose boundary is a vertical line at -0.5 in the case of $\delta = 1$. Let us consider as before $L(j\omega) = x + jy$, then we can obtain contours of constant values of $|T(j\omega)| = |L(j\omega)(1 + L(j\omega))^{-1}| = \delta$ as

$$\delta^2((x+1)^2 + y^2) = x^2 + y^2, \tag{2.20}$$

after factoring, this becomes

$$\frac{1-\delta^2}{\delta^2}x^2 - 2x + \frac{1-\delta^2}{\delta^2}y^2 = 1. \tag{2.21}$$

After straightforward manipulations, it is easy to see that this condition corresponds to the circles given before, when $\delta \neq 1$, and a straight line when $\delta = 1$. In the Nichols plane these curves of constant values of $|T(j\omega)|$ may be obtained by taking the mirror image of the curves of constant values for $|S(j\omega)|$ with respect to the line corresponding to 0 dB, this is due to the fact that $S(j\omega) + T(j\omega) = 1$. Figure 2.7 displays some curves of constant values of $|T|$. Similarly to the previous one, this kind of diagram is known as *Nichols chart*. The same treatment done for the loci of constant magnitude of S and T could also be done for the loci of constant phase of S and T.

Under the assumption that references and load disturbances have low-frequency content and measurement noise has high-frequency content, these objectives may

be achieved by designing the loop transfer function, with adequate gain at different frequency ranges. Bode's gain-phase relation states that the phase lag of any minimum-phase (MP) system is approximately equal to $n\pi/2$ rad, where n is the slope of the Bode plot of $L(j\omega)$, i.e. $d\log|L(j\omega)|/d\log\omega$. (Nonminimum phase (NMP) systems exhibit additional phase lag to the imposed by the latter relation.) This relation implies that an arbitrary fast transition from a range of frequencies where $|L(j\omega)|$ is sufficiently high to another where $|L(j\omega)|$ is sufficiently low cannot be achieved, due to the great amount of phase lag that it would imply.

We can identify three frequency ranges [29, 42, 125, 167], where the feedback controller has different roles:

- *Low frequencies where* $|L(j\omega)| \gg 1$. The role of the feedback controller in this frequency range is to achieve good performance in terms of attenuation of disturbances and changes in the closed-loop due to plant model uncertainty. Therefore, a controller that achieves sufficiently high gain is desired.

- *Intermediate frequencies where* $|L(j\omega)| \approx 1$. In this intermediate frequency range, the feedback controller has to provide adequate stability margins. At this frequency range the gain of the loop transfer function has to decrease, but maintaining adequate stability margin. The existing relation between gain and phase for MP transfer function imposes a certain amount of phase lag per decrement on the gain. Too much phase lag would destabilize the closed-loop system.

- *High frequencies where* $|L(j\omega)| \ll 1$. At high frequencies, the main objective is to attenuate measurement noise. Therefore, a controller that achieves sufficiently low gain is desired. At high frequencies, the benefits of feedback are negligible.

Figure 2.8 shows a usual loop transfer function where the roles of the feedback controller at different frequency ranges are indicated.

2.1.4 Trade-Offs in Control Design

Performance versus Cost of Feedback

A control design approach based on plant inversion is ideally feasible for MP plants, those without RHP poles and zeros and time delay. Then, practically any desired performance specification in terms of disturbance attenuation and changes in the closed-loop behavior due to plan model uncertainty is achievable when the controller

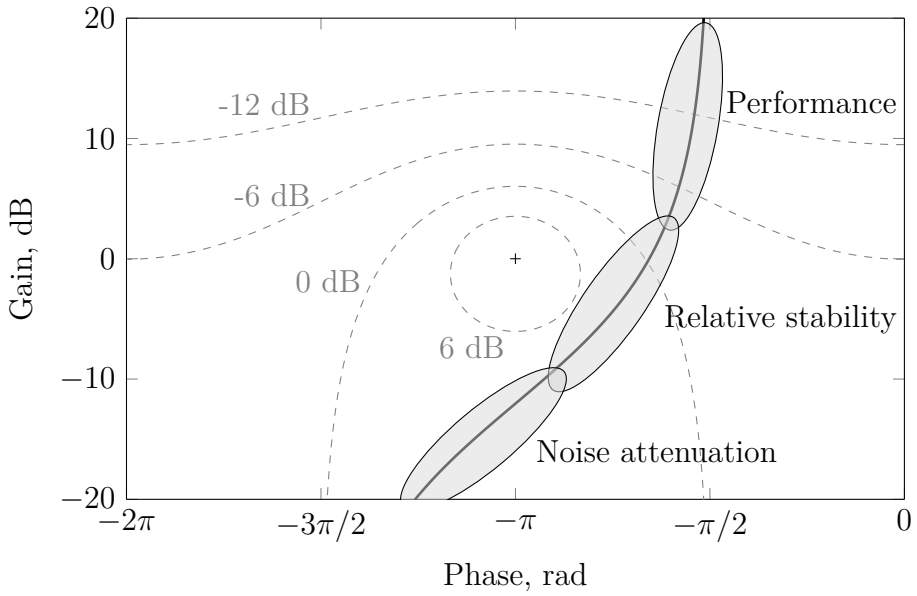

Figure 2.8 Roles of feedback controllers at different frequency ranges

contains an inverse model of the plant, a sufficiently high gain and/or an integrator, and possibly some far poles to ensure realizability. This approach generally leads to controllers with too high bandwidth and neglects specifications about limiting the effect of measurement noise. Most of the cases this design is not realistic and does not care about important drawbacks that arise when the gain of the controller is too large over a wide range of frequencies, for example:

- Sensor noise and disturbances at the plant input may generate control output too large, under these circumstances, there is an instability risk due to actuator saturation.

- Controller output may be too sensitive to sensor noise, leading to expensive wear of actuators.

- There are always unmodeled dynamics at sufficiently high frequencies, at these frequencies the gain of the controller must be low enough.

These drawbacks are related to the notion of *cost of feedback*, term coined by Horowitz [125]. It denotes a range of frequencies where the channel from the measurement noise to the output of the controller is amplified. Figure 2.9 illustrates this concept, the frequency of range where the cost of feedback takes place is approximately from the

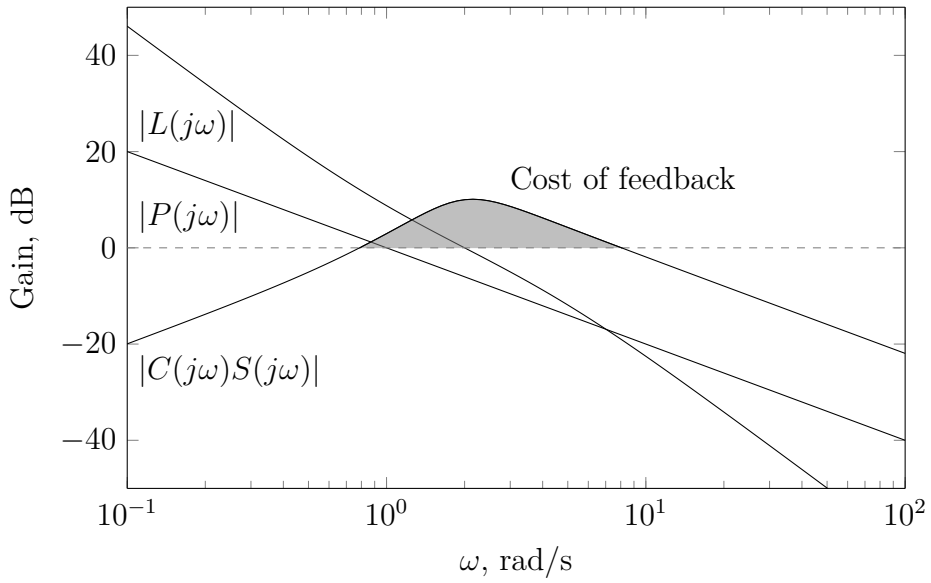

Figure 2.9 Cost of feedback

gain crossover frequency of the plant until the gain crossover frequency of the controller, where the graph of $|L(j\omega)|$ intersects $|P(j\omega)|$.

The trade-off between performance (benefits of feedback) and cost of feedback (drawbacks of feedback) may be solved in different ways. Two approaches are presented here:

- *Maximization of benefits of feedback.* That is achieved by maximizing $|L(j\omega)|$ (or minimizing $|S(j\omega)|$) at low frequencies, subject to constraints that should limit $|L(j\omega)|$ at high frequencies.

- *Minimization of drawbacks of feedback.* That is achieved by minimizing $|L(j\omega)|$ at high frequencies, subject to constraints that impose a desired minimum level of performance in terms of lower bounds on $|L(j\omega)|$ (or upper bounds on $|S(j\omega)|$) at low frequencies.

An analog situation occurs in the portfolio optimization theory developed by the Nobel laureate economist Harry Markowitz [171]. In this approach, the two strategies that may adopt an investor are to maximize return subject to a given level of risk or to minimize the level of risk subject to a given level of expected return. This can be understood as maximization of benefits of inversion and minimization of drawbacks of inversion, respectively. A brief exposition of the modern portfolio theory of Markovitz can be found in [53].

Nonminimum-Phase (NMP) Systems

In addition to the issue of the cost of feedback, the situation is worse for plants containing RHP poles and zeros and/or time delay, since additional theoretical limitations exist on the bandwidth of the loop transfer function. RHP zeros and time delay impose an upper bound on the bandwidth, and RHP poles impose a lower bound on the bandwidth. The latter may seem more benign, but it implies that a plant cannot be stabilizable if the actuator has not sufficiently high bandwidth [241]. In addition, saturation in feedback control systems containing RHP poles may lead to instability. Some rule of thumbs about these limitations over the gain crossover frequency of the loop transfer function are given as follows (see [13] for further details):

$$\begin{aligned} &\omega_{gc} < 1/L, && \text{imposed by a time delay } L, \\ &\omega_{gc} < 0.5b, && \text{imposed by an RHP zero at } s = b, \\ &\omega_{gc} > 2a, && \text{imposed by an RHP pole at } s = a. \end{aligned} \tag{2.22}$$

These limitations are obtained by assuming Bode's ideal loop transfer function and a reasonable value of phase margin. It is worth highlighting that a controller with a bandwidth that does not satisfy these constraints will necessary exhibit poor stability margins.

The Nichols plot of NMP loop transfer functions may also provide some insight into these limitations. Some examples are included below.

Example 2.2. RHP zeros are common in models that have a competing effect of slow and fast dynamics [234]. Let us consider the following loop transfer function with an RHP zero:

$$L(s) = \frac{s-1}{s(s+4)} = \frac{s+1}{s(s+4)}\frac{s-1}{s+1}. \tag{2.23}$$

This transfer function has been factored into two transfer functions, namely an MP and an NMP with unitary gain. Note that the second transfer function provides a phase lag equal to π rad at high frequencies, while it is not possible to cancel it. It clearly imposes a limitation on the gain of the loop transfer function. This situation is illustrated on the Nichols plane in Figure 2.10 (left). The position of the RHP zero is very important, since the addition of phase lag takes place about the frequency $\omega = b$ for an RHP zero that is placed at $s = b$. Time delays impose similar limitations since they can be approximated by a transfer function containing an RHP zero.

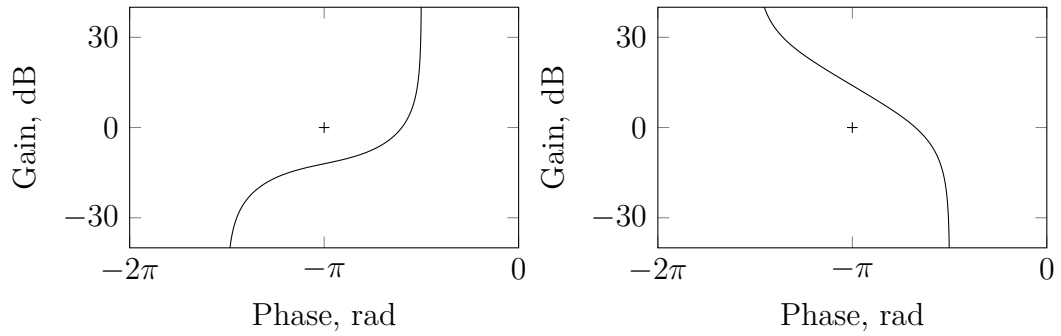

Figure 2.10 Limitations imposed by an RHP zero (left) and an RHP pole (right)

Example 2.3. This example examines the presence of an RHP pole in the loop transfer function. Let us consider the following loop transfer function:

$$L(s) = \frac{5(s+2)}{s(s-1)} = \frac{5(s+2)}{s(s+1)}\frac{s+1}{s-1}. \tag{2.24}$$

As in the previous example, the transfer function can be factored into two transfer functions, an MP and an NMP with gain equal to one. Here, the NMP part provides a phase lag of π rad at low frequencies, and the phase lag decreases to 0 at a frequency $\omega = a$ for an RHP pole that is placed at $s = a$. Then, it is necessary a minimum amount of gain in order to achieve closed-loop stability. This situation is depicted in Figure 2.10 (right).

2.1.5 Limitations of Feedback Control Systems

Another important point regarding limitations of feedback control[6] is the Bode's Integral Formula. Control specifications are usually given in form of constraints over the upper bound of the magnitude of the sensitivity. The question of deciding if a given specifications is or not attainable has attracted the interest of the control community, see for example [13, 223, 234]. A seminal result in this topic is the Bode's sensitivity integral discovered by Hendrik Wade Bode[7], that is presented as follows:

Theorem 2.3 (Bode's sensitivity integral)**.** *Assume that the loop transfer function $L(s)$ of a feedback system goes to zero faster than $1/s$ as $s \to \infty$. If the $L(s)$ has*

[6]We comment here limitations of linear and time-invariant feedback systems, but limitations of nonlinear feedback systems also exist and have been studied, see for example, [224].

[7]This result is a control systems interpretation done by Horowitz from results obtained by Bode [223], and it is sometimes referred as Horowitz's area formula [160].

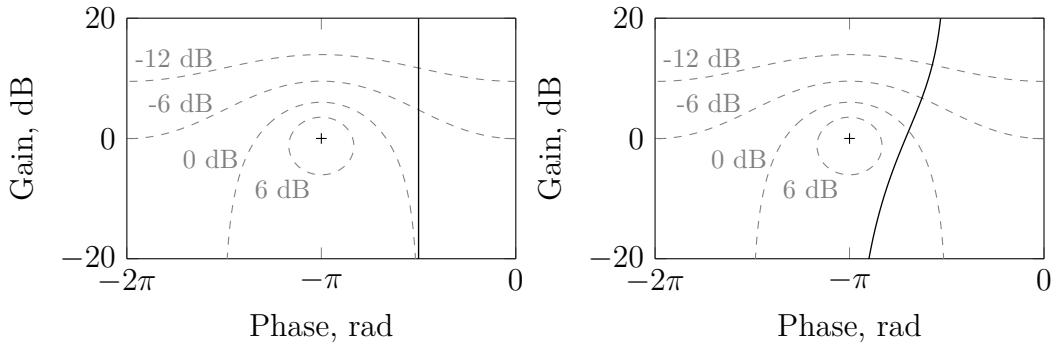

Figure 2.11 Nichols plots of $L_1(s)$ (left) and $L_2(s)$ (right) (Example 2.4)

poles p_k in the open right half-plane, then the sensitivity function satisfies the following integral:

$$\int_0^\infty \log \frac{1}{|1 + L(j\omega)|} d\omega = \pi \sum_k p_k. \tag{2.25}$$

This constraint imposes a limitation on the achievable performance for any practical control system. The benefits of feedback in terms of small sensitivity for a range of frequencies is necessarily paid in terms of a range of frequencies where the magnitude of the sensitivity is higher than 1. It is very illustrative to show the Nichols plots of different loop transfer functions to see how this constraint affects to each one.

Example 2.4. Let us consider the following loop transfer functions:

$$L_1(s) = \frac{1}{s}, \qquad L_2(s) = \frac{1}{s(s+1)}. \tag{2.26}$$

The constraint (2.25) does not apply to $L_1(s)$, but this is not the case of $L_2(s)$. Figure 2.11 shows the Nichols plot of $L_1(s)$ (left) and $L_2(s)$ (right), in addition, loci of constant $|S|$ in dB are overlaid for some values (inverse Nichols chart). In the case of $L_1(s)$, it is possible to increase the gain of the loop transfer function reaching lower values for the sensitivity. On the contrary, if the gain of $L_2(s)$ is increased, it will lead to lower values for the sensitivity at low frequencies, but higher values for the sensitivity in the vicinity of the critical point $[-\pi\ 0]^\top$. This phenomenon is known as waterbed effect.

The extension of Theorem 2.3 to stable strictly proper loop transfer functions with time delay was done in [90], in this case, the constraint holds even in the case of $L(s)$ that goes to zero equal to $1/s$ as $s \to \infty$.

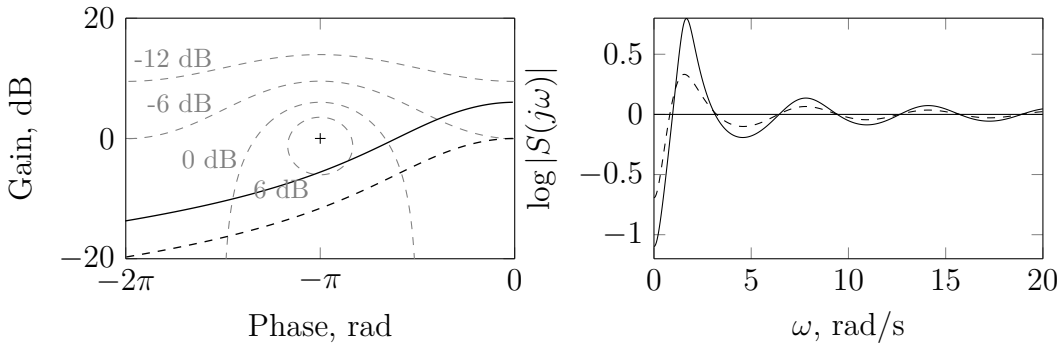

Figure 2.12 Nichols and Bode plots (Example 2.5)

Nichols plot of the loop (left) and Bode plot of the corresponding sensitivity (right) corresponding to $L(s)$ (solid line) and $0.5L(s)$ (dashed line).

Example 2.5. Let us consider the following loop transfer function with time delay:

$$L(s) = \frac{e^{-s}}{s + 0.5}. \tag{2.27}$$

This example shows how the presence of time delay imposes the constraint (2.25), even in the case of loop transfer functions that go to zero equal to $1/s$ as $s \to \infty$. Figure 2.12 compares the Nichols plot and Bode plot of $S(s)$ for $L(s)$ and $0.5L(s)$. While $L(s)$ achieves a higher sensitivity reduction at low frequencies than $0.5L(s)$, the peaks of the sensitivity function are also higher. In the time delay case, the sensitivity function has an infinite number of relative maximums, these correspond to each one of the critical points that appear every 2π rad.

2.2 QFT Design Method

QFT is a control design method mainly developed by Horowitz and coworkers. The seminal works are [124, 133] and some tutorial material can be found in [129, 265]. It is deeply rooted in classical control, extending and generalizing some ideas previously proposed by Bode. In spite of its flavor of classical control, it has also been extended to deal with multiple-input-multiple-output (MIMO) [169, 264, 267] and nonlinear [27, 126, 131] plants.

In the words of Horowitz, QFT addresses "the problem of achieving desired system tolerances from uncertain plants, at minimum cost of feedback" [130]. While most of the robust control literature only uses either the gain or the phase information about the uncertainty of the plant model, QFT uses both gain and phase information

to describe the model uncertainty and to design the loop transfer function[8]. These points allow to obtain controllers with only the necessary bandwidth to cope with the considered amount of uncertainty, i.e. feedback is employed in a quantitative way.

This technique considers a 2-DOF feedback control structure and aims to design a prefilter $F(s)$ and a controller $C(s)$, that achieve performance and stability specifications for an uncertain plant that can be described as a member of a finite or infinite set of transfer functions

$$P(s) \in \mathcal{P}. \tag{2.28}$$

For a given frequency ω, a *template* $\mathcal{P}_\omega$ is defined as the set of all frequency responses values at this frequency. Formally, $\mathcal{P}_\omega$ is defined as

$$\mathcal{P}_\omega = \Big\{ P(j\omega) : P(s) \in \mathcal{P} \Big\}. \tag{2.29}$$

2.2.1 QFT Control Specifications

All specifications must be formulated in the frequency domain, and the ones originally stated in the time domain have to be translated into the frequency domain[9]. The following specifications are typically considered in QFT:

- *Relative stability and output disturbances attenuation*

$$|S(j\omega)| = \left| \frac{1}{1 + L(j\omega)} \right| \leq \delta_S(\omega), \qquad \forall P(j\omega) \in \mathcal{P}_\omega, \qquad \forall \omega \in \Omega_S. \tag{2.30}$$

- *Relative stability and measurement noise attenuation*

$$|T(j\omega)| = \left| \frac{L(j\omega)}{1 + L(j\omega)} \right| \leq \delta_T(\omega), \qquad \forall P(j\omega) \in \mathcal{P}_\omega, \qquad \forall \omega \in \Omega_T. \tag{2.31}$$

- *Input disturbances attenuation*

$$|P(j\omega)S(j\omega)| = \left| \frac{P(j\omega)}{1 + L(j\omega)} \right| \leq \delta_{PS}(\omega), \qquad \forall P(j\omega) \in \mathcal{P}_\omega, \qquad \forall \omega \in \Omega_{PS}. \tag{2.32}$$

[8]This approach is denoted as loop gain-phase shaping in [25], this work presents a comparison that shows the superiority of QFT over other alternative robust control techniques based on loop gain shaping.

[9]There is no an exact method to translate time-domain specifications into frequency-domain specifications, but some heuristic relations exist, see [228, 265].

- *Control effort*

$$|C(j\omega)S(j\omega)| = \left|\frac{C(j\omega)}{1+L(j\omega)}\right| \leq \delta_{CS}(\omega), \qquad \forall P(j\omega) \in \mathcal{P}_\omega, \qquad \forall \omega \in \Omega_{CS}. \tag{2.33}$$

- *Tracking*

$$\delta_l(\omega) \leq |F(j\omega)T(j\omega)| \leq \delta_u(\omega), \qquad \forall P(j\omega) \in \mathcal{P}_\omega, \qquad \forall \omega \in \Omega_{FT}. \tag{2.34}$$

  A simple manipulation of the latter equation results in the following specification for the feedback controller $C(s)$:

$$\max_{P(j\omega)\in\mathcal{P}_\omega} 20\log_{10}|T(j\omega)| - \min_{P(j\omega)\in\mathcal{P}_\omega} 20\log_{10}|T(j\omega)| \leq 20\log_{10}\frac{\delta_u(\omega)}{\delta_l(\omega)}, \quad \forall \omega \in \Omega_{FT}. \tag{2.35}$$

  If this specification is satisfied for a controller $C(s)$, then there exists an MP prefilter $F(s)$ that satisfies (2.34) [128].

The sets $\Omega_\bullet$, considered in the previous specifications, may include a finite or infinite range of frequencies; but in order to obtain a tractable problem, they have to be discretized for solving the design control problem. The same situation occurs with the templates $\mathcal{P}_\omega$. In addition to the presented specifications, alternative specifications for tracking in terms of tracking error specifications are presented in [85], and more general specifications, including phase specifications, are considered in [190].

The QFT design procedure involves several steps that will be explained in the sections ahead.

2.2.2 Generation of Plant Templates

Templates characterize the plant uncertainty by capturing the gain and phase variations of the plant at a given frequency. They are obtained for some frequencies of interest and one arbitrary transfer function from $\mathcal{P}$ is assigned as the nominal. Figure 2.13 illustrates the template generation by showing the templates of the uncertain plant

$$\mathcal{P} = \left\{\frac{k}{\tau s+1} : [k\ \tau]^\top \in \Theta = [1,5]\times[1,5]\right\}, \tag{2.36}$$

at the frequencies $\omega = 0.1, 1, 20$. Several methods have been proposed in the literature to the problem of calculation of templates (also known as value set computation):

- *Grid method.* This approach consists in gridding equidistantly each parameter interval. It is straightforward but computationally expensive. This method suffers from a curse of dimensionality (i.e. the number of points grows exponentially with respect the number of uncertain parameters).

- *Parametric method.* The work [26] presents a method to obtain directly the boundary of the templates, but it assumes that the plant is modeled by rational transfer functions with independent parameters in the numerator and denominator. In [24], the previous approach is extended to the case in which numerator and denominator coefficients are affine functions. The work [92] states conditions under which to map edges is sufficient to generate the templates.

- *Symbolic method.* The work [60] assumes a rational transfer function with numerator and denominator coefficients given as nonlinear functions of uncertain parameters. This method checks the edges and, possibly, some interior lines that satisfy certain conditions obtained by symbolic calculations.

- *Interval method.* The work [192] presents a method applicable to transfer functions whose magnitude and phase are continuous functions of the uncertain parameters. It generates templates with a prescribed accuracy level by means of interval mathematics methods.

- *Recursive method.* The paper [114] constitutes an extension of the grid method, where the gridding is adapted locally in order to achieve a prescribed accuracy level. A Prune algorithm is also presented to find the boundary of the template, this algorithm is also part of the recursive method.

- *Analytic method.* The paper [173] presents a method that combines the use of subtemplates defined by at most two uncertain parameters (analytical functions) with operations between these subtemplates [112, 213] to compose a template.

2.2.3 Generation of Boundaries

The design specifications are translated into certain boundaries (also known as Horowitz-Sidi bounds) on the nominal loop transfer function $L_0(s) = C(s)P_0(s)$. Theses boundaries can be obtained by moving the plant template between the closed-loop magnitude contours in the Nichols chart (or the inverse Nichols chart), that is a very intuitive algorithm to see how QFT works. This procedure is illustrated in Figure 2.14,

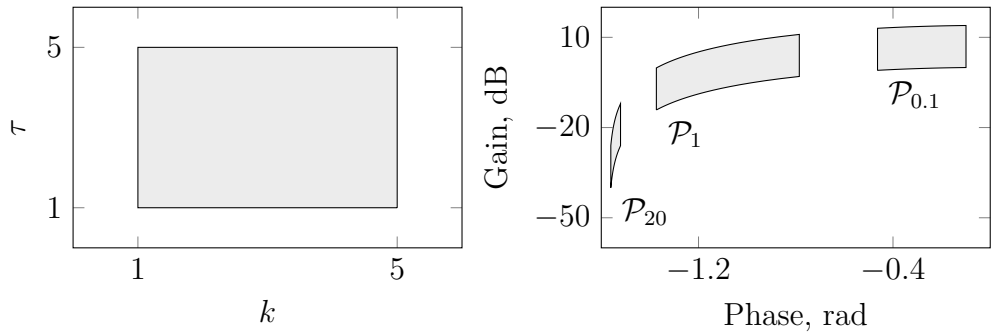

Figure 2.13 Generation of templates

Mapping from the controller parameter space (left) to the Nichols plane (right).

where for a given template (placed in the bottom right corner) corresponding to a frequency $\omega = 0.1$, are obtained the boundaries for the following specifications:

$$\begin{aligned} &\text{Robust stability:} \quad 20\log_{10}|T(j0.1)| \leq 6, \quad \forall P(j0.1) \in \mathcal{P}_{0.1}. \\ &\text{Robust tracking:} \quad \max_{P(j0.1)\in\mathcal{P}_{0.1}} 20\log_{10}|T(j0.1)| - \min_{P(j0.1)\in\mathcal{P}_{0.1}} 20\log_{10}|T(j0.1)| \leq 0.5. \end{aligned} \tag{2.37}$$

The boundary for the first specification is obtained by sliding the rotated (by π rad) template in such a way that the nominal plant coincides with the corresponding M-circle in the Nichols chart. The nominal plant is marked with a circle, it is placed in the upper left part of the template (it is arbitrarily chosen). The boundary for the second specification is obtained (for each controller phase) by moving vertically the template until the specification is satisfied, note that if the controller gain is large enough the specification is met. The procedure to obtain the boundary in both cases is illustrated in Figure 2.14. Boundaries for other specifications can be obtained by following the same procedure.

The boundary calculation has been sketched by using graphical manipulations of the templates, but this task can be done automatically by using computer algorithms. A computer algorithm proposed by Horowitz [128] performs a line search along constant phase grid lines in the Nichols plane, similarly to the procedure presented before for the second specification. A method based on solving quadratic inequalities is proposed in [59]. These methods do not obtain the correct bounds in cases where the bound takes more than two values for a given phase, this phenomenon was firstly described in [26]. A method based on level sets able to compute multivalued boundaries was independently proposed in [114, 189]. More recently, another method able to obtain

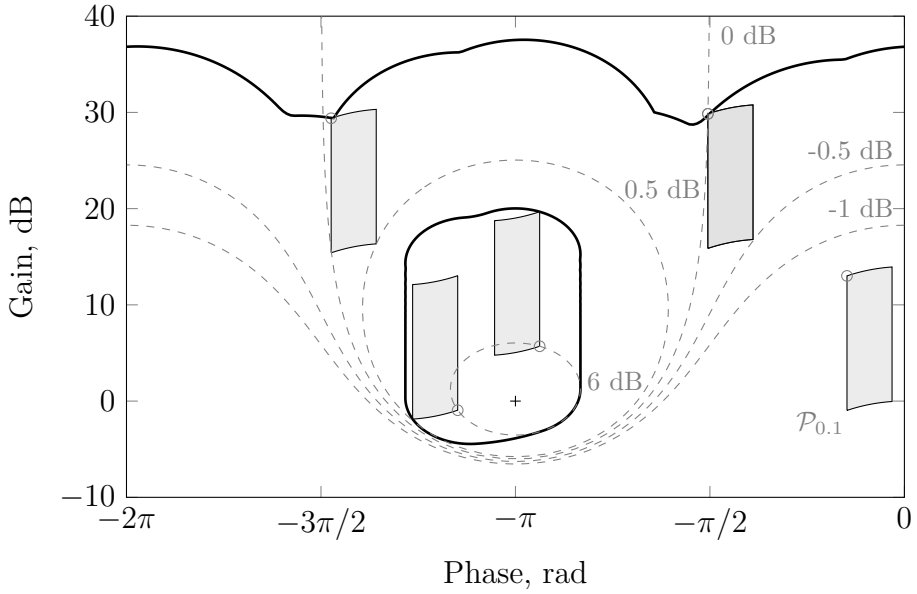

Figure 2.14 Generation of boundaries over the Nichols Chart

multivalued boundaries has been presented in [263], it combines a procedure to test whether a complex point lies in a bound and a pivoting algorithm.

2.2.4 Loop Shaping

The previous stage transforms the simultaneous design problem into a problem for a nominal plant with some extra constraints that account for plant uncertainty and desired specifications. Therefore, a nominal loop transfer function should be designed. That is carried out by adding poles and zeros, in order to obtain a stable nominal closed loop satisfying all specifications imposed by boundaries in the Nichols plane. According to QFT, an optimum loop transfer function is one that satisfies all specifications and its gain decreases as rapidly as possible with frequency to keep the controller bandwidth as low as possible.

Traditionally, the synthesis of QFT controllers has been performed by hand, although this may be a problem for the novel user, this technique offers direct insight into the quantitative trade-off between specifications, controller bandwidth, and controller complexity. Many software packages are available to assist the designer in this steps [46, 74, 96, 110, 134]. In addition, many automatic loop shaping methods have been proposed in the literature. This started with the seminal work of Gera and Horowitz [100]. This work was followed by a multitude of approaches, based on analytic

methods [247], genetic algorithms [61], linear programming [58], interval analysis [193], evolutionary algorithms [56], combined feedforward-feedback design [212], and optimization algorithms [281], among others.

Coming back to the example that we are presenting in this section, let us consider the following specifications:

$$\begin{aligned} &\text{Robust stability:} \quad 20\log_{10}|T(j\omega)| \leq \delta_1(\omega), \quad \forall P(j\omega) \in \mathcal{P}_\omega, \\ &\text{Robust tracking:} \quad \max_{P(j\omega)\in\mathcal{P}_\omega} 20\log_{10}|T(j\omega)| - \min_{P(j\omega)\in\mathcal{P}_\omega} 20\log_{10}|T(j\omega)| \leq \delta_2(\omega), \end{aligned} \tag{2.38}$$

where $\delta_1(0.1) = \delta_1(1) = \delta_1(20) = 6$ dB and $\delta_2(0.1) = 0.5$ dB, $\delta_2(1) = 2$ dB, and $\delta_2(20) = \infty$ dB. (Due to the presence of $20\log_{10}|\cdot|$, δ_1 and δ_2 are expressed in dB.) Figure 2.15 shows the forbidden regions (blue) in the Nichols plane for the designed nominal loop transfer function at each one of the design frequencies. Now, we consider the following controller

$$C(s) = \frac{0.326s^2 + 5.770s + 1}{0.0125s^3 + 0.525s^2 + s}, \tag{2.39}$$

that satisfies the constraints imposed in (2.38). The resulting nominal loop transfer function joint with the Horowitz-Sidi bounds are shown in Figure 2.16.

2.2.5 Design of Prefilter

After designing the feedback compensator $C(s)$, it is necessary to design a prefilter to bring the response within the upper and lower tolerance, $\delta_l(\omega)$ and $\delta_u(\omega)$. The task of designing is relatively easy, the role of the prefilter is only to move the magnitude of transfer function T vertically on a Bode plot. Therefore, if the feedback controller has been designed to cope with the uncertainty, it is possible to design a prefilter that will be able to meet the specification (2.34) [128, 265].

2.3 PID Control

As it was mention in the first chapter, PID control is the most used form of feedback. A PID controller is able to provide a satisfactory design, taking into account the three requisites typically required to a feedback controller when the demanded specifications are not too high:

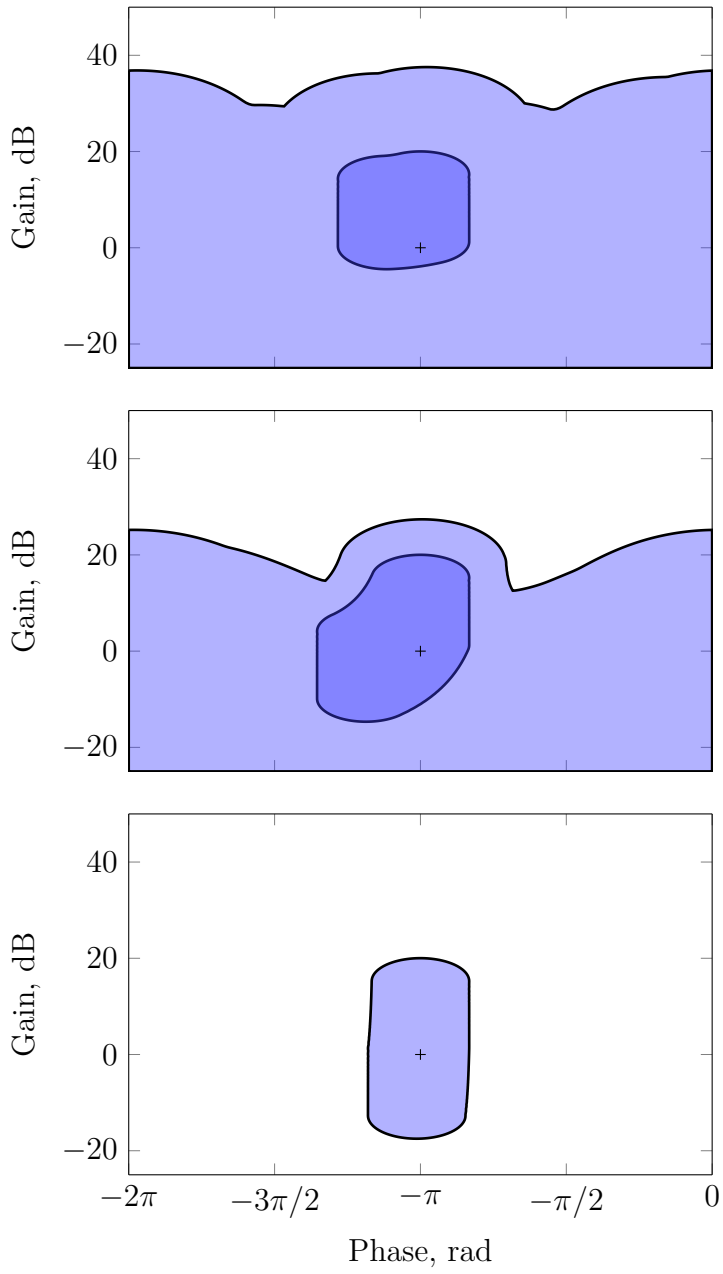

Figure 2.15 Boundaries in the Nichols plane

Boundaries (or Horowitz-Sidi bounds) corresponding to the specifications (2.38) for the frequencies: $\omega = 0.1$ rad/s (top), $\omega = 1$ rad/s (middle), and $\omega = 20$ rad/s (bottom).

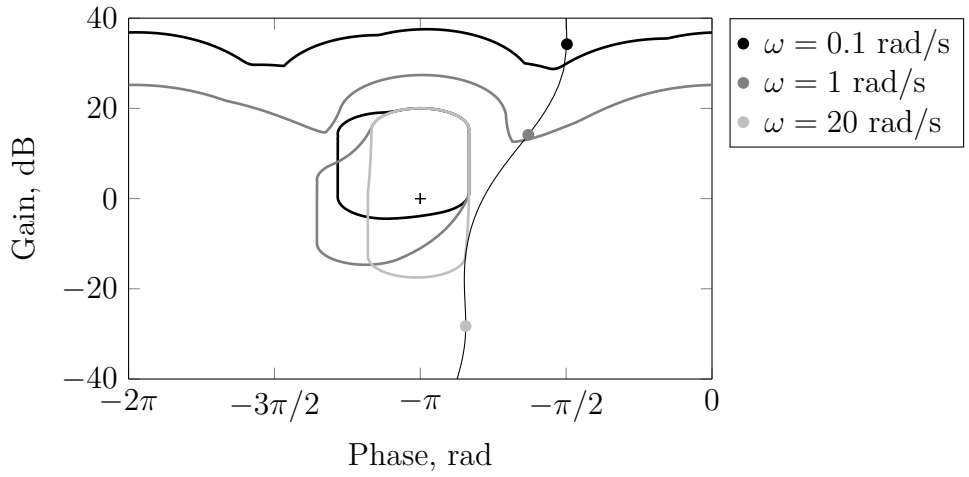

Figure 2.16 Example of feasible loop transfer function

Nominal loop transfer function satisfying the design specifications (2.38).

- *Reduction of the effect of load disturbances and plant model uncertainty.* A PID is able to achieve very high gain at low frequencies due to the presence of an integrator.
- *Guaranteeing closed-loop stability with a prescribed stability margins.* The possibly two zeros of the PID provide phase lead necessary to guarantee adequate stability margins.
- *Feeding a limited or minimum amount of measurement noise to the plant.* The measurement filter is in charge of limiting the undesirable effects of measurement noise.

The choice of a PID controller naturally imposes constraints on the structure of transfer functions to be designed for the feedback controller and the prefilter, implying that they are defined by the equations (1.6) and (1.11), respectively.

2.3.1 PID in the Controller Parameter Space

An advantage of using a controller with a fixed structure is that the *controller parameter space approach* may be used [1, 39]. This is a graphics-oriented approach, whose main caveat is that it is limited to a few controller parameters (less than 3), but it offers figures that provide very valuable insights. Different properties are usually displayed in the controller parameter space such as stability regions and region where performance specifications are met.

Stability in the Controller Parameter Space

A primary concern of a feedback controller is to guarantee closed-loop stability, since feedback control may induce instability. The study of the set of controller parameters that provides closed-loop stability has received considerable attention [107], and in particular for the case of a PID controller [123, 219, 225]. The approach consists on constructing a boundary of the stability domain by performing a mapping of the characteristic equation from the imaginary axis into the controller parameter space. This is performed by obtaining the controller parameters that satisfy the following equation for each frequency

$$1 + L(j\omega) = 0, \qquad -\infty \leq \omega \leq \infty, \tag{2.40}$$

This idea traces back at least to Vishnegradsky [257], he used that to study the stability regions of the Watt's governor for the steam engine. This technique, known as D-partition, was mainly developed by Neimark in the Russian literature and by Mitrovic and Siljak in the Western literature [107]. At the early 1980's, Ackermann extended it to the design of robust controllers [1].

Let us consider a plant model defined by a transfer function with time delay $P(s)$, without zeros on the imaginary axis. On the other hand, we consider a PID controller that is given by

$$C(s) = k_p + \frac{k_i}{s} + k_d s. \tag{2.41}$$

Let us assume that the corresponding loop transfer function is a strictly proper transfer function with time delay. Then, equation (2.40) takes the form

$$1 + P(j\omega)\left(k_p - j\frac{k_i}{\omega} + jk_d\omega\right) = 0, \qquad 0 \leq \omega \leq \infty. \tag{2.42}$$

By symmetric properties, it is only necessary to explore the range of frequencies $0 \leq \omega \leq \infty$. The mapping from (2.42) to the $k_p - k_i$ plane with k_d fixed has nonsingular ($0 < \omega < \infty$) and singular ($\omega = 0$ or $\omega = \infty$) boundaries [225]. From equation (2.42), the nonsingular boundary is given by

$$\begin{aligned} k_p &= -\frac{\Re(P(j\omega))}{|P(j\omega)|^2}, \\ k_i &= \omega^2 k_d - \omega\frac{\Im(P(j\omega))}{|P(j\omega)|^2}, \end{aligned} \tag{2.43}$$

and the singular boundary for $\omega = 0$ is given by

$$k_i P(0) = 0, \tag{2.44}$$

in the case of $P(0) \neq 0$ the singular boundary for $\omega = 0$ is $k_i = 0$. For $\omega = \infty$, equation (2.42) has no solution for a loop transfer function that is given by a strictly proper transfer function with time delay. In addition, note that for $k_i = 0$ there is a drop in the degree of the numerator of $C(s)$, therefore there is a spurious solution, although this line separates regions with different number of stable roots, the parameters placed over this line do not correspond necessarily to closed-loop systems with a pole in the imaginary axis.

The same procedure may be performed for a PID respect to any two selected parameters while the third parameter remains constant. The equations of the corresponding curves can be consulted, for example, in [219, 225]. In the case of a PID endowed with a measurement filter, it may be included in the plant in equation (2.42).

This procedure obtains a division of the controller parameter space into root invariant regions. The nonsingular boundary separates the regions with ± 2 difference in the number of stable roots and singular boundaries separate the regions with ± 1 difference in the number of stable roots [219]. The paper [219] provides results that allow to calculate the number of unstable poles for each region from the number of unstable poles in one of the regions. It allows to obtain the stabilizing region without testing the number of unstable poles in each region.

Example 2.6. This example pretends to illustrate the concept of D-partition using the plant model

$$P(s) = \frac{1}{(s+1)^3}, \tag{2.45}$$

and a PI controller

$$C(s) = k_p + \frac{k_i}{s}. \tag{2.46}$$

Figure 2.17 shows the D-partition for this closed-loop system composed by the previous plant and controller, the number of unstable closed-loop poles of each region is also given. In this case, the singular boundary is the horizontal line $k_i = 0$ and the nonsingular boundary corresponds to the curve starting at $k_p = -1$ and $k_i = 0$. In addition, Figure 2.18 shows the closed-loop poles corresponding to different controllers, that are placed in different regions of the D-partition.

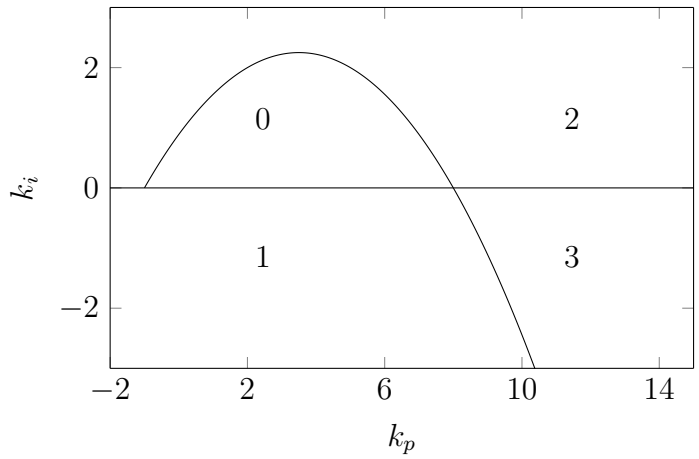

Figure 2.17 D-partition (Example 2.6)

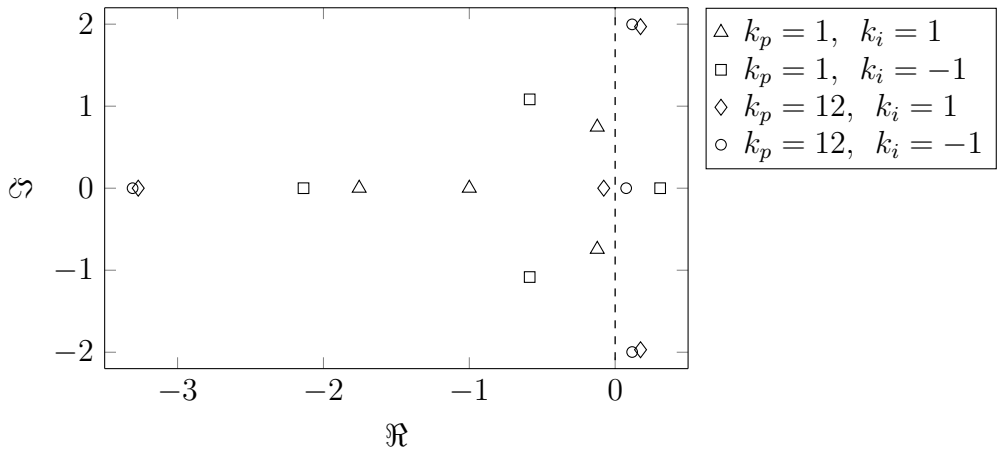

Figure 2.18 Closed-loop poles corresponding to different controllers (Example 2.6)

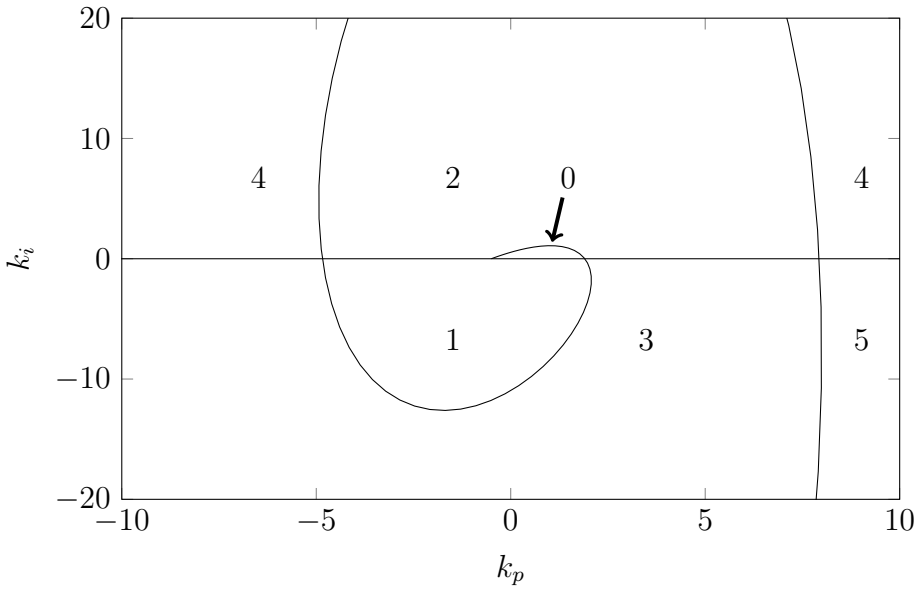

Figure 2.19 D-partition (Example 2.7)

Example 2.7. This example examines the D-partition for a plant with time delay. Let us consider as plant model

$$P(s) = \frac{e^{-s}}{(s + 0.5)}, \tag{2.47}$$

and a PI controller, as in the previous example. The resulting characteristic equation of this system is a transcendental equation (in this case, it contains the exponential function), due to the presence of time delay. This term leads to an infinite number of roots of the characteristic equation. Therefore, it is expected to have regions with an arbitrarily large number of unstable closed-loop poles. The (truncated) D-partition for the considered system is shown in Figure 2.19. In this example, the nonsingular boundary takes the form of a spiral, then each time that it crosses the singular boundary, i.e. $k_i = 0$, a region with an additional unstable pole is generated.

The previous procedure allows to obtain the stability region in the controller parameter space. Figure 2.20 shows some examples of stability regions, where the controller is a PI as the one used in the previous examples. In the left figure, the stabilizing set considering an FOTD plant is shown for different pole values. Note that for a stable plant, the zero controller is included in the stability region. The stability region of an unstable process does not include the zero, in theses cases, a controller with a minimum bandwidth is needed (recall limitations imposed by NMP elements over the

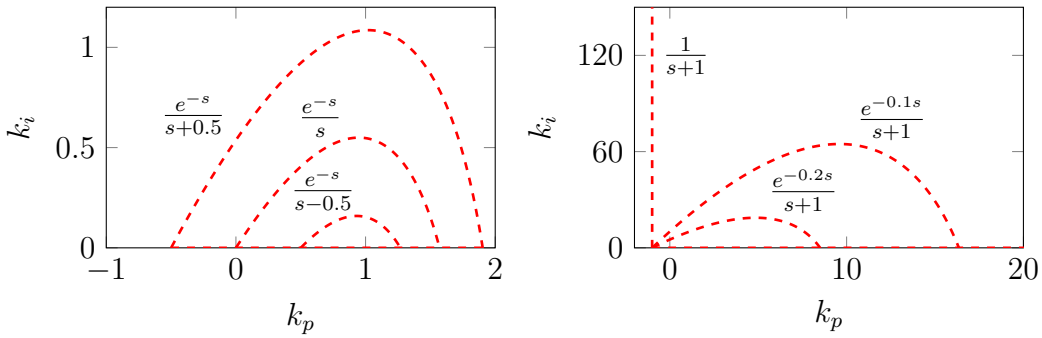

Figure 2.20 Stability regions in the $k_p - k_i$ plane

Plants modeled by an FOTD with different pole values (left) and different time delay values (right).

bandwidth). The right figure shows the stabilizing sets for a time-delay plant as the time delay varies. Note that for the delay-free case the stabilizing region is unbounded, arbitrarily large bandwidth of $L(j\omega)$ are achievable. However, the situation changes for the processes with time delay (recall again limitations imposed by NMP elements). It is worth to note that these limitations are more stringent when a given controller structure is used. As a matter of fact, the use of a given controller structure generally implies limitations that may be circumvented by using a higher-order controller.

Relative Stability and Performance in the Controller Parameter Space

The next step in the process of designing a feedback controller is to guarantee relative stability and performance. An early approach in the controller parameter space to guarantee relative stability was to map a shifted imaginary axis, obtaining in this way a region containing controller parameters that achieve closed-loop poles with their real part less than a prescribed value [107]. In addition to a shifted imaginary axis, other contours could be mapped. Specifications for relative stability and performance in terms of an upper bound on the magnitude of closed-loop transfer functions can also be translated into the controller parameter space. We are going to focus on the upper bound on the magnitude of the sensitivity and complementary sensitivity as control design specifications (for relative stability and performance).

As presented in Section 2.1.3, the constraints $|S(j\omega)| \leq \delta$ and $|T(j\omega)| \leq \delta$ have a graphical interpretation in the complex plane. They impose that the Nyquist plot at a given frequency should lie outside or inside a certain circle. For a PID controller

$$C(s) = k_p + \frac{k_i}{s} + k_d s, \tag{2.48}$$

these circles in the complex plane are mapped into the controller parameter space as ellipses described by the following equation (see [19]):

$$\left(\frac{|P(j\omega)|}{r_c}\right)^2\left(k_p+\frac{\Re(P(j\omega))c_c}{|P(j\omega)|^2}\right)^2+\left(\frac{|P(j\omega)|}{\omega r_c}\right)^2\left(k_i+\frac{\omega\Im(P(j\omega))c_c}{|P(j\omega)|^2}-\omega^2 k_d\right)^2=1, \tag{2.49}$$

where r_c and c_c take the following values depending on the specification

$$\begin{aligned} &c_c=-1, \qquad r_c=\delta^{-1}, \qquad &&\text{for } |S(j\omega)|\leq\delta,\\ &c_c=\frac{\delta^2}{1-\delta^2}, \quad r_c=\frac{\delta^2}{|1-\delta^2|}, \quad &&\text{for } |T(j\omega)|\leq\delta. \end{aligned} \tag{2.50}$$

An alternative (equivalent) procedure to translate these specifications into the controller parameter space is by noting that these specifications are equivalent to simultaneously stabilize a family of plants. This approach is presented in [152, 153]. The specification $\|WS\|_\infty<\gamma$ is equivalent to stabilize $P(s)$ and the family of plants

$$\mathcal{P}=\left\{P(s)\left[\frac{1}{1+\frac{1}{\gamma}e^{j\theta}W(s)}\right]P(s):\theta\in[0,2\pi]\right\}, \tag{2.51}$$

and the specification $\|WT\|_\infty<\gamma$ is equivalent to stabilize $P(s)$ and the family of plants

$$\mathcal{P}=\left\{P(s)\left[1+\frac{1}{\gamma}e^{j\theta}W(s)\right]P(s):\theta\in[0,2\pi]\right\}. \tag{2.52}$$

Example 2.8. This example illustrates the obtainment of regions in the controller parameter space, whose parameters achieve certain specifications on the magnitude of the sensitivity. This example considers the plant model

$$P(s)=\frac{e^{-s}}{(s+0.5)}, \tag{2.53}$$

and a PI controller

$$C(s)=k_p+\frac{k_i}{s}. \tag{2.54}$$

The specification that we consider here is $\|S\|_\infty\leq 1.4$. The region of parameters satisfying this condition is shown in Figure 2.21. The top and bottom left figures show the region obtained using the expression (2.49) that imposes forbidden regions in form of ellipses for each frequency, and the right figure shows the same region but obtained by using multiple stabilization of the family of plant presented in (2.51).

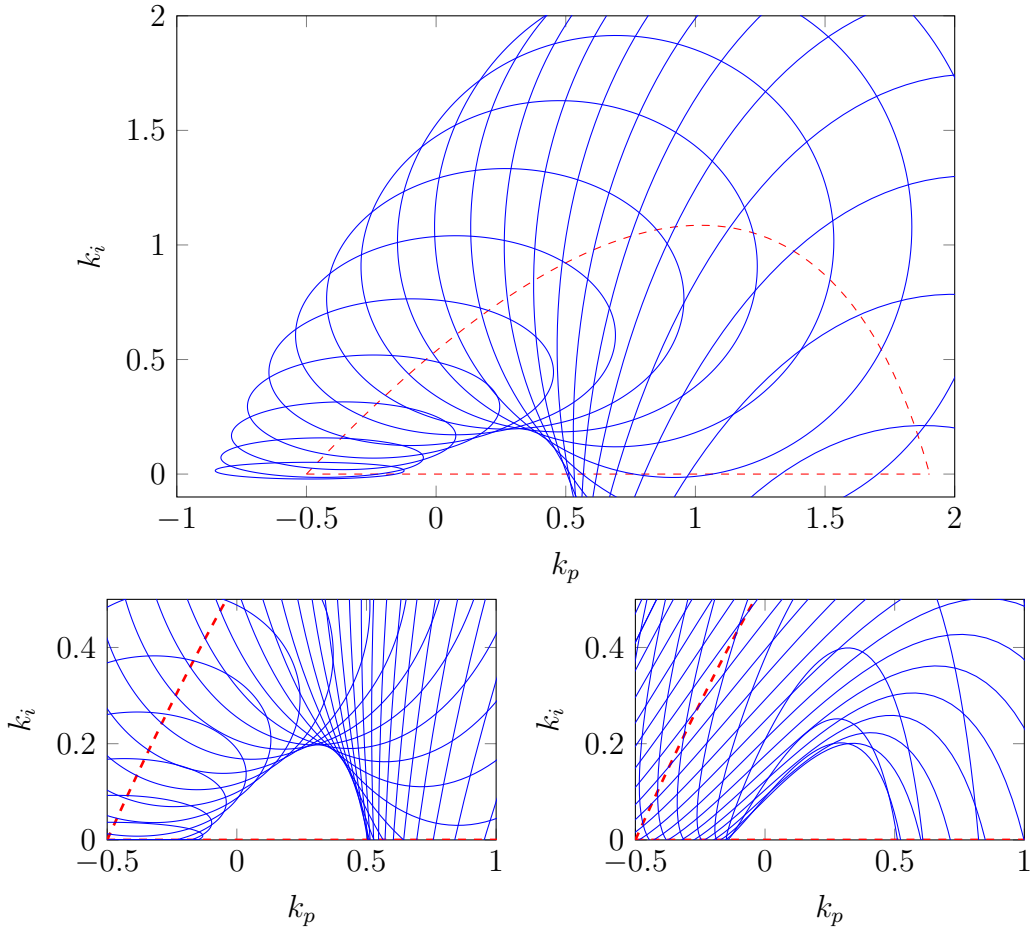

Figure 2.21 Feasible region corresponding to $\|S\|_\infty \leq 1.4$ (Example 2.8)

Feasible region corresponding to $\|S\|_\infty \leq 1.4$ obtained by frequency-wise forbidden ellipses (2.49) (top and bottom left) and multiple stabilization (2.51) (bottom right). The red dashed line corresponds to the boundary of the stability region. Feasible region corresponds to the intersection between stabilizing region and area outside the ellipses in the first case (top and bottom left), and to the intersection between stabilizing region and stabilizing regions of the family of plants in the second case (bottom right).

Performance Indicators in the Time Domain

We have commented before that a controller with sufficiently high gain at low frequencies achieves a good level of performance. It is possible to find links between specifications like that in the frequency domain and specifications in the time domain. One of the most common way to measure the ability to reject load disturbances is usually measured using the *integrated absolute error* (IAE), defined as

$$\text{IAE} = \int_0^\infty |e(t)|\, dt, \tag{2.55}$$

where $e(t)$ is the error due to a unit step disturbance entering at the process input. This integral is difficult (if not impossible) to solve in an analytical manner. An alternative indicator is the *integrated error* (IE) defined as

$$\text{IE} = \int_0^\infty e(t)dt. \tag{2.56}$$

Both indicators yields the same value for a non-oscillatory system, and close values for an oscillatory but well-damped system. This latter property is usually guaranteed by constraining upper bound on the sensitivity function. The great advantage of using the IE is that its value for a control system with a PID as controller is $\text{IE} = 1/k_i$ (see [19]), under the assumption that the steady-state gain of the plant is positive. Therefore, we conclude that

$$\text{maximizing } k_i \qquad \Longleftrightarrow \qquad \text{minimizing IE.} \tag{2.57}$$

This is not surprising since it is equivalent to maximize the gain of the controller at low frequencies (i.e. $\omega \to 0$), and it is well-known that the performance of a control system is provided by the gain of the loop transfer function (typically at low frequencies). The maximization of the integral gain also has a positive impact over reference tracking (or disturbances entering at the process output), since the IE due to a unit step reference is equal to $(P(0)k_i)^{-1}$. However, the reference tracking capability may be improved by using set-point weighting [120], a particular implementation of a control system with 2 DOF when the feedback controller is a PID.

Example 2.9. The aim of this example is to analyze through a particular plant, the relation between the approximation $\text{IAE} \approx \text{IE}$ and the value of $\|S\|_\infty$. We consider the same plant model and controller that were considered in Example 2.8. Figure 2.22 shows the boundary of the stabilizing region (red dashed line), and level curves for the IAE (gray) and $\|S\|_\infty$ (black). Observe that the region where the level curves of the IAE are horizontal, contains the controller parameters that satisfy $\text{IAE} = \text{IE} = k_i^{-1}$.

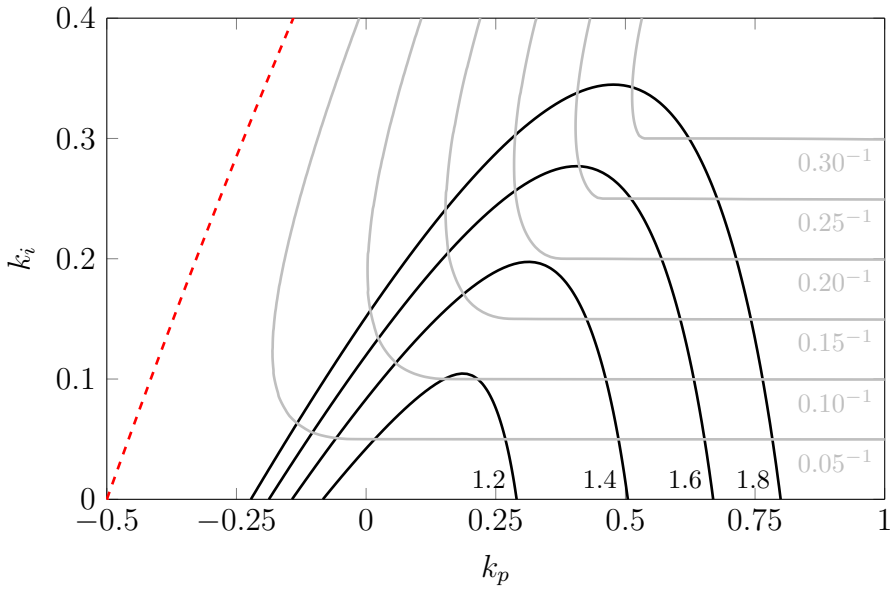

Figure 2.22 Time-domain performance in the controller parameter space

Level curves of IAE (gray) and $\|S\|_\infty$ (black) for Example 2.9. The red dashed line corresponds to the boundary of the stability region.

Regions where the $\mathcal{H}_\infty$-norm of the sensitivity takes relatively low values, i.e. ≤ 1.4, also guarantee that IAE $\approx$ IE.

2.3.2 PID Design via Optimization

A natural way of stating the control design problem is by using a mathematical optimization problem. Several control design methods, such as LQR/LQG or $\mathcal{H}_\infty$, pose the control design problem in this way. A wide variety of problems involving design can be cast in the form of a mathematical optimization problem. This is about making the best possible choice, with respect to a predefined criterion, from a set of candidates choices, that typically have to satisfy some specifications (constraints). In general, an optimization problem has the following form:

$$\begin{array}{ll} \underset{\mathbf{x}}{\text{minimize}} & f_0(\mathbf{x}) \\ \text{subject to} & f_i(\mathbf{x}) \leq 0, \ i = 1, \ldots, m. \end{array} \tag{2.58}$$

In the latter problem, the vector $\mathbf{x} \in \mathbb{R}^n$ is the *optimization variable*, the function $f_0 : \mathbb{R}^n \to \mathbb{R}$ is the *objective* function, and the functions $f_i : \mathbb{R}^n \to \mathbb{R}$, $i = 1, \ldots, m$, are the *constraint* functions.

In the case of PID design, the optimization variable will be the vector of controller parameters, and the specifications will be used as objective and constraint functions. The specification that is considered as most important will play the role of objective function. At this point, it is very important to formulate the optimization problem in a way that it captures all the specifications of the control systems. Although optimization methods are very powerful, they may yield unrealistic solutions, when some specifications are not stated [19]. Unfortunately, this situation is not uncommon in the PID control literature, there are several methods in which some index for performance is optimized, but robustness is not taken into account. These methods may result in controllers with very low robustness levels [19].

Some caveats of optimization methods are that it is possible the presence of many local minimum and the numerical algorithm may be trapped in one of them. On the other hand, the obtainment of a solution may require excessive computational burden. Fortunately, some classes of optimization problem can be efficiently and reliably solved due to is particular structure, e.g. linearity and convexity. See Appendix A for more details about optimization problems.

The design of PID controllers is usually stated as a constrained optimization problem

$$\begin{aligned} \underset{\mathbf{x}}{\text{minimize}} \quad & f_0(\mathbf{x}, \boldsymbol{\theta}) \\ \text{subject to} \quad & f_i(\mathbf{x}, \boldsymbol{\theta}) \leq 0, \ i = 1, \ldots, m. \end{aligned} \tag{2.59}$$

where $\mathbf{x}$ is the design (controller) parameter vector, and $\boldsymbol{\theta}$ is a vector of plant model parameters. A very popular approach is the IE or IAE minimization under constraints on the $\mathcal{H}_\infty$ norm of $S(s)$, $T(s)$, $P(s)S(s)$, and/or $C(s)S(s)$. This has been thoroughly studied. Early work focusing on robustness constrained IE minimization was presented in [22, 203]. Efficient convex-optimization-based algorithms for solving the same problem were recently presented in [119]. Constrained minimization of IAE has been investigated in [98]. Efficient gradient-based algorithms for the same problem were proposed [106]. Simultaneous synthesis of PID controllers and measurement filter was addressed in [236].

In the forthcoming chapters, several control design problems stated as optimization problems will be presented. This thesis addresses the problem of designing PID controllers for plants with large uncertainty. In any real-world control system, the parameters of the plant model are seldom known exactly during the modeling phase, or they usually change as the environment or the operation point changes. In contrast to most of the available tuning methods, that are specifically developed for some nominal values of the plant model parameters, here the goal is to obtain a design

method for plant models with ignorance in its parameters, i.e. it will be assumed that vector of plant parameters belong to a given set that represents the plant model uncertainty. Obviously, it can be argued that available methods already account for plant uncertainty since they usually include some robustness specifications for a nominal plant parameters vector. Here, the design has a stronger emphasis on robustness, since some stability margins are guaranteed for each value of the process parameters in its uncertainty interval.

2.3.3 Literature on PID Design under Parametric Uncertainty

Some approaches that tackle the problem of designing PID controllers under parametric uncertainty are reviewed as follows.

Kharitonov's theorem [155] and related results can be used to study the stability of interval plants (with possibly fixed delay). In order to ensure some margins of stability, a virtual gain-phase margin tester (see [117]) may be added, leading to stability margins in the form of gain and phase margins. Applications of these results to the design of PID controllers has been reported in [135]. The drawbacks of these methods are the inability to deal with stronger stability margins (e.g. maximum sensitivity functions) and uncertainty in the time delay.

Faced with the issue of design PID controllers in presence of interval parametric uncertainty subject to maximum sensitivity functions, several works have been published, see among others [89, 143, 179, 268, 269]. In general, this problem is very hard to solve, since it is necessary to consider all the plants belonging to a given set of plants. Most of them use a brute force approach, which is based on gridding the uncertainty set[10]. Another interesting approach to deal with interval plants is the use of interval techniques [141], these techniques can be applied to a generalized n-th order transfer function, but they rely on some algorithms that are very time-consuming, e.g. SIVIA [141]. Some applications of these techniques to PID control have been reported in [45, 154].

Automatic loop shaping (ALS) methods for QFT that consider a fixed control structure can be particularized to the design of PID controllers. There are several papers that deal with this problem [56, 89, 142, 270, 281, 282]. They differ in the choice of optimization techniques. The paper [89] combines local and global optimization with constraints in the form of Horowitz-Sidi bounds in the Nichols plane. Optimization is done using standard Matlab routines. In [282] the controller is chosen

[10]The QFT approach of using boundaries of the templates is hardly found on the PID literature.

from computations of a set of controllers. In the paper [270] the design specifications are translated into constraints on the controller parameter space and the controller is then chosen by optimization. Similar to [269], it works only with two controller parameters, iterations are necessary with more controller parameters. An approach using evolutionary optimization is proposed in [56]. In [281], the problem is formulated as an unconstrained optimization problem that is solved using the Nelder-Mead method. A procedure based on deterministic interval global optimization techniques and consistency methods is presented in [142].

The chapters ahead will present different design methods for uncertain plants. Some of them are tailored to simple parametric models, while others are able to deal with nonparametric models or probabilistic models.

Chapter 3

PI Design for an Uncertain ITD Plant

3.1 Introduction

This chapter is focused on the problem of tuning PI controllers for ITD plants having interval parametric uncertainty. ITD plant models are common and important in the modeling task for the process industry. This model is extensively used, for example, in level systems, pulp and paper plants, oil-water-gas separators in the oil industry, etc. [254, 256]. It also appears on simplified Saint-Venant equations to model irrigation canals for control design purpose [163–165], where this model is referred to as integrator delay (ID) model. In addition to processes presented in low-level control loops, it is also used to model supply chain management (SCM) processes [71, 75]. Recent works on ITD plants controlled by PID-type controllers have been reported in [10, 70, 158]. The work [10] applies direct synthesis method to design the PID controller, it matches the characteristic equation of the system, after applying a Padé approximation, with a desired characteristic equation. The paper [70] proposes a nonlinear modification of a PI controller, in particular, a reset controller and a design method for ITD plants. The work [158] proposed a design based on Internal Model Control (IMC) principles.

The method proposed here is based on the parameter space approach [1, 229], without using time-delay approximations or ignoring parameter uncertainties. These are two important features. On the one hand, it is well known that some time-delay approximations can lead to instability [230]. On the other hand, most of the tuning rules are usually based on a nominal plant model [201], whereas in practice the model usually varies with the operation point, or simply it is not known precisely. In addition,

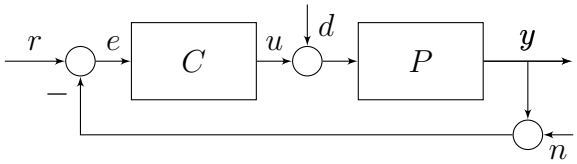

Figure 3.1 1-DOF feedback control system.

since the PI controller has just two tuning parameters, the parameter space approach is quite suitable for control design [219].

Specifically, in PI(D) control, the formulation of the control design problem with parametric uncertainty has previously been approached in a number of works, see for example [136, 143, 269]. However, in all these previous works, the design method comes up with an algorithmic or graphical procedure to obtain the optimum value of the controller parameters. This problem is usually solved with a brute force approach (by gridding the uncertainty set). This chapter will show how to solve this problem by considering only two ITD plants, and that a solution in form of a tuning rule can be obtained without introducing too much conservatism.

The outline of this chapter is as follows. Section 3.2 describes the problem at hand. The main results of this chapter are presented in Sections 3.3 and 3.4. Section 3.3 provides an equivalent control design problem that only involves two plants, making a key simplification of the original problem. Section 3.4 presents a tuning rule for an uncertain ITD plant, which is based on the solution of the simplified control problem. Some design examples that illustrate the proposed tuning rule are given in Section 3.5.

3.2 Problem Statement

The considered control system setup is the 1-DOF feedback control system shown in Figure 3.1, where r is the reference input, y is the plant output, $e = r - y$ is the error, d is the disturbance input, and u is the controller output. Here, C is the controller, and P is the plant.

3.2.1 Plant and Controller Structures

A plant that is modeled by an ITD model is mathematically described by the transfer function

$$P(s) = \frac{k}{s} e^{-sh}, \tag{3.1}$$

where k is the (velocity) gain and h is the time delay. This model is also a good approximation to lag dominant FOTD models. They are given by the transfer function

$$P(s) = \frac{K}{\tau s + 1} e^{-sh}, \tag{3.2}$$

where K is the gain, τ is the time constant, and h is the time delay They may be well-approximated by an ITD model like (3.1) with (velocity) gain $k = K/\tau$, when $\tau \gg h$.

This chapter will consider ITD plants with potentially large parametric uncertainty. An uncertain ITD plant $\mathcal{P}$ is represented by an indexed family of transfer functions like (3.1), where the gain k and the time delay h have values in the intervals $[k_1, k_2]$ and $[h_1, h_2]$, respectively. Therefore, the index set $\Theta = [k_1, k_2] \times [h_1, h_2]$ represents the interval uncertainty of the plant. Without loss of generality, we assume that Θ belongs to the first quadrant of the real plane. That implies that all the processes have positive steady-state gain and positive time delay. The uncertain ITD plant $\mathcal{P}$ is given by

$$\mathcal{P} = \left\{ P(s, \boldsymbol{\theta}) = \frac{k}{s} e^{-sh} : \boldsymbol{\theta} = [k \; h]^\top \in \Theta \right\}. \tag{3.3}$$

On the other hand, the PI controller is given by the following transfer function

$$C(s, \mathbf{x}) = k_p + \frac{k_i}{s}, \tag{3.4}$$

where $\mathbf{x} = [k_p \; k_i]^\top$ is the vector of controller parameters. In control practice, the integration time T_i is often used instead of the integral gain k_i, that is defined as $T_i = k_p/k_i$. However, it is more convenient to use the parameter k_i for the derivation of results in this work. For example, the stabilizing set, in the controller parameter space, is more conveniently expressed in terms of k_p and k_i. By using T_i, the stabilizing sets extend until infinite values of T_i, see for example [136].

Finally, for any vector of plant parameters $\boldsymbol{\theta} \in \Theta$ the corresponding loop transfer function is defined as $L(s, \mathbf{x}, \boldsymbol{\theta}) = C(s, \mathbf{x}) P(s, \boldsymbol{\theta})$.

3.2.2 Control Design Specifications

This section presents a set of specifications for the closed-loop system. These specifications are based on the ones presented in Chapter 2 and must be met for every plant belonging to the set $\mathcal{P}$, or equivalently for any vector of plant parameters $\boldsymbol{\theta}$ belonging to the set Θ.

Robust Stability

A common design specification is to place an upper bound on the magnitude of the sensitivity transfer function, that is

$$\|S(\mathbf{x}, \boldsymbol{\theta})\|_\infty \leq M_s, \qquad \forall \theta \in \Theta, \tag{3.5}$$

where the sensitivity bound has to be $M_s > 1$. Remind that the specification $M_s = 1$ is infeasible, due to the Bode's sensitivity integral presented in the previous chapter.

Note that a sensitivity bound implies certain values for the gain and phase margins (see for example [269]) and that (3.5) guarantees a worst-case sensitivity peak over the uncertain plant $\mathcal{P}$.

Robust Set-Point Response

Tracking specification in an 1-DOF feedback control system may be conveniently specified by an upper bound on the magnitude of the complementary sensitivity transfer function, that is

$$\|T(\mathbf{x}, \boldsymbol{\theta})\|_\infty \leq M_t, \qquad \forall \boldsymbol{\theta} \in \Theta, \tag{3.6}$$

where the complementary sensitivity bound has to be $M_t > 1$. Again, this imposes a worst-case complementary sensitivity peak over the uncertain plant $\mathcal{P}$.

Robust Load Disturbance Rejection

A common way to measure the ability to reject disturbances is the IAE due to a load disturbance in the form of a unit step at the plant input, i.e.

$$\text{IAE} = \int_0^\infty |e(t)|\, dt. \tag{3.7}$$

An analytical solution is difficult (if not impossible) to obtain with this criterion. As it is proposed in [16], a simpler approach is to use the IE defined as

$$\text{IE} = \int_0^\infty e(t) dt. \tag{3.8}$$

The main reason for using this criterion is that IE $= 1/k_i$ [19]. On the other hand, the sensitivity constraints guarantee a well-damped system where IE $\approx$ IAE (see [19]).

Note that this objective (maximize k_i) is very convenient for the problem tackled in this chapter since it does not depend on the uncertain parameters of the plant.

These criteria seem quite suitable for the evaluation of performance and robustness, as it has been pointed out, for example, in [5, 105]. Moreover, minimization of IE (or IAE) without constraints may result in control systems with poor robustness [98]. Thus, the problem of minimizing IE subject to robustness constraints as (3.5)–(3.6) is clearly sound for plants with significant uncertainty. Lastly, note that load disturbances may enter at many different places, here disturbances at the plant input are considered. On the other hand, disturbances at the plant output affect in an equivalent way to set-points responses (both paths are defined by the same transfer function, but with opposite sign), in this way the two extreme cases are considered.

3.2.3 Control Design Problem

Before introducing the control design problem as an optimization problem, we need to define some sets, these are defined as

$$f_s(\boldsymbol{\theta}, M_s) \equiv \{\mathbf{x} \in D(\boldsymbol{\theta}) : \|S(\mathbf{x}, \boldsymbol{\theta})\|_\infty \leq M_s\}, \tag{3.9}$$

$$f_t(\boldsymbol{\theta}, M_t) \equiv \{\mathbf{x} \in D(\boldsymbol{\theta}) : \|T(\mathbf{x}, \boldsymbol{\theta})\|_\infty \leq M_t\}, \tag{3.10}$$

where $D(\boldsymbol{\theta})$ is the set of controller parameters that provide closed-loop stability for the plant with parameters $\boldsymbol{\theta}$. The set $D(\boldsymbol{\theta})$ can be easily obtained in the controller parameter space, a method to obtain it was presented in Section 2.3.1.

Furthermore, are also defined the feasible sets where these constraints are met for a given set Θ. These sets are given by

$$F_s(\Theta, M_s) \equiv \bigcap_{\boldsymbol{\theta} \in \Theta} f_s(\boldsymbol{\theta}, M_s), \tag{3.11}$$

$$F_t(\Theta, M_t) \equiv \bigcap_{\boldsymbol{\theta} \in \Theta} f_t(\boldsymbol{\theta}, M_t). \tag{3.12}$$

The elements in theses sets guarantee a worst-case sensitivity and complementary sensitivity peaks (in addition to closed-loop stability) for a set of plants defined by the box Θ.

After defining these sets, the control design problem is formulated as the following constrained optimization problem:

$$\begin{array}{ll} \underset{\mathbf{x}=[k_p \;\; k_i]^\top}{\text{maximize}} & k_i \\ \text{subject to} & \mathbf{x} \in F_s(\Theta, M_s), \\ & \mathbf{x} \in F_t(\Theta, M_t). \end{array} \tag{3.13}$$

The control design problem (3.13) is based on the well-known MIGO approach for PI design presented in [22], but considering a set of plants representing an uncertain plant. This extension of the MIGO approach to a family of plants is not new and has been studied in some previous work, for example [268, 269]. The novelty here is two-fold. First, we prove that it is only necessary to consider two plants in order to obtain a solution to (3.13) when considering an uncertain ITD like (3.3). Second, an approximate solution to (3.13) in form of a tuning rule, for a given values of M_s and M_t, is presented.

3.3 Reformulation of the Optimization Problem

A previous step for the obtainment of the main results of this chapter is the reformulation of the optimization problem (3.13). The constraints of the optimization problem (3.13) will be translated into a normalized controller parameter space. We use $f(\boldsymbol{\theta}, M_s, M_t)$ to denote a set that contains the controller parameters that satisfy both specifications for a given plant parameters vector. That is

$$f(\boldsymbol{\theta}, M_s, M_t) \equiv f_s(\boldsymbol{\theta}, M_s) \bigcap f_t(\boldsymbol{\theta}, M_t). \tag{3.14}$$

Let us denote by $F(\Theta, M_s, M_t) \subset \mathbb{R}^2$ the feasible set of the optimization problem (3.13). This set is given by the intersection of the indexed family of sets $f(\boldsymbol{\theta}, M_s, M_t)$ over $\boldsymbol{\theta} \in \Theta$, that is

$$F(\Theta, M_s, M_t) \equiv \bigcap_{\boldsymbol{\theta} \in \Theta} f(\boldsymbol{\theta}, M_s, M_t). \tag{3.15}$$

In the following, we will show how the feasible set of the optimization problem (3.13), i.e. $F(\Theta, M_s, M_t)$, can be obtained as the intersection of only two plant parameter vectors instead of an infinite number of plant parameter vectors, greatly simplifying the problem at hand.

3.3.1 A Normalized Feasible Set

The nondimensionalizing (also known as scaling or normalizing) should be taken into account whenever a model is developed, with that technique it is possible to simplify and parameterize certain problems [234]. Here, the goal is to reduce the number of parameters by performing a normalization with respect to $\boldsymbol{\theta}$, and to obtain a normalized feasible set $\bar{f}(M_s, M_t)$ that can be used as a pattern to obtain any feasible set $f(\boldsymbol{\theta}, M_s, M_t)$. Firstly, it is necessary to introduce the following normalized variables (they are denoted with a bar):

$$\begin{aligned} \bar{\omega} &\equiv \omega h, \\ \bar{\mathbf{x}} &\equiv [\bar{k}_p \ \bar{k}_i]^\top = [k_p kh \ k_i kh^2]^\top, \\ \bar{\boldsymbol{\theta}} &\equiv [\bar{k} \ \bar{h}]^\top = [1 \ 1]^\top. \end{aligned} \tag{3.16}$$

By using these normalized variables, the loop transfer function is expressed as

$$L(j\bar{\omega}, \bar{\mathbf{x}}, \bar{\boldsymbol{\theta}}) = \left(\bar{k}_p + \frac{\bar{k}_i}{j\bar{\omega}}\right) \frac{1}{j\bar{\omega}} e^{-j\bar{\omega}}. \tag{3.17}$$

Let us define a normalized loop transfer function as

$$\bar{L}(j\bar{\omega}, \bar{\mathbf{x}}) \equiv \left(\bar{k}_p + \frac{\bar{k}_i}{j\bar{\omega}}\right) \frac{1}{j\bar{\omega}} e^{-j\bar{\omega}}. \tag{3.18}$$

Therefore, by using (3.18), the sensitivity (3.5) and the complementary sensitivity (3.6) constraints are also normalized. The sensitivity constraint, for a given frequency, is directly normalized as

$$\left| \frac{1}{1 + \bar{L}(j\bar{\omega}, \bar{\mathbf{x}})} \right| \leq M_s. \tag{3.19}$$

The above inequality corresponds to a region in the $\bar{k}_p - \bar{k}_i$ plane outside the ellipse

$$\frac{M_s^2}{\bar{\omega}^2} \left(\bar{k}_p - \bar{\omega}\sin(\bar{\omega})\right)^2 + \frac{M_s^2}{\bar{\omega}^4} \left(\bar{k}_i - \bar{\omega}^2\cos(\bar{\omega})\right)^2 = 1. \tag{3.20}$$

This expression is obtained by directly substituting (3.18) in (3.19). On the other hand, it is a particular case of the expression given in (2.49). Note that the centers of these ellipses determine the stabilizing set in the controller parameter space [202],

which consists of the straight line $\bar{k}_i = 0$ and a (parametric) curve given by

$$\begin{cases} \bar{k}_p(\bar{\omega}) = \bar{\omega}\sin(\bar{\omega}), \\ \bar{k}_i(\bar{\omega}) = \bar{\omega}^2\cos(\bar{\omega}). \end{cases} \tag{3.21}$$

The normalized sensitivity constraint (3.19) results in a region of the $\bar{k}_p - \bar{k}_i$ plane whose boundary is the envelope of the family of ellipses (with $\bar{\omega}$ as parameter) given by (3.20). This envelope is easily obtained by using (3.20) and its partial derivative with respect to $\bar{\omega}$:

$$\begin{cases} \dfrac{M_s^2}{\bar{\omega}^2}\left(\bar{k}_p - \bar{\omega}\sin(\bar{\omega})\right)^2 + \dfrac{M_s^2}{\bar{\omega}^4}\left(\bar{k}_i - \bar{\omega}^2\cos(\bar{\omega})\right)^2 = 1, \\ 4(1-M_s^2)\bar{\omega}^3 - 2M_s^2\bar{\omega}\bar{k}_p^2 + 2M_s^2\bar{\omega}\cos(\bar{\omega})(\bar{\omega}^2\bar{k}_p + 2\bar{k}_i) \\ +2M_s^2\bar{\omega}^2\sin(\bar{\omega})(3\bar{k}_p - \bar{k}_i) = 0. \end{cases} \tag{3.22}$$

In the end, a feasible set corresponding to (3.19) is obtained by using the envelope (3.22). The envelope of this family of ellipses has two branches, referred to as inner and outer [22]. Since the outer branch does not intersect the stabilizing set, only the inner branch is used. Thus, by combining the inner branch of the envelope (3.22) with the stabilizing set, it is obtained a feasible set where the closed-loop system is stable and the constraint (3.19) holds, see shadow region in Figure 3.2.

On the other hand, the complementary sensitivity constraint (3.6), but for a given frequency, is also normalized to

$$\left|\frac{\bar{L}(j\bar{\omega},\bar{\mathbf{x}})}{1+\bar{L}(j\bar{\omega},\bar{\mathbf{x}})}\right| \leq M_t, \tag{3.23}$$

and, using similar arguments, it can be shown that this constraint defines a feasible region in the $\bar{k}_p - \bar{k}_i$ plane outside a set of ellipses whose envelope is given by the

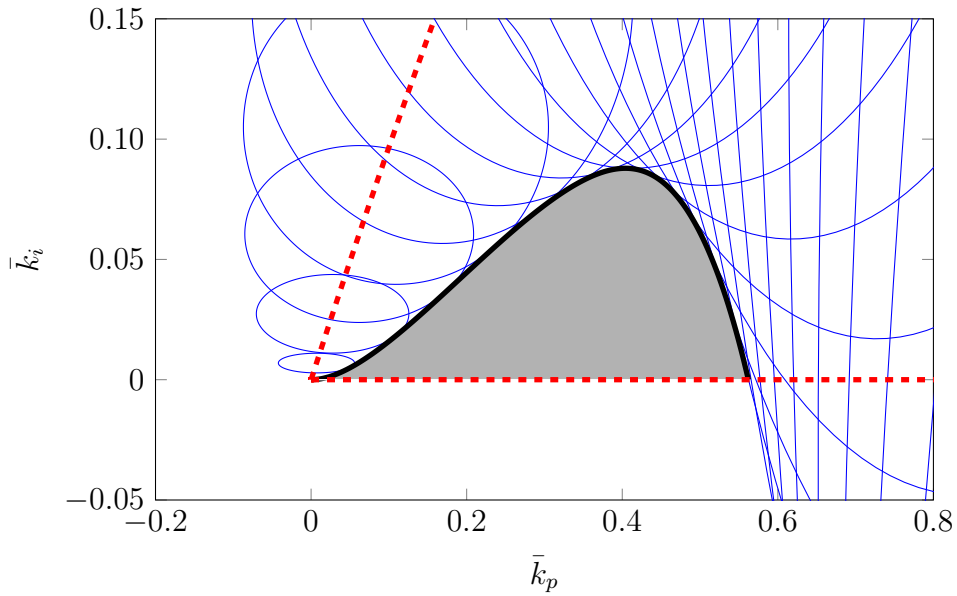

Figure 3.2 Constraint $\|S\|_\infty \leq M_s$ in the controller parameter space

Ellipses sets (blue), stabilizing set boundary (dashed red), envelop inner branch (solid black), and feasible set (shadow region) for $M_s = 1.7$.

following equations:

$$\begin{cases} \dfrac{(M_t^2-1)^2}{M_t^2\bar{\omega}^2}\left(\bar{k}_p - \dfrac{M_t^2\bar{\omega}\sin(\bar{\omega})}{(M_t^2-1)}\right)^2 \\ +\dfrac{(M_t^2-1)^2}{M_t^2\bar{\omega}^4}\left(\bar{k}_i - \dfrac{M_t^2\bar{\omega}^2\cos(\bar{\omega})}{(M_t^2-1)}\right)^2 = 1, \\ (M_t^2-1)(\bar{\omega}^2\bar{k}_p^2 + 2\bar{k}_i^2) + M_t^2\bar{\omega}^2(\bar{\omega}^2\bar{k}_p - 2\bar{k}_i)\cos(\bar{\omega}) \\ -M_t^2\bar{\omega}^3(\bar{k}_p + \bar{k}_i)\sin(\bar{\omega}) = 0. \end{cases} \tag{3.24}$$

Again, we are interested in the inner branch of the envelop of this family of ellipses, see Figure 3.3.

Finally, for some given values M_s and M_t, a normalized feasible set $\bar{f}(M_s, M_t)$ belonging to the $\bar{k}_p - \bar{k}_i$ plane is obtained as the intersection of the two feasible sets obtained above (see the darker area in Figure 3.4). Note that this set is identical to the set $f(\bar{\boldsymbol{\theta}}, M_s, M_t)$ in the $k_p - k_i$ plane. Once $\bar{f}(M_s, M_t)$ has been obtained, the feasible set $F(\Theta, M_s, M_t)$ may be computed by using a mapping from the $\bar{k}_p - \bar{k}_i$ plane to the $k_p - k_i$ plane, directly using (3.16). By definition, for a given vector of plant

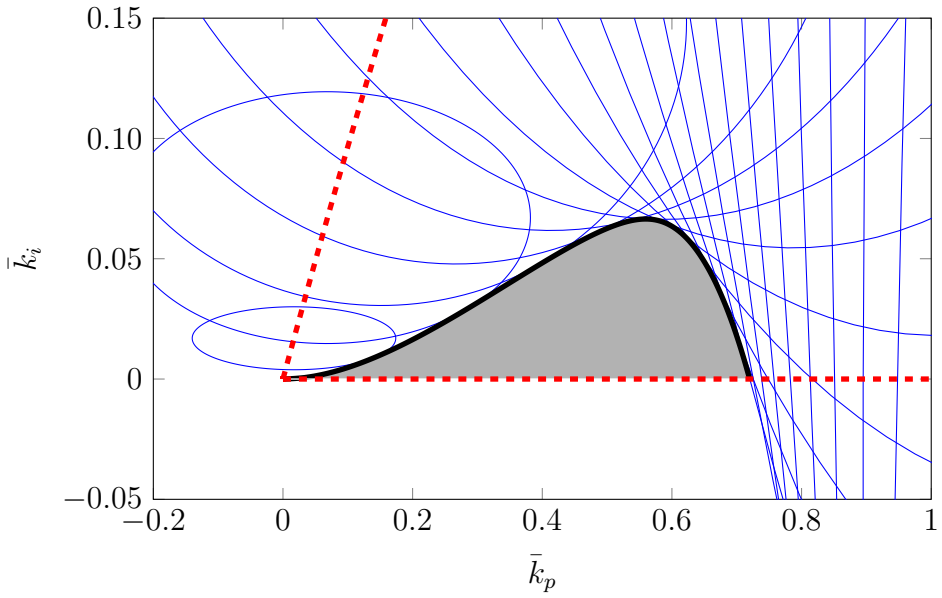

Figure 3.3 Constraint $\|T\|_\infty \leq M_t$ in the controller parameter space

Ellipses sets (blue), stabilizing set boundary (dashed red), envelop inner branch (solid black), and feasible set (shadow region) for $M_t = 1.3$.

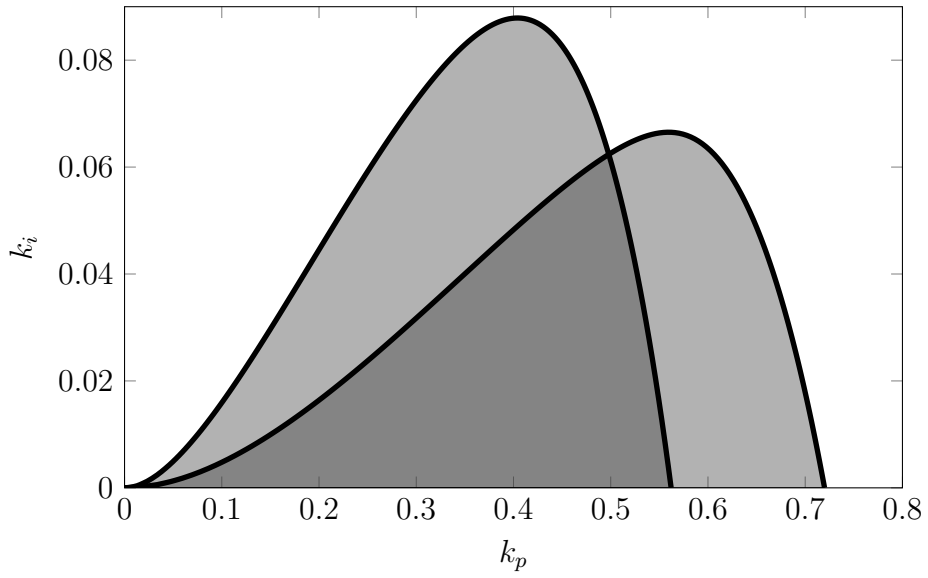

Figure 3.4 Normalized feasible set $\bar{f}(M_s, M_t)$

Normalized feasible set $\bar{f}(M_s, M_t)$ (darker shadow region) for $M_s = 1.7$ and $M_t = 1.3$.

parameters $\boldsymbol{\theta} = [k\ h]^\top$, the mapping $\mathcal{T}_{\boldsymbol{\theta}}$ is defined as

$$[k_p\ k_i]^\top = \mathcal{T}_{\boldsymbol{\theta}}[\bar{k}_p\ \bar{k}_i]^\top \equiv \left[\frac{\bar{k}_p}{kh}\ \frac{\bar{k}_i}{kh^2}\right]^\top. \tag{3.25}$$

Thus, the set $f(\boldsymbol{\theta}, M_s, M_t)$ is directly given by

$$f(\boldsymbol{\theta}, M_s, M_t) = \mathcal{T}_{\boldsymbol{\theta}}\bar{f}(M_s, M_t), \tag{3.26}$$

and finally, using (3.15) and (3.26), the feasible set $F(\Theta, M_s, M_t)$ can be rewritten as

$$F(\Theta, M_s, M_t) = \bigcap_{\boldsymbol{\theta}\in\Theta} \mathcal{T}_{\boldsymbol{\theta}}\bar{f}(M_s, M_t). \tag{3.27}$$

Again with some abuse of notation, the mapping $\mathcal{T}_{\boldsymbol{\theta}}$ is also used to denote the mapping from the $k_p - k_i$ plane to itself, that maps $[k_p\ k_i]^\top$ to $\left[\frac{k_p}{kh}\ \frac{k_i}{kh^2}\right]^\top$. Thus, $\bar{f}(M_s, M_t)$ can be used as a region of the $\bar{k}_p - \bar{k}_i$ plane or of the $k_p - k_i$ plane, indistinctly. In addition, a property of the mapping $\mathcal{T}_{\boldsymbol{\theta}}$ that will be useful is

$$\mathcal{T}_{\boldsymbol{\theta}} f([1\ 1]^\top, M_s, M_t) = \mathcal{T}_{[k\ 1]^\top}\mathcal{T}_{[1\ h]^\top} f([1\ 1]^\top, M_s, M_t) = \mathcal{T}_{[k\ 1]^\top} f([1\ h]^\top, M_s, M_t). \tag{3.28}$$

Now, the mapping $\mathcal{T}_{\boldsymbol{\theta}}$ is acting from the $k_p - k_i$ plane to itself.

Moreover, it is illustrative to show how the mapping $\mathcal{T}_{\boldsymbol{\theta}}$ maps $\bar{f}(M_s, M_t)$ for different values of k and h. Roughly speaking, for a given value of k, $\mathcal{T}_{\boldsymbol{\theta}}\bar{f}(M_s, M_t)$ gives regions as shown in Figure 3.5, in such a way that the intersection of a number of these regions is exactly the region corresponding to the larger value of h (a formal statement and proof will be given in the next section as Proposition 3.1). On the other hand, for a given value of h, $\mathcal{T}_{\boldsymbol{\theta}}\bar{f}(M_s, M_t)$ results in a larger and right-shifted region when $k < 1$, and in a smaller and left-shifted region when $k > 1$. Note that the intersection of a number of these regions corresponds to the intersection of the regions with the extreme values of k as shown in Figure 3.6 (again a formal statement and proof of this fact will be given in the following section as Proposition 3.2).

3.3.2 A Simplified Optimization Problem

Now, it will be shown that in fact the feasible set $F(\Theta, M_s, M_t)$ can be computed by using a finite number of plant parameter vectors $\boldsymbol{\theta}$, greatly simplifying the control design problem.

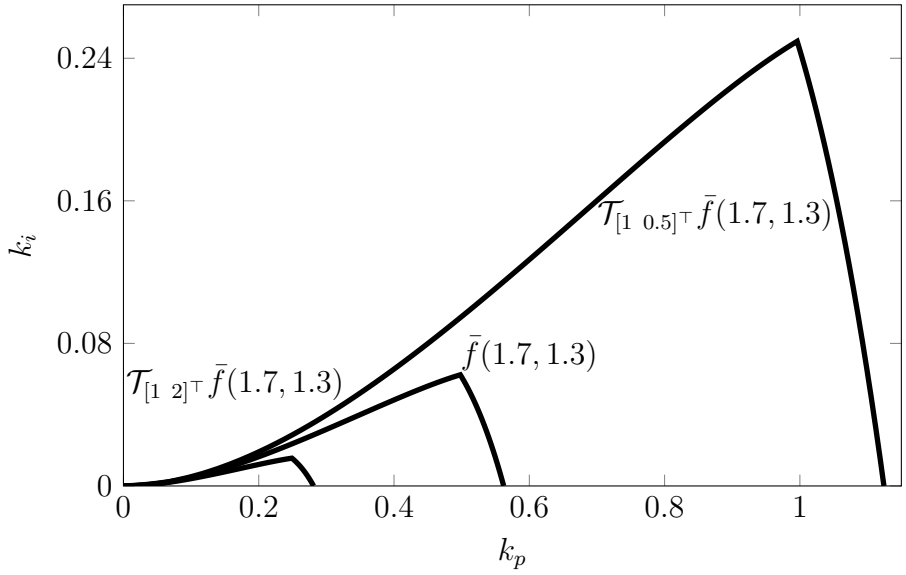

Figure 3.5 Mapping $\mathcal{T}_{[1\ h]^\top}$ over $\bar{f}(M_s, M_t)$

Mapping $\mathcal{T}_{[1\ h]^\top}$ over $\bar{f}(1.7, 1.3)$ for $h = 0.5, 1, 2$.

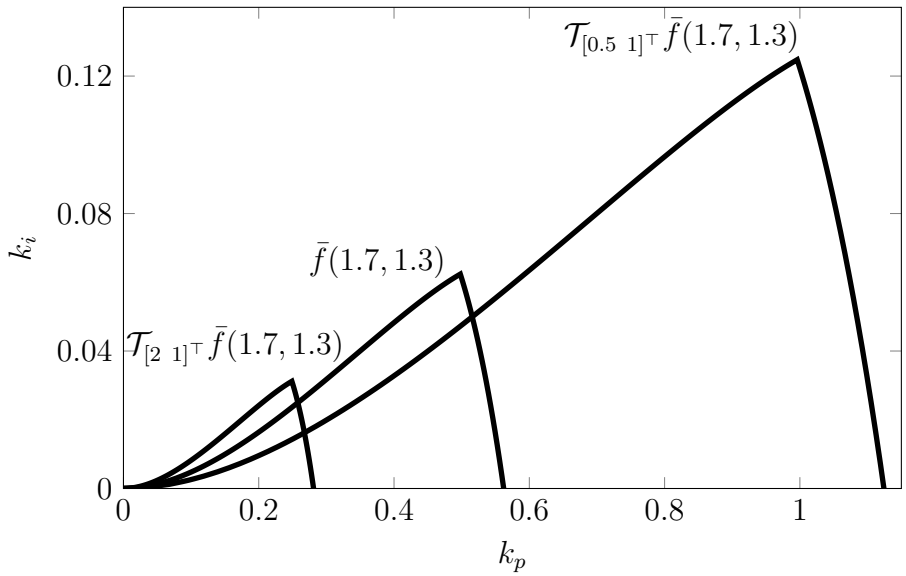

Figure 3.6 Mapping $\mathcal{T}_{[k\ 1]^\top}$ over $\bar{f}(M_s, M_t)$

Mapping $\mathcal{T}_{[k\ 1]^\top}$ over $\bar{f}(1.7, 1.3)$ for $k = 0.5, 1, 2$.

Proposition 3.1. *For a given value of $k \in [k_1, k_2]$,*

$$\bigcap_{h\in[h_1,\,h_2]} f(\boldsymbol{\theta}, M_s, M_t) = f([k\ h_2]^\top, M_s, M_t), \tag{3.29}$$

where $\boldsymbol{\theta} = [k\ h]^\top$.

Proof. Firstly, since the intersection of a number of sets is included in each set, it directly follows that $\bigcap_{h\in[h_1,\,h_2]} f(\boldsymbol{\theta}, M_s, M_t) \subseteq f([k\ h_a]^\top, M_s, M_t)$ for any $h_a \in [h_1, h_2]$, then it is obvious that $\bigcap_{h\in[h_1,\,h_2]} f(\boldsymbol{\theta}, M_s, M_t) \subseteq f([k\ h_2]^\top, M_s, M_t)$.
Secondly, $\bigcap_{h\in[h_1,\,h_2]} f(\boldsymbol{\theta}, M_s, M_t) \supseteq f([k\ h_2]^\top, M_s, M_t)$ will be proved in the following. Consider the controller and plant frequency responses in their polar form

$$\begin{aligned}
C(j\omega, \mathbf{x}) &= k_p + \frac{k_i}{j\omega} = m_c(\omega, \mathbf{x}) e^{j\phi_c(\omega,\mathbf{x})},\\
P(j\omega, \boldsymbol{\theta}) &= \frac{k}{j\omega} e^{-j\omega h} = m_p(\omega, \boldsymbol{\theta}) e^{j\phi_p(\omega,\boldsymbol{\theta})},\\
L(j\omega, \mathbf{x}, \boldsymbol{\theta}) &= C(j\omega, \mathbf{x}) P(j\omega, \boldsymbol{\theta}) = m_l(\omega, \mathbf{x}, \boldsymbol{\theta}) e^{j\phi_l(\omega,\mathbf{x},\boldsymbol{\theta})},
\end{aligned} \tag{3.30}$$

where

$$\begin{aligned}
m_c(\omega, \mathbf{x}) &= \sqrt{k_p^2 + \frac{k_i^2}{\omega^2}}, & \phi_c(\omega, \mathbf{x}) &= -\arctan\frac{k_i}{\omega k_p},\\
m_p(\omega, \boldsymbol{\theta}) &= \frac{k}{\omega}, & \phi_p(\omega, \boldsymbol{\theta}) &= -\frac{\pi}{2} - h\omega,\\
m_l(\omega, \mathbf{x}, \boldsymbol{\theta}) &= m_c(\omega, \mathbf{x}) m_p(\omega, \boldsymbol{\theta}), & \phi_l(\omega, \mathbf{x}, \boldsymbol{\theta}) &= \phi_c(\omega, \mathbf{x}) + \phi_p(\omega, \boldsymbol{\theta}).
\end{aligned} \tag{3.31}$$

The arguments of these functions are dropped most of the time for the sake of brevity. Then, the constraint (3.5) ($\|S(j\omega, \mathbf{x}, \boldsymbol{\theta})\|_\infty \leq M_s$) is equivalent to[1]

$$m_l^2 + 2m_l \cos(\phi_l) + \left(1 - \frac{1}{M_s^2}\right) \geq 0, \tag{3.32}$$

for all nonnegative frequencies. Analogously, the restriction (3.6) ($\|T(j\omega, \mathbf{x}, \boldsymbol{\theta})\|_\infty \leq M_t$) can be stated as

$$m_l^2 \left(1 - \frac{1}{M_t^2}\right) + 2m_l \cos(\phi_l) + 1 \geq 0, \tag{3.33}$$

[1]The quadratic inequalities (3.32) and (3.33) were obtained in [59], within the framework of QFT.

again, for all nonnegative frequencies. In the remain of the proof, it will be demonstrated that $\mathbf{x} = [k_p \ k_i]^\top \in f([k \ h_2]^\top, M_s, M_t)$ implies that $\mathbf{x} \in f(\boldsymbol{\theta}, M_s, M_t)$ for any $h \in [h_1, h_2]$.

Now, $\phi_{l,2}$ and ϕ_l are defined as the angles given by (3.31) corresponding to the time delays h_2 and $h \leq h_2$, respectively. In addition, for a vector of controller parameters $\mathbf{x} \in f([k \ h_2]^\top, M_s, M_t)$, from (3.32)–(3.33) it results that

$$m_l^2 + 2m_l \cos(\phi_{l,2}) + \left(1 - \frac{1}{M_s^2}\right) \geq 0, \tag{3.34}$$

and

$$m_l^2 \left(1 - \frac{1}{M_t^2}\right) + 2m_l \cos(\phi_{l,2}) + 1 \geq 0. \tag{3.35}$$

Regarding restriction (3.32), two cases are possible:

1. $m_l \leq 1 - 1/M_s$. Rewriting as $1 - m_l \geq 1/M_s$ and squaring leads to $m_l^2 - 2m_l + 1 - 1/M_s^2 \geq 0$, therefore (3.32) is met for any value of h.

2. $m_l > 1 - 1/M_s$. By closed-loop stability and by (3.31), it is clear that $-\pi \leq \phi_{l,2} \leq \phi_l < -\pi/2$. As a result, using (3.34) it directly follows that $m_l^2 + 2m_l \cos(\phi_l) + 1 - 1/M_s^2 \geq m_l^2 + 2m_l \cos(\phi_{l,2}) + 1 - 1/M_s^2 \geq 0$, and thus (3.32) is satisfied for any $h \leq h_2$.

Alternatively, regarding restriction (3.33) there are also two possible cases:

1. $m_l \leq (1 + 1/M_t)^{-1}$. Rearranging as $1 - m_l \geq l/M_t$ and squaring leads to $m_l^2(1 - 1/M_t^2) - 2m_l + 1 \geq 0$, therefore (3.33) is met for any value of h.

2. $m_l > (1 + 1/M_t)^{-1}$. Again, since $-\pi \leq \phi_{l,2} \leq \phi_l < -\pi/2$ then $m_l^2(1 - 1/M_t^2) + 2m_l \cos(\phi_l) + 1 \geq m_l^2(1 - 1/M_t^2) + 2m_l \cos(\phi_{l,2}) + 1 \geq 0$ for any $h \leq h_2$.

As a result, restrictions (3.32)–(3.33) are satisfied for any $h \leq h_2$ and thus $\mathbf{x} \in f(\boldsymbol{\theta}, M_s, M_t)$ for any $h \in [h_1, h_2]$. □

Proposition 3.2. *For a given value of* $h \in [h_1, h_2]$,

$$\bigcap_{k \in [k_1, k_2]} f(\boldsymbol{\theta}, M_s, M_t) = f([k_1 \ h]^\top, M_s, M_t) \cap f([k_2 \ h]^\top, M_s, M_t), \tag{3.36}$$

where $\boldsymbol{\theta} = [k \ h]^\top$.

Proof. By using (3.26) and (3.28), it is true that

$$\bigcap_{k\in[k_1,\,k_2]} f(\boldsymbol{\theta}, M_s, M_t) = \bigcap_{k\in[k_1,\,k_2]} \mathcal{T}_{\boldsymbol{\theta}}\bar{f}(M_s, M_t) = \bigcap_{k\in[k_1,\,k_2]} \mathcal{T}_{[k\ 1]^\top} f([1\ h]^\top, M_s, M_t). \quad (3.37)$$

Now, note that $\mathcal{T}_{[k\ 1]^\top}$ acts as a uniform scaling with a scale factor equal to $1/k$, then it follows that the above intersection is given by the extreme values of the interval

$$\bigcap_{k\in[k_1,\,k_2]} f(\boldsymbol{\theta}, M_s, M_t) = \mathcal{T}_{[k_1\ 1]^\top} f([1\ h]^\top, M_s, M_t) \cap \mathcal{T}_{[k_2\ 1]^\top} f([1\ h]^\top, M_s, M_t), \quad (3.38)$$

and using again (3.28) the result directly follows. □

Propositions 3.1 and 3.2 make possible to simplify the optimization problem (3.13) as

$$\begin{aligned} &\underset{\mathbf{x}=[k_p\ k_i]^\top}{\text{maximize}} && k_i \\ &\text{subject to} && \mathbf{x} \in f([k_1\ h_2]^\top, M_s, M_t) \bigcap f([k_2\ h_2]^\top, M_s, M_t). \end{aligned} \quad (3.39)$$

Now, the feasible set of the latter optimization problem is simply given by the intersection of the two sets $f([k_1\ h_2]^\top, M_s, M_t)$ and $f([k_2\ h_2]^\top, M_s, M_t)$, given by some extreme values of the plant parameters.

3.3.3 Illustration of Results in the Nichols Plane

We consider here an example with the aim of illustrating the previous results. Propositions 3.1 and 3.2 guarantee that a design considering the plant parameter vectors $[k_1\ h_2]^\top$ and $[k_2\ h_2]^\top$ will be valid for any plant defined by a vector $\boldsymbol{\theta} \in \Theta = [k_1, k_2] \times [h_1, h_2]$, in terms of satisfaction of specifications over the upper bound on $\|S(\mathbf{x}, \boldsymbol{\theta})\|_\infty$ and $\|T(\mathbf{x}, \boldsymbol{\theta})\|_\infty$, in addition to closed-loop stability.

Let us consider an uncertain ITD plant that is defined by the set $\Theta = [0.5, 1.5] \times [0.5, 1.5]$ and a vector of controller parameters that satisfies $\mathbf{x} = [0.1628\ 0.0156]^\top \in F_s(\Theta, 1.5)$, i.e., $\mathbf{x}$ guarantees closed-loop stability and $\|S(\mathbf{x}, \boldsymbol{\theta})\|_\infty \leq 1.5$ for all $\boldsymbol{\theta} \in \Theta$. Although the results were obtained for $F(\Theta, M_s, M_t)$, by taking a sufficiently high value of M_t, we obtain $F(\Theta, M_s, M_t) = F_s(\Theta, M_s)$.

Figure 3.7 shows the constraint imposed to the loop transfer function by the specification $\|S(\mathbf{x}, \boldsymbol{\theta})\|_\infty \leq 1.5$ (red region), some compensated templates for the frequencies $\omega \in [0.03\ 0.05\ 0.075\ 0.125\ 0.5\ 1.75]$ (green regions), and Nichols plots corresponding to the plants with parameters $[k_1\ h_2]^\top$ and $[k_2\ h_2]^\top$. This figure shows how the satisfaction of $\|S(\mathbf{x}, \boldsymbol{\theta})\|_\infty \leq 1.5$ for these extreme plants guarantees that the same specification is also met for any plant defined by Θ.

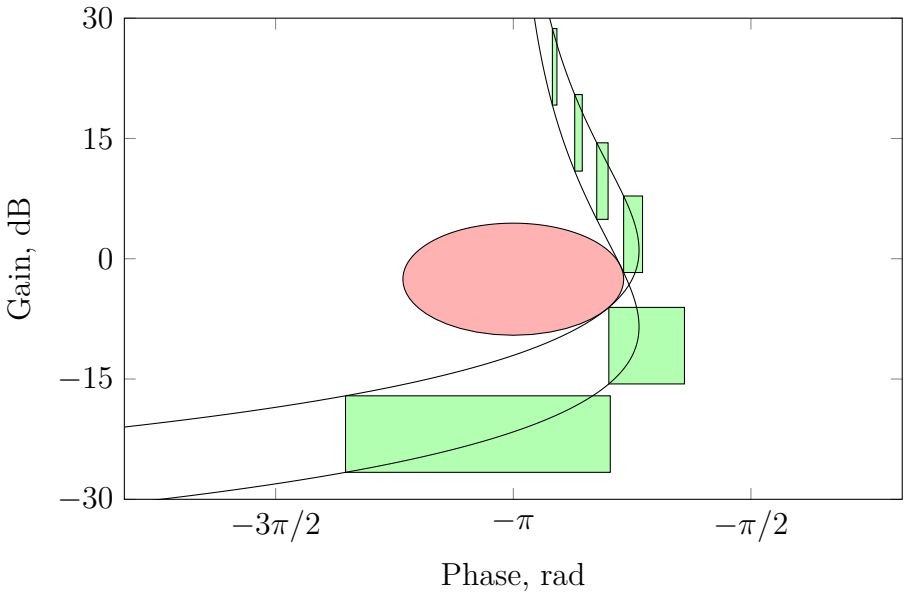

Figure 3.7 Nichols plot of a PI with a family of ITD plants

Compensated templates (green regions), inverse M-circle (red region), and Nichols plots of some extreme plants.

3.4 A PI Tuning Rule for Uncertain ITD Plants

In spite of this simplification for the computation of $F(\Theta, M_s, M_t)$, the optimization problem (3.39) is still hard to solve in a closed form. Nevertheless, it will be shown how an approximation of the normalized set $\bar{f}(M_s, M_t)$ can efficiently solve the optimization problem without introducing an excessive conservatism. The key idea is to use an inner approximation to the set $\bar{f}(M_s, M_t)$. We propose to use a polygon $\bar{f}_p(M_s, M_t)$ satisfying $\bar{f}_p(M_s, M_t) \subset \bar{f}(M_s, M_t)$, in such a way that an inner approximation to any set $f(\boldsymbol{\theta}, M_s, M_t)$ can be obtained as follows:

$$f_p(\boldsymbol{\theta}, M_s, M_t) \equiv \mathcal{T}_{\boldsymbol{\theta}} \bar{f}_p(M_s, M_t) \subset \mathcal{T}_{\boldsymbol{\theta}} \bar{f}(M_s, M_t) = f(\boldsymbol{\theta}, M_s, M_t). \tag{3.40}$$

Here, the polygon $\bar{f}_p(M_s, M_t)$ is defined by approximating $\partial \bar{f}(M_s, M_t)$ by straight line segments, where $\partial \bar{f}(M_s, M_t)$ denotes the boundary of $\bar{f}(M_s, M_t)$. In this way, a feasible set $F_p(\Theta, M_s, M_t) \subset F(\Theta, M_s, M_t)$ defined as

$$F_p(\Theta, M_s, M_t) \equiv f_p([k_1 \ h_2]^\top, M_s, M_t) \bigcap f_p([k_2 \ h_2]^\top, M_s, M_t), \tag{3.41}$$

Table 3.1 Points of polygon $\bar{f}_p(1.7, 1.3)$

Point	k_p	k_i
1	0.0096	0.0000
2	0.0560	0.0009
3	0.1642	0.0104
4	0.4979	0.0623
5	0.5621	0.0000

may be used to formulate an approximate form of the optimization problem (3.13) as

$$\begin{array}{ll} \underset{\mathbf{x}=[k_p \;\; k_i]^\top}{\text{maximize}} & k_i \\ \text{subject to} & \mathbf{x} \in F_p(\Theta, M_s, M_t). \end{array} \tag{3.42}$$

Note that since $F_p(\Theta, M_s, M_t) \subset F(\Theta, M_s, M_t)$, an optimal solution to this problem is a suboptimal solution to the optimization problem (3.13). We will show how an appropriate choice of $\bar{f}_p(M_s, M_t)$ may lead to suboptimal solutions that are very close to the optimal ones.

3.4.1 Proposed Tuning Rule

We define $\bar{f}_p(1.7, 1.3)$ as a pentagon (see Figure 3.8), whose coordinates are given in Table 3.1. In addition, the side of this polygon with vertex i and j is denoted as $\bar{S}_{i,j}(M_s, M_t)$. In this way, the polygons $f_p(\boldsymbol{\theta}, M_s, M_t)$ and its sides $S_{i,j}(\boldsymbol{\theta}, M_s, M_t)$ are obtained by means of

$$\begin{aligned} f_p(\boldsymbol{\theta}, M_s, M_t) &\equiv \mathcal{T}_{\boldsymbol{\theta}} \bar{f}_p(M_s, M_t), \\ S_{i,j}(\boldsymbol{\theta}, M_s, M_t) &\equiv \mathcal{T}_{\boldsymbol{\theta}} \bar{S}_{i,j}(M_s, M_t). \end{aligned} \tag{3.43}$$

Finally two polygons, $f_p([k_1 \;\; h_2]^\top, M_s, M_t)$ and $f_p([k_2 \;\; h_2]^\top, M_s, M_t)$, define the approximated feasible set $F_p(\Theta, M_s, M_t)$. These polygons differ only by a scaling factor, since $\mathcal{T}_{[k \;\; 1]^\top}$ acts as a uniform scaling. Thus, the point with maximum k_i in the approximated feasible set $F_p(\Theta, 1.7, 1.3) = f_p([k_1 \;\; h_2]^\top, 1.7, 1.3) \bigcap f_p([k_2 \;\; h_2]^\top, 1.7, 1.3)$ is given by the intersection of the side $S_{4,5}([k_1 \;\; h_2]^\top, 1.7, 1.3)$ with $S_{3,4}([k_2 \;\; h_2]^\top, 1.7, 1.3)$, $S_{2,3}([k_2 \;\; h_2]^\top, 1.7, 1.3)$ or $S_{1,2}([k_2 \;\; h_2]^\top, 1.7, 1.3)$, depending on the value of the ratio

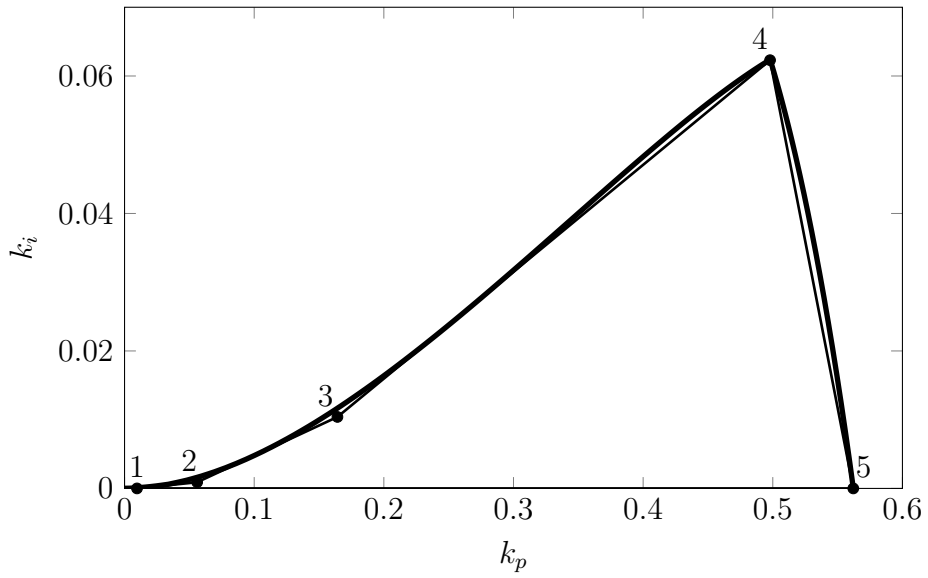

Figure 3.8 Approximation of the normalized feasible set

Approximation of the normalized feasible set by using a polygon $\bar{f}_p(1.7, 1.3) \subset \bar{f}(1.7, 1.3)$.

between k_2 and k_1. These three cases will appear explicitly in the expression of the proposed tuning rule. This fact is illustrated in Figure 3.9, where some polygons are plotted for several values of k and a given value of h. Note that for low values of the ratio k_2/k_1 the solution of the optimization problem lies on the intersection between $S_{4,5}([k_1\ h_2]^\top, 1.7, 1.3)$ and $S_{3,4}([k_2\ h_2]^\top, 1.7, 1.3)$ (see $k_2/k_1 = 1.5$ in Figure 3.9). When this ratio increases, the solution lies on the intersection between $S_{4,5}([k_1\ h_2]^\top, 1.7, 1.3)$ and $S_{2,3}([k_2\ h_2]^\top, 1.7, 1.3)$ (see $k_2/k_1 = 5$ in Figure 3.9). Finally for higher values of this ratio the solution lies on the intersection between $S_{4,5}([k_1\ h_2]^\top, 1.7, 1.3)$ and $S_{1,2}([k_2\ h_2]^\top, 1.7, 1.3)$.

After some straightforward calculations, it is obtained that the value of $\mathbf{x} = [k_p\ k_i]^\top$ that solves the optimization problem (3.42) is

$$[k_p\ k_i]^\top = \begin{cases} S_{3,4}([k_2\ h_2]^\top, 1.7, 1.3) \bigcap S_{4,5}([k_1\ h_2]^\top, 1.7, 1.3), & \dfrac{k_2}{k_1} \in [1, 3.2), \\ S_{2,3}([k_2\ h_2]^\top, 1.7, 1.3) \bigcap S_{4,5}([k_1\ h_2]^\top, 1.7, 1.3), & \dfrac{k_2}{k_1} \in [3.2, 9.9), \\ S_{1,2}([k_2\ h_2]^\top, 1.7, 1.3) \bigcap S_{4,5}([k_1\ h_2]^\top, 1.7, 1.3), & \dfrac{k_2}{k_1} \in [9.9, 50]. \end{cases} \tag{3.44}$$

A direct application of (3.44) (details are omitted for brevity and because it involves straightforward but tedious calculations) results in the following tuning rule. The value

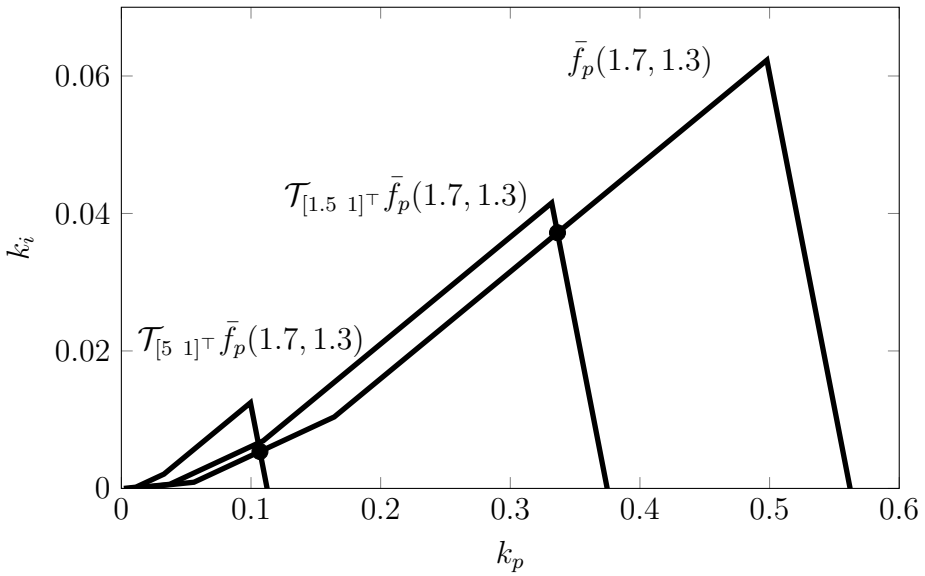

Figure 3.9 Intersections for different values of k_2/k_1

Polygons $\bar{f}_p(1.7, 1.3)$, $f_p([1.5\ 1]^\top, 1.7, 1.3)$ and $f_p([5\ 1]^\top, 1.7, 1.3)$. Intersections for different values of k_2/k_1 are denoted with a dot.

of $\mathbf{x}$ that solves the optimization problem (3.42) is

$$\begin{aligned} k_p &= \frac{\alpha}{h_2 k_2}, \\ k_i &= \frac{\beta}{h_2^2 k_2}, \end{aligned} \tag{3.45}$$

where α and β are given by

$$\begin{aligned} \alpha &= \alpha_0 \left(1 + \alpha_1 \frac{k_2}{k_1}\right), \\ \beta &= \beta_0 \left(1 - \beta_1 \frac{k_2}{k_1}\right). \end{aligned} \tag{3.46}$$

In general, the values of α_0, α_1, β_0, and β_1 depend on the specifications M_s and M_t, and also on the value of k_2/k_1. These values are shown in Table 3.2 for $M_s = 1.7$ and $M_t = 1.3$ (for other values of M_s and M_t these values may be obtained by repeating the procedure exposed here).

The tuning rule presented in this section depends on the approximation of the feasible set. Note that the chosen approximation provides a good trade-off between simplicity and accuracy, since a more accurate approximation of the feasible set will be

Table 3.2 Parameters of the obtained tuning rule

k_2/k_1	α_0	α_1	β_0	β_1
[1, 3.2)	0.485	0.028	0.075	0.173
[3.2, 9.9)	0.516	0.007	0.045	0.081
[9.9, 50]	0.551	0.0003	0.011	0.017

necessarily based on the use of a polygon with more vertices, and thus it would result in a more intricate tuning rule.

3.4.2 Tuning Rule for a Nominal ITD Plant

The proposed tuning rule has been developed for an uncertain ITD plant. Now, the rule is particularized to a nominal plant, i.e. with gain $k = k_1 = k_2$ and time delay $h = h_1 = h_2$. As a result, equations (3.45)–(3.46) give the following tuning rule:

$$\begin{aligned} k_p &= \frac{0.499}{hk}, \\ k_i &= \frac{0.062}{h^2 k}. \end{aligned} \tag{3.47}$$

These values are almost identical to the ones given by the Simple/Skogestad Internal Model Control (SIMC) rule for ITD plants (when using the recommended value for the closed-loop time constant $T_c = h$) [233]. The values given by the latter are

$$\begin{aligned} k_p &= \frac{0.5}{hk}, \\ k_i &= \frac{0.0625}{h^2 k}. \end{aligned} \tag{3.48}$$

The proposed tuning rule (3.45)–(3.46) can be seen as an extension of the SIMC rule for ITD plants with significant uncertainty. As the uncertainty is larger, an SIMC-based tuning (necessarily based on a nominal parameters choice) will result in a poorly tuned PI for the whole set of plants, which can even result in an unstable design for some parameters values. In contrast, the proposed tuning rule will give a close-to-optimal solution to the optimization problem (3.13).

3.4.3 Analysis with the Performance Portrait Method

A tuning rule for a PI controller with an ITD plant can be analyzed with the closed-loop performance portrait method, that has been recently presented in [136, 137]. We consider the following performance indexes for the unit step set-point response:

- IAE,
- overshoot,
- settling time,

and for the unit step disturbance response:

- IAE,
- maximum deviation,
- settling time.

Both settling times are given with respect to the standard 5 % criterion. Note that overshoot and settling time for step set-point response, and maximum deviation and settling time for step disturbance response were not considered in [136], but their use can be easily justified making use of the same arguments that are exposed in [136]. Basically, this work uses normalization properties of the Laplace transform.

In Figure 3.10, level curves of the performances indexes are shown (with values that may depend on k or h), jointly with the boundary of the stabilizing region (red dashed line) and the polygon $\bar{f}_p(1.7, 1.3)$ (black solid line). The presented tuning rule provides controller parameters that remain inside the polygon $\bar{f}_p(1.7, 1.3)$. Some interesting properties of the presented tuning rule are given as follows:

1. The IAE for disturbance response is almost identical to the IE, that implies that the response to step disturbances is not oscillatory. Therefore, the approximation IAE $\approx$ IE in the region $f_p(\boldsymbol{\theta}, 1.7, 1.3)$ is well justified.
2. The overshoot for set-point response is always less than 30 %.

These properties justify the election of the specifications $M_s = 1.7$ and $M_t = 1.3$. Note that higher values of M_s and M_t lead to oscillatory responses to step disturbances and higher overshoots for step references.

Lastly, these figures also allow us to analyze a posteriori these performance indexes for a given plant and controller parameters.

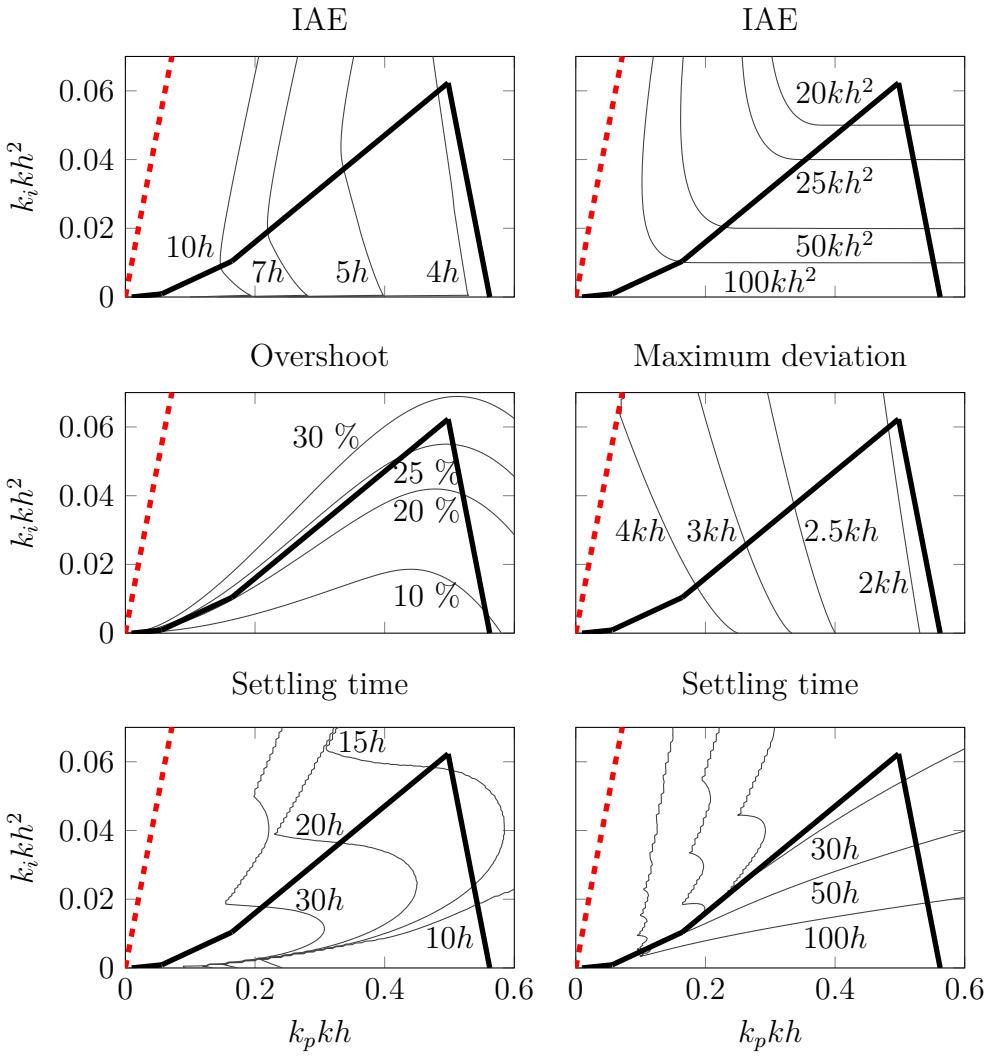

Figure 3.10 Performance indexes in the normalized controller parameter space

Performance indexes for step response (first column) and for disturbance rejection (second column). Stabilizing region (red dashed line) and the polygon $\bar{f}_p(1.7, 1.3)$ (black solid line).

3.5 Examples

This section includes some examples that illustrate the obtained tuning rule. The ultimate goal of this chapter is to present a simple way to tune a PI controller for an uncertain ITD plant. The following examples will show that a PI controller tuned with the rule (3.45)–(3.46) can ensure a close-to-optimum behavior, according to the optimality criterion and constraints of the optimization problem (3.13).

Example 3.1. Consider an ITD plant with parametric uncertainty represented by the set of plants

$$\mathcal{P} = \left\{ \frac{k}{s} e^{-sh} : [k \; h]^\top \in \Theta = [1, 2.5] \times [1, 2.5] \right\}. \tag{3.49}$$

The proposed tuning rule (3.45)–(3.46) provides the PI parameters $k_p = 0.0830$ and $T_i = 30.74$. This solution yields a suboptimal value IE $= 370.37$, while the optimum value is $\text{IE}_{\text{opt}} = 357.14$. (Figure 3.8 showed that the approximation done is not very conservative.)

The obtained controller is compared with other methods from the literature. We obtain the solution to the optimization problem (3.13) by using the numerical method recently proposed in [177] (this method will be presented in Chapter 5), and also a PI tuned with SIMC [233] for a nominal plant corresponding to $k = (k_1 + k_2)/2$ and $h = (h_1 + h_2)/2$. The first method yields the parameters $k_p = 0.0836$ and $T_i = 29.86$, while the latter obtains $k_p = 0.1633$ and $T_i = 14$. The comparison is shown in Figures 3.11 and 3.12, where the plant output and controller output are shown for a unit step disturbance entering at the plant input and for a unit step reference, respectively.

This example has illustrated that the approximation used in order to obtain a simple tuning rule is not overly conservative (proposed tuning rule and optimization method [177] yield very similar results). In addition, it has shown that the application of a nominal tuning rule for an uncertain plant may result in a very poor performance and robustness; in the presented case, very oscillatory responses and worst case for the sensitivity higher than 4 (recommended values are within the range $1.2-2.0$ as indicated in [19]). The proposed tuning rule, that takes into account parametric uncertainty, allows for easily obtaining a robust design; removing the difficulties associated with solving a robust optimization problem or the application of a conventional tuning rule for a nominal plant taken from a set of plants.

Finally, we consider the situation in which the tuning rule is applied to a plant with larger uncertainty intervals. Let us consider an uncertain plant described by the

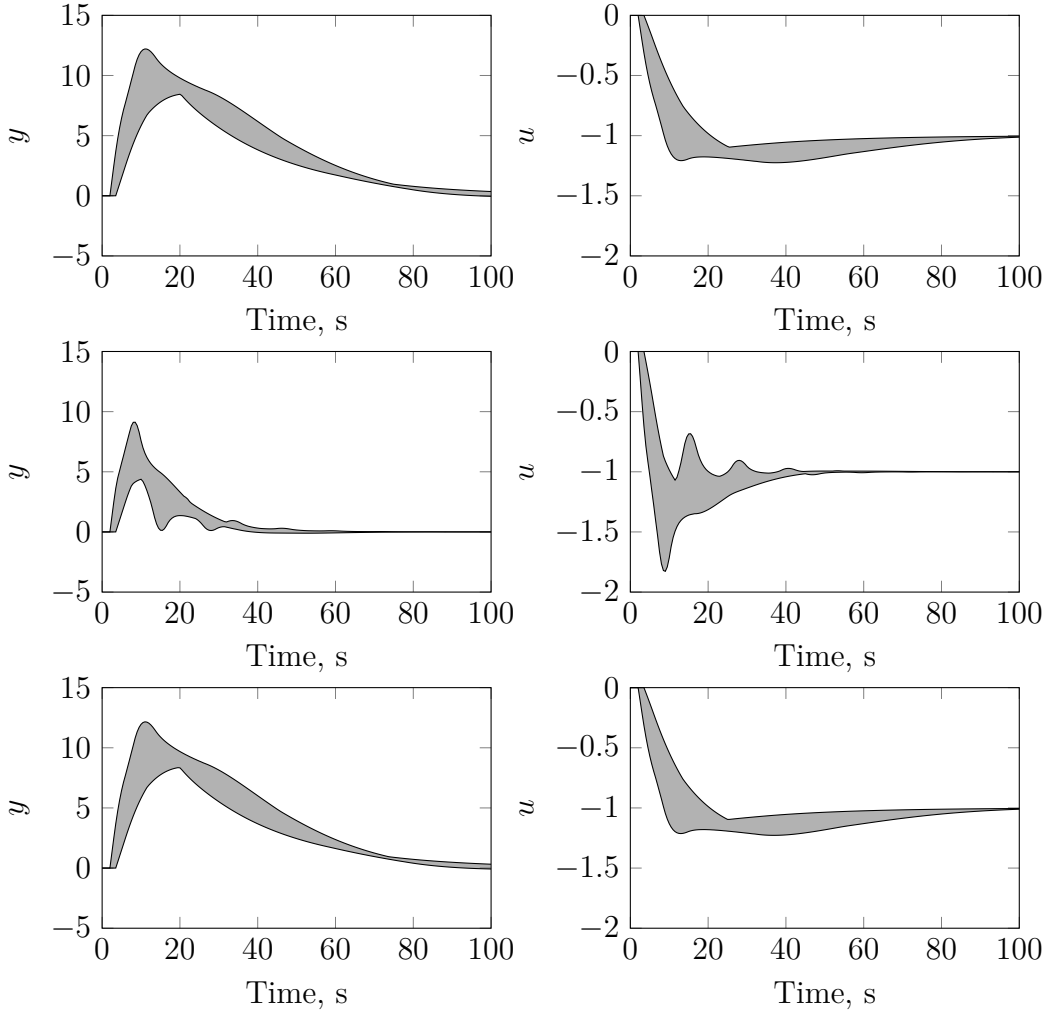

Figure 3.11 Disturbance rejection (Example 3.1)

Plant output (left) and controller output (right) due to a unit step disturbance. Proposed tuning rule (3.45)–(3.46) (top), SIMC tuning rule [233] (middle), and optimization method [177] (bottom).

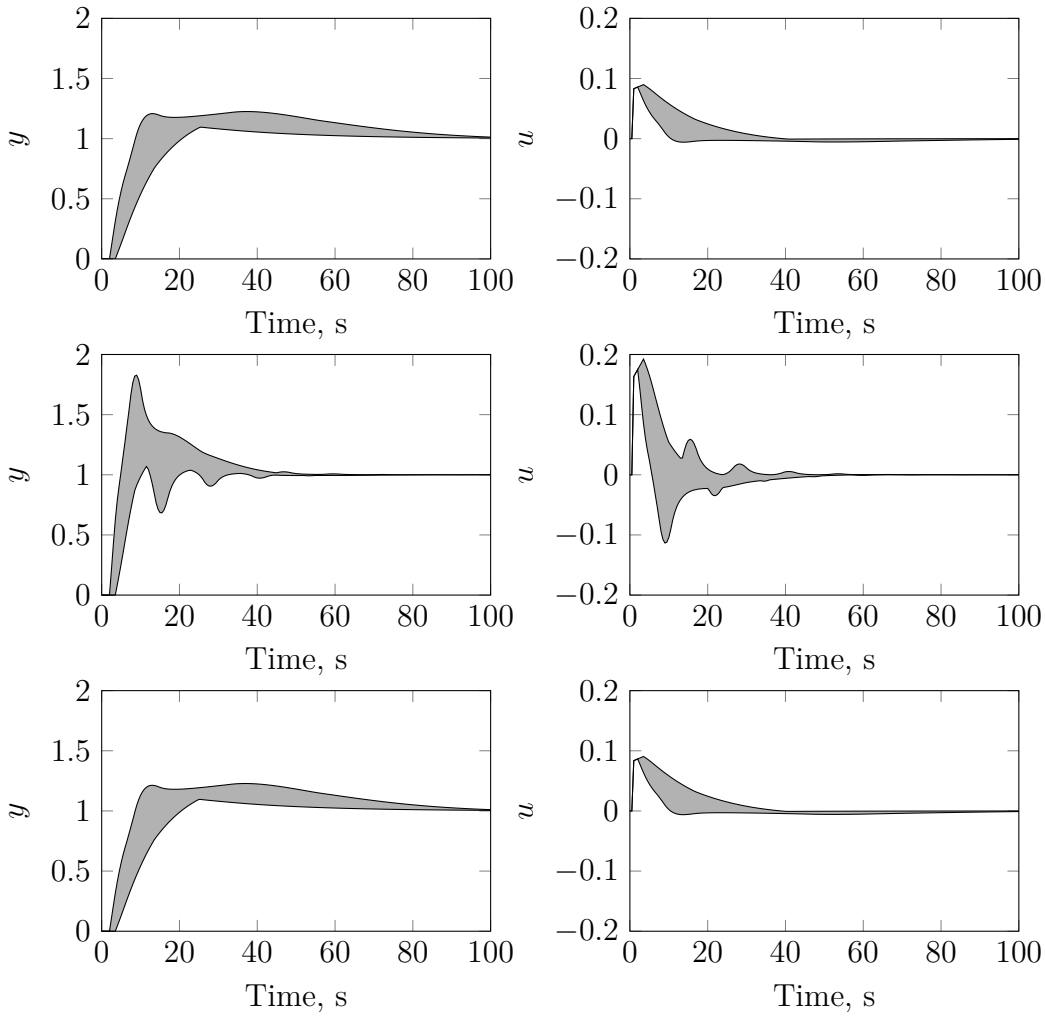

Figure 3.12 Reference tracking (Example 3.1)

Plant output (left) and controller output (right) due to a unit step reference. Proposed tuning rule (3.45)–(3.46) (top), SIMC tuning rule [233] (middle), and optimization method [177] (bottom).

set $\Theta = [1, 5] \times [1, 5]$. In this case, the proposed tuning rule provides the parameters $k_p = 0.0214$ and $T_i = 100$. The obtained value of the IE is 4669, which is close to the optimum value of 4539. Again the application of the SIMC tuning rule for some nominal plant gives a closed-loop system with poor performance (even the closed-loop system is unstable for some plant parameters).

Example 3.2 (Application to an irrigation canal pool)**.** We take this example from the literature [163–165], it considers the problem of distant downstream PI control of irrigation canals. The canal pool is represented by the model

$$Y = P(s)U_1 + P_d(s)(U_2 + P) = \frac{e^{-\tau_d s}}{A_d s}U_1 - \frac{1}{A_d s}(U_2 + P), \tag{3.50}$$

with three inputs u_1, u_2, and p, and one output y. Here, the signal u_1 is the deviation from upstream discharge, u_2 is the deviation from downstream discharge, y is the deviation from downstream water elevation, and finally p is the outlet discharge; in addition, A_d is the equivalent backwater area and τ_d is the delay (for a deeper treatment see [163]). In distant downstream control schemes, the control variable is the upstream discharge u_1 and the controlled variable is the downstream water level y. The feedback control system is shown in Figure 3.13, the inputs u_2 and p enter as a disturbance $d = u_2 + p$.

In practice, the robust control design problem consists of tuning a PI controller for the canal pool operating at different hydraulic conditions (high and low flow conditions and tuned and untuned situations [165]). This can be modeled by an uncertain ITD plant, where different plant parameters correspond to different hydraulic conditions. These parameters, presented in Table 3.3, are taken from [165], and correspond to a real-world example. (The reader is referred to [165] for a more detailed exposition of the different hydraulic conditions.) Note that in this control problem, although the disturbance is at the output, the value of the IE index with respect to a unit step output disturbance is (by using the final value theorem of the Laplace transformation)

$$\text{IE} = \int_0^\infty e(\tau)d\tau = \lim_{s\to 0} s\frac{-P_d(s)}{1 + P(s)C(s)}\frac{1}{s^2} = \lim_{s\to 0}\frac{\frac{1}{A_d s}}{1 + \frac{e^{\tau_d s}}{A_d s}\left(k_p + \frac{k_i}{s}\right)}\frac{1}{s} = \frac{1}{k_i}, \tag{3.51}$$

that is the same value of the IE for a unit step input disturbance. Thus, the control design problem can be recast as the optimization problem (3.13), for which the PI tuning rule (3.45)–(3.46) has been proposed as solution.

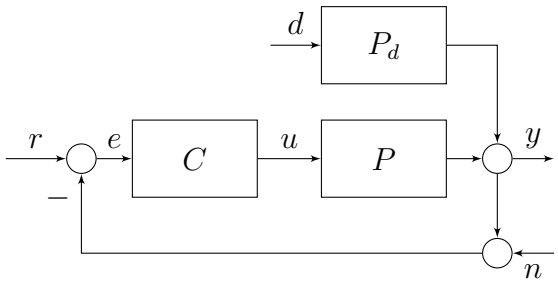

Figure 3.13 Feedback control system of a canal pool (Example 3.2)

Table 3.3 Model parameters (Example 3.2)

τ_d, s	A_d, m^2
308	775
315	752
238	546
247	501

A set of plants corresponding to different hydraulic conditions is characterized by

$$\mathcal{P} = \left\{ \frac{k}{s} e^{-sh} : [k\ h]^\top \in \left[\frac{1}{775}, \frac{1}{501} \right] \times [238, 315] \right\}. \tag{3.52}$$

A direct application of the tuning rule defined by (3.45)–(3.46) and Table 3.2 results in the controller parameters $k_p = 0.8048$ and $T_i = 2874.3$.

Figure 3.14 shows temporal responses, for different hydraulic conditions, to a disturbance of 0.2 m^3/s occurring at time 600 s. Although the PI controller designed in [165] has better performance for some indexes (e.g. a minor settling time after perturbation), this is at the cost of having worse robustness levels in terms of peaks of sensitivity and complementary sensitivity functions. A clear advantage of the proposed method is that it follows directly from a tuning rule, while the method presented in [165] is based on an iterative procedure ("guided trial-and-error" method).

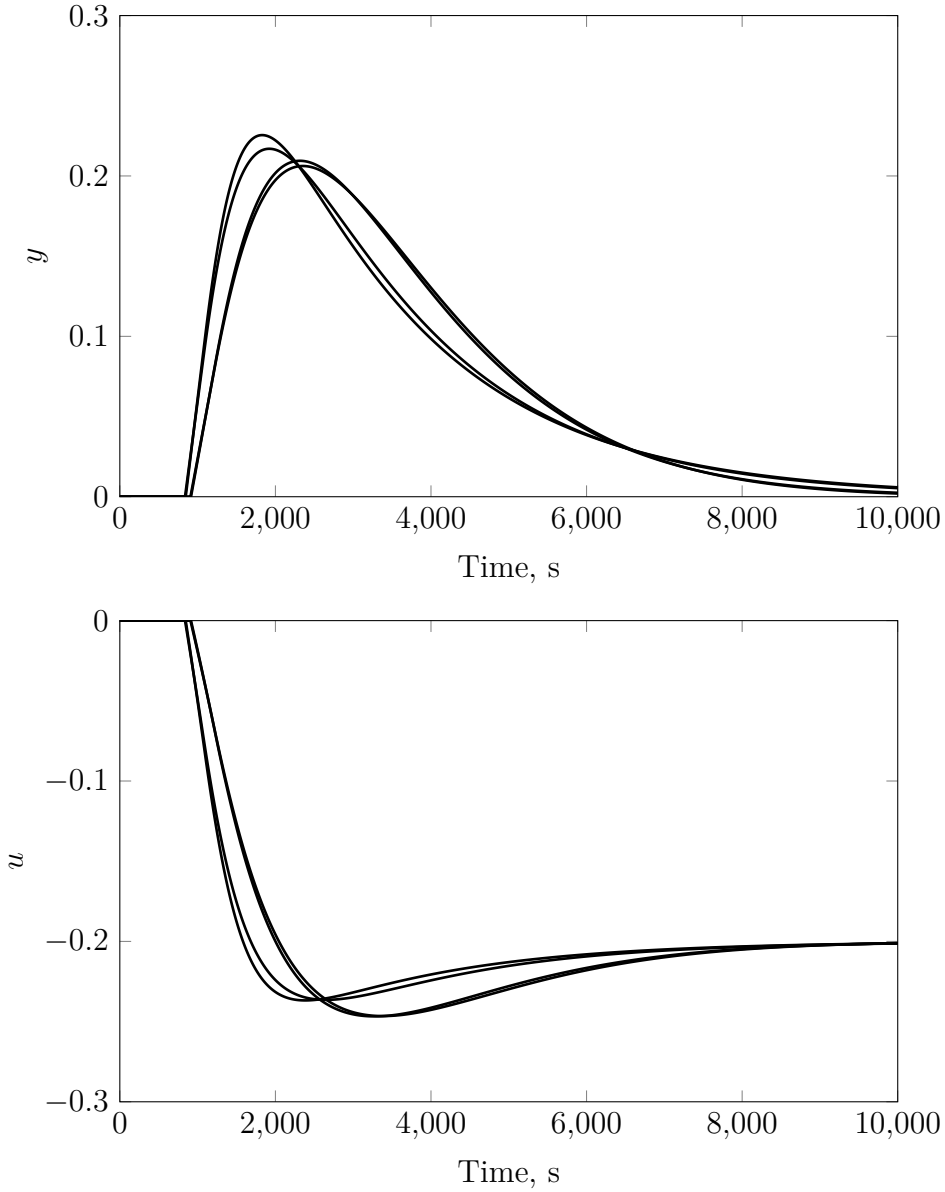

Figure 3.14 Disturbance rejection (Example 3.2)

Disturbance rejection response for different plant parameters (shown in Table 3.3), which correspond to different hydraulic conditions. Plant output (top) and controller output (bottom).

Chapter 4

PID Design for an Uncertain FOTD Plant

4.1 Introduction

This chapter addresses the design of PID controllers for uncertain FOTD plants. The vast majority of process dynamics encountered in industry can be approximately modeled by an FOTD model [227], which is mathematically described by the following transfer function:

$$P(s) = \frac{k}{\tau s + 1} e^{-sh}, \tag{4.1}$$

where k is the steady-state gain, h is the time delay, and τ is the time constant of the process.

The aim of this chapter is to devise a simple method to design PID controllers for FOTD plant models in presence of parametric uncertainty. We will derive conditions under which a solution to the design problem can be obtained by considering only an instrumental fractional-order plant, that is representative in a certain sense of the considered uncertain plant model.

The outline of this chapter is as follows. Section 4.2 describes the problem at hand. Section 4.3 presents the control design problem as a robust optimization problem. Section 4.4 presents the main results of this work that allow to approximate the robust optimization problem. In Section 4.5, some examples are discussed.

4.2 Problem Statement

We consider the same 1-DOF feedback control system of Figure 3.1, that was considered in the previous chapter, where r is the reference input, $e = r - y$ is the error, u is the controller output, d is the disturbance input, n is the measurement noise, and y is the plant output. The controller and the plant are C and P, respectively.

4.2.1 Plant Model and Uncertainty Description

Uncertainty associated with the plant model can be modeled as a set of transfer functions. Here, an FOTD model with unknown-but-bounded parameters is assumed. Therefore, the following set of transfer functions is used throughout this chapter to model an uncertain plant

$$\mathcal{P} = \left\{ P(s,\boldsymbol{\theta}) = \frac{k}{\tau s + 1} e^{-sh} : \boldsymbol{\theta} = [k \; h \; \tau]^\top \in \Theta \right\}, \tag{4.2}$$

where $\Theta = [k_1, k_2] \times [h_1, h_2] \times [\tau_1, \tau_2]$ with $k_1, h_1, \tau_1 \geq 0$. We will use the polar form $P(j\omega,\boldsymbol{\theta}) = m_p(\omega,\boldsymbol{\theta}) e^{j\phi_p(\omega,\boldsymbol{\theta})}$ of the frequency response, where

$$\begin{aligned} m_p(\omega,\boldsymbol{\theta}) &= \frac{k}{\sqrt{1+\tau^2\omega^2}}, \\ \phi_p(\omega,\boldsymbol{\theta}) &= -\arctan \tau\omega - h\omega. \end{aligned} \tag{4.3}$$

As it was introduced in Section 2.2, the interval parametric uncertainty can be graphically represented in the complex plane or Nichols plane using templates (or value sets), these contain information about gain and phase of the frequency response. This representation of uncertainty plays a crucial role in QFT, where it is used to define an open-loop gain-phase shaping procedure (see for example [25, 125]). Here, the purpose is to simplify this problem specifically for FOTD plants, by using a nominal fractional-order plant that is representative of the uncertain plant $\mathcal{P}$.

A template is the set of all frequency response values at a given frequency. More precisely, a template $\mathcal{P}_\omega$ for the uncertain plant $\mathcal{P}$ is defined as

$$\mathcal{P}_\omega = \{ P(j\omega,\boldsymbol{\theta}) : \boldsymbol{\theta} \in \Theta \}. \tag{4.4}$$

A key point in this work is the use of a fractional-order system that is representative of the uncertain plant $\mathcal{P}$. A (nominal) fractional-order plant $P^F(s)$ is proposed to

characterize the set of plants defined by Θ, it is mathematically described by

$$P^F(s) = \sqrt{\frac{(1-\tau_2 s)(1+\tau_2 s)}{(1-\tau_1 s)(1+\tau_1 s)}}\frac{k_2}{\tau_2 s+1}e^{-sh_2}. \tag{4.5}$$

Note that when there is no time-constant uncertainty (i.e. $\tau_1 = \tau_2$), this plant is described by a rational-order transfer function with time delay. This representative plant depends on some of the parameters that define the uncertainty box Θ, this dependence is implicit in the formulation.

Again, it is introduced the polar form $P^F(j\omega) = m_p^F(\omega)e^{j\phi_p^F(\omega)}$, where

$$\begin{aligned} m_p^F(\omega) &= \frac{k_2}{\sqrt{1+\tau_1^2\omega^2}}, \\ \phi_p^F(\omega) &= -\arctan\tau_2\omega - h_2\omega. \end{aligned} \tag{4.6}$$

From (4.3) and (4.6), the following relations are obtained:

$$\begin{aligned} \phi_p^F(\omega) &= \phi_p(\omega, \boldsymbol{\theta}_2) \leq \phi_p(\omega, \boldsymbol{\theta}), \\ m_p^F(\omega) &= m_p(\omega, \boldsymbol{\theta}_1) \geq m_p(\omega, \boldsymbol{\theta}), \end{aligned} \tag{4.7}$$

for $\omega \geq 0$ and $\boldsymbol{\theta} \in \Theta$, where $\boldsymbol{\theta}_1 = [k_2\ h_2\ \tau_1]^\top$ and $\boldsymbol{\theta}_2 = [k_2\ h_2\ \tau_2]^\top$.

Figure 4.1 illustrates the properties presented in equation (4.7), this figure shows the templates (or value sets) and the point corresponding to $P^F(j\omega)$ in the Nichols plane, for an uncertain plant with parameters $k_1 = h_1 = \tau_1 = 0.5$ and $k_2 = h_2 = \tau_2 = 1$. Observe that the point corresponding to $P^F(j\omega)$ is located at the upper left corner of the minimum area rectangle containing $\mathcal{P}_\omega$.

4.2.2 Controller

The PID controller, with a second-order filter with time constant T_f, is given by the transfer function

$$C(s, \mathbf{x}) = \left(k_p + \frac{k_i}{s} + k_d s\right)\left(\frac{1}{1+sT_f+s^2T_f^2/2}\right), \tag{4.8}$$

with the vector of controller parameters $\mathbf{x} = [k_p\ k_i\ k_d\ T_f]^\top$ (design parameters), it is reasonable to assume that all elements belonging to $\mathbf{x}$ are nonnegative, with the exception of k_i that is assumed to be positive (this is necessary in order to guarantee zero steady-state error for a step reference or disturbance). When considering a PI

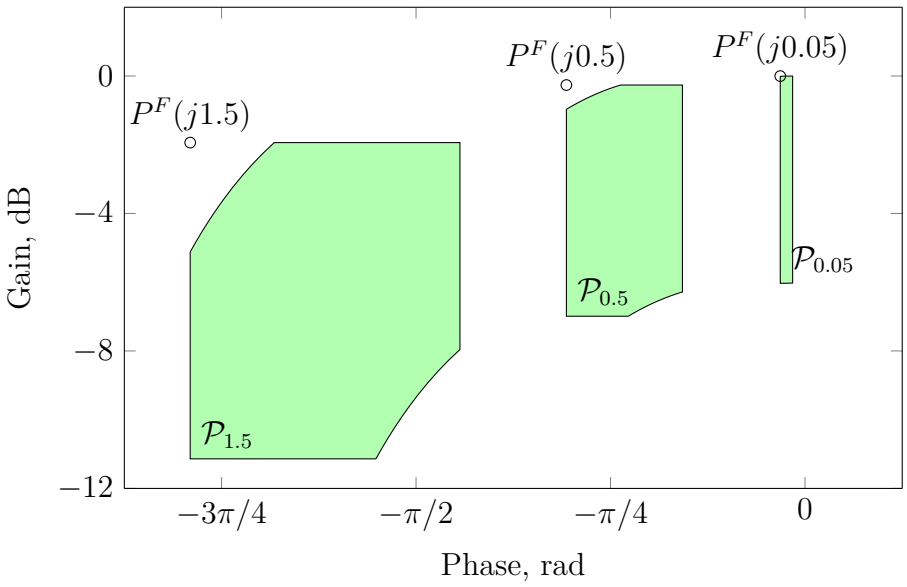

Figure 4.1 Templates for an uncertain FOTD plant

Templates $\mathcal{P}_\omega$ (green regions) and points corresponding to $P^F(j\omega)$ (circles) for some frequencies in the Nichols plane.

controller ($k_d = 0$), a first order filter is recommended. Other filter structures are possible [6, 115], but this choice keeps the number of parameters as low as possible.

4.2.3 Loop Transfer Function

The loop transfer function is denoted as $L(s, \mathbf{x}, \boldsymbol{\theta}) = C(s, \mathbf{x})P(s, \boldsymbol{\theta})$. Using the polar form of the controller $C(j\omega, \mathbf{x}) = m_c(\omega, \mathbf{x})e^{j\phi_c(\omega, \mathbf{x})}$, the polar form of the loop transfer function is given by $L(j\omega, \mathbf{x}, \boldsymbol{\theta}) = m_l(\omega, \mathbf{x}, \boldsymbol{\theta})e^{j\phi_l(\omega, \mathbf{x}, \boldsymbol{\theta})}$, where

$$\begin{aligned} m_l(\omega, \mathbf{x}, \boldsymbol{\theta}) &= m_c(\omega, \mathbf{x})m_p(\omega, \boldsymbol{\theta}), \\ \phi_l(\omega, \mathbf{x}, \boldsymbol{\theta}) &= \phi_c(\omega, \mathbf{x}) + \phi_p(\omega, \boldsymbol{\theta}). \end{aligned} \tag{4.9}$$

A property about $\phi_l(\omega, \mathbf{x}, \boldsymbol{\theta})$, that we will use later, is stated as follows

$$\phi_l(\omega, \mathbf{x}, \boldsymbol{\theta}) \leq \frac{\pi}{2}, \tag{4.10}$$

for all $\omega \geq 0$, under the assumptions made about the design and plant parameters. This property can be easily sketched, at low frequencies $\phi_l(\omega, \mathbf{x}, \boldsymbol{\theta})$ tends to $-\pi/2$ rad due to the presence of the integrator (present in the controller), and the unique elements able to add phase are the two zeros (present in the controller), which add a maximum

of $\pi/2$ rad each one, or equivalently, π rad in the case of a pair of complex zeros. The rest of the elements (i.e. poles and delay) subtract phase.

At this point is important to consider the loop transfer function that will result from considering the previously introduced fractional-order plant. This plant will be used as an auxiliary tool to design a controller for the set of plants $\mathcal{P}$. The nominal (fractional-order) loop transfer function $L^F(s,\mathbf{x}) = C(s,\mathbf{x})P^F(s)$ has the polar representation $L^F(j\omega,\mathbf{x}) = m_l^F(\omega,\mathbf{x})e^{j\phi_l^F(\omega,\mathbf{x})}$, where

$$\begin{aligned} m_l^F(\omega,\mathbf{x}) &= m_c(\omega,\mathbf{x})m_p^F(\omega), \\ \phi_l^F(\omega,\mathbf{x}) &= \phi_c(\omega,\mathbf{x}) + \phi_p^F(\omega). \end{aligned} \tag{4.11}$$

It is worth pointing out that fractional-order system theory is a well-established topic and has been successfully used in many engineering disciplines including control engineering [62, 188] and, in particular, PID control [172]. Regarding the (fractional-order) loop transfer function $L^F(s,\mathbf{x})$, it is worth noting that the most well-known stability criterion in the field of fractional-order systems is only applicable to the particular case of fractional-order systems commonly known as *fractional differential systems of commensurate order* [188], and this is not the case of the fractional-order system under consideration in this chapter (obtained from (4.5)). It should be pointed out that the loop transfer function $L^F(s,\mathbf{x}) = C(s,\mathbf{x})P^F(s)$ has 2 singularities (branch points) in the open right-half plane (ORHP) when $\tau_2 > \tau_1$, at $s = \tau_1^{-1}$ (due to the denominator) and $s = \tau_2^{-1}$ (due to the numerator). Results presented in [187] show that the closed-loop is unstable due to the presence of branch points in the ORHP (instabilities caused by unstable branch points cannot be removed by feedback). This is not a problem and it should not lead to a confusion, since the fractional-order system is only instrumental for the design of the PID controller.

Henceforward, dependency with respect to plant and controller parameters may be omitted for brevity in some cases.

4.2.4 Control Design Specifications

The issue of closed-loop stability is of utmost importance when applying feedback control to any plant. While feedback controllers with sufficiently high gain immunize the closed-loop system against model uncertainties and unknown disturbances, they have a destabilizing effect on any practical plant. However, plain stability is not sufficient (e.g. an asymptotically stable closed-loop system may have a quasi-infinite

settling time or a small variation in a parameter may lead to instability); therefore it is essential to consider any type of stability margin.

As in the previous chapter, we will consider the $\mathcal{H}_\infty$-norm of the sensitivity and complementary sensitivity as stability margins.

Sensitivity. The value of $|S(j\omega, \mathbf{x}, \boldsymbol{\theta})|^{-1} = |1 + L(j\omega, \mathbf{x}, \boldsymbol{\theta})|$ is equal to the distance from the point on the Nyquist curve (corresponding to frequency ω) to the critical point -1. Then, the maximum of the sensitivity (i.e. $\|S(\mathbf{x}, \boldsymbol{\theta})\|_\infty$) is equal to the inverse of the smallest distance to the critical point. Desirable values for $\|S(\mathbf{x}, \boldsymbol{\theta})\|_\infty$ are in the range from 1.2 to 2 (as indicated in the reference [19]).

Complementary sensitivity. The complementary sensitivity as robustness measure indicates how large additive uncertainty can be added to the plant before losing stability. If the plant changes from $P(s, \boldsymbol{\theta})$ to $P(s, \boldsymbol{\theta}) + \Delta P(s)$ being $\Delta P(s)$ stable, a condition for stability is

$$\left|\frac{\Delta P(j\omega)}{P(j\omega, \boldsymbol{\theta})}\right| < \left|\frac{1}{T(j\omega, \mathbf{x}, \boldsymbol{\theta})}\right|, \quad \forall \omega \geq 0. \tag{4.12}$$

Then, $\|T(\mathbf{x}, \boldsymbol{\theta})\|_\infty$ is clearly another robustness measure, which desirable values are in the same range as $\|S(\mathbf{x}, \boldsymbol{\theta})\|_\infty$.

As it is usual in this thesis, a strong emphasis on the robustness is stated. In fact, the same stability margins are required for any instance of the uncertain plant. This is to say, it is required the same stability margins for any plant belonging to set of plants $\mathcal{P}$.

After guaranteeing closed-loop stability with pre-specified stability margins, the following step is to consider the performance of the controller. Load disturbance attenuation is the main concern in process control [227], the ability to reject load disturbances is usually measured using the IAE, defined as

$$\text{IAE} = \int_0^\infty |e(t)|\, dt, \tag{4.13}$$

where $e(t)$ is the error due to a unit step disturbance entering at the plant input. With this criterion it is difficult (if not impossible) to obtain an analytical solution. As it is proposed in [16], a simpler approach is to use the IE defined as

$$\text{IE} = \int_0^\infty e(t) dt. \tag{4.14}$$

The quantity IAE is equal to IE for a non-oscillatory system, and very close to IE for an oscillatory but well-damped system. This desirable behavior is guaranteed by the bounds on the worst-case sensitivity and complementary sensitivity peaks. Moreover, it

has been shown that IE $= 1/k_i$ (see [16]). This is not surprising since it is equivalent to maximize the gain of the controller at low frequencies (i.e. $\omega \to 0$), and it is well-known that the performance of a control system is provided by the gain of the loop transfer function (typically at low frequencies). Note that the choice of this criterion to measure the performance is very convenient for the problem tackled in this work, since it does not depend on the parameters of the plant.

The maximization of the integral gain also has a positive impact on reference tracking (or disturbances entering at the plant output), since the IE due to a unit step reference is equal to $(P(0)k_i)^{-1}$. However, the reference tracking capability may be improved by using a 2-DOF control structure (e.g. set-point weighting is generally used in a PID to obtain a simple control structure with 2 DOF [22, 120]), but this point is out the scope of the work developed in this chapter. In addition, in cases where the disturbance can be measured, a feedforward controller may be used to improve disturbance rejection [216].

4.3 Characterization of the Feasible Set

In a similar way to the done in the previous chapter, the control design problem will be enunciated after introducing some sets. We start introducing a pair of feasible sets (sets whose elements satisfy certain constraints related to the stability margins) that are defined as follows

$$f_s(\boldsymbol{\theta}, M_s) \equiv \{\mathbf{x} \in D(\boldsymbol{\theta}) : \|S(\mathbf{x}, \boldsymbol{\theta})\|_\infty \leq M_s\}, \tag{4.15}$$

$$f_t(\boldsymbol{\theta}, M_t) \equiv \{\mathbf{x} \in D(\boldsymbol{\theta}) : \|T(\mathbf{x}, \boldsymbol{\theta})\|_\infty \leq M_t\}, \tag{4.16}$$

where $D(\boldsymbol{\theta})$ is the set of controller parameters that provide closed-loop stability for the plant with parameters $\boldsymbol{\theta}$. The set $D(\boldsymbol{\theta})$ can be easily obtained in the controller parameter space (see Section 2.3.1).

Furthermore, are also defined the feasible sets where these constraints are met for a given set Θ. These sets are expressed as

$$F_s(\Theta, M_s) \equiv \bigcap_{\boldsymbol{\theta} \in \Theta} f_s(\boldsymbol{\theta}, M_s), \tag{4.17}$$

$$F_t(\Theta, M_t) \equiv \bigcap_{\boldsymbol{\theta} \in \Theta} f_t(\boldsymbol{\theta}, M_t). \tag{4.18}$$

The elements in theses sets guarantee a worst-case sensitivity and complementary sensitivity peaks (in addition to closed-loop stability) for a set of plants defined by the box Θ.

The control design problem considered in this work is a generalization of the well-known MIGO [22], where interval parametric uncertainty is accounted for. It has been motivated by the control requirements presented in the previous section, and it is stated as follows:

$$\begin{array}{ll} \underset{\mathbf{x}=[k_p \;\; k_i \;\; k_d \;\; T_f]^\top}{\text{maximize}} & k_i \\ \text{subject to} & \mathbf{x} \in F_s(\Theta, M_s), \\ & \mathbf{x} \in F_t(\Theta, M_t). \end{array} \tag{4.19}$$

Note that the optimization problem (4.19) implies a simultaneous design considering every plant parameter vectors belonging to the set Θ. In the next section, the simultaneous design for every plant parameter vector will be replaced, at the cost of some conservatism, by a constrained design for the nominal fractional-order plant.

Alternatively to this optimization problem, we could choose any vector of controller parameters $\mathbf{x}$ following any other optimal criteria. For example when considering an unfiltered PI, in order to limit the control effort due to measurement noise, the value of k_p may be limited (since it defines the high-frequency gain of the controller).

4.4 Optimization-Based Design under Uncertainty

The optimization problem (4.19) can be classified as a robust optimization problem, since the constraints depend on uncertain parameters (see equations (4.17) and (4.18)). In general, robust optimization problems are computationally intractable, and the method generally used to obtain an approximate solution is by using a brute force approach, i.e. grid the uncertainty set. Here, the aim is to simplify the robust optimization problem (4.19) by using the nominal fractional-order plant (4.5), and thus reformulating it as a much simpler optimization problem (at the expense of introducing some conservatism).

In the following, with the purpose of generating an inner approximation of the feasible region of the optimization problem (4.19), we isolate the effect of each uncertain parameter by fixing two of them while changing the remaining one.

4.4.1 Uncertain Gain

To analyze the effect of gain uncertainty, we consider a plant parameters set Θ with $h_1 = h_2$ and $\tau_1 = \tau_2$. Before presenting the first result, it is needed to define some additional sets

$$a_s(L(j\omega, \mathbf{x}, \boldsymbol{\theta}), M_s) \equiv \left\{ \mathbf{x} : \pi/2 \geq \phi_l(\omega, \mathbf{x}, \boldsymbol{\theta}) \geq -\arccos\left(-\sqrt{1 - 1/M_s^2}\right), \right. \\ \left. \forall \omega \geq 0 \text{ s.t. } m_l(\omega, \mathbf{x}, \boldsymbol{\theta}) \geq (1 - 1/M_s^2)^{1/2} \right\}, \tag{4.20}$$

$$a_t(L(j\omega, \mathbf{x}, \boldsymbol{\theta}), M_t) \equiv \left\{ \mathbf{x} : \pi/2 \geq \phi_l(\omega, \mathbf{x}, \boldsymbol{\theta}) \geq -\arccos\left(-\sqrt{1 - 1/M_t^2}\right), \right. \\ \left. \forall \omega \geq 0 \text{ s.t. } m_l(\omega, \mathbf{x}, \boldsymbol{\theta}) \geq (1 - 1/M_t^2)^{-1/2} \right\}. \tag{4.21}$$

Controller parameters that belong to $a_s(L(j\omega), M_s)$ (or $a_t(L(j\omega), M_t)$) allow to decrease the gain of $L(j\omega)$ (vertical displacement of the Nichols plot of $L(j\omega)$), without violating the specification $\|S\|_\infty \leq M_s$ (or $\|T\|_\infty \leq M_t$). This fact is illustrated in Figure 4.2 that shows an inverse M-circle corresponding to $M_s = 1.8$ with its interior (red region) and the constraint imposed to the loop transfer function by the controller parameters belonging to the set $a_s(L(j\omega), 1.8)$ (blue rectangle). These forbidden regions may be thought as boundaries (or Horowitz-Sidi bounds) used in the QFT technique.

Proposition 4.1. *If Θ is defined with $h_1 = h_2$ and $\tau_1 = \tau_2$, then*

$$f_s(\boldsymbol{\theta}_2, M_s) \cap a_s(L(j\omega, \mathbf{x}, \boldsymbol{\theta}_2), M_s) \subseteq F_s(\Theta, M_s), \tag{4.22}$$

$$f_t(\boldsymbol{\theta}_2, M_t) \cap a_t(L(j\omega, \mathbf{x}, \boldsymbol{\theta}_2), M_t) \subseteq F_t(\Theta, M_t), \tag{4.23}$$

where $\boldsymbol{\theta}_2 = [k_2 \ h_2 \ \tau_2]^\top$.

Proof. Let start proving (4.22), the condition $\|S(\mathbf{x}, \boldsymbol{\theta})\|_\infty \leq M_s$ is equivalent to

$$m_l^2 + 2m_l \cos(\phi_l) + 1 - 1/M_s^2 \geq 0, \tag{4.24}$$

for all $\omega \geq 0$ (see [59]). Note that only $m_l(\omega, \mathbf{x}, \boldsymbol{\theta})$ depends on k. We consider two cases:

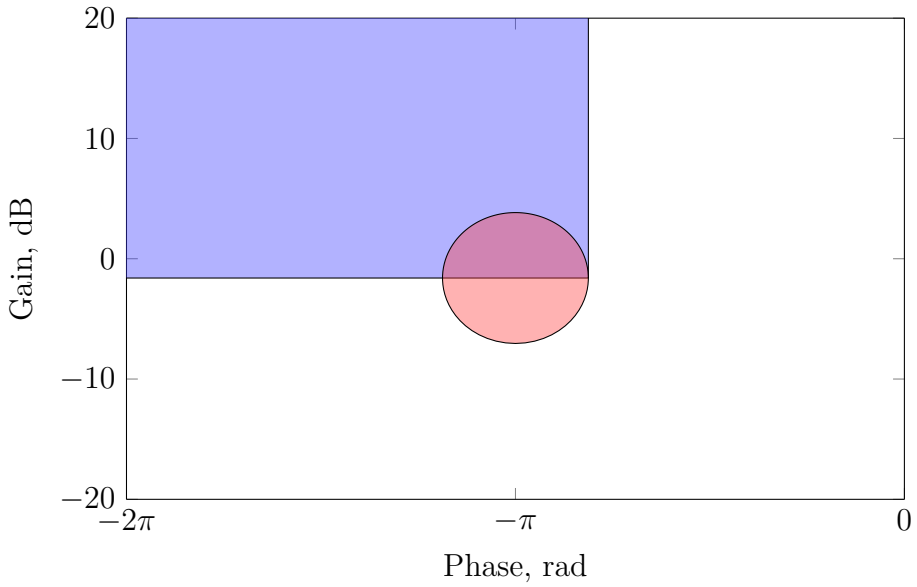

Figure 4.2 Forbidden area imposed to the loop transfer function by $a_s(L(j\omega), M_s)$

Forbidden area imposed to the loop transfer function (blue rectangle) by the controller parameters belonging to the set $a_s(L(j\omega), 1.8)$ in the Nichols plane. The region enclosed by the inverse M-circle corresponding to $M_s = 1.8$ is also shown (red regions).

1) $\pi/2 \geq \phi_l(\omega, \mathbf{x}, \boldsymbol{\theta}_2) \geq -\arccos\left(-\sqrt{1 - 1/M_s^2}\right)$. Under this condition, (4.24) is met independently of the value of k. It is easy to see that (4.24) has not real solutions for m_l, when the equality is considered.
2) $\phi_l(\omega, \mathbf{x}, \boldsymbol{\theta}_2) < -\arccos\left(-\sqrt{1 - 1/M_s^2}\right)$. In this case, we also have that $m_l(\omega, \mathbf{x}, \boldsymbol{\theta}_2) < \sqrt{1 - 1/M_s^2}$. Condition (4.24) is defined by a quadratic function on the variable m_l that attains a unique minimum at $m_l = \cos(\phi_l)$, then if a given $m_l(\omega, \mathbf{x}, \boldsymbol{\theta}_2) < \sqrt{1 - 1/M_s^2}$ satisfies (4.24), it is also satisfied by any $m_l(\omega, \mathbf{x}, \boldsymbol{\theta})$ with $\boldsymbol{\theta} \in \Theta$.

The relation (4.23) is proved using that the condition $\|T(\mathbf{x}, \boldsymbol{\theta})\|_\infty \leq M_t$ is equivalent to

$$m_l^2(1 - 1/M_t^2) + 2m_l \cos(\phi_l) + 1 \geq 0, \tag{4.25}$$

for all $\omega \geq 0$. This case follows similarly to the previous one, and it is omitted here.

Regarding stability, we assume that the controller parameters $\mathbf{x}$ stabilizes the plant with parameters $\boldsymbol{\theta}_2$. Then, the closed-loop system remains stable for any $\boldsymbol{\theta} \in \Theta$, since the boundary between stabilizing and stabilizing parameters corresponds to an infinite value for the sensitivity (and the complementary sensitivity), and it has been proved that when reducing k the sensitivity (and the complementary sensitivity) remains bounded. □

4.4.2 Uncertain Time Delay

The effect of the time-delay uncertainty is studied using a set Θ where $k_1 = k_2$ and $\tau_1 = \tau_2$. Before presenting the result concerning to time-delay uncertainty, it is needed to define some additional sets:

$$b_s(L(j\omega, \mathbf{x}, \boldsymbol{\theta}), M_s) \equiv \Big\{ \mathbf{x} : m_l(\omega, \mathbf{x}, \boldsymbol{\theta}) \leq (1 - 1/M_s), \\ \forall \omega \geq 0 \text{ s.t. } \phi_l(\omega, \mathbf{x}, \boldsymbol{\theta}) \leq -\pi \text{ or } \phi_l(\omega, \mathbf{x}, \boldsymbol{\theta}) \geq \pi/2 \Big\}, \tag{4.26}$$

$$b_t(L(j\omega, \mathbf{x}, \boldsymbol{\theta}), M_t) \equiv \Big\{ \mathbf{x} : m_l(\omega, \mathbf{x}, \boldsymbol{\theta}) \leq (1 + 1/M_t)^{-1}, \\ \forall \omega \geq 0 \text{ s.t. } \phi_l(\omega, \mathbf{x}, \boldsymbol{\theta}) \leq -\pi \text{ or } \phi_l(\omega, \mathbf{x}, \boldsymbol{\theta}) \geq \pi/2 \Big\}. \tag{4.27}$$

These sets have a similar role to the ones presented in the previous section, controller parameters that belong to $b_s(L(j\omega), M_s)$ (or $b_t(L(j\omega), M_t)$) allow to increase the phase of $L(j\omega)$ (horizontal displacement of $L(j\omega)$ in the Nichols plane), without violating the specification $\|S\|_\infty \leq M_s$ (or $\|T\|_\infty \leq M_t$). Analogously to the previous section, Figure 4.3 shows region enclosed by an inverse M-circle corresponding to $M_s = 1.8$ (red region) and the constraint imposed to the loop transfer function by the controller parameters belonging to the set $b_s(L(j\omega), 1.8)$ (blue rectangle) in the Nichols plane.

Proposition 4.2. *If Θ is defined with $k_1 = k_2$ and $\tau_1 = \tau_2$, then*

$$f_s(\boldsymbol{\theta}_2, M_s) \cap b_s(L(j\omega, \mathbf{x}, \boldsymbol{\theta}_2), M_s) \subseteq F_s(\Theta, M_s), \tag{4.28}$$

$$f_t(\boldsymbol{\theta}_2, M_t) \cap b_t(L(j\omega, \mathbf{x}, \boldsymbol{\theta}_2), M_t) \subseteq F_t(\Theta, M_t), \tag{4.29}$$

where $\boldsymbol{\theta}_2 = [k_2 \ h_2 \ \tau_2]^\top$.

Proof. Let start proving (4.28), the condition $\|S(\mathbf{x}, \boldsymbol{\theta})\|_\infty \leq M_s$ is equivalent to (4.24). Note that only $\phi_l(\omega, x, \theta)$ depends on h. We consider two cases:
1) $m_l(\omega, \mathbf{x}, \boldsymbol{\theta}_2) \leq 1 - 1/M_s$. Rewriting as $1 - m_l \geq 1/M_s$ and squaring leads to $m_l^2 - 2m_l + 1 - 1/M_s^2 \geq 0$, therefore (4.24) is met independently of the value of h.
2) $m_l(\omega, \mathbf{x}, \boldsymbol{\theta}_2) > 1 - 1/M_s$. The second term of (4.24) is the only that may be negative,

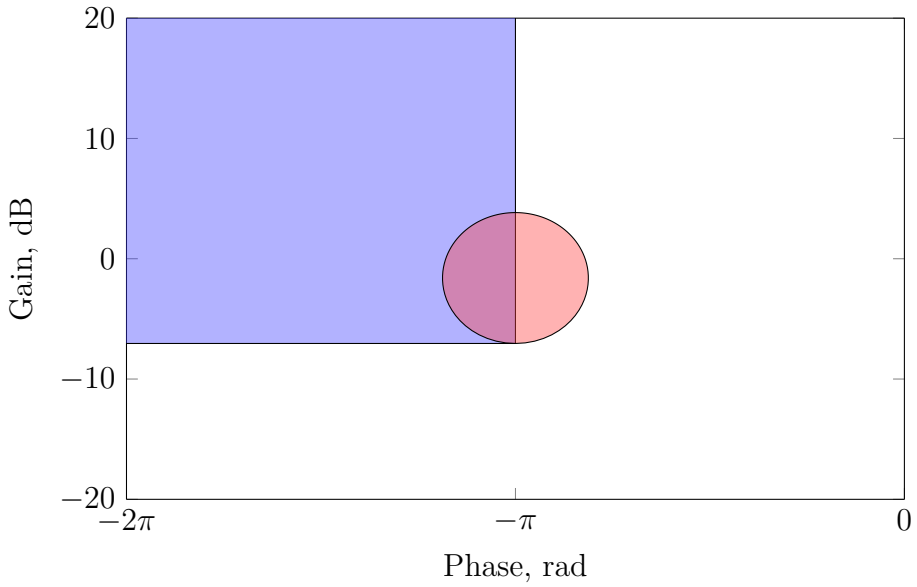

Figure 4.3 Forbidden area imposed to the loop transfer function by $b_s(L(j\omega), M_s)$

Forbidden area imposed to the loop transfer function (blue rectangles) by the controller parameters belonging to the set $b_s(L(j\omega), 1.8)$ in the Nichols plane. The region enclosed by the inverse M-circle corresponding to $M_s = 1.8$ is also shown (red regions).

taking into account that

$$-\pi < \phi_l(\omega, \mathbf{x}, \boldsymbol{\theta}_2) \leq \phi_l(\omega, \mathbf{x}, \boldsymbol{\theta}) < \pi/2. \tag{4.30}$$

That leads to

$$\cos(\phi_l(\omega, \mathbf{x}, \boldsymbol{\theta})) \geq \min(0, \cos(\phi_l(\omega, \mathbf{x}, \boldsymbol{\theta}_2))). \tag{4.31}$$

Then (4.24) is met for any $\boldsymbol{\theta} \in \Theta$.

The proof of (4.29) is similar to that of (4.28), and it is omitted for brevity. On the other hand, we assume that the controller parameters $\mathbf{x}$ stabilizes the plant with parameters θ_2. Then the closed-loop system remains stable for any $\boldsymbol{\theta} \in \Theta$, since the boundary between stabilizing and unstabilizing parameters corresponds to an infinite value for the sensitivity (and the complementary sensitivity), and it has been proved that when reducing h the sensitivity (and the complementary sensitivity) remains bounded.

□

4.4.3 Uncertain Time Constant

In this section, it is initially considered a set Θ where $k_1 = k_2$ and $h_1 = h_2$. Variations in the time constant affect both gain and phase of the plant, that makes the analysis of uncertainty in the time constant more involved. As a consequence of that, $F_s(\Theta, M_s)$ and $F_t(\Theta, M_t)$ are not easily defined by one element belonging to the set Θ. In some cases, the following relations hold

$$f_s(\boldsymbol{\theta}_1, M_s) \cap f_s(\boldsymbol{\theta}_2, M_s) = F_s(\Theta, M_s), \tag{4.32}$$

$$f_t(\boldsymbol{\theta}_1, M_t) \cap f_t(\boldsymbol{\theta}_2, M_t) = F_t(\Theta, M_t). \tag{4.33}$$

But these relations do not hold in general. It is not difficult to find counterexamples where to obtain $F_s(\Theta, M_s)$ and $F_s(\Theta, M_s)$ is needed to take into account more cases in addition to the extremes. This fact motivates the use of the fractional-order plant, introduced in the previous section, to deal with time constant uncertainty. It is needed to define two additional sets that play a similar role to f_s and f_t, but in this case, they are referred to the (fractional-order) loop transfer function $L^F(s, \mathbf{x})$. These sets are defined below:

$$f_s^F(M_s) = \left\{ \mathbf{x} \in D^F : \left\| S^F(x) \right\|_\infty \leq M_s \right\}, \tag{4.34}$$

$$f_t^F(M_t) = \left\{ \mathbf{x} \in D^F : \left\| T^F(x) \right\|_\infty \leq M_t \right\}, \tag{4.35}$$

where D^F is the set of controller parameters that make the loop transfer function $L^F(s, \mathbf{x})$ to have a positive phase margin (that does not imply closed-loop stability for this particular fractional system). This set would be the stabilizing set if Nyquist theorem were applicable to this loop transfer function. $S^F(s, \mathbf{x})$ and $T^F(s, \mathbf{x})$ denote the sensitivity and complementary sensitivity, respectively, for the (fractional-order) loop transfer function $L^F(s, \mathbf{x})$.

As consequence of Propositions 4.1 and 4.2, it is possible to state the following result.

Proposition 4.3. *Considering Θ defined with $k_2 \geq k_1$, $h_2 \geq h_1$, and $\tau_2 > \tau_1$. Then, the following statements hold*

$$f_s^F(M_s) \cap a_s(L^F(j\omega, \mathbf{x}), M_s) \cap b_s(L^F(j\omega, \mathbf{x}), M_s) \subseteq F_s(\Theta, M_s), \tag{4.36}$$

$$f_t^F(M_t) \cap a_t(L^F(j\omega, \mathbf{x}), M_t) \cap b_t(L^F(j\omega, \mathbf{x}), M_t) \subseteq F_t(\Theta, M_t). \tag{4.37}$$

Proof. This proof involves analogous arguments to the used in Propositions 4.1 and 4.2, therefore a complete proof is omitted for brevity. Roughly speaking, $L^F(j\omega, \mathbf{x})$ has greater or equal gain and less or equal phase to $L(j\omega, \mathbf{x}, \boldsymbol{\theta})$ with $\boldsymbol{\theta} \in \Theta$ (see (4.7)). Therefore, the same arguments applied in the proofs of Propositions 4.1 and 4.2 lead to the result presented in this proposition. The only concern is about closed-loop stability, but controller parameters belonging to $f_s^F(M_s)$ and $f_t^F(M_t)$ provides to $L^F(j\omega, \mathbf{x})$ with a positive phase margin, that guarantees a positive phase margin for $L(j\omega, \mathbf{x}, \boldsymbol{\theta})$ with $\boldsymbol{\theta} \in \Theta$, and hence closed-loop stability. □

4.4.4 Illustrative Example

With the purpose of illustrating the previous results, we consider a set Θ defined by the parameters $k_1 = h_1 = \tau_1 = 0.5$ and $k_2 = h_2 = \tau_2 = 1$, and a vector of controller parameters $\mathbf{x} = [0.53\ 0.56\ 0.66\ 1]^\top$. This vector of controller parameter satisfies

$$\mathbf{x}) \in f_s^F(1.8) \cap a_s(L^F(j\omega, \mathbf{x}), 1.8) \cap b_s(L^F(j\omega, \mathbf{x}), 1.8), \tag{4.38}$$

then it also belongs to $F_s(\Theta, 1.8)$ (by Proposition 4.3). This is illustrated in Figure 4.4, that shows the region enclosed by the inverse M-circle corresponding to $M_s = 1.8$ (red region), the restricted regions imposed by the sets $a_s(L^F(j\omega, \mathbf{x}), 1.8)$ and $b_s(L^F(j\omega, \mathbf{x}), 1.8)$ (blue rectangles), some compensated (multiplied by $C(j\omega, \mathbf{x})$) templates corresponding to the set Θ (green regions), and the Nichols plot corresponding to $L^F(j\omega, \mathbf{x})$ (black line).

It is possible to appreciate in Figure 4.4 that being the Nichols plot of $L^F(j\omega, \mathbf{x})$ outside the forbidden regions (red and blue regions), the compensated templates do not enter into the region delimited by the inverse M-circle corresponding to $M_s = 1.8$ (red region). In this way, a simultaneous design for all uncertainty instances is replaced by a constrained design for the nominal fractional-order plant.

4.4.5 Design for the Fractional-Order Plant

After presenting some results that allow us to obtain a subset of the feasible region of the robust optimization problem (4.19), it may be rewritten in the following approximated

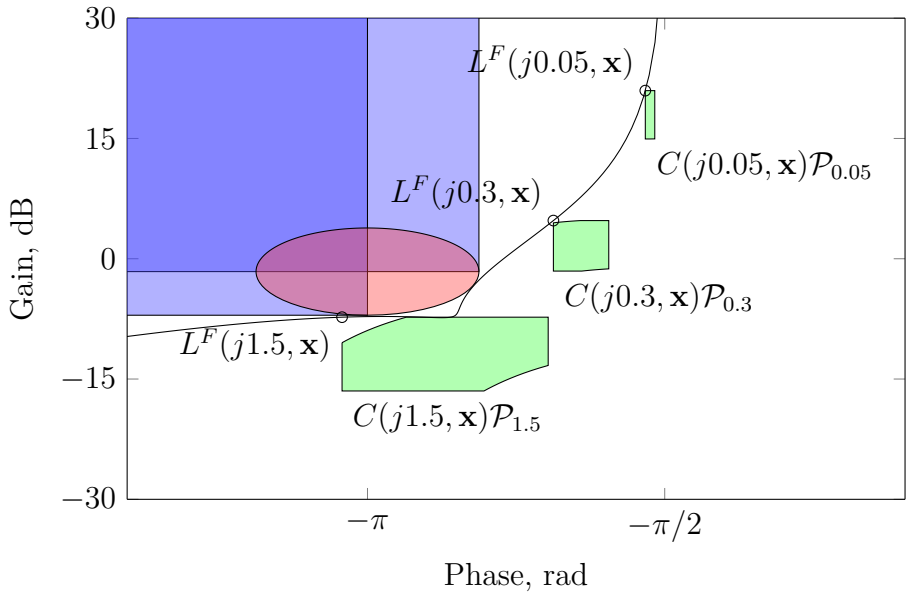

Figure 4.4 Nichols plot of a PID with an uncertain FOTD plant

Compensated templates (green regions) and Nichols plot of $L^F(j\omega, \mathbf{x})$ (black line). Forbidden areas defined by $a_s(L^F(j\omega, \mathbf{x}), 1.8)$ and $b_s(L^F(j\omega, \mathbf{x}), 1.8)$ (blue rectangles) and inverse M-circle corresponding to $M_s = 1.8$ with its interior (red region).

form

$$\begin{aligned} \underset{\mathbf{x}=[k_p\ k_i\ k_d\ T_f]^\top}{\text{maximize}} \quad & k_i \\ \text{subject to} \quad & \mathbf{x} \in f_s^F(M_s) \cap a_s(L^F(j\omega, \mathbf{x}), M_s) \cap b_s(L^F(j\omega, \mathbf{x}), M_s), \\ & \mathbf{x} \in f_t^F(M_t) \cap a_t(L^F(j\omega, \mathbf{x}), M_t) \cap b_t(L^F(j\omega, \mathbf{x}), M_t). \end{aligned} \tag{4.39}$$

Note that the solution to this optimization problem is a sub-optimal solution to the optimization problem (4.19), but in this case, the solution can be obtained by designing for a nominal fractional-order plant and taking into account some restrictions in the loop transfer function.

This optimization problem can be easily solved using several approaches (for simplicity the value of the time constant of the filter T_f will be pre-specified). The resulting optimization problem can be solved using any standard optimization solver without encountering major difficulties. In the many designs that have been carried out, initialization of the local algorithm active-set (implemented in the Matlab function `fmincon`) with the parameter vector $[0\ 0\ 0\ T_f]^\top$ was sufficient to produce the global optimum. (It is easy to see that this vector always belongs to the feasible set of the considered optimization problem.)

The standard form in which most numerical solvers consider optimization problems is

$$\begin{array}{ll} \underset{\mathbf{x}}{\text{minimize}} & f(\mathbf{x}) \\ \text{subject to} & g_i(\mathbf{x}) \leq 0, \quad \forall i = 1, \ldots, m. \end{array} \tag{4.40}$$

The optimization problem (4.39) can be arranged into this form by using some adequate functions. (Determining whether a vector of controller parameters belongs to these sets is easily done by performing basic operations over $L^F(j\omega)$.)

4.5 Examples

The proposed design method will be illustrated by two examples. The first one applies the method to an uncertain plant, motivated by an industrial process. In order to show the applicability of the proposed method to other control structures, the second one considers a PID with an SP.

Example 4.1 (Temperature control problem)**.** This example examines the application of the proposed method to the design of a PID controller for a temperature control problem. The plant that we consider is modeled in [251], it consists of an industrial heat exchanger, commonly used in food industries for thermal treatments, where the steam flow rate is manipulated to control the difference of temperature between the outlet and the inlet of the heat exchanger. The output of the model is the difference of temperature (in degrees centigrade) between the outlet and the inlet of the heat exchanger, and the input is the aperture of a valve. Identification experiments carried out for different operation points (see [251] for further details) obtained the following interval plant

$$\mathcal{P} = \left\{ P(s, \boldsymbol{\theta}) = \frac{k}{\tau s + 1} e^{-sh} : \boldsymbol{\theta} = [k \ h \ \tau]^\top \in \Theta \right\}, \tag{4.41}$$

where $\Theta = [0.31, 0.40] \times [80, 114] \times [50, 88]$. Time constant and time delay are expressed in seconds.

We solve the optimization problem (4.39) (that is an approximate version of the problem (4.19)), considering as specifications $M_s = M_t = 1.4$ and fixing the time constant of the filter to $T_f = 100$. This controller is compared to others obtained with different methods from the literature. Firstly, we use results presented in [177] (this method will be presented in the next chapter) to solve the optimization problem (4.19) (considering as specifications $M_s = M_t = 1.4$ and fixing the value of the time constant

Table 4.1 Different controllers (Example 4.1)

Method	k_p	k_i	k_d	T_f	$\max_{\boldsymbol{\theta}\in\Theta}\|S\|_\infty$	$\max_{\boldsymbol{\theta}\in\Theta}\|T\|_\infty$
Proposed	0.86	$0.77 \cdot 10^{-2}$	101	100	1.39	1.01
[177]	0.92	$0.80 \cdot 10^{-2}$	99	100	1.40	1.02
[119]	1.18	$1.19 \cdot 10^{-2}$	139	100	1.66	1.23
[97]	1.27	$1.09 \cdot 10^{-2}$	111	100	1.64	1.16

of the filter to $T_f = 100$). Secondly, we use the method proposed in [119] to solve the problem (4.42) for the nominal plant parameters $\bar{\boldsymbol{\theta}} = [0.36\ 97\ 69]^\top$, these parameters are the mean parameters of the intervals that define Θ. It is expressed as:

$$\begin{aligned} \underset{\mathbf{x}=[k_p\ \ k_i\ \ k_d\ \ 100]^\top}{\text{maximize}} \quad & k_i \\ \text{subject to} \quad & \mathbf{x} \in f_s(\bar{\boldsymbol{\theta}}, 1.4), \\ & \mathbf{x} \in f_t(\bar{\boldsymbol{\theta}}, 1.4). \end{aligned} \tag{4.42}$$

Lastly, we consider the minimization of the IAE instead of the IE, also for the nominal parameter vector $\bar{\boldsymbol{\theta}}$; that is formulated as follows:

$$\begin{aligned} \underset{\mathbf{x}=[k_p\ \ k_i\ \ k_d\ \ 100]^\top}{\text{minimize}} \quad & \text{IAE} \\ \text{subject to} \quad & \mathbf{x} \in f_s(\bar{\boldsymbol{\theta}}, 1.4), \\ & \mathbf{x} \in f_t(\bar{\boldsymbol{\theta}}, 1.4). \end{aligned} \tag{4.43}$$

This problem is solved using the software that accompanies the paper [97]. The obtained controller parameters and their robustness levels are shown in Table 4.1. In addition, a comparison between the controllers, in terms of temporal responses (plant output and controller output) due to a unit step disturbance and a unit step reference, is shown in Figures 4.5 and 4.6. The proposed method obtains a controller quite similar to the obtained when solving the robust problem optimization (4.19) using [177], but the complexity of the proposed optimization problem (4.39) is comparable to the one corresponding to a nominal design, as (4.42) and (4.43). Note that the controllers obtained by solving (4.42) and (4.43) (using [119] and [97], respectively) result in more oscillatory responses and violation of the constraints, when the controller is evaluated using the uncertain plant.

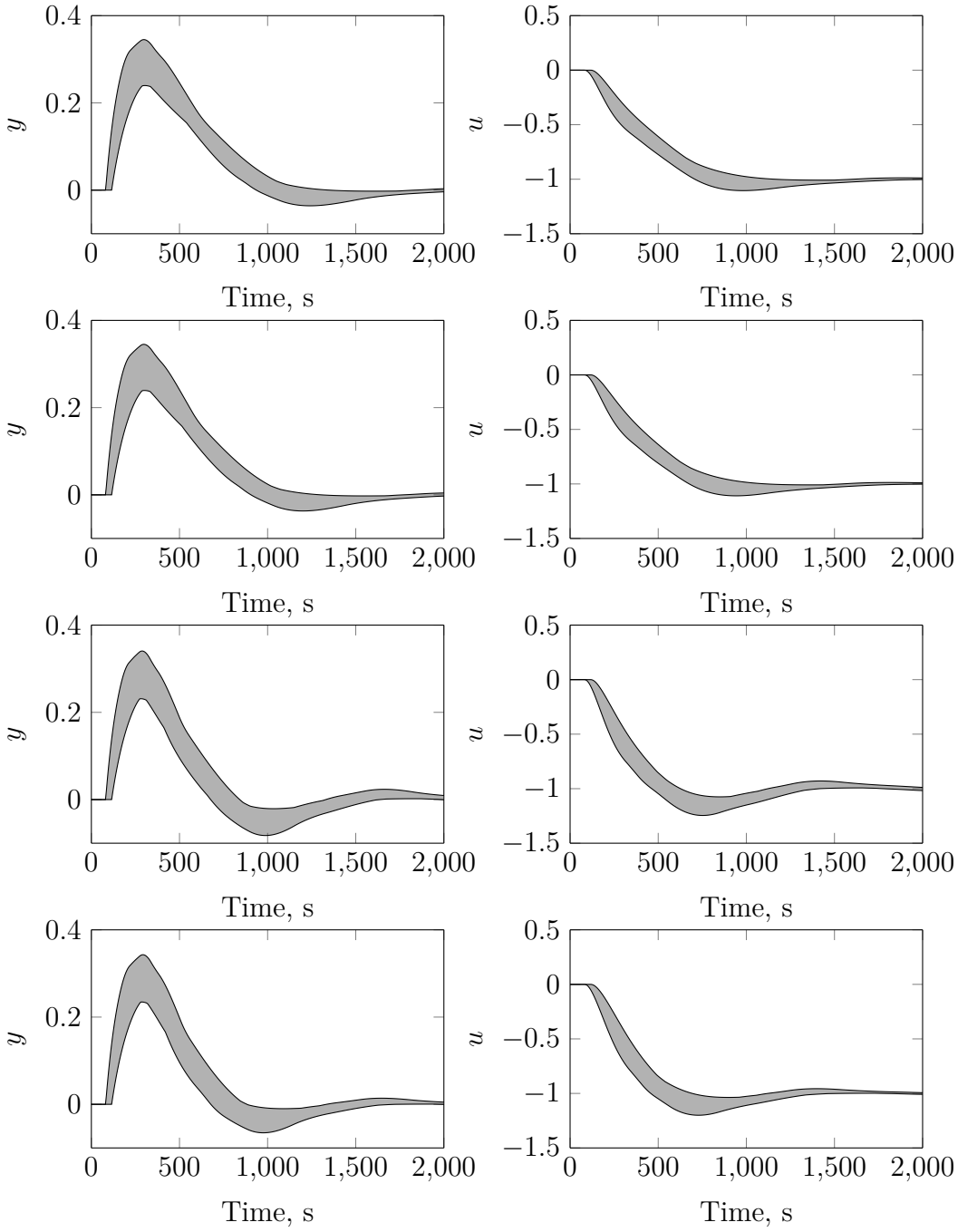

Figure 4.5 Disturbance rejection (Example 4.1)

Plant output (left) and controller output (right) due to a unit step disturbance (right). From top to bottom, proposed method, [177], [119], and [97].

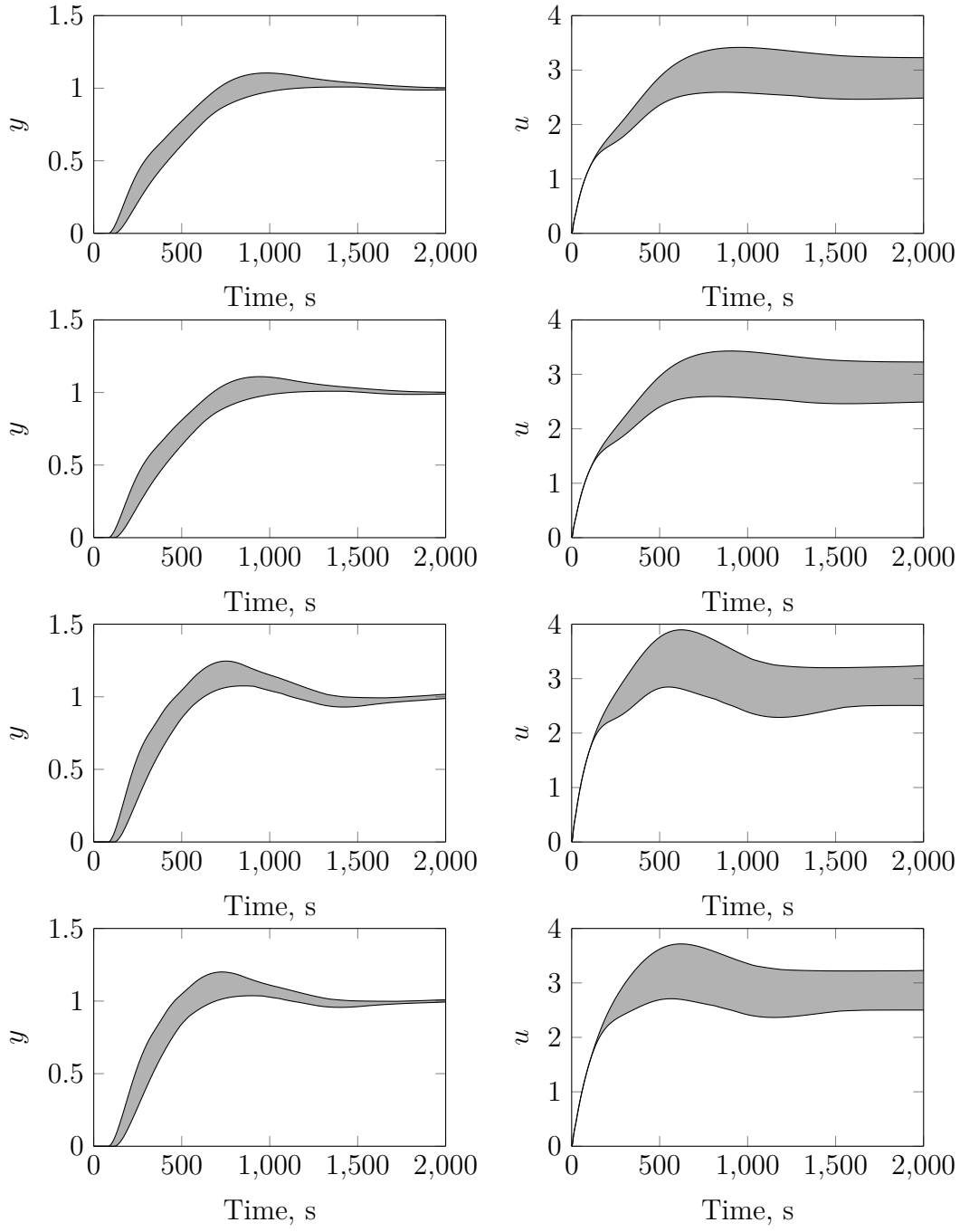

Figure 4.6 Reference tracking (Example 4.1)

Plant output (left) and controller output (right) due to a unit step reference (right). From top to bottom, proposed method, [177], [119], and [97].

Example 4.2 (PID with a Smith Predictor (SP))**.** This example studies the application of Proposition 4.2 to the design of a PID with an SP, a particular case of DTC. This type of controllers is usually regarded as inherently nonrobust, especially with respect to uncertainty in the plant time delay [108, 127]. The reason of that is that they have a tendency to introduce multiple crossover frequencies.

Proposition 4.2 provides conditions that allow for obtaining a design that maintains the stability margins of the nominal plant when reducing the time delay. It should be noted that in the proof of Proposition 4.2, a particular structure of the controller is not used. It is only used that the phase of the loop transfer function less than $\pi/2$. This condition guarantees that when reducing the time delay of the plant, the Nichols plot of the loop transfer function does not enter into the (inverse) M-circles enclosing the critical point $[\pi\ 0]^\top$. Then, provided this last condition is fulfilled, Proposition 4.2 may be applied to any other controller structure.

The traditional SP design procedure involves the tuning of a primary controller (i.e. $C_{\text{PID}}(s)$ in equation (4.44)) as if there were no time delay. It is well-known that this procedure may lead to disastrous designs in terms of very poor robustness properties. Therefore, it is motivated the introduction of some constraints during the design of the primary controller in order to avoid this undesired behavior.

We consider a feedback controller composed of an unfiltered PID with an SP, that has the following transfer function (when a nominal plant modeled by an FOTD is considered)

$$C(s,\mathbf{x},\boldsymbol{\theta}) = \frac{C_{\text{PID}}(s,\mathbf{x})}{1 + C_{\text{PID}}(s,\mathbf{x})\Pi(s,\boldsymbol{\theta})}, \tag{4.44}$$

where

$$C_{\text{PID}}(s,\mathbf{x}) = k_p + \frac{k_i}{s} + k_d s \tag{4.45}$$

and

$$\Pi(s,\boldsymbol{\theta}) = \frac{k}{\tau s + 1}(1 - e^{-sh}), \tag{4.46}$$

being $\mathbf{x} = [k_p\ k_i\ k_d]^\top$ and $\boldsymbol{\theta} = [k\ h\ \tau]^\top$. The same approach to the presented in Section 4.2 is used here to tune this controller. It is possible to prove that the IE due to a unit step disturbance is minimized by maximizing the integral gain. A direct application of the final value theorem leads to

$$\text{IE} = \int_0^\infty e(t)dt = \lim_{s\to 0} s\frac{P(s,\boldsymbol{\theta})}{1 + C(s,\mathbf{x},\boldsymbol{\theta})P(s,\boldsymbol{\theta})}\frac{1}{s^2} = kh + \frac{1}{k_i}. \tag{4.47}$$

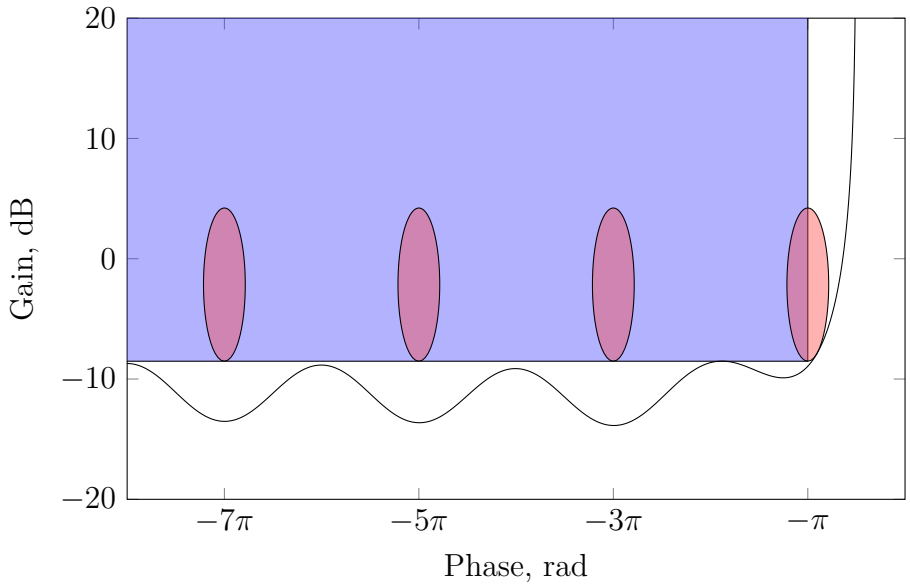

Figure 4.7 Nichols plot (Example 4.2)

Nichols plot of $L(j\omega, \mathbf{x}, \boldsymbol{\theta}_2)$, forbidden areas defined by the set $b_s(L(j\omega, \mathbf{x}, \boldsymbol{\theta}_2), 1.6)$ (blue rectangle) and inverse M-circles corresponding to $M_s = 1.6$ (red regions).

To illustrate the application of Proposition 4.2 to the design of a PID with an SP, we consider the following uncertain plant

$$\mathcal{P} = \left\{ P(s, \boldsymbol{\theta}) = \frac{k}{\tau s + 1} e^{-sh} : \boldsymbol{\theta} = [k \ h \ \tau]^\top \in \Theta \right\}, \tag{4.48}$$

where $\Theta = [1] \times [0, 5] \times [1]$. For simplicity, we choose a plant where uncertainty only affects to the time delay. Using Proposition 4.2, it is stated an optimization problem that only concerns to the plant parameters given by the vector of parameters $\boldsymbol{\theta}_2 = [1 \ 5 \ 1]^\top$. We propose the following optimization problem:

$$\begin{array}{ll} \underset{\mathbf{x}=[k_p \ k_i \ k_d]^\top}{\text{maximize}} & k_i \\ \text{subject to} & \mathbf{x} \in f_s(\boldsymbol{\theta}_2, 1.6) \cap b_s(L(j\omega, \mathbf{x}, \boldsymbol{\theta}_2), 1.6). \end{array} \tag{4.49}$$

The solution to this optimization problem is $\mathbf{x} = [0.523 \ 0.403 \ 0.375]^\top$ (with SP, using the feedback controller of equation (4.44)).

Figure 4.7 shows the Nichols plot for this design, as well as forbidden region imposed to the loop transfer function by the controller parameters belonging to the set $b_s(L(j\omega, \mathbf{x}, \boldsymbol{\theta}_2), 1.6)$ and regions delimited by the inverse M-circles corresponding to $M_s = 1.6$.

In essence, our condition to provide robustness (in terms of maximum sensitivity peak) to a PID with an SP against reduction of time delay is based on limiting the gain of the controller at high-frequencies, similar conditions guaranteeing a gain margin (weaker stability margin) when the time delay is reduced were presented in [159].

Chapter 5

PID Design for an Uncertain General Plant

5.1 Introduction

This chapter tackles the problem of designing PID controllers for an uncertain general plant model, in the sense that the uncertain plant model may be given in terms of a family of frequency response data. Previous chapters have only considered some particular uncertain plant models (parametric models). In addition, this chapter also considers both control approaches already presented in Section 2.1.4, namely maximization of performance and minimization of cost of feedback. The approach of minimizing the cost of feedback requires the specification of a minimum level of performance. Therefore, in addition to constraints for relative stability, constraints for imposing a minimum level of performance are also considered here. Two classes of control design problems are considered in this chapter: MIGO [22, 203] and QFT [128, 265].

In this chapter, optimization problems arising from control design problems are solved by using optimization algorithms based on the convex-concave procedure (CCP) [48, 162]. The main advantages of the approach are:

- Given a plant description and the desired specifications, the control design problem is directly stated in the form of an optimization problem with constraints.
- Many efficient algorithms are available for convex optimization problems.
- The QFT bounds give useful insight into the critical uncertainties.

Convex optimization has been used earlier for PID control [47, 119, 149, 218], but these papers do not use uncertainty specified by (not necessarily convex) templates and Horowitz-Sidi bounds.

The chapter is organized as follows. A problem formulation, which includes plant uncertainty, controller structure, constraints, and optimization criteria, is given in Section 5.2 leading to the optimization problems presented in Section 5.3. The CCP is introduced and applied to loop shaping in Section 5.4. Examples are given in Section 5.5 and a discussion is done in Section 5.6.

5.2 Problem Statement

We consider a 2-DOF feedback control system, as the one represented in the block diagram shown in Figure 1.2, where r is the set-point, e is the error, u is the controller output, d is the load disturbance, n is the measurement noise, and y is the plant output. The transfer functions of the plant, the controller and the prefilter are $P(s)$, $C(s)$ and $F(s)$, respectively. Plant uncertainty is captured by assuming that $P(s)$ belongs to a given set $\mathcal{P}$.

5.2.1 Plant Uncertainty

The approach adopted here to model an uncertain plant is by using a finite or infinite set $\mathcal{P}$ of transfer functions $P(s)$. Typically, this set may represent a physical model of a system with parametric or nonparametric uncertainty, a set of models computed from system identification experiments, or a finite set of models. A template $\mathcal{P}_\omega$ is the set of all frequency responses at the frequency ω, or formally

$$\mathcal{P}_\omega = \Big\{ P(j\omega) : P(s) \in \mathcal{P} \Big\}. \tag{5.1}$$

This way of modeling uncertainty, which is the basis of QFT, has several advantages:

- There is no need for a particular plant model representation, any linear model can be transformed into a frequency response.
- Experimental frequency response data can be used.
- The inclusion of phase uncertainty allows for obtaining less conservative results than the obtained when only gain uncertainty is considered, e.g. unstructured disk uncertainty commonly used in $\mathcal{H}_\infty$ control (it considers a phase uncertainty of $\pm\pi$ rad).

Here, we include a comparison among different approaches to model uncertainty. In particular, we are going to consider templates used in QFT and unstructured disk uncertainty used in $\mathcal{H}_\infty$. Let us consider the same uncertain plant that was studied in Section 2.2.2, that is

$$\mathcal{P} = \left\{ \frac{k}{\tau s + 1} : [k \ \tau]^\top \in \Theta = [1, 5] \times [1, 5] \right\}. \tag{5.2}$$

The use of unstructured disk uncertainty requires the election of a nominal plant, in this case the plant defined by the uncertain parameters in the middle of ranges has been chosen. Then, the uncertain set of plants is modeled by using the following set:

$$\mathcal{P}_{\text{unc}} = \left\{ P(s) : \left| \frac{P(s)}{P_{\text{nom}}(s)} - 1 \right| \leq |W(s)| \right\}, \tag{5.3}$$

where $W(s)$ is known as shaping filter. This is given by a minimum-phase transfer function of a certain order that has to be specified, there are available algorithms to obtain it, for example, `uncover` implemented in Matlab. It is important to clarify that this election of the nominal plant does not necessarily produce the tightest disk, but the election of the nominal plant that leads to the tightest disk is usually a hard task, and the election done here is common in practice. The resulting uncertain sets are shown in Figure 5.1 for the frequencies $\omega = 0.1, 1, 20$. In the case of information about the structure of the uncertainty is available, the use of an unstructured model of the uncertainty will lead to conservative results when comparing with a design performed using a structured model of the uncertainty.

5.2.2 Controller and Prefilter Structures

The PID controller has the following transfer function

$$C_{\text{PID}}(s, \mathbf{x_c}) = k_p + \frac{k_i}{s} + k_d s, \tag{5.4}$$

where $\mathbf{x_c} = [k_p \ k_i \ k_d]^\top$ is a vector of controller parameters. This representation of the PID controller is specially suitable for the techniques used in this chapter, since the parameters depend in a linear way. Other representations of the PID controller and transformations about them are given in Appendix B. The PID controller can be augmented by a low-pass measurement filter, which reduces effects of measurement noise and provides high-frequency roll-off [19]. Then, the resulting controller with a

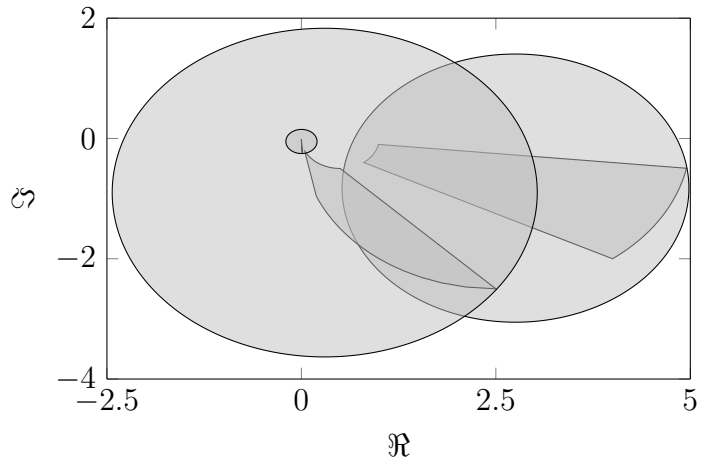

Figure 5.1 Structured (templates) and unstructured (disk) uncertainty

second-order filter is

$$C(s, \mathbf{x_c}) = C_{\text{PID}}(s, \mathbf{x_c}) G_f(s), \tag{5.5}$$

where

$$G_f(s) = \frac{1}{1 + sT_f + s^2 T_f^2/2}. \tag{5.6}$$

This second-order filter has two complex poles with the smallest damping ratio for which there is no amplitude amplification. Other filter structures are possible [115], but this choice keeps the number of parameters as low as possible. The filter time constant does not appear affinely in the controller. It must be determined iteratively when using convex optimization.

Set-point weighting is used to obtain a simple control structure with 2 DOF. It corresponds to the structure in Figure 1.2 with the prefilter $F(s, \mathbf{x_f})$

$$F(s, \mathbf{x_f}) = \frac{ck_d s^2 + bk_p s + k_i}{k_d s^2 + k_p s + k_i}, \tag{5.7}$$

where $\mathbf{x_f} = [b\ c]^\top$ is the vector of prefilter parameters. In some cases, it may be necessary to use more general prefilter structures. In the following the loop transfer function will be denoted $L(s, \mathbf{x_c}) = C(s, \mathbf{x_c})P(s)$. When it is clear from the context, the arguments $\mathbf{x_c}$ and $\mathbf{x_f}$ will be dropped for the sake of brevity.

5.2.3 Control Design Approaches

There is no need for feedback if there are no plant model uncertainty and no disturbances, as pointed out by Horowitz [124]. The effects of uncertainties and disturbances are small if the controller gain is large over a wide frequency range. There are however severe drawbacks with a controller having too high gain. These are related to the cost of feedback, that is paid in terms of bandwidth. The notion of cost of feedback expressed in terms of the frequency band where the controller has high gain was introduced by Horowitz [128], who emphasized the drawbacks inherent to any feedback system (it was presented in Section 2.1.4). In addition, for NMP systems there are theoretical limitations that limit the available bandwidth of the loop transfer function (these limitations were briefly introduced in Section 2.1.4).

To summarize, since load disturbances typically have low frequencies and measurement noise typically has high frequencies, the loop transfer function should be shaped to have high gain at low frequencies and low gain at high frequencies. To have adequate stability the loop transfer function should be shaped so that it has a good phase margin at the crossover frequency ω_{gc} where $|L(j\omega_{gc})| = 1$. Finding the gain crossover frequency ω_{gc} and a good shape of the loop transfer function is a trade-off between performance and robustness.

We present two control design approaches, where the loop shaping trade-off is resolved in different ways.

- *Maximization of performance.* In this approach, the controller gain at low frequencies is maximized under robustness constraints that limit the gain at high frequencies. This approach is well known in the PID literature, for example, the MIGO method. It can be understood as a maximizing criterion of the *benefits of feedback*.

- *Minimization of cost of feedback.* In this case, the high-frequency gain of the controller is minimized under constraints on a lower bound on the low-frequency gain of the controller that correspond to a desired minimum level of performance. This approach is a central issue in QFT, and it can be interpreted as a minimizing criterion of the *drawbacks of feedback*.

5.3 Control Design Problem via Optimization

The control design problem can be stated as a constrained optimization problem. Before introducing the optimization problem, constraints and optimization criteria will be defined.

5.3.1 Constraints

We introduce several design specifications that will play the role of constraints in the optimization problems. The first four constraints impose (frequency-dependent) bounds on the gain of sensitivity functions ("The Gang of Four"), and the fifth constraint (common in the QFT framework) is used to impose a robust tracking specification. All these constraints are used in QFT, as it was already presented in Section 2.2.

Sensitivity

A bound on the peak of the sensitivity is a typical measure of robustness, note that the maximum sensitivity $\|S\|_\infty$ is the inverse of the shortest distance from a point on the Nyquist plot of the loop transfer function to the critical point. A frequency-dependent bound can be used to guarantee attenuation of low-frequency load disturbances.

$$|S(j\omega)| = \left|\frac{1}{1+L(j\omega)}\right| \leq \delta_S(\omega), \quad \forall P(j\omega) \in \mathcal{P}_\omega. \tag{5.8}$$

Complementary Sensitivity

To place an upper bound on the peak of the complementary sensitivity is another way to ensure robustness. When $F(s) = 1$, the complementary sensitivity is the transfer function from set-point to plant output. The peak of the set-point response can be bounded by the constraint

$$|T(j\omega)| = \left|\frac{L(j\omega)}{1+L(j\omega)}\right| \leq \delta_T(\omega), \quad \forall P(j\omega) \in \mathcal{P}_\omega. \tag{5.9}$$

Noise sensitivity

A bound on the noise sensitivity limits the control signal activity due to measurement noise.

$$|G_{un}(j\omega)| = \left|\frac{C(j\omega)}{1+L(j\omega)}\right| \leq \delta_N(\omega), \quad \forall P(j\omega) \in \mathcal{P}_\omega, \tag{5.10}$$

where $G_{un}(s) = C(s)S(s)$ is the transfer function from measurement noise n to control signal u.

Load Disturbance Sensitivity

Attenuation of load disturbances at the plant input can be captured by the inequality

$$|G_{yd}(j\omega)| = \left| \frac{P(j\omega)}{1 + L(j\omega)} \right| \leq \delta_D(\omega), \quad \forall P(j\omega) \in \mathcal{P}_\omega, \tag{5.11}$$

where $G_{yd}(s) = P(s)S(s)$ is the transfer function from load disturbance d to output y.

Robust Tracking Specification

Requirements on set-point tracking can be captured by the inequality

$$\delta_l(\omega) \leq |F(j\omega)T(j\omega)| \leq \delta_u(\omega), \quad \forall P(j\omega) \in \mathcal{P}_\omega. \tag{5.12}$$

Notice that a 2-DOF controller architecture separates disturbance attenuation and robustness from set-point tracking. The feedback controller $C(s)$ is designed to take care of performance and robustness, and the feedforward $F(s)$ handles set-point tracking.

The procedure that will be used here to deal with this constraint is based on [265]. A simple manipulation of (5.12) results in the following specification for the feedback controller $C(s)$:

$$\max_{P(j\omega)\in\mathcal{P}_\omega} 20\log_{10}|T(j\omega)| - \min_{P(j\omega)\in\mathcal{P}_\omega} 20\log_{10}|T(j\omega)| \leq 20\log_{10}\frac{\delta_u(\omega)}{\delta_l(\omega)}. \tag{5.13}$$

If this specification is satisfied for a controller $C(s)$; then there exists a minimum-phase prefilter $F(s)$, that satisfies (5.12) (see [128]). This constraint can also be rewritten in the form (5.9). For a pair of plants $P_1(j\omega), P_2(j\omega) \in \mathcal{P}_\omega$, and by considering

$$L_{\text{aux}}(j\omega) = (1 + P_1(j\omega)C(j\omega))\frac{P_2(j\omega)}{P_1(j\omega) - P_2(j\omega)}, \tag{5.14}$$

this specification can be expressed as follows

$$|T_{\text{aux}}(j\omega)| = \left| \frac{L_{\text{aux}}(j\omega)}{1 + L_{\text{aux}}(j\omega)} \right| \leq \frac{\delta_u(\omega)}{\delta_l(\omega)} = \delta_{Tr}(\omega), \quad \forall P_1(j\omega), P_2(j\omega) \in \mathcal{P}_\omega. \tag{5.15}$$

When $C(s)$ has been determined, the next step is to design the prefilter $F(s)$ or the set-point weights for a PID controller (5.7). Note that with this fixed structure of the PID controller we cannot always guarantee that inequalities (5.13) and (5.15) satisfy the condition (5.12). A relaxation of the constraint (5.12) may, therefore, be required.

5.3.2 Optimization Criteria

Two optimization criteria are proposed namely: maximization of performance and minimization of the cost of feedback.

Maximizing Performance

Control system performance is provided by the gain of the feedback controller (over a range of frequencies). Therefore, a natural choice for an optimal criterion is to maximize the gain of the feedback controller at low frequencies, with some constraints that limit the gain of the controller at high frequencies. For PID control this criterion is equivalent to maximize the integral gain k_i. It is also equivalent to minimize the IE due to a load disturbance at the plant input or a unit step in the set-point, since

$$\mathrm{IE_d} = k_i^{-1}, \qquad \mathrm{IE_s} = (P(0)k_i)^{-1}, \tag{5.16}$$

where the subscripts d and s stand for disturbance and set-point, respectively.

The criterion (5.16) for the case of disturbances combined with constraints on the maximum sensitivities $\|S\|_\infty$ and $\|T\|_\infty$ corresponds to the MIGO design method.

Minimizing the Cost of Feedback

This is the optimal criterion used in QFT, where the control design problem is defined as the minimization of the cost of feedback, subject to a constraint on the minimum level of performance for every plant. In the words of Horowitz, that is "the problem of achieving desired system tolerances from uncertain plants, at minimum cost of feedback" [130]. The controller gain at low frequencies is given by the tracking specifications (5.12) and by the disturbance rejection at the plant input (or plant output) specification (5.11) (or (5.8)).

Minimization of the high-frequency gain of the controller corresponds to minimization of proportional gain k_p for a PI controller or derivative gain k_d for a controller with derivative action.

To pose the design problem we choose one criterion to be optimized while keeping the others as constraints. Different optimization problems are obtained depending on what criterion we choose to optimize.

5.3.3 Extension of MIGO Method to a Set of Plants

Adopting the disturbance attenuation in terms of minimization of IE as the specification to be placed as objective function, we arrive at an extension of MIGO method by considering a set of plants instead of a nominal plant. This is presented as follows:

$$\begin{aligned} \underset{\mathbf{x_c}}{\text{maximize}} \quad & k_i \\ \text{subject to} \quad & \|S(\mathbf{x_c})\|_\infty \leq M_s, \\ & \|T(\mathbf{x_c})\|_\infty \leq M_t, \\ & \|G_{un}(\mathbf{x_c})\|_\infty \leq M_n, \\ & \forall P(s) \in \mathcal{P}. \end{aligned} \tag{5.17}$$

If all plants have positive gain at low frequencies, then the integral gain must be positive to ensure closed-loop stability.

5.3.4 Control Design Problem Based on QFT Specifications

A control design problem with specifications and optimal criterion from QFT is stated in two stages. Firstly, the feedback controller is designed and later the prefilter. The feedback controller is determined by solving the following optimization problem:

$$\begin{aligned} \underset{\mathbf{x_c}}{\text{minimize}} \quad & |k_d| \\ \text{subject to} \quad & |T_{\text{aux}}(j\omega, \mathbf{x_c})| \leq \delta_{Tr}(\omega), \\ & |G_{yd}(j\omega, \mathbf{x_c})| \leq \delta_D(\omega), \\ & |S(j\omega, \mathbf{x_c})| \leq \delta_S(\omega), \\ & |T(j\omega, \mathbf{x_c})| \leq \delta_T(\omega), \\ & |G_{un}(j\omega, \mathbf{x_c})| \leq \delta_N(\omega), \\ & \forall P_1(j\omega), P_2(j\omega) \in \mathcal{P}_\omega, \\ & \forall P(j\omega) \in \mathcal{P}_\omega, \\ & \forall \omega \geq 0. \end{aligned} \tag{5.18}$$

The prefilter is then determined as the solution of the following optimization problem:

$$\begin{aligned} \underset{\mathbf{x_f}}{\text{maximize}} \quad & b \\ \text{subject to} \quad & |F(j\omega, \mathbf{x_f})T(j\omega)| \leq \delta_u(\omega), \\ & \forall P(j\omega) \in \mathcal{P}_\omega, \\ & \forall \omega \geq 0. \end{aligned} \tag{5.19}$$

The design of the set-point weights is a convex optimization problem, which was solved recently [120].

The requirement of closed-loop stability is assumed in both optimization problems, i.e., the feasible set of each problem is the intersection of the controller parameters satisfying the constraints with the set of parameters that provide closed-loop stability.

5.4 Loop Shaping Using the CCP

This section describes the application of the CCP to the optimization problems described in the previous section. The key idea is to describe the constraints and the optimization criteria as convex functions or differences of convex functions. Since CCP is an iterative method it is also necessary to give initial conditions. Gridding of the frequency range will be also discussed. Finally, we give a simple example that illustrates the use of the CCP for a simple design problem.

5.4.1 The CCP Method

Convex optimization has the advantage that there is a unique minimum and that very efficient and reliable computation algorithms are available. The CCP extends convex optimization to the case when the criterion and the constraint can be expressed as a difference of convex functions. That is

$$\begin{aligned} \underset{\mathbf{x}}{\text{minimize}} \quad & f_0(\mathbf{x}) - g_0(\mathbf{x}) \\ \text{subject to} \quad & f_i(\mathbf{x}) - g_i(\mathbf{x}) \leq 0, \quad i = 1, ..., m, \end{aligned} \tag{5.20}$$

where $f_i(\mathbf{x})$ and $g_i(\mathbf{x})$ (for $i = 0, 1, ..., m$) are convex functions. This is not a convex problem since $-g_i(\mathbf{x})$ is concave (see Appendix A for more details about optimization problems). To obtain a convex criterion or constraint $f_i(\mathbf{x}) - g_i(\mathbf{x})$ around a point $\mathbf{x}^k$,

$g_i(\mathbf{x})$ is substituted by its affine approximation

$$\hat{g}_i(\mathbf{x}, \mathbf{x}^k) = g_i(\mathbf{x}^k) + \nabla g_i(\mathbf{x}^k)^\top (\mathbf{x} - \mathbf{x}^k), \tag{5.21}$$

where $\nabla g_i(\mathbf{x}^k)$ is the gradient of $g_i(\mathbf{x})$ evaluated at $\mathbf{x}^k$. Since

$$f_i(\mathbf{x}) - \hat{g}_i(\mathbf{x}, \mathbf{x}^k) \geq f_i(\mathbf{x}) - g_i(\mathbf{x}), \tag{5.22}$$

the convex objective and constraints are more conservative than the originals. In this way, the feasible set will be a convex subset of the original feasible set. The convexified problem can be solved efficiently, and by using a new feasible point $\mathbf{x}^{k+1}$ the procedure is iterated. The iterative procedure converges to a saddle point or a local minimum [276]. The procedure is stopped when there is no significant improvement from the last iteration. Even though there is no guarantee of convergence to a global minimum, experience has shown the method to often be effective in obtaining good solutions [119]. Note that the algorithm requires a feasible starting point $\mathbf{x}^0$, some guidelines for determining a starting point for the control problems under consideration will be given later.

5.4.2 Circle Constraints

Consider a circle with center c_c and radius r_c. The constraint that the Nyquist plot of $L(s, \mathbf{x_c})$ should lie outside the circle at a given frequency ω is equivalent to

$$r_c - |L(j\omega, \mathbf{x_c}) - c_c| = r_c - g(\mathbf{x_c}) \leq 0, \tag{5.23}$$

where $\mathbf{x_c} = [k_p \ k_i \ k_d]^\top$. The inequality constraint (5.23) is not a convex constraint, since $g(\mathbf{x_c})$ is a convex function. By using the approximation (5.21) of (5.23), we get

$$\hat{g}(\mathbf{x_c}, \mathbf{x_c}^k) = \Re\left(\frac{(L(j\omega, \mathbf{x_c}^k) - c_c)^*}{|L(j\omega, \mathbf{x_c}^k) - c_c|}(L(j\omega, \mathbf{x_c}^k) - c_c)\right), \tag{5.24}$$

where $\Re$ and $*$, denotes the real part and complex conjugate. This linearization of $g(\mathbf{x_c})$ was introduced in [119]. The vector $\mathbf{x_c}^k$ represents the controller parameters from iteration k that leads to the convex constraint

$$r_c - \hat{g}(\mathbf{x_c}, \mathbf{x_c}^k) \leq 0. \tag{5.25}$$

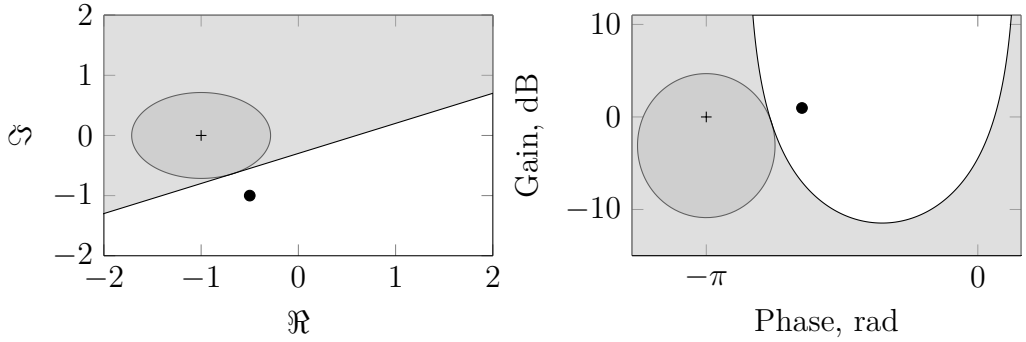

Figure 5.2 Linearization of circle constraints

Linearization of circle constraints in the complex plane (left) and the corresponding situation in the Nichols plane (right).

Figure 5.2 illustrates graphically this linearization both in the complex plane (left) and the Nichols plane (right), the linearization is done with respect to the point denoted with a dot.

This constraint is used to impose an upper bound on the magnitude of the sensitivity at a given frequency; and to impose an upper bound on the complementary sensitivity at a given frequency, when this upper bound is greater than or equal to 1. When this upper bound is less than or equal to 1, the constraint that the Nyquist plot should lie inside the circle at a given frequency ω is used, that is equivalent to

$$|L(j\omega, \mathbf{x_c}) - c_c| - r_c = g(\mathbf{x_c}) - r_c \leq 0, \tag{5.26}$$

which is also a convex constraint.

For a given plant $P(s) \in \mathcal{P}$ and a given frequency ω, the design specifications can be expressed in the form of (5.23) or (5.26), where the values of c_c and r_c are given in Table 5.1 (see [265]). The constraint (5.13) can be rewritten in the form (5.15), where $L_{\text{aux}}(s)$ depends affinely on the controller parameters $\mathbf{x_c}$. The previous method can thus also be used for the robust tracking specification. Finally, note that for the cases $\delta_T = 1$ and $\gamma_G = 1$ the circles are distorted into straight lines.

5.4.3 Initialization

The proposed method needs an initial controller that stabilizes the system and satisfies the constraints for all plants in $\mathcal{P}$. In some relevant cases this choice is quite simple, a controller with all parameters equal to zero can be used for problems as (5.17), if all plants are stable. More care is required if some plants in $\mathcal{P}$ are unstable, see [119].

Table 5.1 Values of c_c and r_c for different closed-loop specifications

Specification	Constraint	c_c	r_c
$\lvert S(j\omega)\rvert \leq \delta_S(\omega)$	(5.23)	-1	$\frac{1}{\delta_S(\omega)}$
$\lvert T(j\omega)\rvert \leq \delta_T(\omega)$, with $\delta_T(\omega) \geq 1$	(5.23)	$\frac{\delta_T^2(\omega)}{1-\delta_T^2(\omega)}$	$\frac{\delta_T(\omega)}{\lvert 1-\delta_T^2(\omega)\rvert}$
$\lvert T(j\omega)\rvert \leq \delta_T(\omega)$, with $\delta_T(\omega) \leq 1$	(5.26)	$\frac{\delta_T^2(\omega)}{1-\delta_T^2(\omega)}$	$\frac{\delta_T(\omega)}{\lvert 1-\delta_T^2(\omega)\rvert}$
$\lvert G_{un}(j\omega)\rvert \leq \delta_G(\omega)$, with $\delta_G(\omega)\lvert P(j\omega)\rvert \geq 1$	(5.23)	$\frac{\gamma_G^2(\omega)}{1-\gamma_G^2(\omega)}$	$\frac{\gamma_G(\omega)}{\lvert 1-\gamma_G^2(\omega)\rvert}$
$\lvert G_{un}(j\omega)\rvert \leq \delta_G(\omega)$, with $\delta_G(\omega)\lvert P(j\omega)\rvert \leq 1$	(5.26)	$\frac{\gamma_G^2(\omega)}{1-\gamma_G^2(\omega)}$	$\frac{\gamma_G(\omega)}{\lvert 1-\gamma_G^2(\omega)\rvert}$
$\lvert G_{yd}(j\omega)\rvert \leq \delta_D(\omega)$	(5.23)	-1	$\frac{1}{\gamma_D(\omega)}$

$\gamma_G(\omega) = \delta_G(\omega)\lvert P(j\omega)\rvert$ and $\gamma_D(\omega) = \delta_D(\omega)\lvert P(j\omega)\rvert$.

A two-step procedure can be used for the optimization problem (5.18). An optimization problem of the type (5.17) is first solved in order to provide adequate controller parameters to the optimization problem (5.18). The controller obtained by optimizing (5.17) has high gain at low frequencies, because the integral gain k_i is maximized, and it is expected that this controller will satisfy the constraints of (5.18). This procedure is illustrated in Example 5.3.

Finally, simple tuning rules like approximate MIGO method (AMIGO) [18] and SIMC [233] can also be used for initialization.

5.4.4 Insight from QFT Analysis

When using CCP it is necessary to grid the templates $\mathcal{P}_\omega$. Several ideas from QFT may help to reduce the number of plants to consider in the proposed optimization problems, in order to reduce the computational burden. Methods for doing this will be discussed. Techniques for dealing with worst-case robust optimization problems will also be briefly presented, together with relations to standard methods used in QFT design.

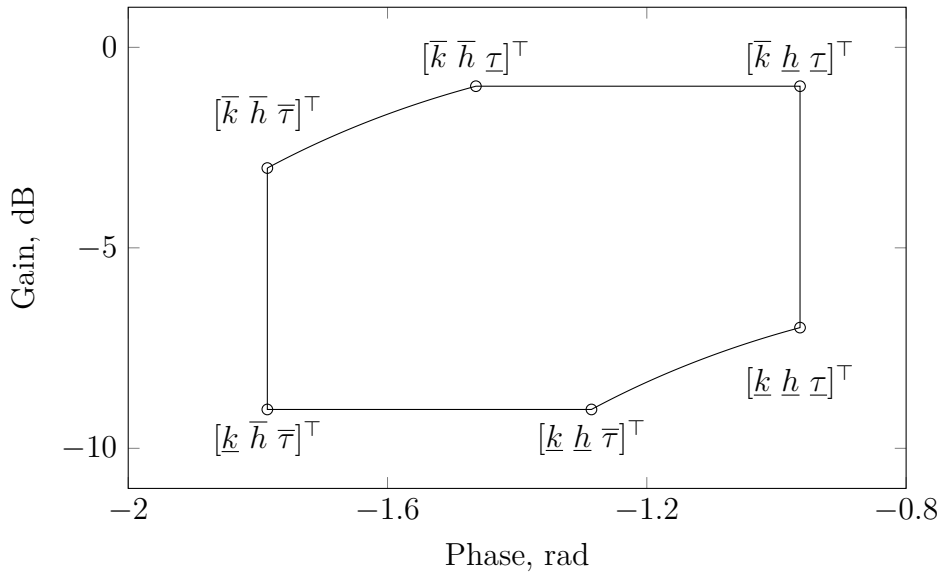

Figure 5.3 Template for an uncertain FOTD plant

Template for FOTD plant with interval parametric uncertainty (described in (5.27)) at a given frequency.

Simply Connected Templates

For simply connected templates (templates that consist of one piece and do not have any holes in the extended Nichols chart that spans over all Riemann surfaces) and $L(s)$ with a fixed number of unstable poles, it is necessary and sufficient to work only with the boundary of the templates [57].

The FOTD plant model with interval parametric uncertainty is commonly used in industry. It can be represented by

$$\mathcal{P} = \left\{ \frac{k}{\tau s + 1} e^{-sh} : [k\ h\ \tau]^\top \in \Theta \subset \mathbb{R}^3_+ \right\}. \tag{5.27}$$

where $\Theta = [\underline{k}, \overline{k}] \times [\underline{h}, \overline{h}] \times [\underline{\tau}, \overline{\tau}]$. The boundaries of the templates for this case are easily parametrized, since these boundaries can be decomposed into several sections, where only one parameter changes. The boundary of the plant template can be obtained by mapping the boundary of the plant parameter uncertainty region, as illustrated in Figure 5.3, where the template of an FOTD model with $\underline{k} = \underline{h} = \underline{\tau} = 0.5$, $\overline{k} = \overline{h} = \overline{\tau} = 1$, and $\omega = 1$ is shown.

Although templates computation may be efficiently solved for some uncertainty types (for plants like in Figure 5.3 by gridding over the edges of the parameter set [92], or using interval analysis [192]), in general templates computation must be solved by

gridding the whole parameter set. This approach has to be followed with some care [114], since it may result in spurious computations because it generates a large number of internal points of no interest for optimization, and on the other hand some critical point of the templates could be missed. A brief overview of the generation of plant templates has been presented in Section 2.2.2.

Simplifications for some Fixed Controller Structures

There are cases in which some conditions related to the gain and phase of the loop transfer function may reduce the dimensionality of the problem.

Remark 5.1. *Consider an uncertain ITD model given by the following set of transfer functions*

$$\mathcal{P} = \left\{ \frac{k}{s} e^{-sh} : [k \ h]^\top \in [\underline{k}, \overline{k}] \times [\underline{h}, \overline{h}] \subset \mathbb{R}^2_+ \right\}, \tag{5.28}$$

a PI controller $C(s) = k_p + \frac{k_i}{s}$*, and the specifications of robustness,* $\|S\|_\infty \leq M_s$ *and* $\|T\|_\infty \leq M_t$*. Then, a vector of controller parameters* $[k_p \ k_i]^\top$ *that solves the problem for*

$$\mathcal{P}_r = \left\{ \frac{\underline{k}}{s} e^{-s\overline{h}}, \frac{\overline{k}}{s} e^{-s\overline{h}} \right\} \subseteq \mathcal{P}, \tag{5.29}$$

is also a solution for the set $\mathcal{P}$*. The insight from the QFT analysis is that it is sufficient to explore only two systems, corresponding to plants with the longest time delay and the largest and smallest steady-state gains. A formal proof of that has been presented in Chapter 3.*

Remark 5.2. *Consider an uncertain FOTD model given by the following set of transfer functions*

$$\mathcal{P} = \left\{ \frac{k}{\tau s + 1} e^{-sh} : [k \ h \ \tau]^\top \in \Theta \subset \mathbb{R}^3_+ \right\}, \tag{5.30}$$

where $\Theta = [\underline{k}, \overline{k}] \times [\underline{h}, \overline{h}] \times [\underline{\tau}, \overline{\tau}]$*, a PI controller* $C(s) = k_p + \frac{k_i}{s}$*, and the specifications of robustness,* $\|S\|_\infty \leq M_s$ *and* $\|T\|_\infty \leq M_t$*. Then, a pair of values* $[k_p \ k_i]^\top$ *that solves the problem for*

$$\mathcal{P}_r = \left\{ \frac{k}{\tau s + 1} e^{-sh} : [k \ h \ \tau]^\top \in [\overline{k}] \times [\overline{h}] \times [\underline{\tau}, \overline{\tau}] \right\} \subseteq \mathcal{P}, \tag{5.31}$$

is also a solution for the set $\mathcal{P}$*, if the following property is satisfied*

$$\frac{dArg(L(j\omega))}{d\omega} \leq 0, \quad \forall P(s) \in \mathcal{P}_r, \tag{5.32}$$

where $L(s)$ is the open-loop transfer function. The intuitive idea behind that can be devised by using the Nichols chart and the inverse Nichols chart. The proof of this statement follows with the same arguments as in [179].

Remark 5.3. *Consider an uncertain FOTD model given by the following set of transfer functions*

$$\mathcal{P} = \left\{ \frac{k}{\tau s/q + 1} e^{-sh/q} : q \in [\underline{q}, \bar{q}] \subset \mathbb{R}_+ \right\}, \tag{5.33}$$

a PI controller $C(s) = k_p + \frac{k_i}{s}$, and the specifications of robustness, $\|S\|_\infty \leq M_s$ and $\|T\|_\infty \leq M_t$. Then, a pair of values $[k_p \ k_i]^\top$ that solves the problem for

$$\mathcal{P}_r = \left\{ \frac{k}{\tau s/\underline{q} + 1} e^{-sh/\underline{q}} \right\} \subseteq \mathcal{P}, \tag{5.34}$$

is also a solution for the set $\mathcal{P}$. Uncertain models of this type appear in the process industry, where the variable q is typically a flow. Plant dynamics changes with flow, see [23]. An insight gained from the QFT analysis is that it is sufficient to explore only one plant, namely the one with the lowest value of $\bar{q}$. By using normalization properties, it is easy to see that increasing q is equivalent to decreasing (in absolute value) k_i, and it is well known that such decrement of integral gain does not lead to a violation of these constraints.

Note that the gain of the open-loop frequency response in these three cases is always nonincreasing with respect to the frequency; in fact, it is decreasing for all controller parameters except for the trivial parameters ($k_p = 0$ and $k_i = 0$).

Iterative Design in QFT

In the QFT framework, it is common to solve the problem for a (modest) number of frequencies, and later validate the solution (some iterations may be needed to obtain a satisfactory solution) [46]. This procedure bares similarity to some methods used to solve worst-case robust optimization problems. The optimization problems presented in this work can be seen as worst-case robust optimization problems, with arbitrary dependence on the uncertain parameters (in our case points belonging to the boundary of the templates at different frequencies), then some techniques used in such problems can be applied to the problems presented here, for example, cutting-set methods [191]. These methods obtain a solution for an uncertainty set $\mathcal{U}$ by solving a sequence of sampled problems, with expanding sets of scenarios $\hat{\mathcal{U}}_i \subset \mathcal{U}$, which are found by evaluation in the original set $\mathcal{U}$ (it alternates between optimization and worst-case

analysis). It can be viewed as a generalization of the common procedure in QFT, but considering an adaptive sampling not only in the frequency but also in the boundaries of the templates.

The robust optimization problems presented in this works can be recast in the following form:

$$\begin{aligned} \underset{\mathbf{x}}{\text{maximize}} \quad & f_0(\mathbf{x}) \\ \text{subject to} \quad & f_i(\mathbf{x}, \mathbf{u}) \leq 0, \quad \forall \mathbf{u} \in \mathcal{U}, \quad i = 1, \ldots, m. \end{aligned} \tag{5.35}$$

where the set $\mathcal{U}$ is a finite set of points, but with a large number of points, corresponding to the (boundary) templates at different frequencies.

In order to give an overview of the methods presented in [191], it is necessary to define some concepts. The *worst-case constraint functions* are defined as

$$F_i(\mathbf{x}) \equiv \max_{\mathbf{u} \in \mathcal{U}} f_i(\mathbf{x}, \mathbf{u}). \tag{5.36}$$

This function is evaluated to perform a worst-case analysis. A *sequence of sampled optimization problem* (indexed by k) is defined as

$$\begin{aligned} \underset{\mathbf{x}}{\text{maximize}} \quad & f_0(\mathbf{x}) \\ \text{subject to} \quad & f_i(\mathbf{x}, \mathbf{u}) \leq 0, \quad \forall \mathbf{u} \in \hat{\mathcal{U}}_i^k, \quad i = 1, \ldots, m, \end{aligned} \tag{5.37}$$

where $\hat{\mathcal{U}}_i^k$ are finite subsets of $\mathcal{U}$. The solution of the k-th optimization problem is denoted as $\mathbf{x}^k$.

A basic cutting-set method consists in solving a sequence of sampled optimization problem (5.37), with expanding set of scenarios $\hat{\mathcal{U}}_i^k$, that are found by performing a worst-case analysis, i.e. evaluating (5.36). The expanding of the set of scenarios $\hat{\mathcal{U}}_i^k$ is obtained by appending to the previous ones, i.e. $\hat{\mathcal{U}}_i^{k-1}$, the elements $\mathbf{u} \in \mathcal{U}$ for which $f_i(\mathbf{x}^{k-1}, \mathbf{u})$ are maximum. The iterative process is stopped when $\max_{i=1,\ldots,m} F_i(\mathbf{x}^{k-1})$ is less than a predefined threshold, typically, a small positive number.

5.5 Examples

To illustrate the effectiveness of the proposed method we will explore some examples that have been investigated previously with other methods. The package CVX is used to formulate and solve the optimization problems [103, 104].

Example 5.1 (An illustrative example)**.** The following simple example illustrates how the CCP works. The plant and the controller have the transfer functions

$$P(s) = \frac{e^{-s}}{s+1}, \tag{5.38}$$

and

$$C(s, \mathbf{x_c}) = k_p + \frac{k_i}{s}. \tag{5.39}$$

The optimization problem is given as follows:

$$\begin{array}{ll} \underset{\mathbf{x_c}}{\text{maximize}} & k_i \\ \text{subject to} & \|S(\mathbf{x_c})\|_\infty \leq 1.6, \end{array} \tag{5.40}$$

where $\mathbf{x_c} = [k_p \ k_i]^\top$. To obtain a tractable problem, a grid of frequencies is chosen, for each frequency the constraint of the optimization problem takes the form of (5.23). A sparse discretization of the frequency is used to obtain an easy visualization of the constraints in the $k_p - k_i$ plane. These constraints have a nice geometrical interpretation in the controller parameter space, $k_p - k_i$ plane; each constraint is translated into an ellipse of forbidden parameters [22], whose centers define the stabilizing set. To obtain convex constraints the constraints are linearized for each frequency (5.23) resulting in constraints as half planes (5.25). Hence for each frequency, the exterior of each ellipse is replaced by a half plane. The iterations are illustrated in Figure 5.4. Black dots mark the point used in the linearization and the point that maximizes the integral gain is marked with squares. The dashed line is the border of the stability region. In this simple example, a good solution was obtained after only three iterations.

Example 5.2 (Temperature control problem)**.** This example of temperature control of an industrial heat exchanger is the one considered in Example 4.1. The steam flow rate in one loop of the heat exchanger is manipulated to control the temperature difference between outflow and inflow in the other loop. A model in the form of FOTD transfer functions, is given in [251]. The input is the valve opening and the output is a temperature difference. The parameters of the model for different operating points are given in Table 5.2.

Uncertain dynamics will be modeled in two different ways. The set $\mathcal{P}_1$ is modeled as

$$\mathcal{P}_1 = \left\{ \frac{k}{\tau s + 1} e^{-sh} : [k \ h \ \tau]^\top \in \Theta \right\}, \tag{5.41}$$

where $\Theta = [0.31, 0.40] \times [50, 88] \times [80, 114]$, if the parameters vary independently.

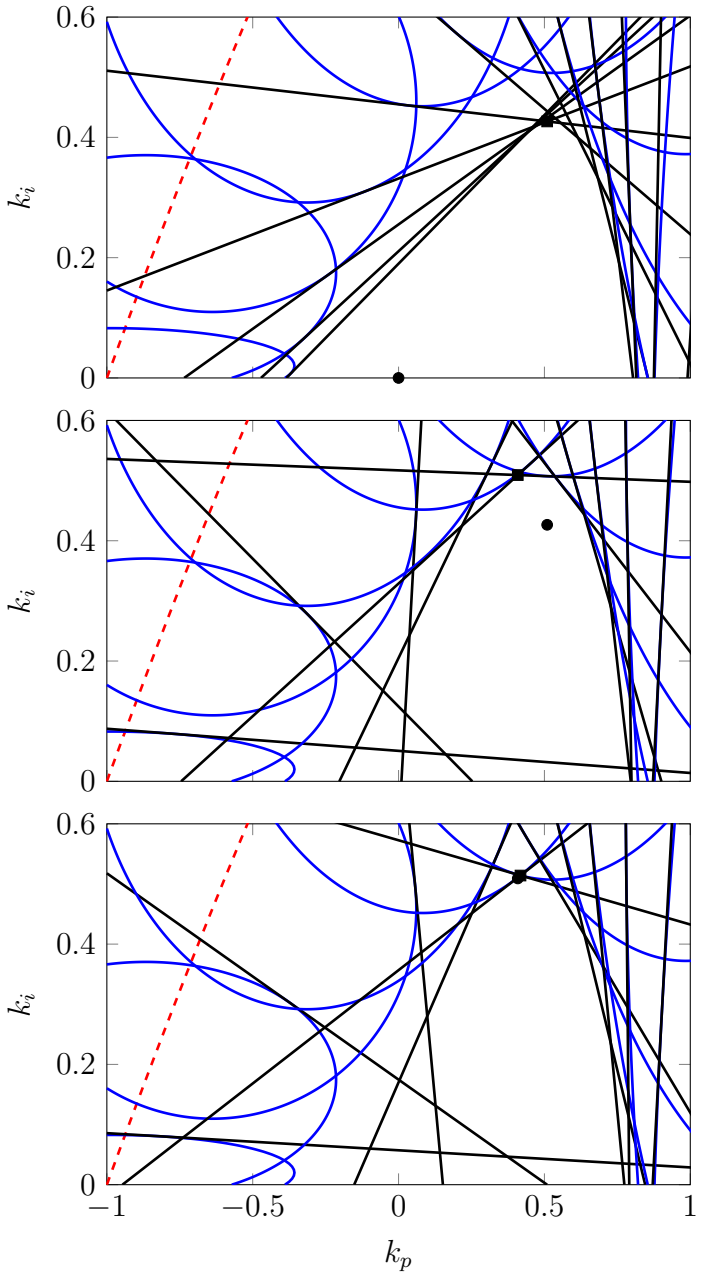

Figure 5.4 Illustration of the CCP (Example 5.1)

The feasible point used to linearize the non convex constraints (ellipses) is marked with a dot, and the optimal point is marked with a square. The dashed line delimits the stabilizing set.

Table 5.2 Plant model uncertainty (Example 5.2)

Plant	k	h	τ
$P_1(s)$	0.32	88	87
$P_2(s)$	0.35	83	82
$P_3(s)$	0.40	65	80
$P_4(s)$	0.40	50	89
$P_5(s)$	0.35	76	95
$P_6(s)$	0.31	84	114

Another way is to model the uncertainty by the smallest simple polygon $\mathcal{P}_2$ in the Nichols plane that contains the six points in Table 5.2. This is appropriate if the there are dependencies between the parameter variations. The set $\mathcal{P}_2$ can be generated using tools from computational geometry. We use the alpha shape procedure [83], with the alpha radius that gives only one region with the tightest fitting alpha shape (containing all the points); the result is the smallest simple polygon enclosing all the points in this particular case. This approach remains feasible for sets with large cardinality. The problem of finding the simple polygon containing a set of points with minimum enclosed area is NP-complete [87].

Figure 5.5 shows the templates $\mathcal{P}_{1\omega}$ and $\mathcal{P}_{2\omega}$ for some frequency values. The figure indicates that the template $\mathcal{P}_{1\omega}$ is more conservative than $\mathcal{P}_{2\omega}$

We choose a PI controller with no filtering, with the transfer function

$$C(s, \mathbf{x_c}) = k_p + \frac{k_i}{s}, \tag{5.42}$$

where $\mathbf{x_c} = [k_p \; k_i]^\top$.

The following optimization problem maximizes performance subject to a robustness constraint:

$$\begin{aligned} \underset{\mathbf{x_c}}{\text{maximize}} \quad & k_i \\ \text{subject to} \quad & \|S(\mathbf{x_c})\|_\infty \leq 1.4, \\ & \forall P(s) \in \mathcal{P}. \end{aligned} \tag{5.43}$$

A discretization of the frequency range and the boundaries of the templates are required to obtain a tractable problem. Solving the optimization problem using CCP for the

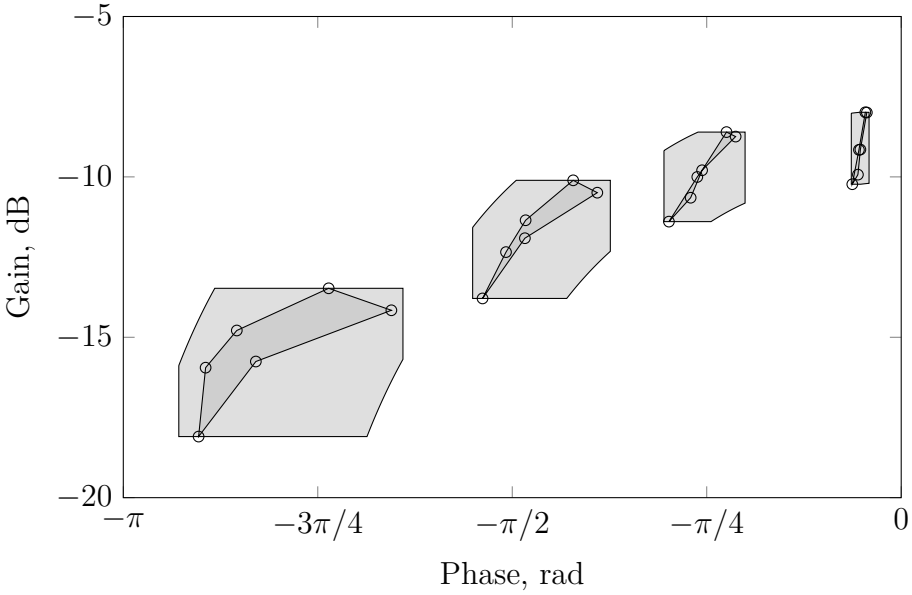

Figure 5.5 Different templates (Example 5.2)

Templates $\mathcal{P}_{1\omega}$ (interval templates) and $\mathcal{P}_{2\omega}$ (polygonal templates) at frequencies $\omega \in [0.001\ 0.005\ 0.01\ 0.02]$.

sets $\mathcal{P}_1$ and $\mathcal{P}_2$ gives the controllers

$$C_1(s) = 0.93 + \frac{0.011}{s}, \qquad C_2(s) = 1.04 + \frac{0.013}{s}. \tag{5.44}$$

The controllers $C_1(s)$ and $C_2(s)$ correspond to the sets $\mathcal{P}_1$ and $\mathcal{P}_2$, respectively. The integral gain in $C_2(s)$ is about 20 % higher than the integral gain in $C_1(s)$. Figure 5.6 shows the responses from unit step disturbances at the plant input d for controllers C_1 (solid lines) and C_2 (dashed lines) for the six plants shown in Table 5.2.

The method applies to arbitrary templates and is less conservative than methods based on a particular class of templates, for example, templates based on interval parameters (as this example has shown).

Example 5.3 (Control of an exhaust gas recirculation (EGR) valve)**.** Design of a PID controller with typical QFT specifications is illustrated in this example. The problem is to control the air-to-fuel ratio of exhaust gas by manipulating the EGR valve. This loop is part of a MIMO system, where each control loop includes a PID controller with prefilter. There are also static decouplers with gains designed to reduce cross-couplings. Models and a detailed problem description are given in [207].

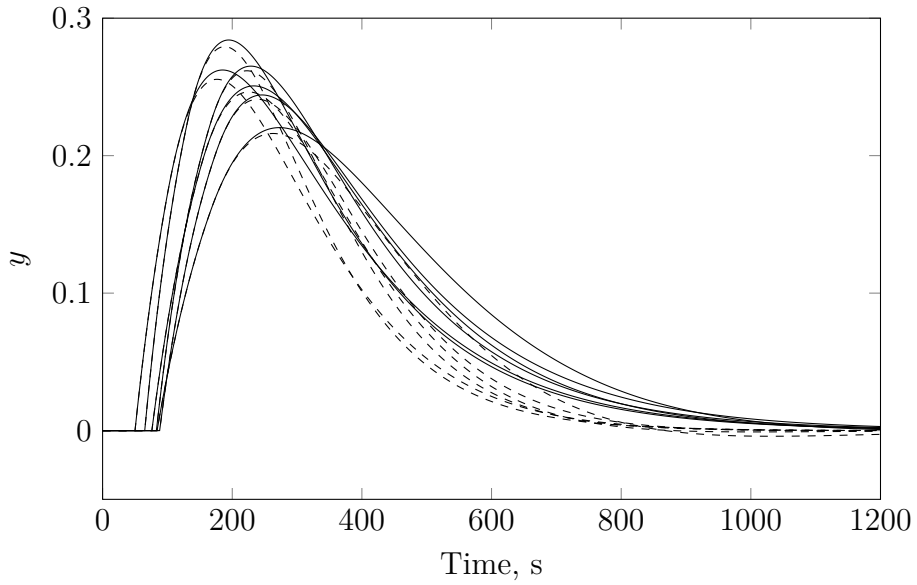

Figure 5.6 Temporal responses (Example 5.2)

Step responses due to a unit step disturbance at the plant input d for controllers C_1 (solid lines) and C_2 (dashed lines).

The plant model is given by the set

$$\mathcal{P} = \left\{ \frac{k}{\tau s + 1} e^{-sh} : [k \ h \ \tau]^\top \in \Theta \right\}, \tag{5.45}$$

where $\Theta = [0.23, 0.64] \times [0.12, 0.24] \times [0.43, 0.50]$.

The specifications cover robust stability and tracking performance. Robust stability is ensured by an upper bound on the gain of the complementary sensitivity transfer function. That is

$$|T(j\omega)| \leq 1.1, \ \forall P(j\omega) \in \mathcal{P}_\omega, \ \forall \omega \in \Omega, \tag{5.46}$$

where $\Omega = 2\pi \, [0.01 \ 0.05 \ 0.1 \ 0.2 \ 0.4 \ 0.5 \ 1 \ 1.5 \ 2]$.

Robust tracking performance is specified by

$$\delta_l(\omega) \leq |F(j\omega)T(j\omega)| \leq \delta_u(\omega), \quad \forall P(j\omega) \in \mathcal{P}_\omega, \ \forall \omega \in \Omega, \tag{5.47}$$

where

$$\delta_u(\omega) = \left| \frac{1.02 j\omega + 5.09}{(j\omega)^2 + 2.67 j\omega + 5.09} \right|, \tag{5.48}$$

$$\delta_l(\omega) = \left| \frac{21.95}{(j\omega)^3 + 12.67 (j\omega)^2 + 28.86 j\omega + 21.95} \right|. \tag{5.49}$$

The requirements are captured by minimizing the cost of feedback subject to a robustness constraint, hence

$$\begin{aligned} \underset{\mathbf{x_c}}{\text{minimize}} \quad & |k_d| \\ \text{subject to} \quad & |T_{\text{aux}}(j\omega, \mathbf{x_c})| \leq \frac{\delta_u(\omega)}{\delta_l(\omega)} = \delta_{Tr}(\omega), \\ & |T(j\omega, \mathbf{x_c})| \leq 1.1, \\ & \forall P_1(j\omega), P_2(j\omega) \in \mathcal{P}_\omega, \\ & \forall P(j\omega) \in \mathcal{P}_\omega, \\ & \forall \omega \in \Omega. \end{aligned} \tag{5.50}$$

The frequency set Ω is finite, but the sets $\mathcal{P}_\omega$ are infinite. The problem will be solved for a subset of points belonging to the boundaries of each template $\mathcal{P}_\omega$. The first step is to find a controller $C(s)$, the design of the prefilter $F(s)$ is then straightforward.

To compare with [207] we will design a controller without the measurement filter. The first controller is obtained by maximizing performance subject to a robustness constraint. This is captured by the following optimization problem:

$$\begin{aligned} \underset{x_c}{\text{maximize}} \quad & k_i \\ \text{subject to} \quad & |T(j\omega, \mathbf{x_c})| \leq 1.1, \\ & \forall P(j\omega) \in \mathcal{P}_\omega, \\ & \forall \omega \in \Omega. \end{aligned} \tag{5.51}$$

A controller with all its parameters equal to zero is used for initialization. The CCP procedure gives the following controller

$$C_{\text{PID}}(s) = 2.64 + \frac{6.60}{s} + 0.33s. \tag{5.52}$$

Since this controller maximizes integral gain subject to a constraint on the complementary sensitivity peak, it is expected that it satisfies the constraints of the optimization problem (5.50). Using the controller (5.52) to initialize CCP for the optimization problem (5.50) gives the controller

$$C_{\text{PID}}(s) = 1.97 + \frac{4.66}{s} + 0.14s. \tag{5.53}$$

In [207], the controller was obtained by manual loop shaping using a computer aided design package. The following controller was obtained:

$$C_{\text{PID}}(s) = 2.04 + \frac{4.20}{s} + 0.24s. \tag{5.54}$$

Figure 5.7 (top) shows the gain of the PID controllers (5.52), (5.53), and (5.54). The controller (5.52) (dashed line) was obtained by maximizing the integral gain, as a consequence of that this controller has higher gain than the others for all frequencies because it maximizes performance at the cost of having a higher cost of feedback. The controller (5.53) (solid line) that minimizes the derivative gain has similar low-frequency properties compared to (5.54) (dotted line) but it is clearly superior at high frequencies, where its gain is about 5 dB less than (5.54). These properties are illustrated in Figure 5.7 (middle), where $\max |T_{\text{aux}}(j\omega)|$ is plotted for the three controllers (with the specification $\delta_{Tr}(\omega)$), and in Figure 5.7 (bottom), where $\max |G_{un}(j\omega)|$ is plotted for the three controllers.

To explore the effects of measurement noise filtering, we introduce a second-order filter with time constant $T_f = 1/30$. This value has been chosen to have a filter with a cutoff frequency greater than (but not very far from) the significant frequencies of the previous PID controllers. Solving the optimization problems (5.51) and (5.50) gives the controllers

$$C_{\text{PID}}(s) = 2.18 + \frac{5.88}{s} + 0.35s, \tag{5.55}$$

and

$$C_{\text{PID}}(s) = 1.98 + \frac{4.57}{s} + 0.23s, \tag{5.56}$$

respectively.

The properties of the closed-loop system with these controllers are illustrated in Figure 5.8. Note that the inclusion of the filter degrades the maximum performance achievable, compare integral gains of controllers (5.52) and (5.55).

The design of the prefilter $F(s)$ is straightforward when the feedback controller $C(s)$ is known. A prefilter $F(s)$ with the structure given by (5.7) can be obtained by solving the following convex optimization problem:

$$\begin{aligned} \underset{\mathbf{x_f}}{\text{maximize}} \quad & b \\ \text{subject to} \quad & |F(j\omega, \mathbf{x_f})T(j\omega)| \leq \delta_u(\omega), \\ & \forall P(j\omega) \in \mathcal{P}_\omega, \\ & \omega \in \Omega. \end{aligned} \tag{5.57}$$

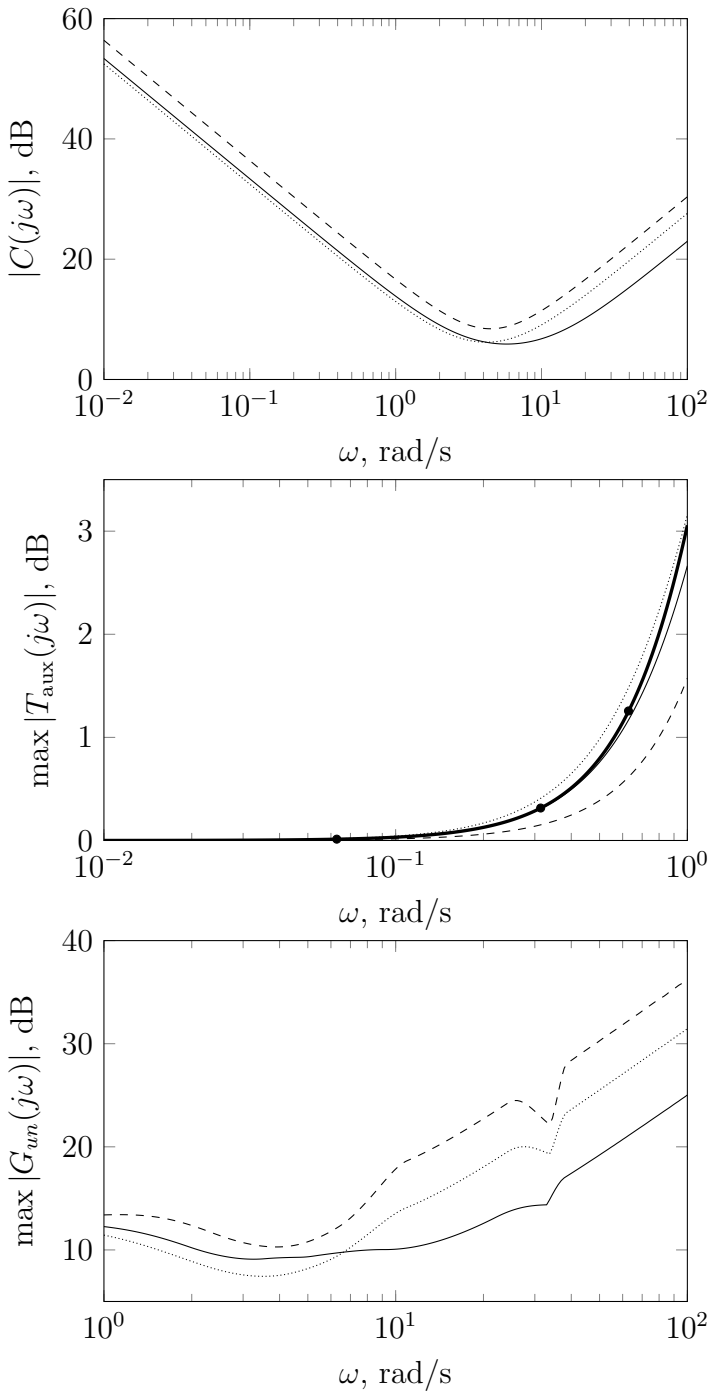

Figure 5.7 Magnitude of relevant transfer functions without the measurement filter (Example 5.3)

These graphs show $|C(j\omega)|$ (top), $\max|T_{\text{aux}}(j\omega)|$ (middle), and $\max|G_{un}(j\omega)|$ (bottom), for the controllers (5.52) (dashed line), (5.53) (solid line), and (5.54) (dotted line). The bound $\delta_{Tr}(\omega)$ is shown in a thick line in the middle graph. Frequencies in Ω are marked with a dot.

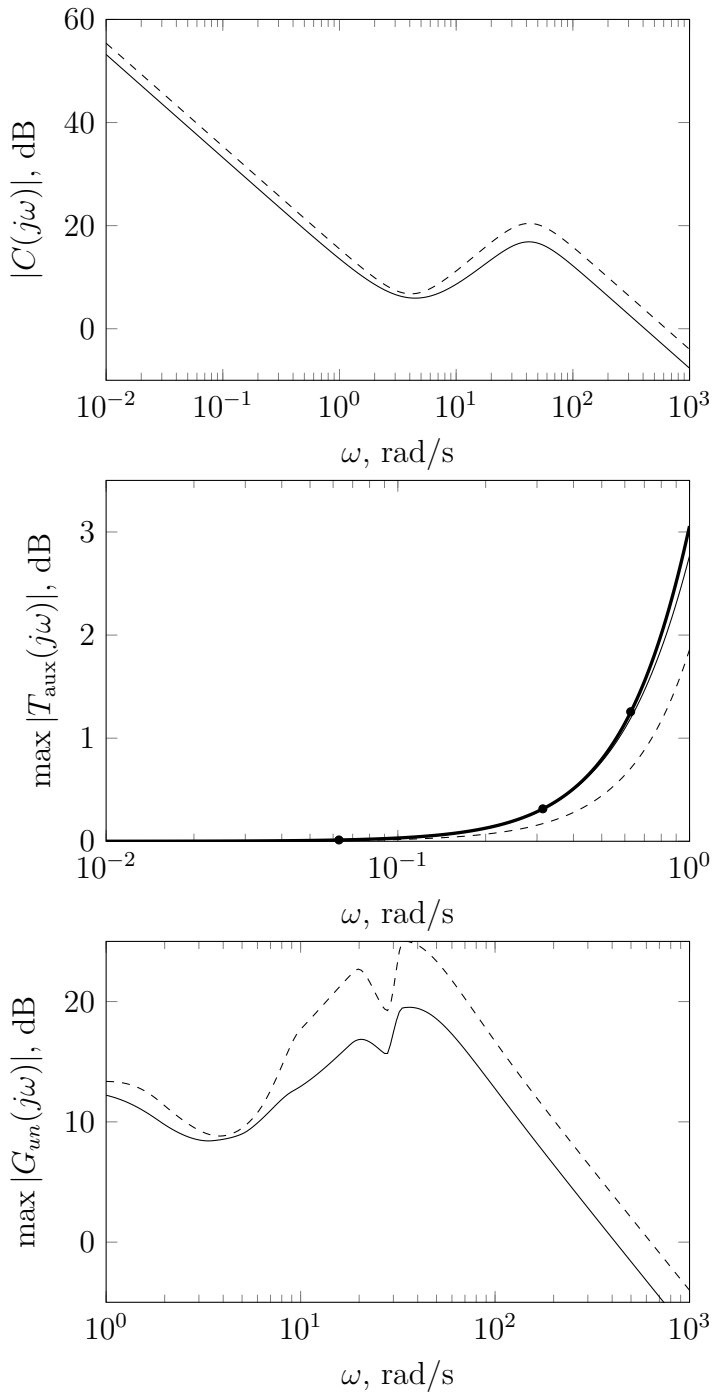

Figure 5.8 Magnitude of relevant transfer functions with the measurement filter (Example 5.3)

These graphs show $|C(j\omega)|$ (top), $\max|T_{\text{aux}}(j\omega)|$ (middle), and $\max|G_{un}(j\omega)|$ (bottom), for the controllers (5.55) (dashed line) and (5.56) (solid line). The bound $\delta_{Tr}(\omega)$ is shown in a thick line in the middle graph. Frequencies in Ω are marked with a dot.

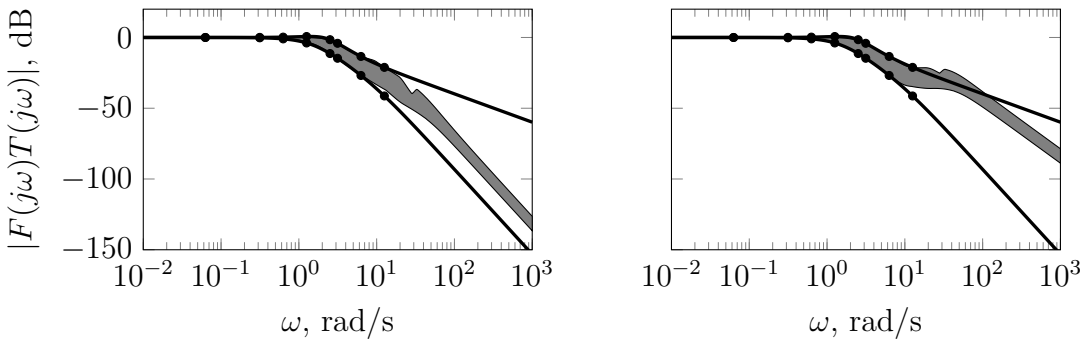

Figure 5.9 Prefilter design (Example 5.3)

The graphs show $|F(j\omega)T(j\omega)|$ for (5.55) and (5.58) (left), and for (5.56) and (5.7) (with $b = 0.22$ and $c = 0.19$) (right). Tracking specifications are shown in thick lines and frequencies belonging to Ω are marked with a dot.

The parameters obtained for the controller (5.56), are $b = 0.22$ and $c = 0.19$. The optimization problem for the controller (5.55) is not feasible and the prefilter was designed by manual loop shaping resulting in the following prefilter

$$F(s) = \frac{(s/12+1)(s/20+1)}{(s/3.5+1)(s/5+1)(s/7+1)}. \tag{5.58}$$

The properties of the prefilter designs are illustrated in Figure 5.9, where the gain of $F(s)T(s)$ is plotted for all $P(s) \in \mathcal{P}$ with the tracking specification bounds $\delta_l(\omega)$ and $\delta_u(\omega)$.

Example 5.4 (ACC'90 benchmark)**.** This example is a benchmark problem from ACC'90 [261]. The plant is an undamped spring-mass system modeled by the set of transfer functions

$$\mathcal{P} = \left\{ \frac{k}{s^2(s^2+2k)} : k \in [0.5,\ 2] \right\}. \tag{5.59}$$

The problem is to design a controller that robustly stabilizes the system and gives a settling time around 15 seconds for an impulse disturbance at the plant output for the whole range of k with a reasonable control effort.

This problem has been tackled using a low-order controller (PD with a second-order filter) in [128, pp. 198–203] and [46, Example 5]. We will attempt a design for a PD controller with a second order filter

$$C(s, \mathbf{x_c}) = \frac{k_p + k_d s}{1 + sT_f + s^2 T_f^2/2}. \tag{5.60}$$

where $\mathbf{x_c} = [k_p\ k_d]^\top$ and the value of the time constant of the filter is fixed to $T_f = 2.5$. Notice that the plant cannot be stabilized by an ideal PD controller, as can be shown by a root locus analysis.

A design that maximizes performance k_p, subject to robustness constraints is captured by the following optimization problem:

$$\begin{array}{ll} \underset{\mathbf{x_c}}{\text{maximize}} & k_p \\ \text{subject to} & |S(j\omega, \mathbf{x_c})| \leq 2, \\ & |T(j\omega, \mathbf{x_c})| \leq 2, \\ & \forall P(j\omega) \in \mathcal{P}_\omega, \quad \forall \omega \in \Omega. \end{array} \tag{5.61}$$

The set Ω is chosen as 500 frequencies logarithmically spaced between 0.01 and 10. The templates were discretized by taking 50 values of k equidistant between 0.5 and 2. The iteration was initialized by the controller parameters $k_p = 0$ and $k_d = 0.01$. Solving the problem (5.61) gives the controller parameters $k_p = 0.035$ and $k_d = 0.331$.

The top plot in Figure 5.10 shows the gain of the sensitivity (solid line) and complementary sensitivity (dashed line) for the plant gains $k = 0.5, 1, 2$. The bound on the sensitivities $M_s = M_t = 2$ is shown as a thick line in the figure. The lower plot in Figure 5.10 shows the gain curve of the transfer function G_{un} from measurement noise to control action. Notice that the gains are very low.

Figure 5.11 shows responses of an impulse at the plant output for $k = 0.5, 1, 2$. The required specification for the settling time is not satisfied and the response is oscillatory. Notice however that the controller has low order compared with other solutions proposed for this problem.

5.6 Discussion

Computation Aspects

The algorithms used in this chapter have been implemented in Matlab using CVX on a standard notebook (2.4 GHz dual-core and 8 GB RAM). Solution of the optimization problem (5.61) with 500 frequencies and 50 plants took about 5 seconds. The computation time can be reduced significantly by using the cutting-set methods discussed in Section 5.4.4. For example, by initializing the algorithm with 50 randomly chosen scenarios and iteratively expanding this set with the one that maximizes the individual constraint violations reduces the time to about 1 second. In addition, use of cutting-set

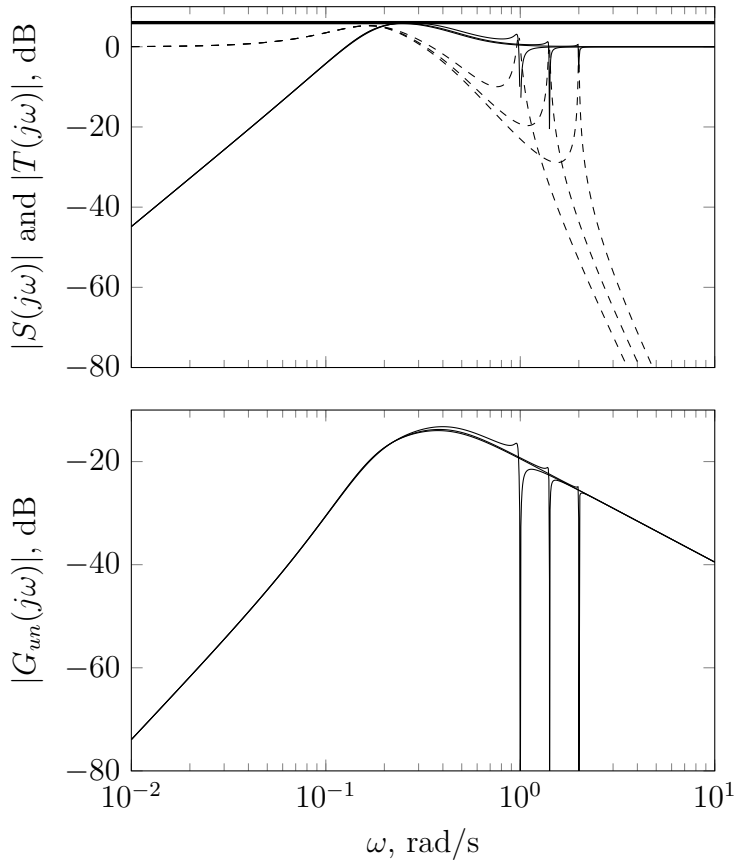

Figure 5.10 Magnitude of relevant transfer functions (Example 5.4)

The graphs show $|S(j\omega)|$ (solid line), $|T(j\omega)|$ (dashed line), and the upper bound (thick line) (top), and $|G_{un}(j\omega)|$ (bottom) (for $k = 0.5, 1, 2$).

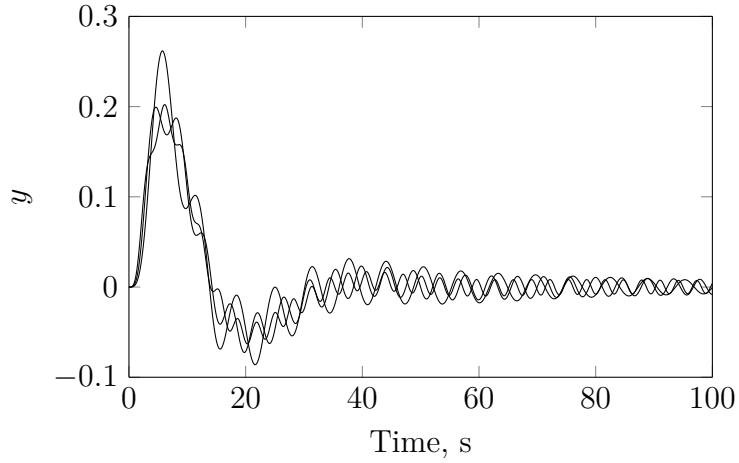

Figure 5.11 Plant response with PD (Example 5.4)

Plant output due to an impulse disturbance at the plant output (for $k = 0.5, 1, 2$).

methods makes it possible to increase the accuracy. For example, 500 values of k can be used instead of 50 without significantly increasing the computing time.

Comparison with other ALS Methods

Most of the available ALS methods use the Horowitz-Sidi bounds as a starting point, see [56, 89, 142, 212, 281, 282]. Computing the Horowitz-Sidi bounds with the QFT Toolbox in Matlab [46] for Example 5.4 took about 8 seconds, using a phase vector with 180 equidistant points between -2π and 0 rad. This is more time than the required for the presented method to obtain a solution. In addition, the generation of bounds considering more frequencies or plant cases implies a significant increment of the computation time. For example, the computing time increases by a factor of 10 if 500 values of k are used instead of 50.

Use of Higher-order Control Structures

The presented method can be applied to a higher-order controller. We consider again the plant model of Example 5.4. We propose the following structure

$$C(s, \mathbf{x_c}) = \frac{k_0 + k_1 s + k_2 s^2 + k_3 s^3}{(1 + sT_f + s^2 T_f^2/2)^2}, \tag{5.62}$$

where $\mathbf{x_c} = [k_0 \ k_1 \ k_2 \ k_3]^\top$ and $T_f = 1/15$. A higher-order controller allows for considering more demanding specifications, we consider $\|T\|_\infty \leq 1.5$ and $\|S\|_\infty \leq 1.6$ under the criterion of maximizing k_0. The initial feasible controller is obtained by manual loop-shaping $\mathbf{x_c} = [0.01 \ 0.16 \ 0.07 \ 0.64]^\top$, the proposed method obtain as solution the following parameters $\mathbf{x_c} = [0.890 \ 1.630 \ 0.891 \ 1.633]^\top$. It is interesting to note that the obtained controller have a pair of RHP complex zeros, the use of these elements in loop shaping for bending modes is discussed in [128, pp. 198–203]. Figure 5.12 shows responses of an impulse at the plant output. This solution satisfies specification for the settling time.

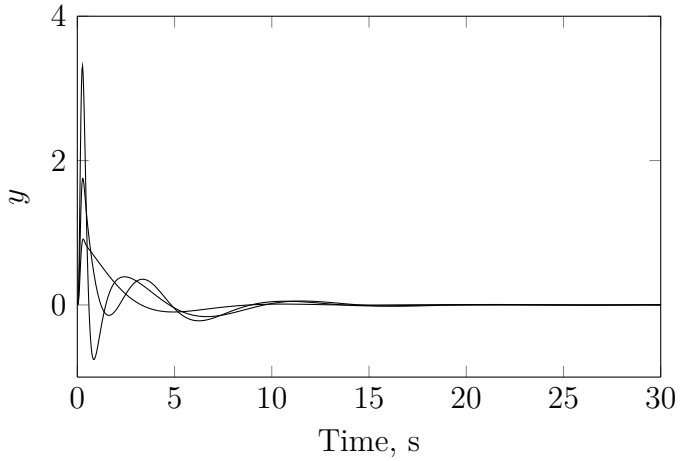

Figure 5.12 Plant response with higher-order controller (Example 5.4)

Plant output due to an impulse disturbance at the plant output (for $k = 0.5, 1, 2$) using a higher-order control structure.

Chapter 6

PID Design under Probabilistic Parametric Uncertainty

6.1 Introduction

Designing a feedback control system comprises a trade-off between achieving a good performance level and maintaining adequate stability margins. When model uncertainty is explicitly incorporated into the problem formulation, it impacts the achievable performance level. Most of the robust control literature (e.g. QFT, $\mathcal{H}_\infty$, interval methods, etc.) deals with deterministic uncertainty descriptions [209], resulting in worst-case specifications for performance and robustness. It is well-known that a deterministic approach may potentially lead to conservative designs, since the occurrence of the worst-case scenario may be very unlikely. A probabilistic uncertainty model enables computation of constraint violation probabilities; in this way, higher performance levels may be achieved at the cost of having some probability of constraint violation – typically small, and predefined by the user.

The robust design of PID controllers is usually stated as a constrained optimization problem (see [19])

$$\begin{aligned} \underset{\mathbf{x}}{\text{minimize}} \quad & J(\mathbf{x}, \boldsymbol{\theta}) \\ \text{subject to} \quad & \boldsymbol{\varphi}(\mathbf{x}, \boldsymbol{\theta}) \leq \mathbf{0}, \end{aligned} \tag{6.1}$$

where $\mathbf{x}$ is the design (controller) parameter vector, and $\boldsymbol{\theta}$ is a deterministic vector of plant model parameters. This approach has been the one used in the previous chapters. The rationale of the problem (6.1) is that minimization of the objective J aims at maximizing performance over $\mathbf{x}$, while the constraint vector $\boldsymbol{\varphi}$ (with components φ_i,

and $\leq$ corresponding to the component-wise inequality) is in place to ensure robustness (i.e. to guarantee adequate stability margins).

If the model parameter vector $\boldsymbol{\theta}$ is instead assumed to be a random variable, both the cost function $J(\mathbf{x}, \boldsymbol{\theta})$ and the constraints $\boldsymbol{\varphi}(\mathbf{x}, \boldsymbol{\theta})$ also become random variables. Two possible extensions of (6.1), taking this into account, are given below:

- *Expectation-variance specifications:*

$$\begin{aligned} \underset{\mathbf{x}}{\text{minimize}} \quad & \mathbb{E}[J(\mathbf{x}, \boldsymbol{\theta})] \\ \underset{\forall i}{\text{subject to}} \quad & \mathbb{E}[\varphi_i(\mathbf{x}, \boldsymbol{\theta})] + \alpha_i \sqrt{\mathbb{V}[\varphi_i(\mathbf{x}, \boldsymbol{\theta})]} \leq \mathbf{0}. \end{aligned} \tag{6.2}$$

  The parameters α_i in (6.2) enables the user to specify a confidence for constraint fulfillment. This optimization problem maximizes performance while honoring constraints in terms of mean plus a number of standard deviations.

- *Chance-constrained specifications:*

$$\begin{aligned} \underset{\mathbf{x}}{\text{minimize}} \quad & \mathbb{E}[J(\mathbf{x}, \boldsymbol{\theta})] \\ \underset{\forall i}{\text{subject to}} \quad & \Pr[\varphi_i(\mathbf{x}, \boldsymbol{\theta}) \leq 0] \geq 1 - \alpha_i, \end{aligned} \tag{6.3}$$

  where α_i specify permissible probabilities of constraint violation. The formulation (6.3) aims to minimize the expected cost, subject to a fulfillment of the constraints with at least a predefined level of probability.

In this context, it is highly recommended to include a stability constraint for all (or almost all) cases [111]. Another option is to analyze, a posteriori, the closed-loop stability by means of randomized algorithms (RAs).

Note that both formulations are extensions of (6.1) in the sense that they are equivalent to (6.1) in the case of deterministic plant parameters $\boldsymbol{\theta}$ and $\alpha_i = 0$ for each possible value of i. While providing a feasible formulation in order to exploit the stochastic nature of the plant parameters, it is typically not possible to solve either (6.2) or (6.3) exactly, as there exists no explicit way to evaluate the objective and constraints. Their evaluation comprises the computation of multidimensional expectation integrals. However, numerical methods can be used to obtain approximations of these integrals [49, 68]. Once the expectation integrals have been approximated, the problem may be solved using standard optimization techniques. Finally, RAs may be used to probabilistically validate the obtained (approximate) solution.

Related prior works are briefly presented below: In [44], a Taylor series expansion was used to approximate the integrand of the expectation integral. This approach is the one utilized in the extended Kalman filter (EFK) to propagate the uncertainty. Test-points methods were proposed in [186] to approximate these integrals in the context of PID design. The latter approach has been integrated into an autotuner method [239] able to exploit the uncertainty that arises as a result of least-square-based identification methods (the next chapter will present these two works). In [81, 82] a polynomial chaos approach was applied to optimize temporal responses, see Section 6.2 for details. All these works consider specifications in form of *mean plus a number of standard deviations* as in (6.2), in contrast to probabilistic constraints as in (6.3). Probability estimates can also be obtained from expectation and variance by using the Chebychev inequality [206], but these estimates are expected to be very conservative, since this inequality is independent of the involved probability density function (PDF). The latter inequality states that being X an integrable random variable with finite expected value μ and finite nonzero variance σ^2, then for any positive real k

$$\Pr\left[|X-\mu| \geq k\sigma\right] \leq \frac{1}{k^2}. \tag{6.4}$$

This inequality is only useful when $k > 1$. In general, the statement of the control design problem in terms of probability constraints makes the problem more difficult to address. On the other hand, the work [258] considers the design of decentralized (multivariable) PID controllers with probabilistic robustness via Monte Carlo (MC) simulations and genetic algorithms. Other applications of stochastic methods to the design of PID controllers, not necessarily for plant models with probabilistic parameterization, have been reported, for example, in [116, 204, 271].

This chapter is organized as follows. The problem statement is given in Section 6.2. An approach to approximately solve the resulting chance-constrained optimization problem is presented in Section 6.3. RAs for numerical verification are presented in Section 6.4. To conclude, the synthesis method is illustrated through several examples in Section 6.5.

6.2 Problem Statement

We consider the 1-DOF feedback control system shown in Figure 3.1, with a plant P and controller C. The plant model is given by the arbitrary-order time-delayed transfer

function

$$P(s,\boldsymbol{\theta}) = \frac{b_B s^B + b_{B-1}s^{B-1} + \cdots + b_0}{a_A s^A + a_{A-1}s^{A-1} + \cdots + a_0} e^{-hs}, \tag{6.5}$$

where A and B are known constants satisfying $B \leq A$, and

$$\boldsymbol{\theta} = [b_B \; b_{B-1} \; \ldots \; b_0 \; a_A \; a_{A-1} \; \ldots \; a_0 \; h]^\top \tag{6.6}$$

is the stochastic plant model parameter vector. The joint PDF of $\boldsymbol{\theta}$ will be denoted as $f(\boldsymbol{\theta}) : \mathbb{R}^n \to \mathbb{R}$, where $n = A + B + 3$. A multivariate uniform PDF is assumed, being the probabilistic counterpart of the (unknown-but-bounded) interval parametric uncertainty. A rigorous justification for the use of the uniform PDF in this setting was done in [32].

We consider as controller a PID described by the following transfer function

$$C(s,\mathbf{x}) = k_p + \frac{k_i}{s} + k_d s, \tag{6.7}$$

where $\mathbf{x} = [k_p \; k_i \; k_d]^\top$ is a deterministic vector of its parameters.

The control design problem is formulated as a constrained optimization problem, in the spirit of the chance-constrained optimization problem (6.3). The main design challenge in this context is disturbance attenuation [19]. Tracking is not treated here, since it could be improved by using a 2-DOF control structure, with a reference pre-filter [19]. Similarly, attenuation of high-frequency measurement noise n is not explicitly addressed, as it can be accomplished by considering an extended plant, being the series connection of (6.5) and a low-pass filter. Regarding performance in terms of disturbance attenuation, two well-known ways of achieving it are the minimization of either the IE

$$\mathrm{IE}(\mathbf{x},\boldsymbol{\theta}) = \int_0^\infty e(t,\mathbf{x},\boldsymbol{\theta})dt, \tag{6.8}$$

or the IAE

$$\mathrm{IAE}(\mathbf{x},\boldsymbol{\theta}) = \int_0^\infty |e(t,\mathbf{x},\boldsymbol{\theta})|\, dt. \tag{6.9}$$

The error e in both (6.8) and (6.9) is caused by a unit load disturbance step d, applied with the control system in an equilibrium state, see Figure 3.1.

For well-damped systems, it holds that IE $\approx$ IAE. However, oscillatory systems with consecutive zero-crossings in e can yield small IE, while providing a large IAE. Obviously, from a performance measure point, this is not desired. Despite this, there remains one reason to consider minimization of IE in favor of IAE. It was shown in [19] that minimization of IE is equivalent to maximization of k_i in (6.7). That is, IE

minimization results in a convex objective, that, in addition, does not depend on plant parameters, and thus takes a deterministic value. Unfortunately, this is not the case for the IAE. In this work, we minimize IE while honoring a constraint on the $\mathcal{H}_\infty$-norm of the sensitivity function

$$S(s, \mathbf{x}, \boldsymbol{\theta}) = \frac{1}{1 + C(s, \mathbf{x})P(s, \boldsymbol{\theta})}. \tag{6.10}$$

Alongside enforcing robust stability, the latter ensures a well-damped closed-loop system. It is straightforward to introduce additional constraints on complementary sensitivity $T = 1 - S$ and noise sensitivity $-CS$. In a deterministic setting, this approach is known as MIGO [22, 203].

By combining (6.3), with the IE objective (6.8) expressed as maximization of k_i, and an $\mathcal{H}_\infty$-constraint on $S(s, \mathbf{x}, \boldsymbol{\theta})$, we arrive at the chance-constrained optimization problem:

$$\begin{aligned} \underset{\mathbf{x}}{\text{minimize}} \quad & -k_i \\ \text{subject to} \quad & \Pr[\|S(\mathbf{x}, \boldsymbol{\theta})\|_\infty - M_s \leq 0] \geq 1 - \alpha, \end{aligned} \tag{6.11}$$

where M_s is greater than 1, and α is nonnegative and less than 1. Note that the solution to the optimization problem (6.11) for $\alpha = 0$ is the same as the solution to the deterministic counterpart of this problem.

6.3 Chance-Constrained Optimization Problem

Our aim is to solve the chance-constrained optimization problem (6.11) in an efficient way, using a gradient-based algorithm, such as sequential quadratic programming (SQP) or interior point methods [50, 198]. This approach relies on numerous evaluations of the objective and constraint, calling for an efficient method to calculate them. Motivated by that, the multidimensional expectation integrals resulting from the constraint of (6.11) are approximated by a weighted sum defined by a quadrature rule (Section 6.3.1). The (sharp) indicator function, that is necessary to obtain probability values, have to be approximated by a (smooth) differentiable function in order to obtain reliable gradient information using numerical differences (Section 6.3.2). Finally, guidelines to obtain good initialization candidates to be used in the optimization algorithm need to be established (Section 6.3.3).

6.3.1 Constraint Evaluation

Constraint evaluation implies the calculation of expectation integrals. For example, the probability value of constraint satisfaction of (6.11) is

$$\Pr[\|S(\mathbf{x},\boldsymbol{\theta})\|_\infty - M_s \leq 0] = \mathbb{E}\left[\mathcal{I}[\|S(\mathbf{x},\boldsymbol{\theta})\|_\infty - M_s]\right], \tag{6.12}$$

where $\mathcal{I}[\cdot]$ is the indicator function, given by

$$\mathcal{I}[x] = \begin{cases} 1, & \text{if } x \leq 0, \\ 0, & \text{if } x > 0. \end{cases} \tag{6.13}$$

In this section, we introduce a function $g(\mathbf{x},\boldsymbol{\theta})$, which takes on the role of $\mathcal{I}[\|S(\mathbf{x},\boldsymbol{\theta})\|_\infty - M_s]$. The expectation of $g(\mathbf{x},\boldsymbol{\theta})$ is defined by the multivariate integral

$$\mathbb{E}\left[g\right] = \int_\Lambda g(\mathbf{x},\boldsymbol{\theta}) f(\boldsymbol{\theta}) d\boldsymbol{\theta}, \tag{6.14}$$

where Λ is the support of $f(\boldsymbol{\theta})$, i.e., the set of values for which $\boldsymbol{\theta}$ is nonzero. In general, an analytical solution to this type of integral does not exist for nonlinear $g(\mathbf{x},\boldsymbol{\theta})$. Henceforward, in this section, the dependence with respect to $\mathbf{x}$ will be omitted, whenever possible, to simplify the notation. Several numerical approaches have been presented in the literature to obtain approximate values of expectation integrals, among others, linearization of the integrand, MC methods, and quadrature rules [49]. In this work, the expectation integral (6.14) is approximated by a quadrature rule

$$I\left[g\right] \equiv \sum_{i=1}^{N} w_i g(\boldsymbol{\theta}_i), \tag{6.15}$$

comprising nodes $\boldsymbol{\theta}_i$ and weights w_i, $i = 1, \ldots, N$. An important feature of (6.15) is that nodes and weights depend solely on f. Hence they can be obtained for a given f, and subsequently used for an arbitrary g. As nodes and weights are independent of the problem instance, there exist repositories of them [66, 243].

A quadrature rule, such as (6.15), is said to have a *degree of polynomial exactness* D, if it delivers exact integral values, $I[g] = \mathbb{E}[g]$, for any n-dimensional polynomial g of total order at most D. The total order of a polynomial is defined as the maximum total order of its monomials, and the total order of a monomial is defined as the sum of orders with respect to the individual variables. (For example, a 2-dimensional polynomial of total order 2 may contain terms as θ_1, θ_2, θ_1^2, θ_2^2, and $\theta_1\theta_2$.) This issue is

of utmost importance when using a quadrature rule, since high degree of polynomial exactness translates to good integral approximations whenever g is approximable by polynomial functions (through e.g. Taylor expansion).

We will start presenting the univariate case, and then extend it to its multivariate counterpart. Focus will lie on avoiding the curse of dimensionality naturally introduced through this extension.

Univariate Quadrature

Consider first the one-dimensional case, i.e., $n = 1$. A sequence of quadrature rules for a PDF (or more general, for a given weight function) f defines, for every $\nu \in \mathbb{N}$ (accuracy level), a set of N_ν nodes $\theta_{\nu,i}$ and weights $w_{\nu,i}$, $i = 1, \ldots, N_\nu$, which are used to approximate the expectation integral (6.14) as the following weighted sum

$$I_\nu [g] \equiv \sum_{i=1}^{N_\nu} w_{\nu,i} g(\theta_{\nu,i}). \tag{6.16}$$

Here, the degree of polynomial exactness is denoted D_ν, since it depends on the accuracy level ν. A well-known example is the sequence of Gauss–Legendre (GL) quadrature rules. It comprises $N_\nu = \nu$ nodes and achieves the maximum possible polynomial exactness, $D_\nu = 2\nu - 1$ [49]. By considering the interval $[-1, 1]$ with weighting function $f(\theta) = 1$, it uses as nodes the roots of the ν-th order Legendre polynomial and as weights the integral of the associated Lagrange polynomials. Note that the previous quadrature rule would need to be normalized when using to compute expectation values for an univariate uniform distribution. Finally, by means of an affine transformation applied to the nodes, it is possible to transfer to an arbitrary interval the quadrature rule obtained for a given interval.

An interesting class of sequences of quadrature rules is the nested one. For these, the set of nodes used for a given accuracy is a subset of the nodes used for any higher accuracy. The GL quadrature rules do not have this property (see Figure 6.1 (left)). The nested sequences of quadrature rule are of interest when extending to the multivariate case. Herein, a delayed sequence of the Kronrod–Patterson (dKP) nested quadrature rules will be used, see [210]. An early nested scheme was proposed by Kronrod, he extended an n-point GL quadrature rule by $n + 1$ points such that the degree of polynomial exactness of the resulting $2n + 1$ rule is maximal. Patterson iterated the Kronrod's scheme recursively obtaining a sequence of nested quadrature rules. That scheme typically uses the 1-point and 3-point GL formulas and then iterates to form a sequence of quadrature rules. The dKP sequence of quadrature rules is

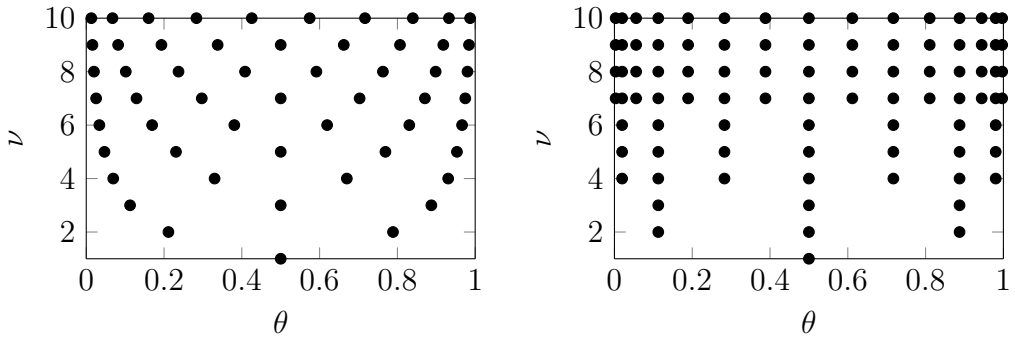

Figure 6.1 Nodes employed by different univariate quadrature rules

Nodes used by the univariate GL (left) and dKP (right) quadratures for different accuracy levels ν, from 1 to 10.

recommended for numerical computations, details about its construction can be found in [210].

Figure 6.1 shows the nodes employed by the univariate GL and dKP quadratures for the univariate uniform distribution over the interval $[0, 1]$. Observe that due to the restriction that all nodes corresponding a lower value of ν have to be used, the number of nodes is in general higher that the employed by the GL rule for the same value of ν. Although both integration rules comprise the same nodes (and weights) for the cases corresponding to $\nu = 1$ and $\nu = 3$.

Multivariate Quadrature

The extension from univariate to multivariate quadrature can be performed by using the tensor product

$$\left(I_{\nu_1} \otimes \cdots \otimes I_{\nu_n}\right)[g] \equiv \sum_{i_1=1}^{N_{\nu_1}} \cdots \sum_{i_n=1}^{N_{\nu_n}} w_{\nu_1,i_1} \cdots w_{\nu_n,i_n} g\left(\left[\theta_{\nu_1,i_1} \ \ldots \ \theta_{\nu_n,i_n}\right]^\top\right). \tag{6.17}$$

This formula for multivariate integration based on a tensor product is referred to as full grid, as opposed to sparse grid, which will be presented later. The degree of exactness of (6.17) is the same as the minimum degree of exactness of the underlying univariate quadratures. The main drawback is that it exhibits an exponential growth of nodes with respect to the dimension n (it suffers from a *curse of dimensionality*). This is due to the quadrature rule not being exact in a class of polynomials of a bounded total order, but for a tensor product of univariate polynomials [122]. (For example, considering $n = 2$ and $D = 2$, in addition to the polynomials θ_1, θ_2, $\theta_1\theta_2$, θ_1^2, and θ_2^2, it is also exact for polynomials involving the higher-order terms $\theta_1^2\theta_2$, $\theta_1\theta_2^2$, and $\theta_1^2\theta_2^2$.)

An alternative to the multivariate rules based on tensor product (full grid) is available through Smolyak's product [235]. The expression presented originally by Smolyak was given in terms of the difference of quadrature rules for different accuracy levels, but we will present one that is given directly in terms of the univariate quadrature rules, presented in [260]. The Smolyak product rule with accuracy level q, for n-dimensional integration, was formulated in [260] as

$$S_{q,n}[g] = \sum_{q+1 \leq \|\boldsymbol{\nu}\|_1 \leq q+n} (-1)^{q+n-\|\boldsymbol{\nu}\|_1} \binom{n-1}{\|\boldsymbol{\nu}\|_1 - \nu - 1} (I_{\nu_1} \otimes \cdots \otimes I_{\nu_n})[g], \tag{6.18}$$

where $\boldsymbol{\nu} = [\nu_1 \ \ldots \ \nu_n]^\top$. This rule consists of a weighted sum of product rules with accuracy levels defined by $\boldsymbol{\nu}$. Bounds on $\|\boldsymbol{\nu}\|_1$ imply that if a high level of accuracy is used in one dimension, relatively low accuracy levels are used in the others.

Two important properties of the Smolyak's product rule regarding degree of polynomial exactness and dimensional complexity are stated below (see [49] for a more detailed exposition):

- Assume that the sequence of univariate quadrature rules I_ν, with $\nu \in \mathbb{N}$, is exact for all univariate polynomial of order $2\nu - 1$. Then, the Smolyak product rule $S_{q,n}$ is exact for n-dimensional polynomials of total order $2q - 1$ or less.

- The number of nodes grows polynomially with respect to the dimension n, as opposed to the exponential growth of the tensor-product quadrature (6.17).

Both sequences of univariate quadrature rules presented here, GL and dKP, satisfy the previous assumption on polynomial exactness degree.

Nested quadrature rules, which are usually less efficient in the univariate case, become attractive when combined with Smolyak's product, since the nested quadrature rules make the union of the tensor products in (6.18) a much smaller set than when using a non-nested quadrature rule, in which each set contains different nodes.

Figure 6.2 shows the number of nodes for different integration product rules, with underlying univariate quadrature rules GL and dKP. The tensor product yields quadratures with fewer nodes than Smolyak's product rules for dimension $n = 2$, but this situation changes as the dimension increases. However, a weakness of Smolyak's product rules is that some weights may be negative, leading to erroneous results for ill-behaved integrands, e.g., a nearly Dirac's delta function on a node where the weight is negative.

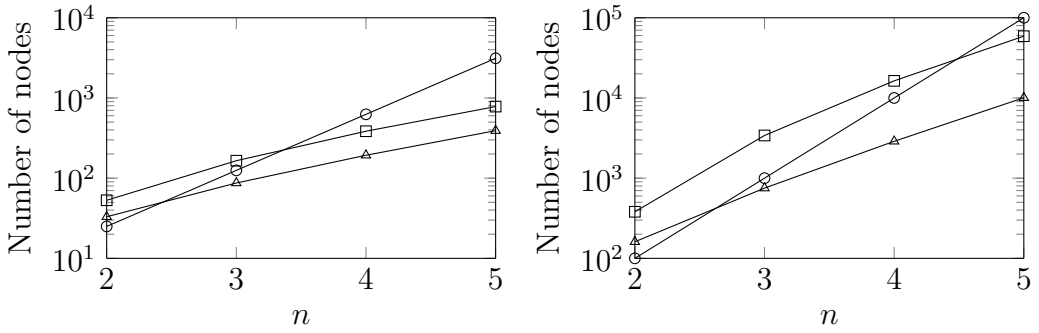

Figure 6.2 Number of nodes for different integration quadrature rules

Number of nodes versus dimension for: Full grid GL (circles), Smolyak GL (squares), and Smolyak dKP (triangles). The left graph shows the situation when $\nu = 5$ and the right graph corresponds to $\nu = 10$.

6.3.2 Constraint Gradient Evaluation

Gradient-based algorithms use the objective and constraints gradients with respect to the controller parameter vector, to find a (local) minimum to the optimization problem (6.11). The gradient of the objective function is trivial; on the other hand, the gradient of the constraint requires more attention. An analytic expression for the constraint gradient is generally not available. It may be approximated by finite differences, but the combination of the (nonsmooth) indicator function with the quadrature rule does not provide reliable gradient information. Several differentiable functions have been suggested as smooth approximations to the indicator function, including the sigmoid

$$\sigma_a(x) = \frac{1}{1 + e^{ax}}, \tag{6.19}$$

where $a \geq 0$. This is a smooth and tight approximation (it tightens as a increases), used in several other applications [250]. The mentioned approximation to the indicator function is shown in Figure 6.3 for the values $a = 50, 100, 250$. The use of approximations (quadrature rule and sigmoid function) calls for verification of numeric results. This is the topic of the next section.

6.3.3 Selection of Initial Points

To solve the chance-constrained optimization problem (6.11), a feasible initial point has to be provided to the gradient-based algorithm. Controller parameters given by the zero vector (i.e. $\mathbf{x} = [k_p \; k_i \; k_d]^\top = [0 \; 0 \; 0]^\top$) satisfy the constraints for any stable

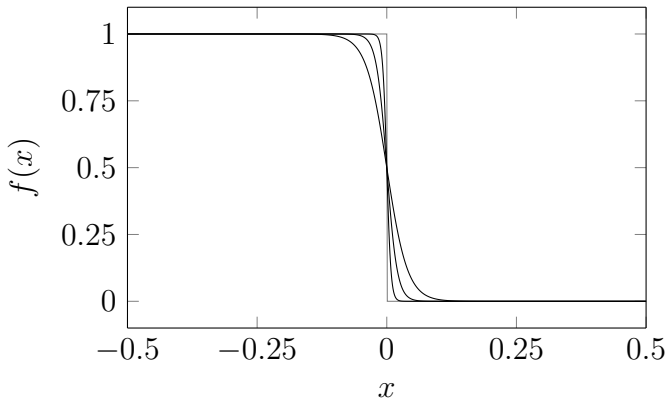

Figure 6.3 Sigmoid functions

Sigmoid approximations (black lines) to the indicator function (gray line).

plant. Otherwise, a stabilizing and feasible initial controller candidate has to be found [119].

The solution of the deterministic counterpart of the considered probabilistic design problem is an appealing alternative to the zero controller (the method presented in the previous chapter could be used here). In addition to being feasible, the corresponding controller is associated with a lower objective. This translates to a faster convergence of the method used to solve the optimization problem.

6.4 Probabilistic Verification

It is of particular interest to investigate how the approximations involved in solving the presented optimization problems affect the final result. Tools from the RAs for control analysis framework [51, 52, 246] can be used to evaluate the obtained (approximate) solutions. Let us denote the constraint fulfillment probability by

$$p = \Pr\left[\|S(\mathbf{x}, \boldsymbol{\theta})\|_\infty - M_s \leq 0\right]. \tag{6.20}$$

The RA framework provides estimates $\hat{p}$ of p, lying within an *a priori* specified accuracy $\epsilon \in (0, 1)$, with probability $1 - \delta$. This is formally stated as

$$\Pr\left[|p - \hat{p}| \leq \epsilon\right] \geq 1 - \delta. \tag{6.21}$$

A simple RA for constraint verification can be obtained through the MC method [246]. The constraint fulfillment probability estimates $\hat{p}$ are defined as

$$\hat{p} = \frac{1}{N}\sum_{i=1}^{N} \mathcal{I}\left[\|S(\mathbf{x}, \boldsymbol{\theta}^{(i)})\|_\infty - M_s\right], \tag{6.22}$$

where the samples $\boldsymbol{\theta}^{(1)}, \ldots, \boldsymbol{\theta}^{(N)}$ are generated by the PDF $f(\boldsymbol{\theta})$. A lower bound on the number of samples required to meet (6.21) is given by the so-called Chernoff bound [246]

$$\frac{1}{2\epsilon^2}\log\frac{2}{\delta} \leq N. \tag{6.23}$$

A related analysis problem is to assess the worst-case constraint violation. That is, for a given δ and ρ, to obtain with probability $1-\delta$, a level $\hat{\gamma}$ such that

$$\Pr\left[\|S(\mathbf{x}, \boldsymbol{\theta})\|_\infty \leq \hat{\gamma}\right] \geq \rho. \tag{6.24}$$

A simple RA for obtaining $\hat{\gamma}$ of (6.24) is

$$\hat{\gamma} = \max_{i=1,\ldots,N} \|S(\mathbf{x}, \boldsymbol{\theta}^{(i)})\|_\infty, \tag{6.25}$$

where $\boldsymbol{\theta}^{(1)}, \ldots, \boldsymbol{\theta}^{(N)}$ are, again, generated by the PDF $f(\boldsymbol{\theta})$ with a minimum number of samples given by

$$\frac{\log\delta}{\log\rho} \leq N. \tag{6.26}$$

An interesting property of these minimum numbers of samples is that they do not depend on the dimension of the random variable $\boldsymbol{\theta}$. On the other hand, the number of samples becomes prohibitively high for obtaining very accurate estimates. That is why we propose these techniques for analysis, but not for synthesis.

6.5 Examples

This section aims at illustrating the proposed method through some examples and presenting the benefit of considering probabilistic specifications (in terms of reduction of conservatism with respect to designs using worst-case specifications). The examples were obtained with the aid of a software package [122] to generate nodes and weights for the quadrature rules. Expectation integrals have been computed by using a sparse grid with dKP as underlying univariate quadrature. Estimates of constraint fulfillment

probability $\hat{p}$ and worst-case constraint violation $\hat{\gamma}$ presented in this section are based on $\epsilon = \delta = 0.005$ for $\hat{p}$, and $\delta = 10^{-4}$ and $\rho = 1 - \delta$ for $\hat{\gamma}$.

Example 6.1 (Plants with different normalized time delays)**.** This example considers three uncertain FOTD plant models: one lag dominant, one balanced, and one delay dominant:

$$P_1(s, \boldsymbol{\theta}) = \frac{k}{s} e^{-hs}, \quad P_2(s, \boldsymbol{\theta}) = \frac{k}{\tau s + 1} e^{-hs}, \quad P_3(s, \boldsymbol{\theta}) = k e^{-hs}, \tag{6.27}$$

where $\boldsymbol{\theta} = [k \ h \ \tau]^\top$, $k \in [0.5, 1.5]$, $h \in [0.5, 1.5]$, and $\tau \in [0.5, 1.5]$. In spite of its simplicity, this type of models captures a majority of dynamics encountered in process industry [19, 227]. The PID controller (6.7) is considered for each of these uncertain plants.

Figure 6.4 shows level curves in the $k_p - k_i$ space (when $k_d = 0$), corresponding to the probability of constraint violation for the specification $\|S\|_\infty \leq 1.4$. This figure illustrates how allowing for a higher probability of constraint violation can significantly improve the performance. Note the considerable increase in k_i, with respect to the worst-case design, that is achieved when allowing only a 2 % for the probability constraint violation.

In the rest of this example, we study with greater detail the plant P_1. Table 6.1 presents the solution to the chance-constrained optimization problem (6.11) corresponding to the uncertain plant model P_1 and different values of α, when $k_d = 0$. Also shown are the estimated mean IAE, the estimated probability of constraint violation $1 - \hat{p}$, and the estimated worst-case constraint violation $\hat{\gamma}$. Temporal responses due to a unit step disturbance entering at the plant input for different controllers are shown in Figure 6.5. The solid line corresponds to the median response and the area enclosed by dashed lines corresponds to the $5 - 95$ % quantiles. In this example, performance improves considerably with small increases in constraint violation probability, while the worst-case of $\|S\|_\infty$ does not reach very high values. Even with a value of constraint violation equal to 0.18 (the highest value of α considered in Table 6.1), the estimated worst-case of $\|S\|_\infty$ is below 1.8.

Example 6.2 (Comparison with an alternative stochastic optimization design)**.** This example considers the uncertain FOTD plant model

$$P(s, \boldsymbol{\theta}) = \frac{1}{\tau s + 1} e^{-hs}, \tag{6.28}$$

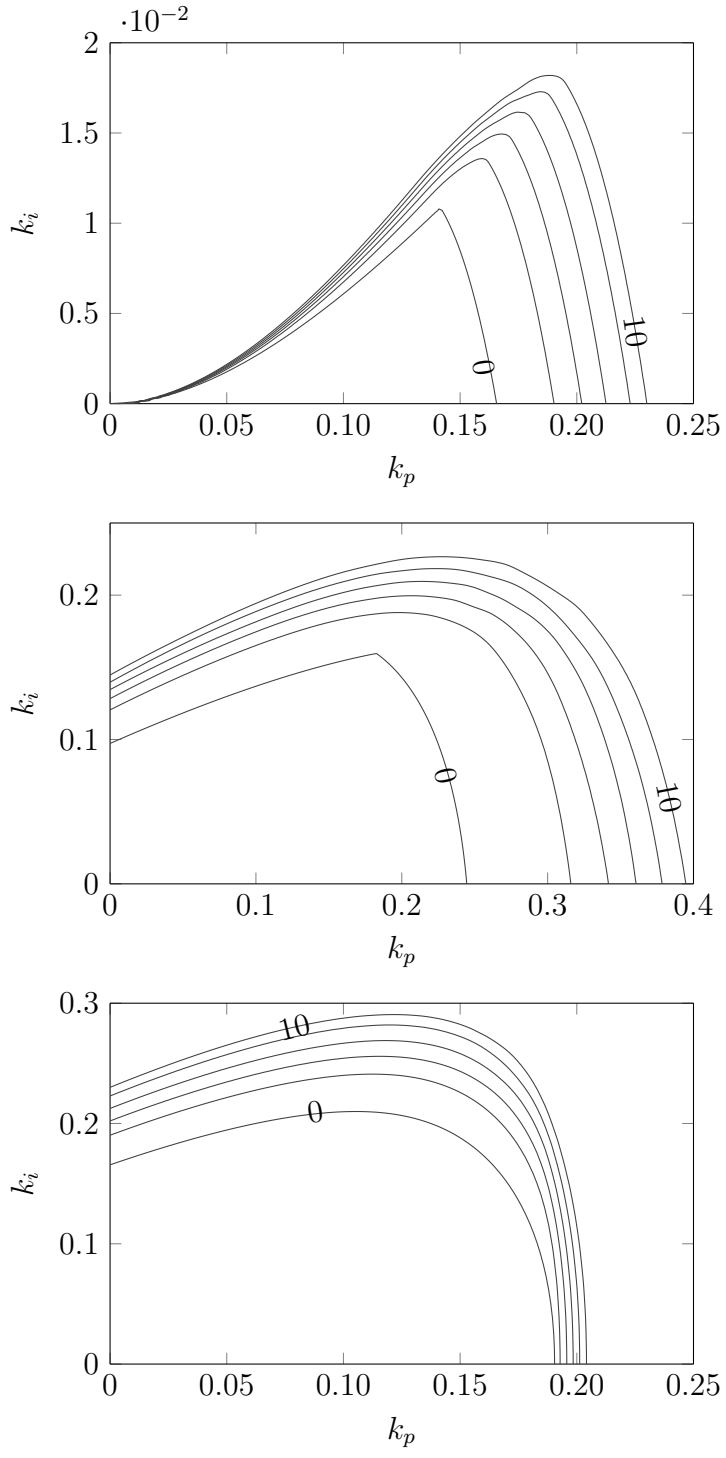

Figure 6.4 Level curves for the probability of constraint violation (Example 6.1)

Level curves in the controller parameter space for the values 0, 2, 4, 6, 8, and 10 % probability of constraint violation, i.e. 100α, for the specification $\|S\|_\infty \leq 1.4$ and the plant models P_1 (top), P_2 (middle), and P_3 (bottom).

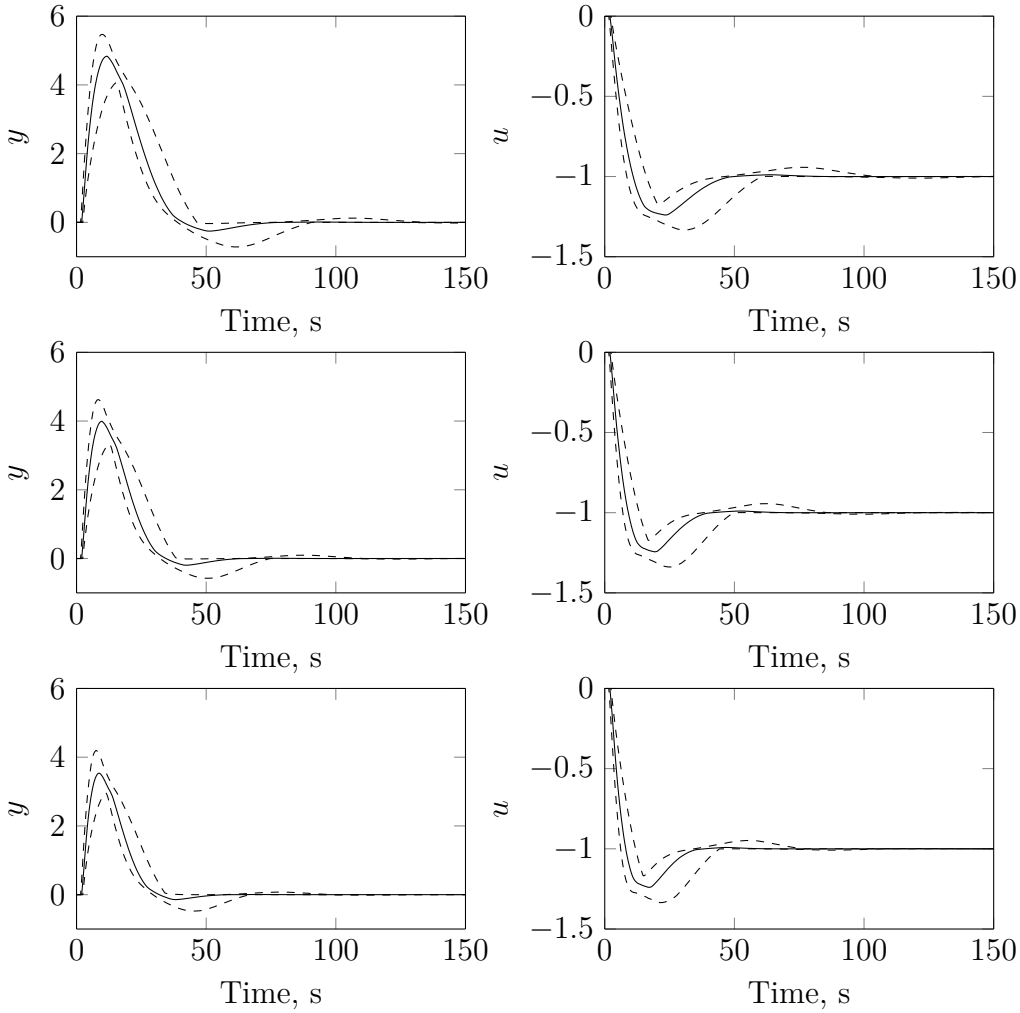

Figure 6.5 Disturbance rejection considering the plant P_1 (Example 6.1)

Load step response (left) and controller output (right) for $\alpha = 0$ (top), $\alpha = 0.06$ (middle), and $\alpha = 0.14$ (bottom). The solid line corresponds to the median response and the area enclosed by dashed lines corresponds to the $5 - 95$ % quantiles.

Table 6.1 Results considering the plant P_1 (Example 6.1)

α	k_p	k_i	IE	$\mathbb{E}$[IAE]	$1-\hat{p}$	$\hat{\gamma}$
0.00	0.142	0.0109	91.74	106.68	0.000	1.40
0.02	0.159	0.0136	73.53	85.10	0.020	1.47
0.06	0.176	0.0161	62.11	71.08	0.060	1.53
0.10	0.190	0.0182	54.94	62.52	0.099	1.59
0.14	0.203	0.0202	49.50	55.75	0.139	1.65
0.18	0.216	0.0220	45.45	50.74	0.177	1.71

Table 6.2 Comparison of controllers (Example 6.2)

Method	k_p	k_i	k_d	IE	$\mathbb{E}$[IAE]	$1-\hat{p}$	$\hat{\gamma}$
[81]	1.957	2.012	0.320	0.497	0.512	0.516	6.74
Proposed	0.807	1.150	0.132	0.870	0.955	0.049	1.53

where $\boldsymbol{\theta} = [\tau \; h]^\top$, $\tau \in [0.5, 1.5]$, and $h \in [0, 0.5]$. This uncertain plant was considered in [81], where a PID controller was designed by solving the stochastic optimization problem:

$$\begin{aligned} \underset{\mathbf{x}}{\text{minimize}} \quad & \mathbb{E}[\text{IAE}(\mathbf{x}, \boldsymbol{\theta})] \\ \text{subject to} \quad & \max_{0 \le t \le T} \mathbb{V}[y(t, \mathbf{x}, \boldsymbol{\theta})] \le D_y, \end{aligned} \tag{6.29}$$

where $\mathbb{V}[\cdot]$ denotes variance, and the value of D_y is a design specification. The solution was obtained by approximating the stochastic temporal response of the plant output, due to a unit step disturbance, using a polynomial chaos approach. The obtained controller for $D_y = 0.01$ is shown in Table 6.2. We compare this controller with the one resulting from (6.11) with $\alpha = 0.05$ and $M_s = 1.4$; controller parameters are shown in Table 6.2, where the IE and average IAE values, the estimated probability of constraint violation of $\|S\|_\infty \le 1.4$, and the estimated worst-case constraint violation of $\|S\|_\infty \le 1.4$, are also shown. Load step responses are shown in Figure 6.6. Line styles correspond to those of Figure 6.5.

The solution proposed in [81], in spite of considering uncertainty in the design stage, yields a very low level of robustness. Note that the worst case of $\|S\|_\infty$ is higher than 6 and acceptable values of $\|S\|_\infty$ are in the interval $1.2 - 2$ [22]. Furthermore, the

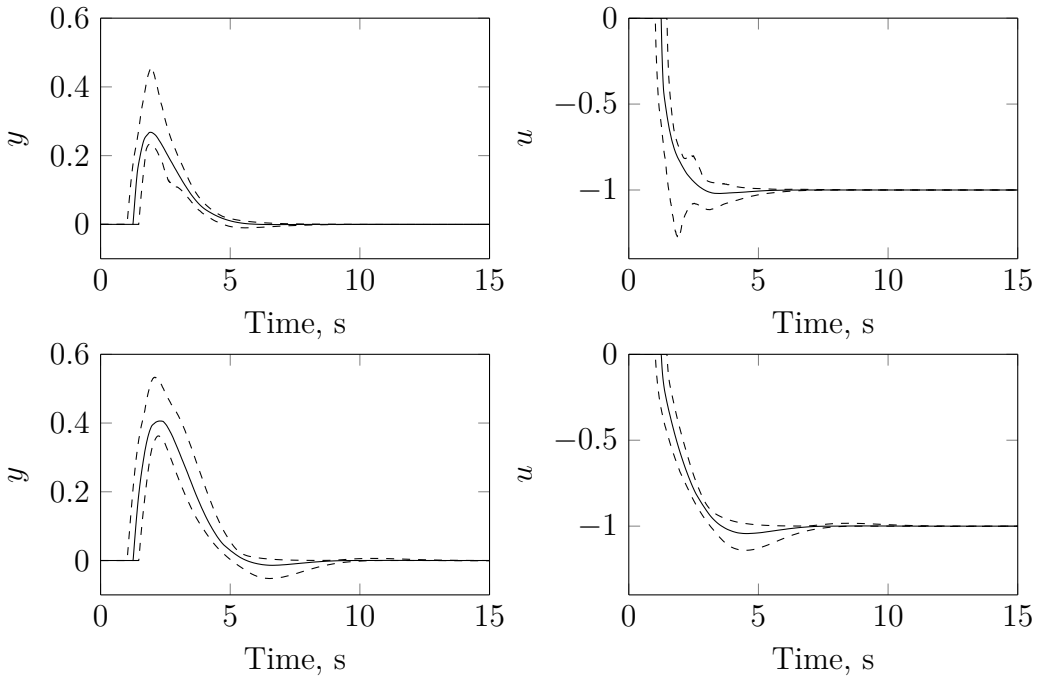

Figure 6.6 Disturbance rejection (Example 6.2)

Plant output (left) and controller output (right) due to a unit step disturbance for the controllers obtained in [81] (top) and the obtained with the proposed method (bottom). The solid line corresponds to the median response and the area enclosed by dashed lines corresponds to the $5 - 95$ % quantiles.

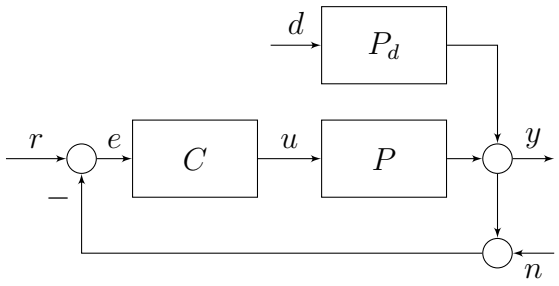

Figure 6.7 Feedback control system of an elastic two-mass system (Example 6.3)

specification used in the problem (6.29) is not very intuitive. Although this constraint implicitly guarantees closed-loop stability in a probabilistic sense, it is difficult to associate values of D_y with values of any known stability margin.

Example 6.3 (Plant with a large number of uncertain coefficients)**.** This example illustrates that the proposed method is applicable in cases with more general parameter dependencies than intervals of transfer function coefficients, as in (6.5), and in cases with a large number of uncertain coefficients. The uncertain elastic two-mass system defined by the following transfer functions is considered (see Figure 6.7):

$$P(s,\boldsymbol{\theta}) = \frac{c_s s + k_s}{d(s,\boldsymbol{\theta})}, \tag{6.30}$$

$$P_d(s,\boldsymbol{\theta}) = -\frac{J_m s^2 + (c_m + c_s)s + k_s}{d(s,\boldsymbol{\theta})}, \tag{6.31}$$

where

$$\begin{aligned} d(s,\boldsymbol{\theta}) &= J_m J_l s^3 + (J_l(c_m + c_s) + J_m(c_m + c_s))s^2 \\ &+((J_l + J_m)k_s + c_m c_l + c_m c_s + c_l c_s)s + (c_m + c_l)k_s. \end{aligned} \tag{6.32}$$

Here, $\boldsymbol{\theta} = [J_m\ c_m\ J_l\ c_l\ k_s\ c_s]^\top$ denotes the vector of plant parameters. These two transfer functions represent the paths from plant input and disturbance, respectively, to plant output. The reader is referred to [199] for a more detailed description of this model. The following numerical values, taken from [199], are used in this example:

$$\begin{aligned} &J_m = 0.4 \text{ kg m}^2, && c_m \in [0, 0.1] \text{ Nm/(rad/s)}, \\ &J_l \in [5.5, 6.0] \text{ kg m}^2, && c_l \in [0, 1] \text{ Nm/(rad/s)}, \\ &k_s \in [3000, 4000] \text{ Nm/rad}, && c_s \in [1, 20] \text{ Nm/(rad/s)}. \end{aligned} \tag{6.33}$$

Table 6.3 Controllers for different values of α (Example 6.3)

α	k_p	k_i	$1-\hat{p}$	$\hat{\gamma}$
0.000	5.816	12.048	0.000	1.60
0.010	9.131	29.695	0.011	2.37
0.015	9.942	35.054	0.016	2.75
0.020	10.626	40.598	0.021	3.00

Although the disturbance acts on the output through P_d, minimization of the corresponding IE is equivalent to maximization of k_i:

$$\text{IE} = \int_0^\infty e(\tau, \mathbf{x}, \boldsymbol{\theta}) d\tau = \lim_{s \to 0} s \frac{P_d(s)}{1 + P(s)C(s)} \frac{1}{s^2} = -\frac{1}{k_i}. \tag{6.34}$$

A PI is often used for this kind of system, in particular, when actuator dynamic (including delays) is relatively slow, since it limits the advantage of high bandwidth controllers [199]. This motivates the following problem formulation:

$$\begin{aligned} \underset{\mathbf{x}}{\text{minimize}} \quad & -k_i \\ \text{subject to} \quad & \Pr[\|S(\mathbf{x}, \boldsymbol{\theta})\|_\infty - 1.6 \leq 0] \geq 1 - \alpha. \end{aligned} \tag{6.35}$$

Table 6.3 shows the solution of (6.35) for different values of α. Estimates of the probability of constraint violation and worst-case specification are also shown. In this example, the level of performance increases considerably even for small (e.g. $1-2$ %) probabilities of constraint violation. The load step responses corresponding to the extreme values of α in Table 6.3 are displayed in Figure 6.8. Line styles have the same meaning as in the previous figures.

Finally, it is worth mentioning that, in this example, the computational time required by using the sparse grid with dKP is shorter, by a factor of 10, than the one required by full grid with GL.

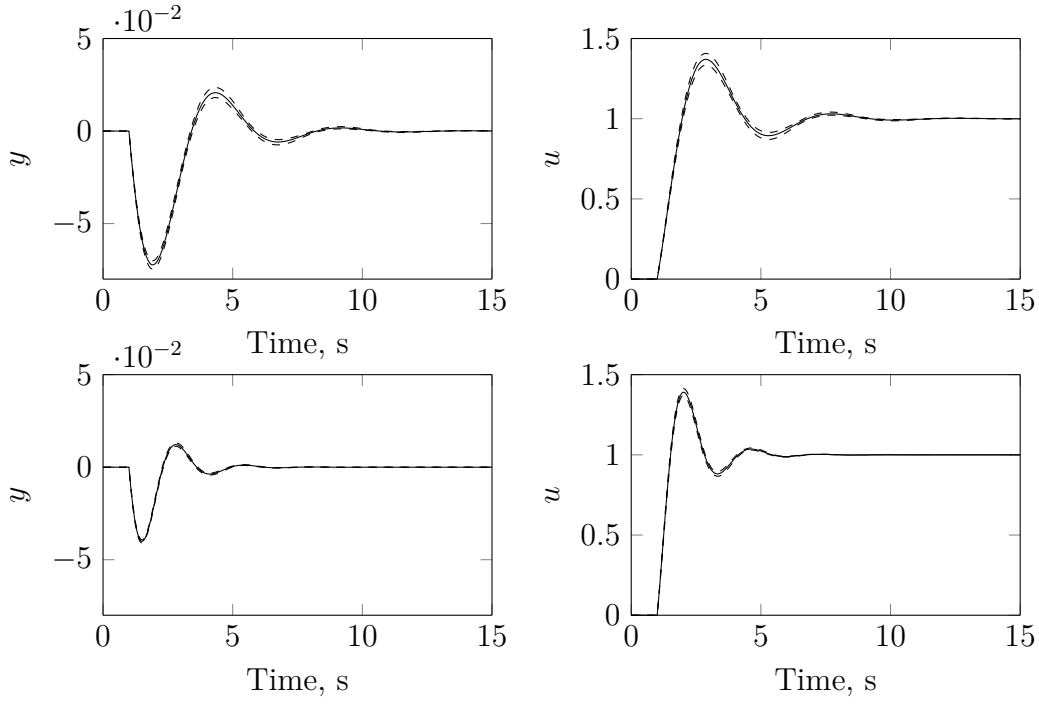

Figure 6.8 Disturbance rejection (Example 6.3)

Load step response (left) and controller output (right) for the plant P_1 considering $\alpha = 0$ (top) and $\alpha = 0.02$ (bottom). The solid line corresponds to the median response and the area enclosed by dashed lines corresponds to the $5 - 95$ % quantiles.

Chapter 7

Autotuning of PID Controllers

7.1 Introduction

Most process industrial plants can be adequately controlled using either the PI or PID controller [254]. However, an accurate model of the plant to be controlled is a pre-requisite for successful tuning of the controller. Obtaining such a model is usually time-consuming and expensive [98]. A typical process industrial manufacturing plant has thousands of PID controllers, and consequently, many of them are left poorly tuned, or running at their factory default parameters [72]. In [72], the average tuning price per loop is estimated to lie between USD 250 and USD 1000 in labor, while a representative process industrial factory typically has hundreds or thousands of such loops.

The previous facts explain the popularity of automatic controller tuning methods, also known as autotuners. These methods combine an identification experiment with a controller tuning. The basic idea behind the most commonly used autotuner is to close a negative feedback loop over the plant in series with a relay, as shown in Figure 7.1. For most industrial processes, this results in a stable limit cycle oscillation close to the cross-over frequency of the plant [161]. This ability – to automatically produce an input signal with adequate excitation – is a key property of relay autotuners. Controller tuning is subsequently based on the switching time instants (the oscillation period) and peak values of the output (used to compute process gain) [14]. The identification experiment yields a model consisting of the system response at the plant phase crossover frequency. An approximate criterion for predicting limit cycles is available by means of the describing function. The inverse describing function of the relay intersects the plant Nyquist plot along the negative axis as shown in Figure 7.2 (left), the same

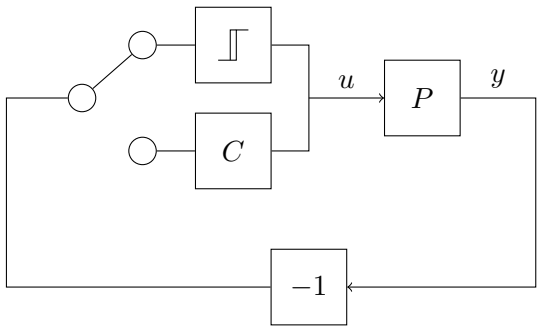

Figure 7.1 Relay autotuner

Block diagram of relay autotuner with plant P, controller C, control signal u, and plant output y.

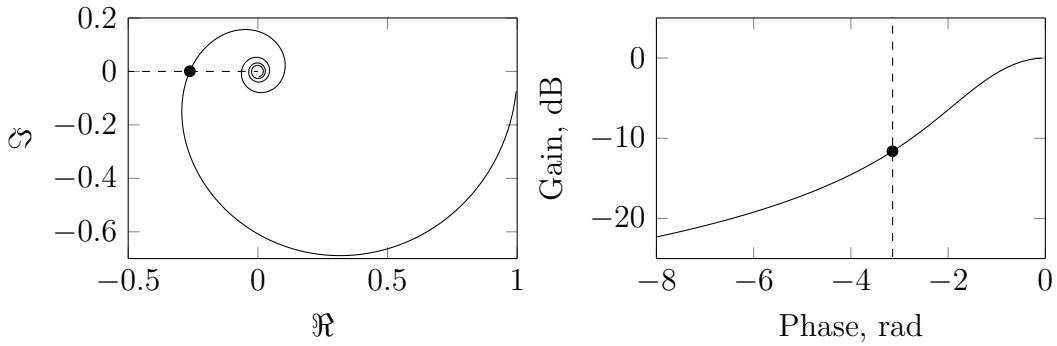

Figure 7.2 Model obtained with the relay autotuner method

Nyquist (left) and Nichols (right) plot with obtained model (dot).

situation in the Nichols plane is depicted in Figure 7.2 (right). The fact that only one frequency response point is identified is its major caveat, which has resulted in the development of several variants of the method. In [91], an integrator was connected in series with a second relay, to change the phase shift of the plant at which the limit cycle occurs. The method proposed in [138] utilizes the original experiment, but makes use of the identified frequency response differently to obtain the PID parameters. Other modifications include extensions to MIMO systems as covered by the survey [176].

In this chapter, an improved version of the relay method is utilized. It voids the requirement for limit cycle convergence, by using all recorded data, as opposed to only peak and switch values. Furthermore, the identification procedure, that enables this, also yields a parameter uncertainty model, which we utilize for robust controller synthesis.

This chapter is structured in four sections. The novel autotuning procedure is presented in Section 7.2. It is applied to an in-line pH control system, which is

commonly occurring in the chemical production industry and often regarded as difficult to control. A brief presentation of the pH control system is then given in Section 7.3. Finally, the results of identification and control experiments carried out on the physical plant are shown in Section 7.4.

7.2 Autotuning Method

Relay autotuning methods are very common in industrial practice. A key feature of these methods is that they produce an experiment that excites the plant at frequencies relevant for controller synthesis, without the need of a priori plant information. However, the classic relay autotuner only utilizes plant output peaks and relay switch times for modeling. This makes it noise sensitive and requires convergence of a stable limit cycle. These caveats can be overcome by utilizing the entire experiment data set, as suggested in [238, 239], and adopted in this chapter.

7.2.1 Identification

The use of an asymmetric relay (also known as biased-relay) has been proposed in the literature for obtaining better signal excitation than the obtained by the symmetric relay (see for example [151, 226, 240]). The relay output takes on the value u_{on}, when its input is positive, and u_{off}, when its input is negative. The proposed experiment utilizes an asymmetric relay, with output levels $u_{\text{on}} = -\gamma u_{\text{off}}$, and $\gamma = 1.5$, as suggested in [37, 38]. However, instead of the $6 - 8$ switches typically needed for convergence, the experiment is terminated after only 3 switches [239].

The relay hysteresis is set according to the level of noise in the process output, in order to avoid chattering triggered by the measurement noise. Assuming white noise with zero mean and variance σ_n^2, the hysteresis level $\mu = 2\sigma_n^2$ is recommended. A negative feedback is generally used during the relay experiments. In the application case that will be presented in this chapter, due to the reverse characteristic of the process (increment in the control signal implies a decrement in the plant output), a positive feedback loop is instead used during relay experiments.

After performing the asymmetric relay experiment, the plant input u and output y, sampled at period t_s, are used to estimate parameters $\boldsymbol{\theta} = [k\ h\ \tau]^\top$ corresponding to the FOTD model structure:

$$\hat{P}(s, \boldsymbol{\theta}) = \frac{k}{\tau s + 1} e^{-sh}. \tag{7.1}$$

Continuous time representation is utilized to limit the number of elements of the parameter vector $\boldsymbol{\theta}$. The same approach could be applied to estimate the parameters of any other model structure, possibly with a more elaborate experiment design. A more thorough analysis of the number of parameters one can expect to estimate from a given experiment is available through the persistency of excitation of the input signal, defined as the number of singular values of the input covariance matrix exceeding a certain threshold [166].

The parameters identification procedure is posed as an optimization problem, as suggested in [237], aiming to minimize the output error $\mathcal{L}_2$-norm:

$$J(\boldsymbol{\theta}) = \frac{1}{2}\int_0^{t_f} e^2(t)dt, \tag{7.2}$$

where $e = y - \hat{y}$, $\hat{y}$ is the resulting output when $\hat{P}$ is driven by u, and t_f is the experiment duration. The optimization is handled by an active-set solver. To improve convergence, the exact parameter sensitivity gradient and an approximation of the corresponding Hessian are provided in each iteration to the optimization algorithm. The gradient with respect to $\boldsymbol{\theta}$ is given by

$$\nabla J = \int e\nabla\hat{y}dt, \tag{7.3}$$

and the Hessian is

$$\Delta J = \int \left(\nabla\hat{y}\nabla\hat{y}^\top + e\Delta\hat{y}\right)dt. \tag{7.4}$$

The first term of the integrand (7.4) is positively semidefinite, $\nabla\hat{y}\nabla\hat{y}^\top \geq 0$, while the integral of the second term is small, $e\Delta\hat{y} \approx 0$, under the realistic assumption that the output error is uncorrelated with its second derivative, $\mathbb{E}\left[e\Delta\hat{y}\right] = 0$. It is therefore fair to approximate the Hessian by the integral of the first term (although it is straightforward to extend the method outlined below, to include also the second term). Technical details surrounding the computations yielding these expressions are available in [238, 239].

In addition to the expectation $\bar{\boldsymbol{\theta}}$, the optimization provides the asymptotic covariance matrix

$$R_{\bar{\boldsymbol{\theta}}} = \mathbb{E}\left[(\boldsymbol{\theta} - \bar{\boldsymbol{\theta}})(\boldsymbol{\theta} - \bar{\boldsymbol{\theta}})^\top\right] = \frac{2}{N}\bar{J}(\Delta\bar{J})^{-1}, \tag{7.5}$$

where N is the number of samples [12]. The standard deviations of the parameter estimates decrease proportional to $1/\sqrt{N}$, meaning that one cannot expect significantly improved estimation precision, by (small) increases in experiment duration.

7.2.2 Controller Design

Upon obtaining estimates of the parameter expectations and covariances, a control design problem is formulated. The aim is to synthesize a PI controller, robust to the model uncertainty, as expressed through the parameter covariance matrix (7.5). The synthesis method is similar to the one presented in the previous chapter, but considering a design problem like (6.2) instead of (6.3). Hence, expectation-variance specifications will be considered instead of probabilistic specifications, that makes the resulting optimization problem more easily to solve. In order to integrate it in an autotuner method, it is important that the resulting optimization problem does not require of user supervision.

The controller is parametrized in continuous time as

$$C(s, \mathbf{x}) = k_p + \frac{k_i}{s}, \tag{7.6}$$

where $\mathbf{x} = [k_p \ k_i]^\top$ is the vector of controller parameters. The synthesis problem formulation is based on propagating the model uncertainty (assuming that model parameter uncertainty obeys a multivariate Gaussian distribution) through to a performance index, which is optimized, and robustness measures, which are constrained. A common performance index, quantifying disturbance attenuation (the main concern in process control), is the IAE:

$$\mathrm{IAE}(\mathbf{x}, \boldsymbol{\theta}) = \int_0^\infty |e(t, \mathbf{x}, \boldsymbol{\theta})| dt, \tag{7.7}$$

where $e(t)$ is the error due to a unit step disturbance entering at the plant input. Analytic computation of the IAE is very seldom possible. As a tractable alternative it is common to use the IE:

$$\mathrm{IE}(\mathbf{x}, \boldsymbol{\theta}) = \int_0^\infty e(t, \mathbf{x}, \boldsymbol{\theta}) dt. \tag{7.8}$$

This choice simplifies the problem since minimization of (7.8) is equivalent to maximization of the integral gain, k_i in (7.6), as pointed out in [19]. The IAE and IE coincide for control loops with non-oscillatory load step responses and are similar for loops with well-damped responses. The latter is a desirable feature, and it can be enforced by imposing robustness constraints. Herein this is achieved by stochastic $\mathcal{H}_\infty$ constraints on the sensitivity, $S = (1 + \hat{P}C)^{-1}$, and complementary sensitivity, $T = 1 - S$. Since $\boldsymbol{\theta}$ is Gaussian, there is a finite probability of attaining *any* value, and generally it is not possible to guarantee specification of the kind worst-case constraints.

Motivated by the above requirements, the control design problem is posed as the following stochastic optimization problem:

$$\begin{aligned} \underset{\mathbf{x}=[k_p \;\; k_i]^\top}{\text{maximize}} \quad & k_i \\ \text{subject to} \quad & \mathbb{E}\left[\|S(\mathbf{x},\boldsymbol{\theta})\|_\infty\right] + \alpha_s \sqrt{\mathbb{V}\left[\|S(\mathbf{x},\boldsymbol{\theta})\|_\infty\right]} \leq M_s, \\ & \mathbb{E}\left[\|T(\mathbf{x},\boldsymbol{\theta})\|_\infty\right] + \alpha_t \sqrt{\mathbb{V}\left[\|T(\mathbf{x},\boldsymbol{\theta})\|_\infty\right]} \leq M_t. \end{aligned} \tag{7.9}$$

The design parameters α_s and α_t let the user specify the confidence with which each robustness constraint should be met. Note that when there is no uncertainty, i.e. zero covariance matrices, the design problem (7.9) is equivalent to the well-known MIGO approach for PI design [19].

The proposed approach to solve the stochastic optimization problem (7.9) is very similar to the one exposed in the previous chapter. Here, the method to approximately solve (7.9) is based on propagating the uncertainty by means of the unscented transform (UT) [146, 147, Julier and Uhlmann], and the conjugate unscented transform (CUT) [2–4]. To illustrate how these techniques are employed to propagate the uncertainty, we consider an arbitrary (nonlinear) function $g(\boldsymbol{\theta})$, where

$$\boldsymbol{\theta} = \left[\theta_1 \;\; \theta_2 \;\; \ldots \;\; \theta_n\right]^\top, \tag{7.10}$$

is a random variable, with a multivariate Gaussian PDF. It is well-known that any Gaussian can be transformed into one with zero expectation and unitary covariance, through an affine transformation. This transformation can be applied to g, and consequently, it is sufficient to consider $\boldsymbol{\theta}$ with $\mathbb{E}[\boldsymbol{\theta}] = \mathbf{0}$ and $\mathbb{V}[\boldsymbol{\theta}] = I_n$, where I_n denotes the identity matrix of size n. In order to consider a Gaussian $\mathbf{z}$ with $\mathbb{E}[\mathbf{z}] = \bar{\mathbf{z}}$ and $\mathbb{V}[\mathbf{z}] = Z$, it is sufficient to transform samples $\boldsymbol{\theta}^{(i)}$ of $\boldsymbol{\theta}$ as

$$\mathbf{z}^{(i)} = \bar{\mathbf{z}} + S\boldsymbol{\theta}^{(i)}, \tag{7.11}$$

where $Z = SS^\top$, which can be found using Cholesky decomposition.

Denote by f the PDF of a Gaussian zero expectation and unitary covariance. The expectation $\mathbb{E}[g(\boldsymbol{\theta})]$ is defined as

$$\mathbb{E}\left[g(\boldsymbol{\theta})\right] = \int_{\mathbb{R}^n} g(\boldsymbol{\theta}) f(\boldsymbol{\theta}) d\boldsymbol{\theta}. \tag{7.12}$$

Test-point methods approximate $\mathbb{E}[g(\boldsymbol{\theta})]$ as a weighted sum

$$\mathbb{E}\left[g(\boldsymbol{\theta})\right] \approx \sum_{i=0}^{N-1} w_i g(\boldsymbol{\theta}^{(i)}), \tag{7.13}$$

where

$$\boldsymbol{\theta}^{(i)} = \left[\theta_1^{(i)}\ \theta_2^{(i)}\ \ldots\ \theta_n^{(i)}\right]^\top, \tag{7.14}$$

are known as the test points. The approximation of (7.12) as the weighted sum (7.13) is exact for a given class of functions g. Note that MC can be considered a test-point method with weights $\omega_i = 1/N$, and test points $\boldsymbol{\theta}^{(i)}$ randomly generated by the underlying PDF. What makes the UT, CUT, and related test-points methods interesting is a clever choice of *deterministic* test-points and weights, removing the requirement of many samples (large N). Using the Taylor series expansion of $g(\boldsymbol{\theta})$ about the expected value $\boldsymbol{\theta} = \mathbf{0}$ [68], (7.12) can be rewritten as

$$\mathbb{E}\left[g(\boldsymbol{\theta})\right] = \sum_{N_1=0}^{\infty} \cdots \sum_{N_n=0}^{\infty} \frac{\mathbb{E}\left[\theta_1^{N_1} \cdots \theta_n^{N_n}\right]}{N_1! \cdots N_n!} \frac{\partial^{N_1+\cdots+N_n} g}{\partial \theta_1^{N_1} \cdots \partial \theta_n^{N_n}}(\mathbf{0}). \tag{7.15}$$

Assume that g belong to the class of functions for which (7.16) is exact, then by combining (7.15) with (7.13) yields the following equation

$$\mathbb{E}\left[g(\boldsymbol{\theta})\right] = \sum_{N_1=0}^{\infty} \cdots \sum_{N_n=0}^{\infty} \frac{\sum_{i=0}^{N-1} w_i \left((\theta_1^{(i)})^{N_1} \cdots (\theta_n^{(i)})^{N_n}\right)}{N_1! \cdots N_n!} \frac{\partial^{N_1+\cdots+N_n} g}{\partial \theta_1^{N_1} \cdots \partial \theta_n^{N_n}}(\mathbf{0}). \tag{7.16}$$

Equating (7.15) and (7.16) leads to a set of equations

$$\sum_{i=0}^{N-1} w_i \left((\theta_1^{(i)})^{N_1} \cdots (\theta_n^{(i)})^{N_n}\right) = \mathbb{E}\left[\theta_1^{N_1} \cdots \theta_n^{N_n}\right], \tag{7.17}$$

referred to as the moment constraint equations (MCE). These equations were obtained with some abuse of notation due to the approximate nature of (7.13), but note that this relation is exact for a given class of functions g, for which is valid the relation (7.17).

The idea behind test-point methods is to choose test points and corresponding weights, to fulfill all MCEs for which $N_1 + \cdots + N_n \leq d$, where d is referred to as the order of the MCE. This allows for *exact* integration of monomials up to order d, and Taylor approximation of other functions through such monomials.

Due to the symmetry of the considered Gaussian PDF f, odd moments are 0. The even moments up to order $d = 6$ are

$$\begin{aligned} &\mathbb{E}\left[\theta_i^2\right] = 1, \quad \mathbb{E}\left[\theta_i^4\right] = 3, \quad \mathbb{E}\left[\theta_i^2\theta_j^2\right] = 1, \\ &\mathbb{E}\left[\theta_i^6\right] = 15, \quad \mathbb{E}\left[\theta_i^4\theta_j^2\right] = 3, \quad \mathbb{E}\left[\theta_i^2\theta_j^2\theta_k^2\right] = 1, \end{aligned} \tag{7.18}$$

for distinct $i, j, k \in \{1, 2, \ldots, n\}$.

Unscented Transform (UT)

The UT [146, Julier and Uhlmann] relies on the selection of $N = 2n + 1$ test-points, satisfying the MCEs (7.17) up to order $d = 3$. This leaves some degree of freedom in choosing the test points. For the UT, they are constrained to lie on the principal axes. The resulting test points and corresponding weights are

$$\begin{aligned} \boldsymbol{\theta}^{(0)} &= \mathbf{0}, & w_0 &= \frac{\kappa}{n+\kappa}, \\ \boldsymbol{\theta}^{(i)} &= \sqrt{n+\kappa}\mathbf{e}_i, & w_i &= \frac{1}{2(n+\kappa)}, \\ \boldsymbol{\theta}^{(i+n)} &= -\sqrt{n+\kappa}\mathbf{e}_i, & w_{i+n} &= \frac{1}{2(n+\kappa)}, \end{aligned} \tag{7.19}$$

where $i = 1, 2, \ldots, n$, $\mathbf{e}_i$ is the unit vector along the i^{th} principal axis, and κ is a tuning parameter. For the considered Gaussian, the choice

$$n + \kappa = 3 \tag{7.20}$$

was recommended by Julier and Uhlmann [Julier and Uhlmann], since it minimizes the error in higher order moments. Adopting this recommendation, the test points and corresponding weights of (7.19) satisfy

$$\begin{aligned} &\sum_{m=0}^{N-1} w_m = 1, && \sum_{m=0}^{N-1} w_m \left(\theta_i^{(m)}\right)^2 = 1 = \mathbb{E}\left[\theta_i^2\right], \\ &\sum_{m=0}^{N-1} w_m \left(\theta_i^{(m)}\right)^4 = n+\kappa = 3 = \mathbb{E}\left[\theta_i^4\right], && \sum_{m=0}^{N-1} w_m \left(\theta_i^{(m)}\right)^2 \left(\theta_j^{(m)}\right)^2 = 0 \neq \mathbb{E}\left[\theta_i^2\theta_j^2\right] = 1, \end{aligned} \tag{7.21}$$

for distinct $i, j \in \{1, 2, \ldots, n\}$. With the choice (7.20), the UT fulfills one of the 4^{th} order MCEs through $\mathbb{E}[\theta_i^4] = 3$. However, due to the fact that all UT test points lie along the principal axes, all cross moments are 0, as can be seen in the last equation of (7.21). This fact makes impossible to satisfy the last equation of (7.21). Furthermore, the weight w_0 corresponding to the central point is negative for $n > 3$, leading to higher quadrature error compared to an equivalent method with positive weights [243]. These two aspects motivate the introduction of additional test points, not lying along the principal axes. That is the basis of the CUT, that is presented in the next section.

Conjugate Unscented Transform (CUT)

The CUT [2–4] proposes an extension of the UT test point set, by adding test points along conjugate coordinate axes. The conjugate-m axes lie in the directions of the vectors $\mathbf{c}_m^{(i)}$, generated by

$$\left\{\mathbf{c}_m^{(i)}, 1 \leq i \leq 2n\binom{n}{m}\right\} = \mathrm{FS}\Big[[\underbrace{1 \ \ldots \ 1}_{m} \ \underbrace{0 \ \ldots \ 0}_{m-n}]^\top\Big]. \tag{7.22}$$

The $\mathrm{FS}[\cdot]$ operator generates a fully symmetric set, closed under all sign and coordinate permutations. For instance, the unit vectors $\mathbf{e}_i$ along the principal axes together with their negated counterparts $-\mathbf{e}_i$, used in the UT, are generated by

$$\left\{\mathbf{s}^{(i)}, 1 \leq i \leq 2n\right\} = \mathrm{FS}\left[[1 \ 0 \ \ldots \ 0]^\top\right]. \tag{7.23}$$

Including test points along conjugate coordinate axes enables solving the MCEs up to higher order d than the one achieved by UT, while maintaining positive weights. This comes at the cost of additional test points. To illustrate, we will consider the CUT4 method, which fulfills all MCEs up to order $d = 4$ (actually $d = 5$). It has $N = 1 + 2n + 2^n$ test points for $2 \leq n \leq 5$:

- 1 central test point $\boldsymbol{\theta}^{(0)} = \mathbf{0}$ with weight W_0,
- $2n$ principal test points $\boldsymbol{\theta}^{(i)} = r_1\mathbf{s}^{(i)}$ with weight W_1,
- 2^n conjugate-n test points $\boldsymbol{\theta}^{(i+2n)} = r_2\mathbf{c}_n^{(i)}$ with weight W_2.

Table 7.1 Test points for CUT4 (first three rows) and CUT6 (all rows)

Test points	Weights	
$\boldsymbol{\theta}^{(0)} = \mathbf{0}$	$w_0 = W_0$	
$\boldsymbol{\theta}^{(i)} = r_1 \mathbf{s}^{(i)}$	$w_i = W_1$	$1 \leq i \leq 2n$
$\boldsymbol{\theta}^{(i+2n)} = r_2 \mathbf{c}_n^{(i)}$	$w_{i+2n} = W_2$	$1 \leq i \leq 2^n$
$\boldsymbol{\theta}^{(i+2n+2^n)} = r_3 \mathbf{c}_2^{(i)}$	$w_{i+2n+2^n} = W_3$	$1 \leq i \leq 2n(n-1)$

The scaling factors r_1, r_2, and weights W_0, W_1, W_2 for $n > 2$ utilized by CUT4 are given by

$$\begin{aligned} r_1 &= \sqrt{\frac{n+2}{2}}, \quad r_2 = \sqrt{\frac{n+2}{n-2}}, \\ W_1 &= \frac{4}{(n+2)^2}, \quad W_2 = \frac{(n-2)^2}{2^n(n+2)^2}, \quad W_0 = 0. \end{aligned} \tag{7.24}$$

For $n \leq 2$ numerical values are presented in [3].

The CUT4 method corresponds to the first three rows of Table 7.1. It is evident from the table that CUT4 is an extension of the UT (with different weights and scaling factors).

By adding $2n(n-1)$ conjugate-2 test points, one arrives at the CUT6 method, corresponding to rows 1–4 of Table 7.1. Numeric values of corresponding weights and scaling factors can be found in [3]. The same work also presents parameters values for the CUT8 method.

7.3 The In-Line pH Control System

The control of pH processes has motivated many works in the literature and a wide variety of control strategies have been applied to it (see [262] and references therein). Most pH control loops are based on the Continuous Stirred Tank Reactor (CSTR) model, comprising a tank with an agitator used to reach a perfect mixture. Another possible setup is the in-line process, where mixing occurs in the production line itself [55]. The process that will be studied here is the latter. The considered experimental setup is part of a canned food industry pilot plant, shown in Figure 7.3. The same industrial plant has been considered in previous works that apply reset control strategies [30, 55, 208].

Figure 7.3 Photograph of the pilot plant containing the in-line pH control system

The pH control loop consists of the following elements:

- A tank with a capacity of about 50 liters where the product is stored;
- A progressive cavity pump that produces a continuous product flow;
- An electromagnetic metering pump[1] (LMI Milton Roy AA9), which injects acid into the product;
- A 350 mm long static mixer;
- A pH sensor (Endress & Hauser, Orbisint CPS 11).

The product is potable water from the water supply network, the acid is an aqueous solution of nitric acid with a 10 % concentration, and the steady product flow rate generated by the progressive cavity pump is around 300 liters per hour (lph). The identification and control experiments are carried out around the operating point defined by the control output 15 spm, and its corresponding steady-state value of pH 7. The sampling time of the controller is 0.5 s.

[1]The pump can only make a natural number of strokes per minute (spm), between 0 and 100. At 100 spm, the pump creates a flow rate of 1.6 liters per hour (lph).

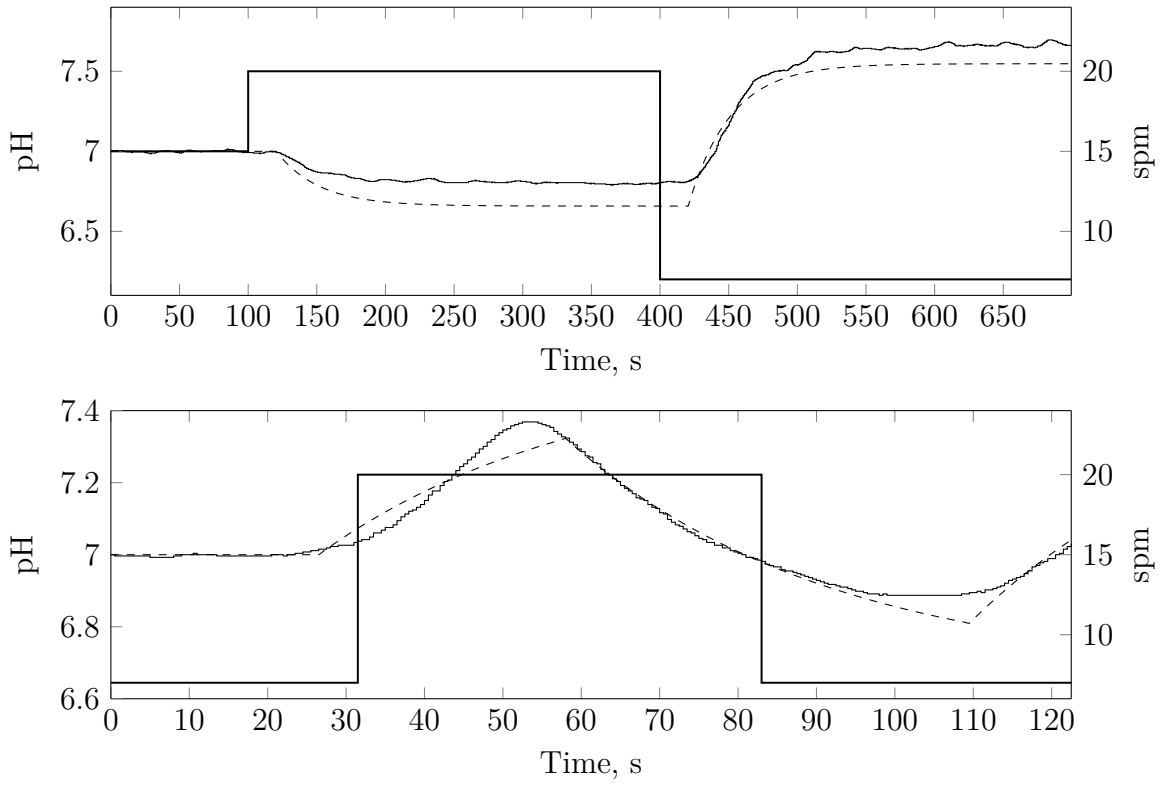

Figure 7.4 Identification experiments

Step response (top) and relay (bottom). Curves show measured output (solid thin), simulated output of the identified model (dashed), and input (solid thick).

7.4 Experimental Results

In this section, we demonstrate the proposed autotuning method on the industrial in-line pH control loop described in Section 7.3.

The identification experiment was carried out using relay output levels $u_{\text{on}} = 5$ and $u_{\text{off}} = -\gamma u_{\text{on}} = -7.5$ (corresponding to $\gamma = 1.5$, as previously mentioned). Taking operation point offset and quantification of the control signal into account, the corresponding control signal values become 20 and 7, respectively. The relay hysteresis was set to 0.025.

The proposed experiment and identification procedure yielded the parameter vector $\boldsymbol{\theta} = [k\ h\ \tau]^\top = [-0.067\ 26.5\ 33.7]^\top$ (and corresponding covariance matrix). The gain k is given in spm^{-1}; while the time parameters, τ and h, are given in seconds. A much longer (700 vs 122 s) step response experiment yielded a very similar model parametrized by $\boldsymbol{\theta} = [k\ h\ \tau]^\top = [-0.068\ 20.3\ 30.8]^\top$), as shown in Figure 7.4.

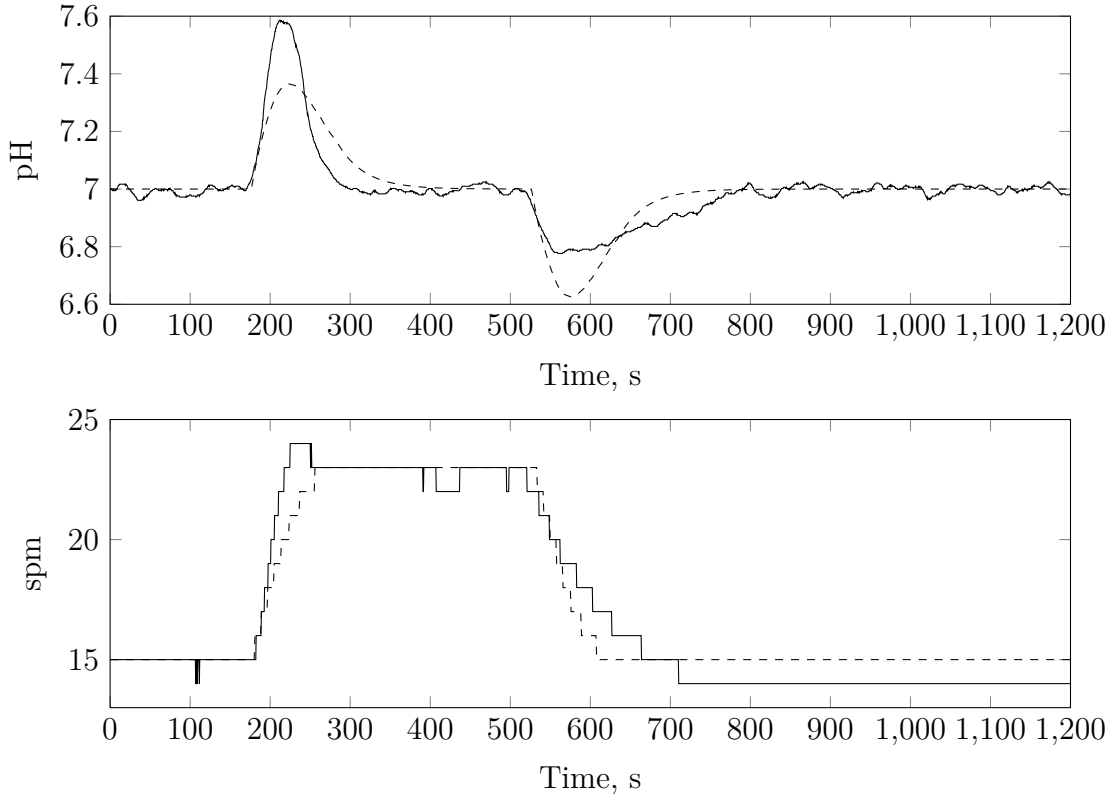

Figure 7.5 Disturbance rejection experiment

Plant output (top) and controller output (bottom). Experimental data is shown in solid and simulated in dashed.

Next, an optimization problem as (7.9) was solved, using the design parameters $\alpha_s = \alpha_t = 1$ and $M_s = M_t = 1.5$. That is formulated as follows:

$$\begin{aligned} \underset{\mathbf{x}=[k_p \;\; k_i]^\top}{\text{maximize}} \quad & k_i \\ \text{subject to} \quad & \mathbb{E}\left[\|S(\mathbf{x},\boldsymbol{\theta})\|_\infty\right] + \sqrt{\mathbb{V}\left[\|S(\mathbf{x},\boldsymbol{\theta})\|_\infty\right]} \leq 1.5, \\ & \mathbb{E}\left[\|T(\mathbf{x},\boldsymbol{\theta})\|_\infty\right] + \sqrt{\mathbb{V}\left[\|T(\mathbf{x},\boldsymbol{\theta})\|_\infty\right]} \leq 1.5, \end{aligned} \tag{7.25}$$

where $\boldsymbol{\theta}$ is a random variable obeying a multivariate Gaussian with expectation and variance given by the ones obtained in the identification stage. The obtained vector of controller parameter, $\mathbf{x} = [-7.379 \;\; -0.247]^\top$, was implemented on an industrial controller. Figure 7.5 shows both the experimental and simulated disturbance attenuation capabilities of the resulting closed-loop system. The load disturbance resulting in the response of Figure 7.5 was a pulse of height -8, active from the instant 50 to 500 s.

Chapter 8

Conclusions and Future Works

In this final chapter, we summarize the main results presented throughout this thesis and provide some potential future works on this research field.

8.1 Conclusions

The exposition of the conclusions of this thesis will be performed by discussing each chapter separately, due to the variety of the topics that have been addressed.

Chapter 1: Introduction

The first chapter has presented the context in which this thesis is placed, namely, the design of PID controllers for uncertain plants. The position of the PID controller as the most used form of feedback has been tried to justify by its desirable properties. Emphasis has been made on the importance of considering explicitly the uncertainty of the model in the control design stage.

Chapter 2: Background

The second chapter is devoted at providing a background on the issues that are covered throughout the forthcoming chapters. In particular, it provided a general overview of feedback control, and later, some issues like QFT and PID control are treated in a more detailed way.

Chapter 3: PI Design for an Uncertain ITD Plant

The design of PI controller for an uncertain ITP plant has been tackled in Chapter 3, by formulating the control design problem in terms of minimizing IE subject to worst-case peak values of the sensitivity and complementary sensitivity functions. The contribution of this chapter is two-fold. On the one hand, the design considering an infinite number of plant cases is replaced by one that only considers two extreme plant cases. On the other hand, an approximate solution in form of a tuning rule is presented to the mentioned control design problem. To the best of the author's knowledge, this is the first tuning rule for PI control that considers explicitly interval parametric uncertainty. The proposed tuning rule yields a close-to-optimum robust design, removing the difficulties associated with solving a robust optimization problem or the application of a conventional tuning rule for a nominal plant. It effectiveness has been proved by its application to several design examples.

Chapter 4: PID Design for an Uncertain FOTD Plant

Chapter 4 has studied the design of filtered PID controllers for uncertain FOTD plants. As in the previous chapter, the uncertainty has been modeled by an interval parametric uncertainty model, and the control design problem has been formulated in terms of minimizing IE subject to worst-case peak values of the sensitivity and complementary sensitivity functions. The control design problem was initially posed as a robust optimization problem; then, it is approximated by a nominal optimization problem by using an instrumental nominal fractional-order plant and some extra conditions. The major strength of the proposed approach is that it allows to take into account interval plant uncertainty, while the design is carried out for a nominal plant. Two examples have been studied. The first example has demonstrated that practically at the same computational cost of designing for a nominal, we can design for a given uncertain plant. A second example illustrates that the obtained conditions are applicable to a more general class of controller, in this case, it is analyzed a PID with an SP (a control structure that may exhibit a particularly high sensitivity to time-delay uncertainty).

Chapter 5: PID Design for an Uncertain General Plant

Chapter 5 considers a more general problem than the considered in the previous chapter. The uncertain plant model considered in Chapter 5 is given by a finite set of frequency responses. This way of modeling is very general since any SISO LTI model can be transformed into a frequency response. In addition, many input/output

identification experiments yield a model in form of a frequency response. Many control design problems are considering by generalizing the ones considered in Chapters 3 and 4. Control design problems based on QFT specifications and optimality criterion are also considered. The method is studied in the context of PID control, but it can also be applied to any controller structure, where the transfer function depends affinely on the controller parameters. In other words, the controller poles are fixed, and the synthesis method gives the zeros of the controller. The proposed design method has been illustrated by several numerical examples.

Chapter 6: PID Design under Probabilistic Parametric Uncertainty

The three previous chapters had adopted a deterministic description of the uncertainty. This approach to model the uncertainty leads to (hard) worst-case specifications. Chapter 6 adopts another approach to model it. In this case, the uncertain parameters are assumed to be described by a random variable. The uniform distribution is used to model the interval parametric uncertainty. A probabilistic description of the uncertainty enables us to obtain a probability of constraint violation, and hence to formulate the control design problem by using (soft) probabilistic specifications. The probabilistic design problem is posed in terms of minimizing IE subject to chance-constrained specifications on the peak values of the sensitivity. The calculation of probability values for this specification is a challenging problem. We have employed quadrature schemes based on combining Smolyak's product with nested univariate quadrature rules. RAs are suggested to probabilistically validate the obtained designs. The synthesis method has been illustrated by several examples. They show that significant performance gains can be made, if (small) probabilities for constraint violations are permitted.

Chapter 7: Autotunning of PID Controllers

Chapter 7 has presented the successful application of a novel autotuning method on an in-line pH control system. The method combines a modified relay experiment, output error identification and controller design. Its main strengths lie in the short experiment duration, combined with a robust synthesis method, explicitly accounting for identified model parameter uncertainty.

8.2 Future Works

In this section, we provide several potential lines of research related to the content of this thesis.

Extension to MIMO Control

Any ALS method for SISO controllers could be extended to a method of design for MIMO controllers based on the sequential QFT method, for example, in the spirit of the work [266]. It is worth pointing out that [47] presents a technique based on iterative convex optimization for the design of MIMO PID controllers and able to handle nonparametric models. In fact, this technique has been employed by the author of this thesis resulting in a successfully application to a benchmark problem[1]. However, this technique, as most of the multivariable control literature, considers specifications in terms of principal gains, i.e., global matrix performances. This approach for assessing performance may be quite conservative under some realistic circumstances, see [129, 169]. That is why, in the author's opinion, it is worth exploring an alternative approach based on typical QFT specifications, i.e., performance specifications over the elements of relevant closed-loop matrix transfer functions.

Extension to Constrained Control

A caveat of virtually any feedback control design method, in the continuous-time case, is the inability to deal systematically with constraints, both control and plant output constraints. There are several approaches in the discrete-time case that overcome this caveat, being the most popular by far MPC. However, finding the weights for its optimality criterion is often nontrivial. Consequently, important issues like sensitivity and robustness are generally not taken into account in its design. Recall that an MPC controller behaves like a linear controller when the constraints are not active. That has motivated several works that address the problem of reproducing an existing controller as an MPC controller, e.g., [73, 118, 156]. Moreover, as pointed out in a recent survey on MPC [174], some of the topics that require more attention are the problem of linking MPC to an existing control law, robustness, and the use of output feedback, among others issues.

In the author's opinion, these issues can be efficiently treated using a novel control approach known as interpolation based control [195–197]. It constitutes an appealing

[1]Competition on Control Engineering organized by the Spanish Committee of Automation CEA-IFAC.

alternative to MPC. It is less computationally demand than MPC. The price to paid is that the controller is optimal (in MPC sense) only locally. This technique is built over an existing controller, and the control signal is given by it when this control law is feasible (state belongs to the maximum admissible set). Otherwise, the control signal is generated by interpolating between the existing controller and another control law (feasible in a controlled positively invariant set).

Therefore, this technique could be applied to any controller designed in this thesis (once it has been discretized), endowing it with the ability to handle constraints. Work on this topic is currently ongoing.

Extension to Reset Control

Reset control attempts to overcome the limitations of linear controllers by a nonlinear controller. A reset controller has a dynamic governed by a lineal differential equation between the reset instants, in which the dynamic is governed by an impulsive equation. In terms of the (approximate) describing function approach, this kind of controllers has the attractive property of yielding the same gain characteristic of a linear controller, but with less phase lag than the linear counterpart. It has received considerable attention in the literature during the last twenty years, see, for example, the recent monographs [28, 109] and PhD theses [69, 249]. Most of the literature deals with the problem of stability analysis, but there are a few results on control synthesis, see, for example, [30, 70]. Nevertheless, the current state-of-the-art is far from providing a general methodology able to incorporate important issues like robustness, sensitivity, noise attenuation, etc.

An appealing solution is to resort to the describing function approach to extend the methods presented here to the design of reset controllers. However, the main disadvantage is that a rigorous justification for its use with reset control systems is an open problem, and it seems to be a very challenging one.

Bibliography

[1] Ackermann, J. (2002). *Robust Control: The Parameter Space Approach*. Springer-Verlag London.

[2] Adurthi, N. and Singla, P. (2015). Conjugate unscented transformation-based approach for accurate conjunction analysis. *Journal of Guidance, Control, and Dynamics*, 38(9):1642–1658.

[3] Adurthi, N., Singla, P., and Singh, T. (2012). The conjugate unscented transform-an approach to evaluate multi-dimensional expectation integrals. In *Proceedings of the 2012 American Control Conference*, pages 5556–5561, Montreal, Canada.

[4] Adurthi, N., Singla, P., and Singh, T. (2013). Conjugate unscented transform rules for uniform probability density functions. In *Proceedings of the 2013 American Control Conference*, pages 2454–2459, Washington, USA.

[5] Alcántara, S., Vilanova, R., and Pedret, C. (2013). PID control in terms of robustness/performance and servo/regulator trade-offs: A unifying approach to balanced autotuning. *Journal of Process Control*, 23(4):527–542.

[6] Alfaro, V. M. and Vilanova, R. (2013). Performance and robustness considerations for tuning of proportional integral/proportional integral derivative controllers with two input filters. *Industrial & Engineering Chemistry Research*, 52(51):18287–18302.

[7] Alfaro, V. M. and Vilanova, R. (2016). *Model-Reference Robust Tuning of PID Controllers*. Springer International Publishing.

[8] Anderson, B. D. and Moore, J. B. (1971). *Linear Optimal Control*. Prentice-Hall, Inc.

[9] Ang, K. H., Chong, G., and Li, Y. (2005). PID control system analysis, design, and technology. *IEEE Transactions on Control Systems Technology*, 13(4):559–576.

[10] Anil, C. and Sree, R. P. (2015). Tuning of PID controllers for integrating systems using direct synthesis method. *ISA Transactions*, 57(1):211–219.

[11] Araki, M. (1984). PID control system with reference feedforward (PID-FF control system). In *Proceedings of the 23rd Society of Instrument and Control Engineers Annual Conference*, pages 31–32.

[12] Åström, K. J. (1980). Maximum likelihood and prediction error methods. *Automatica*, 16(5):551–574.

[13] Åström, K. J. (2000). Limitations on control system performance. *European Journal of Control*, 6(1):2–20.

[14] Åström, K. J. and Hägglund, T. (1984). Automatic tuning of simple regulators with specifications on phase and amplitude margins. *Automatica*, 20(5):645–651.

[15] Åström, K. J. and Hägglund, T. (1988). *Automatic Tuning of PID Controllers*. Instrument Society of America.

[16] Åström, K. J. and Hägglund, T. (1995). *PID Controllers: Theory, Design, and Tuning*. Instrument Society of America.

[17] Åström, K. J. and Hägglund, T. (2001). The future of PID control. *Control engineering practice*, 9(11):1163–1175.

[18] Åström, K. J. and Hägglund, T. (2004). Revisiting the Ziegler–Nichols step response method for PID control. *Journal of Process Control*, 14(6):635–650.

[19] Åström, K. J. and Hägglund, T. (2006). *Advanced PID Control*. The Instrumentation, Systems, and Automation Society.

[20] Åström, K. J. and Kumar, P. (2014). Control: A perspective. *Automatica*, 50(1):3–43.

[21] Åström, K. J. and Murray, R. M. (2008). *Feedback Systems: An Introduction for Scientists and Engineers*. Princeton University Press.

[22] Åström, K. J., Panagopoulos, H., and Hägglund, T. (1998). Design of PI controllers based on non-convex optimization. *Automatica*, 34(5):585–601.

[23] Åström, K. J. and Wittenmark, B. (1995). *Adaptive Control*. Addison-Wesley.

[24] Bailey, F. and Hui, C.-H. (1989). A fast algorithm for computing parametric rational functions. *IEEE Transactions on Automatic Control*, 34(11):1209–1212.

[25] Bailey, F. and Hui, C.-H. (1991). Loop gain-phase shaping for single-input-single-output robust controllers. *IEEE Control Systems*, 11(1):93–101.

[26] Bailey, F., Panzer, D., and Gu, G. (1988). Two algorithms for frequency domain design of robust control systems. *International Journal of Control*, 48(5):1787–1806.

[27] Baños, A. (2007). Nonlinear quantitative feedback theory. *International Journal of Robust and Nonlinear Control*, 17(2-3):181–202.

[28] Baños, A. and Barreiro, A. (2012). *Reset Control Systems*. Springer-Verlag London.

[29] Baños, A., Cervera, J., Lanusse, P., and Sabatier, J. (2011). Bode optimal loop shaping with CRONE compensators. *Journal of Vibration and Control*, 17(13):1964–1974.

[30] Baños, A. and Davó, M. A. (2014). Tuning of reset proportional integral compensation with a variable reset ratio and reset band. *IET Control Theory and Applications*, 8(17):1949–1962.

[31] Baños, A. and Horowitz, I. M. (2004). Nonlinear quantitative stability. *International Journal of Robust and Nonlinear Control*, 14(3):289–306.

[32] Barmish, B. and Lagoa, C. M. (1997). The uniform distribution: A rigorous justification for its use in robustness analysis. *Mathematics of Control, Signals and Systems*, 10(3):203–222.

[33] Bartlett, A. C., Hollot, C. V., and Lin, H. (1988). Root locations of an entire polytope of polynomials: It suffices to check the edges. *Mathematics of Control, Signals and Systems*, 1(1):61–71.

[34] Bennett, S. (1993). Development of the PID controller. *IEEE Control Systems*, 13(6):58–62.

[35] Bennett, S. (1996). A brief history of automatic control. *IEEE Control Systems Magazine*, 16(3):17–25.

[36] Bennett, S. (2001). The past of PID controllers. *Annual Reviews in Control*, 25:43–53.

[37] Berner, J., Åström, K. J., and Hägglund, T. (2014). Towards a new generation of relay autotuners. In *Proceedings of the 19th IFAC World Congress*, Cape Town, South Africa.

[38] Berner, J., Hägglund, T., and Åström, K. J. (2016). Asymmetric relay autotuning – Practical features for industrial use. *Control Engineering Practice*, 54:231–245.

[39] Bhattacharyya, S., Chapellat, H., and Keel, L. (1995). *Robust Control: The Parametric Approach*. Prentice-Hall.

[40] Black, H. S. (1934). Stabilized feedback amplifiers. *Bell System Technical Journal*, 13(1):1–18.

[41] Blondel, V. D. and Tsitsiklis, J. N. (2000). A survey of computational complexity results in systems and control. *Automatica*, 36(9):1249–1274.

[42] Bode, H. W. (1945). *Network Analysis and Feedback Amplifier Design*. van Nostrand.

[43] Boiko, I. (2013). *Non-Parametric Tuning of PID Controllers – A Modified Relay-Feedback-Test Approach*. Springer-Verlag London.

[44] Boje, E. (2007). Quantitative feedback design for systems with probabilistic parameterizations. *International Journal of Robust and Nonlinear Control*, 17(2–3):173–179.

[45] Bondia, J., Kieffer, A., Walter, E., Monreal, J., and Pico, J. (2004). Guaranteed tuning of PID controllers for parametric uncertain systems. In *Proceedings of the 43rd IEEE Conference on Decision and Control*, pages 2948–2953, Nassau, Bahamas. IEEE.

[46] Borghesani, C., Chait, Y., and Yaniv, O. (1994). *Quantitative feedback theory toolbox for use with MATLAB®: User's guide*. MathWorks, Incorporated.

[47] Boyd, S., Hast, M., and Åström, K. J. (2016). MIMO PID tuning via iterated LMI restriction. *International Journal of Robust and Nonlinear Control*, 26(8):1718–1731.

[48] Boyd, S. and Vandenberghe, L. (2004). *Convex Optimization*. Cambridge University Press.

[49] Bungartz, H.-J. and Griebel, M. (2004). Sparse grids. *Acta numerica*, 13:147–269.

[50] Byrd, R. H., Gilbert, J. C., and Nocedal, J. (2000). A trust region method based on interior point techniques for nonlinear programming. *Mathematical Programming*, 89(1):149–185.

[51] Calafiore, G., Dabbene, F., and Tempo, R. (2007). A survey of randomized algorithms for control synthesis and performance verification. *Journal of Complexity*, 23(3):301–316.

[52] Calafiore, G., Dabbene, F., and Tempo, R. (2011). Research on probabilistic methods for control system design. *Automatica*, 47(7):1279–1293.

[53] Calafiore, G. and El Ghaoui, L. (2014). *Optimization Models*. Cambridge University Press.

[54] Camacho, E. F. and Bordons, C. (2007). *Model Predictive Control*. Springer-Verlag London.

[55] Carrasco, J. and Baños, A. (2012). Reset control of an industrial in-line pH process. *IEEE Transactions on Control Systems Technology*, 2(4):1100–1106.

[56] Cervera, J. and Baños, A. (2009). Nonlinear nonconvex optimization by evolutionary algorithms applied to robust control. *Mathematical Problems in Engineering*, 2009. Article ID 671869.

[57] Chait, Y., Borghesani, C., and Zheng, Y. (1995). Single-loop QFT design for robust performance in the presence of non-parametric uncertainties. *Journal of Dynamic Systems, Measurement, and Control*, 117(3):420–425.

[58] Chait, Y., Chen, Q., and Hollot, C. (1999). Automatic loop-shaping of QFT controllers via linear programming. *Journal of Dynamic Systems, Measurement, and Control*, 121(3):351–357.

[59] Chait, Y. and Yaniv, O. (1993). Multi-input/single-output computer-aided control design using the quantitative feedback theory. *International Journal of Robust and Nonlinear Control*, 3(1):47–54.

[60] Chen, W.-H. and Ballance, D. J. (1999). Plant template generation for uncertain plants in Quantitative Feedback Theory. *Journal of Dynamic Systems, Measurement, and Control*, 121(3):358–364.

[61] Chen, W.-H., Ballance, D. J., Feng, W., and Li, Y. (1999). Genetic algorithm enabled computer-automated design of QFT control systems. In *Proceedings of the 1999 IEEE International Symposium on Computer Aided Control System Design*, pages 492–497.

[62] Chen, Y., Petras, I., and Xue, D. (2009). Fractional order control - a tutorial. In *Proceedings of the 2009 American Control Conference*, pages 1397–1411, St. Louis, USA.

[63] Choi, Y. and Chung, W. K. (2004). *PID Trajectory Tracking Control for Mechanical Systems*. Springer-Verlag Berlin Heidelberg.

[64] Clegg, J. C. (1958). A nonlinear integrator for servomechanisms. *Transactions of the American Institute of Electrical Engineers, Part II: Applications and Industry*, 77(1):41–42.

[65] Cohen, N., Chait, Y., Yaniv, O., and Borghesani, C. (1994). Stability analysis using Nichols charts. *International Journal of Robust and Nonlinear Control*, 4(1):3–20.

[66] Cools, R. (2003). An encyclopaedia of cubature formulas. *Journal of Complexity*, 19(3):445–453.

[67] Datta, A., Ho, M.-T., and Bhattacharyya, S. P. (2000). *Structure and Synthesis of PID Controllers*. Springer-Verlag London.

[68] Davis, P. J. and Rabinowitz, P. (1984). *Methods of Numerical Integration*. Academic Press, Inc.

[69] Davó, M. A. (2015). *Analysis and design of reset control systems*. PhD thesis, University of Murcia.

[70] Davó, M. A. and Baños, A. (2016). Reset control of integrating plus dead time processes. *Journal of Process Control*, 38:22–30.

[71] Dejonckheere, J., Disney, S. M., Lambrecht, M. R., and Towill, D. R. (2003). Measuring and avoiding the bullwhip effect: A control theoretic approach. *European Journal of Operational Research*, 147(3):567–590.

[72] Desborough, L. and Miller, R. (2002). Increasing customer value of industrial control performance monitoring-Honeywell's experience. In *Proceedings of the 6th AIChE International Conference on Chemical Process Control*, pages 169–189, Tucson, USA.

[73] Di Cairano, S. and Bemporad, A. (2010). Model predictive control tuning by controller matching. *IEEE Transactions on Automatic Control*, 55(1):185–190.

[74] Díaz, J., Dormido, S., and Aranda, J. (2007). An interactive software tool for learning robust control design using Quantitative Feedback Theory methodology. *International Journal of Engineering Education*, 23(5):1011–1023.

[75] Disney, S. M., Towill, D. R., and Warburton, R. D. (2006). On the equivalence of control theoretic, differential, and difference equation approaches to modeling supply chains. *International Journal of Production Economics*, 101(1):194–208.

[76] Doyle, J. C. (1978). Guaranteed margins for LQG regulators. *IEEE Transactions on Automatic Control*, AC-23(4):756–757.

[77] Doyle, J. C. (1982). Analysis of feedback systems with structured uncertainties. *IEE Proceedings D (Control Theory and Applications)*, 129:242–250.

[78] Doyle, J. C. (1983). Synthesis of robust controllers and filters. In *Proceedings of the 22nd IEEE Conference on Decision and Control*, pages 109–114.

[79] Doyle, J. C., Francis, B. A., and Tannenbaum, A. R. (1992). *Feedback Control Theory*. Macmillan Publishing Co.

[80] Doyle, J. C., Glover, K., Khargonekar, P. P., and Francis, B. A. (1989). State-space solutions to standard H_2 and H_∞ control problems. *IEEE Transactions on Automatic control*, 34(8):831–847.

[81] Duong, P. L. T. and Lee, M. (2012). Robust PID controller design for processes with stochastic parametric uncertainties. *Journal of Process Control*, 22(9):1559–1566.

[82] Duong, P. L. T. and Lee, M. (2014). Probabilistic analysis and control of systems with uncertain parameters over non-hypercube domain. *Journal of Process Control*, 24(4):358–367.

[83] Edelsbrunner, H., Kirkpatrick, D. G., and Seidel, R. (1983). On the shape of a set of points in the plane. *IEEE Transactions on Information Theory*, 29(4):551–559.

[84] Eitelberg, E. (1987). A regulating and tracking PI (D) controller. *International Journal of Control*, 45(1):91–95.

[85] Eitelberg, E. (2000). Quantitative feedback design for tracking error tolerance. *Automatica*, 36(2):319–326.

[86] Eitelberg, E. and Houpis, C. H. (2007). Isaac M. Horowitz: an essential singularity in the complex domain of control theory (1920–2005). *International Journal of Robust and Nonlinear Control*, 17(2-3):95–105.

[87] Fekete, S. P. (2000). On simple polygonalizations with optimal area. *Discrete & Computational Geometry*, 23(1):73–110.

[88] Foster, W. C., Gieseking, D. L., and Waymayer, W. K. (1966). A nonlinear filter for independent gain and phase (with applications). *Journal of Basic Engineering*, 88:457–462.

[89] Fransson, C.-M., Wik, T., Lennartson, B., Saunders, M., and Gutman, P.-O. (2009). Nonconservative robust control: optimized and constrained sensitivity functions. *IEEE Transactions on Control Systems Technology*, 17(2):298–308.

[90] Freudenberg, J. and Looze, D. (1987). A sensitivity tradeoff for plants with time delay. *IEEE Transactions on Automatic Control*, 32(2):99–104.

[91] Friman, M. and Waller, K. V. (1997). A two-channel relay for autotuning. *Industrial and Engineering Chemistry Research*, 36(7):2662–2671.

[92] Fu, M. (1990). Computing the frequency response of linear systems with parametric perturbation. *Systems & Control Letters*, 15(1):45–52.

[93] Fu, M., Olbrot, A. W., and Polis, M. (1989). Robust stability for time-delay systems: the edge theorem and graphical tests. *IEEE Transactions on Automatic Control*, 34(8):813–820.

[94] Gaing, Z.-L. (2004). A particle swarm optimization approach for optimum design of PID controller in AVR system. *IEEE Transactions on Energy Conversion*, 19(2):384–391.

[95] Garcia-Sanz, M. (2016). The Nyquist stability criterion in the Nichols chart. *International Journal of Robust and Nonlinear Control*, 26(12):2643–2651.

[96] Garcia-Sanz, M., Mauch, A., and Philippe, C. (2009). QFT Control Toolbox: an interactive object-oriented Matlab CAD tool for Quantitative Feedback Theory. In *Proceedings of the 6th IFAC Symposium on Robust Control Design*, Haifa, Israel.

[97] Garpinger, O. and Hägglund, T. (2015). Software-based optimal PID design with robustness and noise sensitivity constraints. *Journal of Process Control*, 33:90–101.

[98] Garpinger, O., Hägglund, T., and Åström, K. J. (2014). Performance and robustness trade-offs in PID control. *Journal of Process Control*, 24(5):568–577.

[99] Gelb, A. and Vander Velde, W. E. (1968). *Multiple-Input Describing Functions and Nonlinear System Design*. McGraw-Hill.

[100] Gera, A. and Horowitz, I. M. (1980). Optimization of the loop transfer function. *International Journal of Control*, 31(2):389–398.

[101] Goodwin, G. C., Graebe, S. F., and Salgado, M. E. (2001). *Control System Design*. Prentice Hall.

[102] Gorodnichenko, Y. and Shapiro, M. D. (2007). Monetary policy when potential output is uncertain: Understanding the growth gamble of the 1990s. *Journal of Monetary Economics*, 54(4):1132–1162.

[103] Grant, M. and Boyd, S. (2008). Graph implementations for nonsmooth convex programs. In Blondel, V., Boyd, S., and Kimura, H., editors, *Recent Advances in Learning and Control*, Lecture Notes in Control and Information Sciences, pages 95–110. Springer-Verlag Limited.

[104] Grant, M. and Boyd, S. (2014). CVX: Matlab software for disciplined convex programming, version 2.1. http://cvxr.com/cvx.

[105] Grimholt, C. and Skogestad, S. (2012). Optimal PI-control and verification of the SIMC tuning rule. *IFAC Proceedings Volumes*, 45(3):11–22.

[106] Grimholt, C. and Skogestad, S. (2015). Improved optimization-based design of PID controllers using exact gradients. In *Proceedings of the 25th European Symposium on Computer Aided Process Engineering*, pages 1751–1756, Copenhagen, Denmark.

[107] Gryazina, E. N. and Polyak, B. T. (2006). Stability regions in the parameter space: D-decomposition revisited. *Automatica*, 42(1):13–26.

[108] Gudin, R. and Mirkin, L. (2007). On the delay margin of dead-time compensators. *International Journal of Control*, 80(8):1316–1332.

[109] Guo, Y., Xie, L., and Wang, Y. (2015). *Analysis and Design of Reset Control Systems*. Institution of Engineering and Technology.

[110] Gutman, P.-O. (1996). *QSYN – The Toolbox for Robust Control Systems Design for use with Matlab*.

[111] Gutman, P.-O. (2003). Robust and adaptive control: fidelity or an open relationship? *Systems & Control Letters*, 49(1):9–19.

[112] Gutman, P.-O., Baril, C., and Neumann, L. (1994). An algorithm for computing value sets of uncertain transfer functions in factored real form. *IEEE Transactions on Automatic Control*, 39(6):1268–1273.

[113] Gutman, P.-O. and Cwikel, M. (1986). Admissible sets and feedback control for discrete-time linear dynamical systems with bounded controls and states. *IEEE Transactions on Automatic Control*, 31(4):373–376.

[114] Gutman, P.-O., Nordin, M., and Cohen, B. (2007). Recursive grid methods to compute value sets and Horowitz–Sidi bounds. *International Journal of Robust and Nonlinear Control*, 17(2-3):155–171.

[115] Hägglund, T. (2013). A unified discussion on signal filtering in PID control. *Control Engineering Practice*, 21(8):994–1006.

[116] Hajiloo, A., Nariman-Zadeh, N., and Moeini, A. (2012). Pareto optimal robust design of fractional-order PID controllers for systems with probabilistic uncertainties. *Mechatronics*, 22(6):788–801.

[117] Han, K.-W. and Chang, C.-H. (1990). Gain margins and phase margins for control systems with adjustable parameters. *Journal of Guidance, Control, and Dynamics*, 13(3):404–408.

[118] Hartley, E. N. and Maciejowski, J. M. (2013). Designing output-feedback predictive controllers by reverse-engineering existing LTI controllers. *IEEE Transactions on Automatic Control*, 58(11):2934–2939.

[119] Hast, M., Åström, K., Bernhardsson, B., and Boyd, S. (2013). PID design by convex-concave optimization. In *Proceedings of the 12th biannual European Control Conference*, pages 4460–4465, Zürich, Switzerland.

[120] Hast, M. and Hägglund, T. (2015). Optimal proportional–integral–derivative set-point weighting and tuning rules for proportional set-point weights. *IET Control Theory & Applications*, 9(15):2266–2272.

[121] Hawkins, R. J., Speakes, J. K., and Hamilton, D. E. (2015). Monetary policy and PID control. *Journal of Economic Interaction and Coordination*, 10(1):183–197.

[122] Heiss, F. and Winschel, V. (2008). Likelihood approximation by numerical integration on sparse grids. *Journal of Econometrics*, 144(1):62–80.

[123] Ho, M.-T., Datta, A., and Bhattacharyya, S. (1997). A linear programming characterization of all stabilizing PID controllers. In *Proceedings of the 1997 American Control Conference*, pages 3922–3928, Albuquerque, USA.

[124] Horowitz, I. M. (1959). Fundamental theory of automatic linear feedback control systems. *IRE Transactions on Automatic Control*, 4(3):5–19.

[125] Horowitz, I. M. (1963). *Synthesis of Feedback Systems*. Academic Press.

[126] Horowitz, I. M. (1976). Synthesis of feedback systems with nonlinear time-varying uncertain plants to satisfy quantitative performance specifications. *Proceedings of the IEEE*, 64(1):123–130.

[127] Horowitz, I. M. (1983). Some properties of delayed controls (Smith regulator). *International Journal of Control*, 38(5):977–990.

[128] Horowitz, I. M. (1993). *Quantitative Feedback Design*. QFT Publications.

[129] Horowitz, I. M. (2001). Survey of quantitative feedback theory (QFT). *International Journal of Robust and Nonlinear Control*, 11(10):887–921.

[130] Horowitz, I. M. (2003). Some ideas for QFT research. *International Journal of Robust and Nonlinear Control*, 13(7):599–605.

[131] Horowitz, I. M. and Baños, A. (2001). Fundamentals of nonlinear quantitative feedback theory. In Baños, A., Lamnabhi-Lagarrigue, F., and Montoya, F. J., editors, *Advances in the Control of Nonlinear Systems*, Lecture Notes in Control and Information Sciences, pages 63–132. Springer-Verlag London.

[132] Horowitz, I. M. and Shaked, U. (1975). Superiority of transfer function over state-variable methods in linear time-invariant feedback system design. *IEEE Transactions on Automatic Control*, 20(1):84–97.

[133] Horowitz, I. M. and Sidi, M. (1972). Synthesis of feedback systems with large plant ignorance for prescribed time-domain tolerances. *International Journal of Control*, 16(2):287–309.

[134] Houpis, C. and Sating, R. (1997). MIMO QFT CAD package (version 3). *International Journal of Robust and Nonlinear Control*, 7(6):533–549.

[135] Huang, Y. J. and Wang, Y.-J. (2000). Robust PID tuning strategy for uncertain plants based on the Kharitonov theorem. *ISA Transactions*, 39(4):419–431.

[136] Huba, M. (2013a). Performance measures, performance limits and optimal PI control for the IPDT plant. *Journal of Process Control*, 23(4):500–515.

[137] Huba, M. (2013b). Performance portrait method: a new CAD tool. *IFAC Proceedings Volumes*, 46(17):315–320.

[138] Ionescu, C. M. and De Keyser, R. (2012). The next generation of relay-based PID autotuners (part 1): Some insights on the performance of simple relay-based PID autotuners. *IFAC Proceedings Volumes*, 45(3):122–127.

[139] Iwasaki, T. and Skelton, R. E. (1994). All controllers for the general H_∞ control problem: LMI existence conditions and state space formulas. *Automatica*, 30(8):1307–1317.

[140] James, H. M., Nichols, N. B., and Phillips, R. S. (1947). *Theory of Servomechanisms*. McGraw-Hill Book Co.

[141] Jaulin, L., Kieffer, M., Didrit, O., and Walter, E. (2001). *Applied Interval Analysis - With Examples in Parameter and State Estimation, Robust Control and Robotics*. Springer-Verlag London.

[142] Jeyasenthil, R. and Nataraj, P. (2017). An interval-consistency-based hybrid optimization algorithm for automatic loop shaping in quantitative feedback theory design. *Journal of Vibration and Control*, 23(3):414–431.

[143] Jin, Q., Liu, Q., and Huang, B. (2015). Control design for disturbance rejection in the presence of uncertain delays. *IEEE Transactions on Automation Science and Engineering*, PP(99):1–12.

[144] Johnson, M. A. and Moradi, M. H. (2005). *PID Control - New Identification and Design Methods*. Springer-Verlag London.

[Julier and Uhlmann] Julier, S. J. and Uhlmann, J. K. New extension of the Kalman filter to nonlinear systems. In *Proceedings of the SPIE 3068, Signal Processing, Sensor Fusion, and Target Recognition VI*, pages 182–193.

[146] Julier, S. J. and Uhlmann, J. K. (1996). A general method for approximating nonlinear transformations of probability distributions. Technical report, Department of Engineering Science, University of Oxford.

[147] Julier, S. J. and Uhlmann, J. K. (2004). Unscented filtering and nonlinear estimation. *Proceedings of the IEEE*, 92(3):401–422.

[148] Kalman, R. E. (1964). When is a linear control system optimal? *Journal of Basic Engineering*, 86(1):51–60.

[149] Karimi, A. and Galdos, G. (2010). Fixed-order H_∞ controller design for nonparametric models by convex optimization. *Automatica*, 46(8):1388–1394.

[150] Karybakas, C. (1977). Nonlinear integrator with zero phase shift. *IEEE Transactions on Industrial Electronics and Control Instrumentation*, 24(2):150–152.

[151] Kaya, I. and Atherton, D. (2001). Parameter estimation from relay autotuning with asymmetric limit cycle data. *Journal of Process Control*, 11(4):429–439.

[152] Keel, L. H. and Bhattacharyya, S. P. (2008). Controller synthesis free of analytical models: Three term controllers. *IEEE Transactions on Automatic Control*, 53(6):1353–1369.

[153] Keel, L. H. and Bhattacharyya, S. P. (2012). Modern PID control: Stabilizing sets and multiple performance specifications. In Vilanova, R. and Visioli, A., editors, *PID Control in the Third Millennium*, Advances in Industrial Control, pages 319 – 348. Springer-Verlag London.

[154] Khadraoui, S., Rakotondrabe, M., and Lutz, P. (2012). Interval modeling and robust control of piezoelectric microactuators. *IEEE Transactions on Control Systems Technology*, 20(2):486–494.

[155] Kharitonov, V. (1978). Asympotic stability of an equilibrium position of a family of systems of linear differntial equations. *Differntia Uravnen*, 14(11):1483–1485.

[156] Kong, H., Goodwin, G., and Seron, M. M. (2013). Predictive metamorphic control. *Automatica*, 49(12):3670–3676.

[157] Kucera, V. (1975). Stability of discrete linear feedback systems. In *Proceedings of the 6th IFAC World Congress*, Boston, USA.

[158] Kumar, D. S. and Sree, R. P. (2016). Tuning of IMC based PID controllers for integrating systems with time delay. *ISA Transactions*, 63:242 – 255.

[159] Lennartson, B. and Kristiansson, B. (2009). Evaluation and tuning of robust PID controllers. *IET Control Theory & Applications*, 3(3):294–302.

[160] Lewis, A. D. (2003). *A Mathematical Approach to Classical Control*.

[161] Lin, C., Wang, Q.-G., and Lee, T. H. (2004). Relay feedback: A complete analysis for first-order systems. *Industrial & Engineering Chemistry Research*, 43(26):8400–8402.

[162] Lipp, T. and Boyd, S. (2016). Variations and extension of the convex–concave procedure. *Optimization and Engineering*, 17(2):263–287.

[163] Litrico, X. and Fromion, V. (2004). Simplified modeling of irrigation canals for controller design. *Journal of Irrigation and Drainage Engineering*, 130(5):373–383.

[164] Litrico, X. and Fromion, V. (2006). Tuning of robust distant downstream PI controllers for an irrigation canal pool. I: Theory. *Journal of Irrigation and Drainage Engineering*, 132(4):359–368.

[165] Litrico, X., Fromion, V., and Baume, J.-P. (2006). Tuning of robust distant downstream PI controllers for an irrigation canal pool. II: Implementation issues. *Journal of Irrigation and Drainage Engineering*, 132(4):369–379.

[166] Ljung, L. (1999). *System Identification - Theory For the User*. Prentice Hall.

[167] Lurie, B. and Enright, P. (2000). *Classical Feedback Control: with MATLAB*. CRC Press.

[168] MacFarlane, A. G. J. and Postlethwaite, I. (1977). The generalized Nyquist stability criterion and multivariable root loci. *International Journal of Control*, 25(1):81–127.

[169] Maciejowski, J. M. (1989). *Multivariable Feedback Design*. Addison-Wesley.

[170] Maciejowski, J. M. (2001). *Predictive Control with Constraints*. Prentice Hall.

[171] Markowitz, H. (1952). Portfolio selection. *The Journal of Finance*, 7(1):77–91.

[172] Martín, F., Monje, C. A., Moreno, L., and Balaguer, C. (2015). DE-based tuning of PIλDμ controllers. *ISA Transactions*, 59:398–407.

[173] Martin-Romero, J. J. and Martin-Romero, A. (2007). QFT templates for plants with a high number of uncertainty parameters. *IEEE Transactions on Automatic Control*, 52(4):754–758.

[174] Mayne, D. Q. (2014). Model predictive control: Recent developments and future promise. *Automatica*, 50(12):2967–2986.

[175] Mees, A. and Bergen, A. (1975). Describing functions revisited. *IEEE Transactions on Automatic Control*, 20(4):473–478.

[176] Menani, S. and Koivo, H. (2001). A comparative study of recent relay autotuning methods for multivariable systems. *International Journal of System Science*, 32(4):443–466.

[177] Mercader, P., Åström, K. J., Baños, A., and Hägglund, T. (2017a). Robust PID design based on QFT and convex-concave optimization. *IEEE Transactions on Control Systems Technology*, 25(2):441–452.

[178] Mercader, P. and Baños, A. (2014a). Robust PI compensators design for FOPDT systems with large uncertainty. In *Proceedings of the 2014 14th International Conference on Control, Automation and Systems*, pages 1261–1266, Seoul, Korea.

[179] Mercader, P. and Baños, A. (2014b). Tuning of PI compensators for integrating systems with large parametric uncertainty. In *Proceedings of the 19th IEEE Conference on Emerging Technologies & Factory Automation*, pages 1–6, Barcelona, Spain.

[180] Mercader, P. and Baños, A. (2017). A PI tuning rule for integrating plus dead time processes with parametric uncertainty. *ISA Transactions*.

[181] Mercader, P., Baños, A., and Vilanova, R. (2017b). Robust PID design for processes with interval parametric uncertainty. *IET Control Theory & Applications*.

[182] Mercader, P., Carrasco, J., and Baños, A. (2013a). IQC analysis for time-delay reset control systems with first order reset elements. In *Proceedings of the 52nd IEEE Conference on Decision and Control*, pages 2251–2256, Florence, Italy.

[183] Mercader, P., Davó, M. A., and Baños, A. (2013b). $\mathcal{H}_\infty/\mathcal{H}_2$ analysis for time-delay reset control systems. In *Proceedings of the 3rd International Conference on Systems and Control*, pages 518–523, Algiers, Algeria.

[184] Mercader, P., Davó, M. A., and Baños, A. (2015). Performance analysis of PI and PI+CI compensation for an IPDT process. In *Proceedings of the 23rd Mediterranean Conference on Control and Automation*, Torremolinos, Spain.

[185] Mercader, P., Soltesz, K., and Baños, A. (2016a). Autotuning of an in-line pH control system. In *21st International Conference on Emerging Technologies and Factory Automation (ETFA)*, pages 1–4, Berlin, Germany.

[186] Mercader, P., Soltesz, K., and Baños, A. (2016b). PID synthesis under probabilistic parametric uncertainty. In *Proceedings of the 2016 American Control Conference*, pages 5467–5472, Boston, USA.

[187] Merrikh-Bayat, F. and Karimi-Ghartemani, M. (2008). On the essential instabilities caused by fractional-order transfer functions. *Mathematical Problems in Engineering*, 2008. Article ID 419046.

[188] Monje, C. A., Chen, Y., Vinagre, B. M., Xue, D., and Feliu-Batlle, V. (2010). *Fractional-order Systems and Controls: Fundamentals and Applications*. Springer-Verlag London.

[189] Moreno, J. C., Baños, A., and Berenguel, M. (2006). Improvements on the computation of boundaries in QFT. *International Journal of Robust and Nonlinear Control*, 16(12):575–597.

[190] Moreno, J. C., Baños, A., and Berenguel, M. (2011). The design of QFT robust compensators with magnitude and phase specifications. *Mathematical Problems in Engineering*, 2010. Article ID 105143.

[191] Mutapcic, A. and Boyd, S. (2009). Cutting-set methods for robust convex optimization with pessimizing oracles. *Optimization Methods & Software*, 24(3):381–406.

[192] Nataraj, P. and Sardar, G. (2000). Template generation for continuous transfer functions using interval analysis. *Automatica*, 36(1):111 – 119.

[193] Nataraj, P. and Tharewal, S. (2007). An interval analysis algorithm for automated controller synthesis in QFT designs. *Journal of Dynamic Systems, Measurement, and Control*, 129(3):311–321.

[194] Nemirovskii, A. (1993). Several NP-hard problems arising in robust stability analysis. *Mathematics of Control, Signals and Systems*, 6(2):99–105.

[195] Nguyen, H.-N. (2014). *Constrained Control of Uncertain, Time-Varying, Discrete-Time Systems: An Interpolation-Based Approach*. Springer International Publishing.

[196] Nguyen, H.-N., Gutman, P.-O., Olaru, S., and Hovd, M. (2013). Implicit improved vertex control for uncertain, time-varying linear discrete-time systems with state and control constraints. *Automatica*, 49(9):2754–2759.

[197] Nguyen, H.-N., Gutman, P.-O., Olaru, S., and Hovd, M. (2014). Control with constraints for linear stationary systems: An interpolation approach. *Automation and Remote Control*, 75(1):57–74.

[198] Nocedal, J. and Wright, S. (2006). *Numerical Optimization*. Springer-Verlag New York.

[199] Nordin, M. and Gutman, P.-O. (2002). Controlling mechanical systems with backlash—a survey. *Automatica*, 38(10):1633–1649.

[200] Nyquist, H. (1932). Regeneration theory. *Bell system technical journal*, 11(1):126–147.

[201] O'Dwyer, A. (2006). *Handbook of PI and PID Controller Tuning Rules*. World Scientific.

[202] Padula, F. and Visioli, A. (2012). On the stabilizing PID controllers for integral processes. *IEEE Transactions on Automatic Control*, 57(2):494–499.

[203] Panagopoulos, H., Åström, K. J., and Hägglund, T. (2002). Design of PID controllers based on constrained optimisation. *IEE Proceedings-Control Theory and Applications*, 149(1):32–40.

[204] Panda, S., Sahu, B., and Mohanty, P. (2012). Design and performance analysis of PID controller for an automatic voltage regulator system using simplified particle swarm optimization. *Journal of the Franklin Institute*, 349(8):2609–2625.

[205] Papadopoulos, K. G. (2015). *PID Controller Tuning Using the Magnitude Optimum Criterion*. Springer International Publishing.

[206] Papoulis, A. and Pillai, S. U. (2002). *Probability, Random Variables, and Stochastic Processes*. McGraw-Hill.

[207] Park, I., Hong, S., and Sunwoo, M. (2014). Robust air-to-fuel ratio and boost pressure controller design for the EGR and VGT systems using quantitative feedback theory. *IEEE Transactions on Control Systems Technology*, 22(6):2218–2231.

[208] Perez, F., Baños, A., and Cervera, J. (2011). Periodic reset control of an in-line pH process. In *Proceedings of the 16th IEEE Conference on Emerging Technologies & Factory Automation*, pages 1–4, Toulouse, France.

[209] Petersen, I. R. and Tempo, R. (2014). Robust control of uncertain systems: Classical results and recent developments. *Automatica*, 50(5):1315–1335.

[210] Petras, K. (2003). Smolyak cubature of given polynomial degree with few nodes for increasing dimension. *Numerische Mathematik*, 93(4):729–753.

[211] Poljak, S. and Rohn, J. (1993). Checking robust nonsingularity is NP-hard. *Mathematics of Control, Signals and Systems*, 6(1):1–9.

[212] Purohit, H., Goldsztejn, A., Jermann, C., Granvilliers, L., Goualard, F., Nataraj, P., and Patil, B. (2016). Simultaneous automated design of structured QFT controller and prefilter using nonlinear programming. *International Journal of Robust and Nonlinear Control*.

[213] Rantzer, A. and Gutman, P.-O. (1991). Algorithm for addition and multiplication of value sets of uncertain transfer functions. In *Proceedings of the 30th IEEE Conference on Decision and Control*, pages 3056–3057, Brighton, UK.

[214] Rivera, D. E., Morari, M., and Skogestad, S. (1986). Internal model control: PID controller design. *Industrial & Engineering Chemistry Process Design and Development*, 25(1):252–265.

[215] Roberts, G. (2008). Trends in marine control systems. *Annual Reviews in Control*, 32(2):263–269.

[216] Rodríguez, C., Normey-Rico, J. E., Guzmán, J. L., and Berenguel, M. (2016). Robust design methodology for simultaneous feedforward and feedback tuning. *IET Control Theory & Applications*, 10(1):84–94.

[217] Rosenbrock, H. and McMorran, P. (1971). Good, bad, or optimal? *IEEE Transactions on Automatic Control*, 16(6):552–554.

[218] Sadeghpour, M., De Oliveira, V., and Karimi, A. (2012). A toolbox for robust PID controller tuning using convex optimization. *IFAC Proceedings Volumes*, 45(3):158–163.

[219] Saeki, M. (2007). Properties of stabilizing PID gain set in parameter space. *IEEE Transactions on Automatic Control*, 52(9):1710–1715.

[220] Safonov, M. G. (1983). L_∞-optimal sensitivity vs. stability margin. In *Proceedings of the 22nd IEEE Conference on Decision and Control*, pages 115–118, San Antonio, USA.

[221] Safonov, M. G. (2012). Origins of robust control: Early history and future speculations. *Annual Reviews in Control*, 36(2):173–181.

[222] Safonov, M. G. and Athans, M. (1977). Gain and phase margin for multiloop LQG regulators. *IEEE Transactions on Automatic Control*, 22(2):173–179.

[223] Seron, M. M., Braslavsky, J. H., and Goodwin, G. C. (1997). *Fundamental Limitations in Filtering and Control*. Springer-Verlag London.

[224] Seron, M. M. and Goodwin, G. C. (1996). Sensitivity limitations in nonlinear feedback control. *Systems & Control Letters*, 27(4):249–254.

[225] Shafiei, Z. and Shenton, A. (1994). Tuning of PID-type controllers for stable and unstable systems with time delay. *Automatica*, 30(10):1609–1615.

[226] Shen, S.-H., Wu, J.-S., and Yu, C.-C. (1996). Use of biased-relay feedback for system identification. *AIChE Journal*, 42(4):1174–1180.

[227] Shinskey, F. G. (1996). *Process Control Systems: Application, Design and Tuning*. McGraw-Hill Inc.

[228] Sidi, M. J. (2001). *Design of Robust Control Systems: From Classical to Modern Practical Approaches*. Krieger Publishing Company.

[229] Siljak, D. D. (1989). Parameter space methods for robust control design: a guided tour. *IEEE Transactions on Automatic Control*, 34(7):674–688.

[230] Silva, G. J., Datta, A., and Bhattacharyya, S. (2001). Controller design via Padé approximation can lead to instability. In *Proceedings of the 40th IEEE Conference on Decision and Control*, volume 5, pages 4733–4737, Orlando, USA.

[231] Silva, G. J., Datta, A., and Bhattacharyya, S. P. (2002). New results on the synthesis of PID controllers. *IEEE Transactions on Automatic Control*, 47(2):241–252.

[232] Silva, G. J., Datta, A., and Bhattacharyya, S. P. (2005). *PID Controllers for Time-Delay Systems*. Birkhäuser Basel.

[233] Skogestad, S. (2003). Simple analytic rules for model reduction and PID controller tuning. *Journal of Process Control*, 13(4):291–309.

[234] Skogestad, S. and Postlethwaite, I. (2005). *Multivariable Feedback Control: Analysis and Design*. John Wiley & Sons.

[235] Smolyak, S. A. (1963). Quadrature and interpolation formulas for tensor products of certain classes of functions. *Soviet Mathematics Doklady*, 4:240–243.

[236] Soltesz, K., Grimholt, C., and Skogestad, S. (2017). Simultaneous design of proportional–integral–derivative controller and measurement filter by optimisation. *IET Control Theory & Applications*, 11(3):341–348.

[237] Soltesz, K., Hägglund, T., and Åström, K. J. (2010). Transfer function parameter identification by modified relay feedback. In *Proceedings of the 2010 American Control Conference*, pages 2164–2169, Baltimore, USA.

[238] Soltesz, K. and Mercader, P. (2016). Identification for control of biomedical systems using a very short experiment. In *Proceedings of the 2016 International Conference on Systems in Medicine and Biology*, Kharagpur, India.

[239] Soltesz, K., Mercader, P., and Baños, A. (2016). An automatic tuner with short experiment and probabilistic plant parameterization. *International Journal of Robust and Nonlinear Control*.

[240] Srinivasan, K. and Chidambaram, M. (2003). Modified relay feedback method for improved system identification. *Computers & Chemical Engineering*, 27(5):727–732.

[241] Stein, G. (2003). Respect the unstable. *IEEE Control Systems*, 23(4):12–25.

[242] Stelling, J., Sauer, U., Szallasi, Z., Doyle, F. J., and Doyle, J. (2004). Robustness of cellular functions. *Cell*, 118(6):675–685.

[243] Stroud, A. H. (1971). *Approximate Calculation of Multiple Integrals*. Prentice Hall Inc.

[244] Sung, S. W., Lee, J., and Lee, I.-B. (2009). *Process Identification and PID Control*. John Wiley & Sons.

[245] Tan, K. K., Wang, Q.-G., and Hang, C. C. (1999). *Advances in PID Control*. Springer-Verlag London.

[246] Tempo, R., Calafiore, G., and Dabbene, F. (2012). *Randomized Algorithms for Analysis and Control of Uncertain Systems: With Applications*. Springer-Verlag London.

[247] Thompson, D. F. and Nwokah, O. D. (1994). Analytic loop shaping methods in quantitative feedback theory. *Journal of Dynamic Systems, Measurement, and Control*, 116(2):169–177.

[248] Tsypkin, Y. Z. (1979). Stability of sistems with delayed feedback. In MacFarlane, A. G. J., editor, *Frequency-Response Methods in Control Systems*, pages 45–56. IEEE Press.

[249] van Loon, S. J. L. M. (2016). *Hybrid control for performance improvement of linear systems*. PhD thesis, Technische Universiteit Eindhoven.

[250] Vapnik, V. N. (1999). An overview of statistical learning theory. *IEEE Transactions on Neural Networks*, 10(5):988–999.

[251] Vidal, A. and Baños, A. (2010). Reset compensation for temperature control: Experimental application on heat exchangers. *Chemical Engineering Journal*, 159(1):170–181.

[252] Vidyasagar, M. (2002). *Nonlinear Systems Analysis*. SIAM: Society for Industrial and Applied Mathematics.

[253] Vidyasagar, M., Bertschmann, R., and Sallaberger, C. (1988). Some simplifications of the graphical Nyquist criterion. *IEEE Transactions on Automatic Control*, 33(3):301–305.

[254] Vilanova, R. and Visioli, A. (2012). *PID Control in the Third Millennium: Lessons Learned and New Approaches*. Springer-Verlag London.

[255] Visioli, A. (2006). *Practical PID Control*. Springer-Verlag London.

[256] Visioli, A. and Zhong, Q. (2011). *Control of Integral Processes with Dead Time*. Springer-Verlag London.

[257] Vyshnegradskii, I. (1876). Sur la théorie générale des régulateurs. *Comptes rendus de l'Académie des Sciences*, 83:318–321.

[258] Wang, C. and Li, D. (2011). Decentralized PID controllers based on probabilistic robustness. *Journal of Dynamic Systems, Measurement, and Control*, 133(6):061015.

[259] Wang, Q.-G., Ye, Z., Cai, W.-J., and Hang, C.-C. (2008). *PID Control for Multivariable Processes*. Springer-Verlag Berlin Heidelberg.

[260] Wasilkowski, G. W. and Wozniakowski, H. (1995). Explicit cost bounds of algorithms for multivariate tensor product problems. *Journal of Complexity*, 11(1):1–56.

[261] Wie, B. and Bernstein, D. S. (1991). Benchmark problems for robust control design. In *Proceedings of the 1991 American Control Conference*, pages 1929–1930, Boston, USA.

[262] Wright, R. A. and Kravaris, C. (2001). On-line identification and nonlinear control of an industrial pH process. *Journal of Process Control*, 11(4):361–374.

[263] Yang, S.-F. (2010). Efficient algorithm for computing QFT bounds. *International Journal of Control*, 83(4):716–723.

[264] Yaniv, O. (1995). MIMO QFT using non-diagonal controllers. *International Journal of Control*, 61(1):245–253.

[265] Yaniv, O. (1999). *Quantitative Feedback Design of Linear and Nonlinear Control Systems*. Springer US.

[266] Yaniv, O. (2006). Automatic loop shaping of MIMO controllers satisfying sensitivity specifications. *Journal of Dynamic Systems, Measurement, and Control*, 128(2):463–471.

[267] Yaniv, O. and Horowitz, I. M. (1986). A quantitative design method for MIMO linear feedback systems having uncertain plants. *International Journal of Control*, 43(2):401–421.

[268] Yaniv, O. and Nagurka, M. (2003). Robust PI controller design satisfying sensitivity and uncertainty specifications. *IEEE Transactions on Automatic Control*, 48(11):2069–2072.

[269] Yaniv, O. and Nagurka, M. (2004). Design of PID controllers satisfying gain margin and sensitivity constraints on a set of plants. *Automatica*, 40(1):111–116.

[270] Yaniv, O. and Nagurka, M. (2005). Automatic loop shaping of structured controllers satisfying QFT performance. *Journal of Dynamic Systems, Measurement, and Control*, 127(3):472–477.

[271] Yeroğlu, C. and Ateş, A. (2014). A stochastic multi-parameters divergence method for online auto-tuning of fractional order PID controllers. *Journal of the Franklin Institute*, 351(5):2411–2429.

[272] Yi, T.-M., Huang, Y., Simon, M. I., and Doyle, J. (2000). Robust perfect adaptation in bacterial chemotaxis through integral feedback control. *Proceedings of the National Academy of Sciences*, 97(9):4649–4653.

[273] Youla, D., Bongiorno, J., and Jabr, H. (1976a). Modern Wiener–Hopf design of optimal controllers Part I: The single-input-output case. *IEEE Transactions on Automatic Control*, 21(1):3–13.

[274] Youla, D., Jabr, H., and Bongiorno, J. (1976b). Modern Wiener–Hopf design of optimal controllers Part II: The multivariable case. *IEEE Transactions on Automatic Control*, 21(3):319–338.

[275] Yu, C.-C. (2006). *Autotuning of PID Controllers: A Relay Feedback Approach*. Springer-Verlag London.

[276] Yuille, A. L. and Rangarajan, A. (2003). The concave-convex procedure. *Neural Computation*, 15(4):915–936.

[277] Zames, G. (1981). Feedback and optimal sensitivity: Model reference transformations, multiplicative seminorms, and approximate inverses. *IEEE Transactions on Automatic Control*, 26(2):301–320.

[278] Zames, G. and Francis, B. (1983). Feedback, minimax sensitivity, and optimal robustness. *IEEE Transactions on Automatic Control*, 28(5):585–601.

[279] Zhou, K., Doyle, J. C., and Glover, K. (1995). *Robust and Optimal Control*. Pearson.

[280] Ziegler, J. G. and Nichols, N. B. (1942). Optimum settings for automatic controllers. *Transactions of the ASME*, 64(11).

[281] Zimmerman, Y. and Gutman, P.-O. (2014). An innovative method for optimization based, high order controller autotuning. *Journal of Dynamic Systems, Measurement, and Control*, 136(2):021010.

[282] Zolotas, A. and Halikias, G. (1999). Optimal design of PID controllers using the QFT method. *IEE Proceedings-Control Theory and Applications*, 146(6):585–589.

Glossary

Symbols

$\mathbb{N}$	Set of natural numbers
$\mathbb{Z}$	Set of integer numbers
$\mathbb{R}$	Set of real numbers
$\mathbb{R}_+$	Set of nonnegative real numbers (including 0).
$\mathbb{R}^n$	Real coordinate space of n dimensions
$\mathbf{0}$	The zero vector
$[a, b]$	A closed interval in $\mathbb{R}$
$[a\ b]$	A row vector
:	"Such that"
$\in$	"Is an element of"
$\subset$	"Is a subset of"
$\bigcap$	Intersection
j	Imaginary unit $\sqrt{-1}$. Sometimes an index
$\arg z$	Argument of the complex number z
$\Re(z)$	Real part of the complex number z
$\Im(z)$	Imaginary part of the complex number z
z^*	Complex conjugate of z
$\log_{10}$	Logarithm to base 10
dB	Decibels, x dB represents a gain of $10^{x/20}$
$\|G\|_\infty$	$\sup_\omega \|G(j\omega)\|$ where G is a transfer function
$A^\top$	Transpose of the real matrix A
∇	Gradient operator
Δ	Hessian operator
$\mathbb{E}[\cdot]$	Expectation operator
$\mathbb{V}[\cdot]$	Variance operator

$\Pr[\cdot]$	Probability
$\otimes$	Tensor product
$\|\mathbf{x}\|_1$	1-norm, $\sum_i \|x_i\|$

Acronyms

ALS	Automatic Loop Shaping
CCP	Convex-Concave Procedure
CUT	Conjugate Unscented Transform
dKP	delayed Kronrod–Patterson
DOF	Degrees Of Freedom
DTC	Dead-Time Compensator
FOTD	First-Order Time-Delay
GL	Gauss–Legendre
IAE	Integral Absolute Error
IE	Integral Error
IMC	Internal Model Control
ITD	Integrating Time-Delay
LQG	Linear Quadratic Gaussian
LQR	Linear Quadratic Regulator
LTI	Linear Time-Invariant
MC	Monte Carlo
MCE	Moment Constraint Equation
MIGO	M-Constrained Integral Gain Optimization
MIMO	Multiple-Input-Multiple-Output
MPC	Model Predictive Control
MP	Minimum Phase
NMP	Nonminimum Phase
OLHP	Open Left Half-Plane
ORHP	Open Right Half-Plane
PDF	Probability Density Function
PI	Proportional-Integral
PID	Proportional-Integral-Derivative

QFT	Quantitative Feedback Theory
RA	Randomized Algorithm
RHP	Right Half-Plane
SIMC	Simple/Skogestad Internal Model Control
SISO	Single-Input-Single-Output
SP	Smith Predictor
SQP	Sequential Quadratic Programming
UT	Unscented Transform

Appendix A

Optimization Problems

A continuous mathematical optimization problem has the form

$$\begin{array}{ll} \underset{\mathbf{x}}{\text{minimize}} & f_0(\mathbf{x}) \\ \text{subject to} & f_i(\mathbf{x}) \leq 0,\ i = 1, \ldots, m. \end{array} \tag{A.1}$$

Where $\mathbf{x} \in \mathbb{R}^n$ is the *decision variable*, the function $f_0 : \mathbb{R}^n \to \mathbb{R}$ is the *objective* function, and the functions $f_i : \mathbb{R}^n \to \mathbb{R}$, $i = 1, \ldots, m$, are the *constraint* functions. A decision variable is called a *global optimizer* or *optimal solution* if it minimizes the objective over all feasible points, i.e., points that satisfy the constraints. On the other hand, a decision variable is called *local optimizer* if it minimizes the objective function among feasible points that are near.

The optimizations problem can be classified into several classes depending on its structure. An optimization problem is *linear* if the objective and constraint functions $f_0, \ldots, f_m$ are linear, i.e., they satisfy the following condition

$$f_i(\alpha \mathbf{x}_1 + \beta \mathbf{x}_2) = \alpha f_i(\mathbf{x}_1) + \beta f_i(\mathbf{x}_2), \tag{A.2}$$

for all $\mathbf{x}_1, \mathbf{x}_2 \in \mathbb{R}^n$ and all $\alpha, \beta \in \mathbb{R}$. Otherwise, the optimization problem is *nonlinear*. Another important class of optimization problems is the one in which the objective and constraint functions are convex, i.e., objective and constraint functions satisfy

$$f_i(\alpha \mathbf{x}_1 + \beta \mathbf{x}_2) \leq \alpha f_i(\mathbf{x}_1) + \beta f_i(\mathbf{x}_2), \tag{A.3}$$

for all $\mathbf{x}_1, \mathbf{x}_2 \in \mathbb{R}^n$ and all $\alpha, \beta \in \mathbb{R}$ with $\alpha + \beta = 1$, $\alpha \geq 0$, and $\beta \geq 0$. This class of problems is a generalization of the linear optimization problems.

An important property of convex optimization problems is that local optimizers are also global optimizers [48].

In general, the solution of an optimization problem (A.1) is a difficult task, even in the case that objective and constraint functions are smooth. Some important exceptions are optimization problems that are linear or convex. In these cases, there are very effective algorithms for solving them. Nonconvex optimization problems are usually solved by iterating between the solution of convex subproblems.

Appendix B

Different Representations of the PID Controller

Along this thesis, the chosen representation of the PID controller has been

$$C_{\text{par}}(s) = k_p + \frac{k_i}{s} + k_d s. \tag{B.1}$$

This representation is generally referred to as *parallel* representation. It has the advantage of particularizing to P, I, ID, PI, or PD with finite values of its parameters. A representation that is equivalent to the latter, but with different values of the parameter are the so-called *standard* or *non-interacting*, that is given by the following equation

$$C_{\text{std}}(s) = K\left(1 + \frac{1}{sT_i} + sT_d\right). \tag{B.2}$$

The relation between the parameters of the representation (B.1) and (B.2) are given as follows

$$\begin{aligned} K &= k_p, \\ T_i &= \frac{k_p}{k_i}, \\ T_d &= \frac{k_d}{k_p}. \end{aligned} \tag{B.3}$$

Another alternative representation, known as *series* or *interacting*, is given by

$$C_{\text{ser}}(s) = K'\left(1 + \frac{1}{sT_i'}\right)(1 + sT_d'). \tag{B.4}$$

In this case, not any controller in the representation (B.1) has an equivalent in the representation (B.4). The reason is that representation (B.1) allows a pair of complex zeros, while the representation (B.4) require two real zeros. Remind that the transfer function of a PID controller in the parallel representation is composed by a gain, an integrator (pole at the origin), and two zeros (two real zeros or a pair of complex zeros). It is easy to show that the following transfer function

$$C_{\text{par}}(s) = \frac{k_d s^2 + k_p s + k_i}{s}, \tag{B.5}$$

that describes a PID controller in the parallel representation, has two real zeros, when $k_p^2 - 4k_d k_i \geq 0$, and a pair of complex zeros, when $k_p^2 - 4k_d k_i < 0$. Therefore, a PID controller in the parallel representation can be transformed into a series representation if $k_p^2 - 4k_d k_i \geq 0$. In this case, the relation between the parameters of the representation (B.1) and (B.4) are given as follows

$$\begin{aligned} K' &= \frac{k_p}{2}\left(1 + \sqrt{1 - 4\frac{k_d k_i}{k_p^2}}\right), \\ T_i' &= \frac{k_p}{2k_i}\left(1 + \sqrt{1 - 4\frac{k_d k_i}{k_p^2}}\right), \\ T_d' &= \frac{k_p}{2k_i}\left(1 - \sqrt{1 - 4\frac{k_d k_i}{k_p^2}}\right). \end{aligned} \tag{B.6}$$

It has been assumed that each parameter k_p, k_i, and k_d is nonzero. It is worth to note that both representations are equivalent when k_i or k_d is zero. In these cases, the relation between the parameters of both representations can be obtained in an easier manner. For example, a PI controller in the parallel representation

$$C_{\text{par}}(s) = k_p + \frac{k_i}{s}, \tag{B.7}$$

can always be transformed to the series representation

$$C_{\text{ser}}(s) = K'\left(1 + \frac{1}{sT_i'}\right), \tag{B.8}$$

and the relation between their parameters is given by

$$\begin{aligned} K' &= k_p, \\ T_i' &= \frac{k_p}{k_i}. \end{aligned} \tag{B.9}$$

Any other relation can be obtained without major difficulties.